NASA CR-178,201

NASA Contractor Report **178201**

NASA-CR-178201
19870011940

SUMMARY OF THE MODELING AND TEST CORRELATIONS OF A NASTRAN FINITE ELEMENT VIBRATIONS MODEL FOR THE AH-1G HELICOPTER

J.D. Cronkhite, V.L. Berry, and R.V. Dompka

FOR REFERENCE

NOT TO BE TAKEN FROM THIS ROOM

Bell Helicopter TEXTRON
A Subsidiary of Textron Inc.
Ft. Worth, TX 76101

Contract NAS1-17496
January 1987

LIBRARY COPY

MAY 7 1987

LANGLEY RESEARCH CENTER
LIBRARY, NASA
HAMPTON, VIRGINIA

NASA
National Aeronautics and
Space Administration

Langley Research Center
Hampton, Virginia 23665-5225

NF00197

FOREWORD

Bell Helicopter Textron Inc. (BHTI) has been conducting a study of finite element modeling of helicopter airframes to predict vibration. This work is being performed under U.S. Government Contract NAS1-17496. The contract is monitored by the NASA Langley Research Center, Structures Directorate.

This report summarizes the development and validation of a vibration finite element model for the AH-1G airframe which was used as the basis for evaluating extant analysis methods for predicting coupled rotor-fuselage vibrations. Key NASA and BHTI personnel are listed below:

NASA Langley

Michael F. Cavelli, Contracting Officer
Joseph W. Owens, Contract Specialist
John Cline, Technical Representative
Raymond G. Kvaternik, Leader, Rotorcraft Structural Dynamics Group

Bell Helicopter Textron

W. Young, Manager, Research
J.D. Cronkhite, Group Engineer, Research Structures
V.L. Berry, Senior Research Engineer
R.V. Dompka, Senior Research Engineer

N87-21373 #

TABLE OF CONTENTS

Section Page

FOREWORD i

1. INTRODUCTION 1

2. MODELING 7

3. STATIC TESTING 105

4. GROUND VIBRATION TESTING 139

5. FLIGHT VIBRATION TESTING 193

6. TAILBOOM EFFECTIVE SKIN INVESTIGATION 245

7. REFERENCES 269

APPENDIX A - KAMAN FREQUENCY RESPONSE COMPARISONS 273
(Low, Mean, High GW Configurations)

1. INTRODUCTION

The NASA Langley Research Center is sponsoring a rotorcraft structural dyanmics program with the overall objective to establish in the United States a superior capability to utilize finite element analysis models for calculations to support industrial design of helicopter airframe structures. Viewed as a whole, the program is planned to include efforts by NASA, universities, and the U.S. helicopter industry. In the initial phase of the program, teams from the major U.S. manufacturers of helicopter airframes will apply extant finite element analysis methods to calculate static internal loads and vibrations of helicopter airframes of both metal and composite construction, conduct laboratory measurements of the structural behavior of these airframes, and perform correlations between analysis and measurements to build up a basis upon which to evaluate the results of the applications. To maintain the necessary scientific observation and control, emphasis throughout these activities will be on advance planning, documentation of methods and procedures, and thorough discussion of results and experiences, all with industry-wide critique to allow maximum technology transfer between companies. The finite element models formed in this phase will then serve as the basis for the development, application, and evaluation of both improved modeling techniques and advanced analytical and computational techniques, all aimed at strengthening and enhancing the technology base which supports industrial design of helicopter airframe structures. Here again, procedures for mutual critique have been established, and these procedures call for a thorough discussion among the program participants of each method prior to the applications and of the results and experiences after the applications. The aforementioned rotorcraft structural dynamics program has been given the acronym DAMVIBS (Design Analysis Methods for VIBrationS). Under the DAMVIBS program, the four industry participants (BHTI, Boeing-Vertol, McDonnell-Douglas Helicopter, and Sikorsky Aircraft) are to apply existing company methods for coupled rotor-fuselage analysis to calculate vibrations of the AH-1G helicopter and to correlate with data available from an Operational Load Survey (OLS) flight test program (Refs. 1 and 2). In support of this common activity, BHTI, the manufacturer of the subject aircraft, was tasked to prepare and provide to the other participants the data needed to independently make these analyses and correlations. Specifically, BHTI was tasked to:

1. Present a detailed description of the modeling rationale and techiques used to develop the AH-1G NASTRAN fuselage vibration model under previous contract (Ref. 3). A NASTRAN data deck of this model was provided to all participating manufacturers.

2. Present a detailed description of all previous correlation work used to verify the fuselage vibration model (two versions - stick and built-up tailboom), including the following:

   a. Ground vibration tests (GVT), static deflection tests and in-flight excitation simulation (Refs. 4 and 5).

    b. Application of the built-up tailboom model predictions to the previous static and vibration ground tests of Reference 4.

    c. Correlation of both models with other prior AH-1G results contained in References 6 and 7.

3. Describe the OLS flight-test program on the AH-1G and assemble the vibration data to be used in the correlations.

4. Present the AH-1G rotor system mechanical and aerodynamic coefficient data to all participants.

This report addresses items 1 and 2, i.e., presents a summary of the modeling techniques used to develop the NASTRAN finite element model (FEM) of the AH-1G airframe and a detailed description of all previous correlation work used to validate the airframe model.

In particular, this report describes BHTI involvement in a program initiated by the Army in 1973 to evaluate NASTRAN as a workable tool for satisfying the needs of industry and government as well as to develop a useful helicopter airframe model of the AH-1G. The first part of the program concerned the development of the three-dimensional finite element model (FEM) to represent the low frequency (below 30 Hz) vibration characteristics of the AH-1G airframe. In addition, clear and complete documentation was provided to allow government personnel the option of changing the model for in-house analysis, in particular, to determine the response of the airframe to automatic weapon firing and rotor vibration. Following development and documentation of the NASTRAN model, correlation with static and vibration tests was performed to assess the validity of the model. Static load deflection testing of the AH-1G fuselage, wing, tailboom, and vertical fin was performed to verify the stiffness modeling and two separate sinusoidal vibration tests were performed to verify the dynamic characteristics (including both stiffness and mass effects) of the NASTRAN FEM.

Finally, a two part study was conducted to further correlate the NASTRAN analysis of the AH-1G helicopter airframe structure. The first study was a comparative evaluation of the analysis for calculating level flight airframe vibration at main rotor excitation frequencies. The second was a comparison of a NASTRAN tailboom analysis with test data for evaluation of methods used to determine effective skin in a semimonocoque sheet-stringer structure.

AH-1G NASTRAN MODELING
(1973 - 1976)

- MODELING
- STATIC AND GROUND VIBRATION TESTING
- FLIGHT VIBRATION TESTING
- TAILBOOM EFFECTIVE SKIN INVESTIGATION

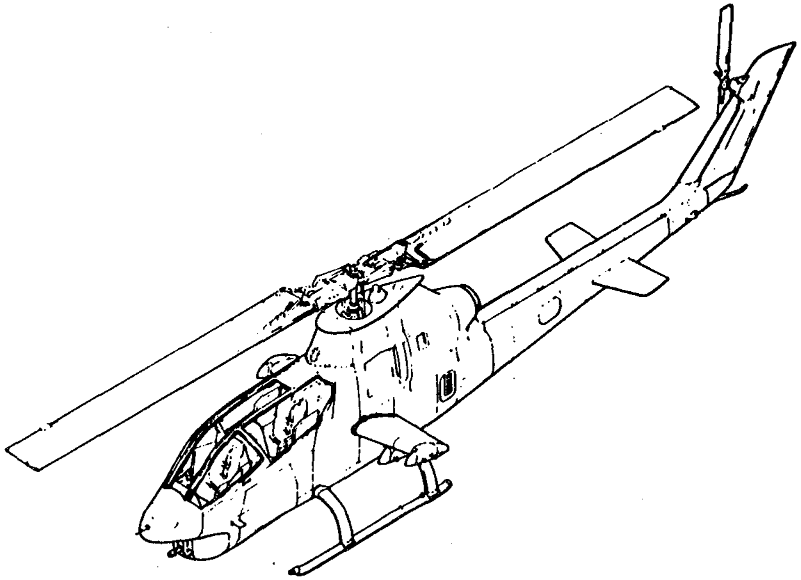

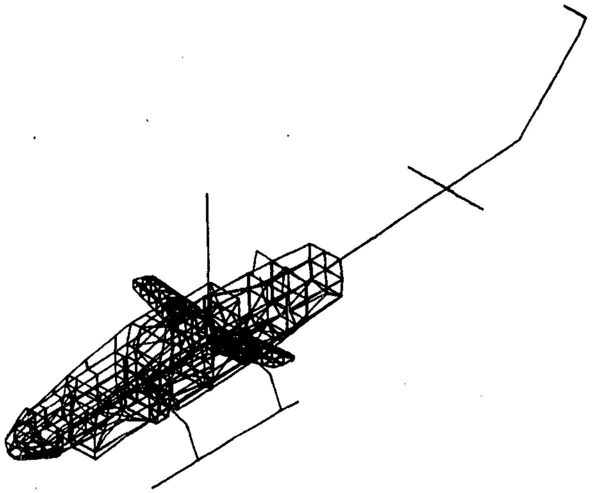

2. MODELING

DEVELOPMENT AND DOCUMENTATION

The two principal goals of the work reported herein were:

1. To produce a NASTRAN model of the AH-1G helicopter which would enable the Government to determine time dependent deformations of the airframe structure produced by on-board weapon systems, as well as rotor induced vibrations.
2. To provide documentation which was clear and altogether comprehensible, showing in what manner and upon what judgments the actual helicopter was idealized as a NASTRAN finite element model.

In the following sections, the actual structure is described, the idealization of the structure is discussed in general, and assumptions and modeling philosophy used in the idealization are presented. Modeling techniques used repetitively are listed and are referenced later in the stiffness modeling section.

DEVELOPMENT AND DOCUMENTATION

- MODEL REQUIREMENTS REPRESENT AIRFRAME RESPONSE DUE TO:
  - AUTOMATIC WEAPON FIRE
  - ROTOR VIBRATION
- TRANSFERRABLE MODEL
  - WILL RUN ON DIFFERENT GOVERNMENT COMPUTERS
  - DOCUMENTATION SUFFICIENT FOR GOVERNMENT USE OF IN-HOUSE ANALYSIS

AH-1G HELICOPTER

BHTI initiated the Model 209 in March 1965 as a company-funded development of the UH-1B/C Iroquois intended specifically for armed helicopter missions. The original design combined the basic transmission and rotor system and the power plant of the UH-1C with a new, streamlined fuselage designed for maximum speed, armament load, and crew efficiency. Tandem seating is provided for the crew of two with the copilot/gunner forward and the pilot aft.

The Model 209 prototype made its first flight on 7 September 1965, and the U.S. Army's intention to order the aircraft was announced on 11 March 1966, the initial model being known as the AH-1G Huey Cobra. Total orders to date for all versions of the Huey Cobra/Sea Cobra exceed 1800.

The original version for the U.S. Army was powered by a single 1400 shp Avco Lycoming T53-L-13 turboshaft engine derated to 1100 shp for take off and maximum continuous rating. The AH-1G uses a Model 540 two-bladed wide-chord 'door hinge' 44 ft diameter main rotor system similar to that of the UH-1C. The interchangeable blades are built-up of extruded aluminum spars and laminates. The tail rotor is a two-bladed all-metal flex-beam tractor tail rotor located on the starboard side and is of honeycomb construction. The main rotor rpm is 294 to 324. The 44-1/2 ft long AH-1G fuselage is a conventional all metal semimonocoque structure with low silhouette and narrow profile. The small mid-mounted stub wings carry armament and off-load the rotor in flight. The landing gear is a nonretractable tubular skid type gear.

The AH-1G maximum takeoff and landing weight is 9500 lb. The never exceed speed is 190 knots while the maximum level speed at sea level is 149 knots.

AH-1G HELICOPTER

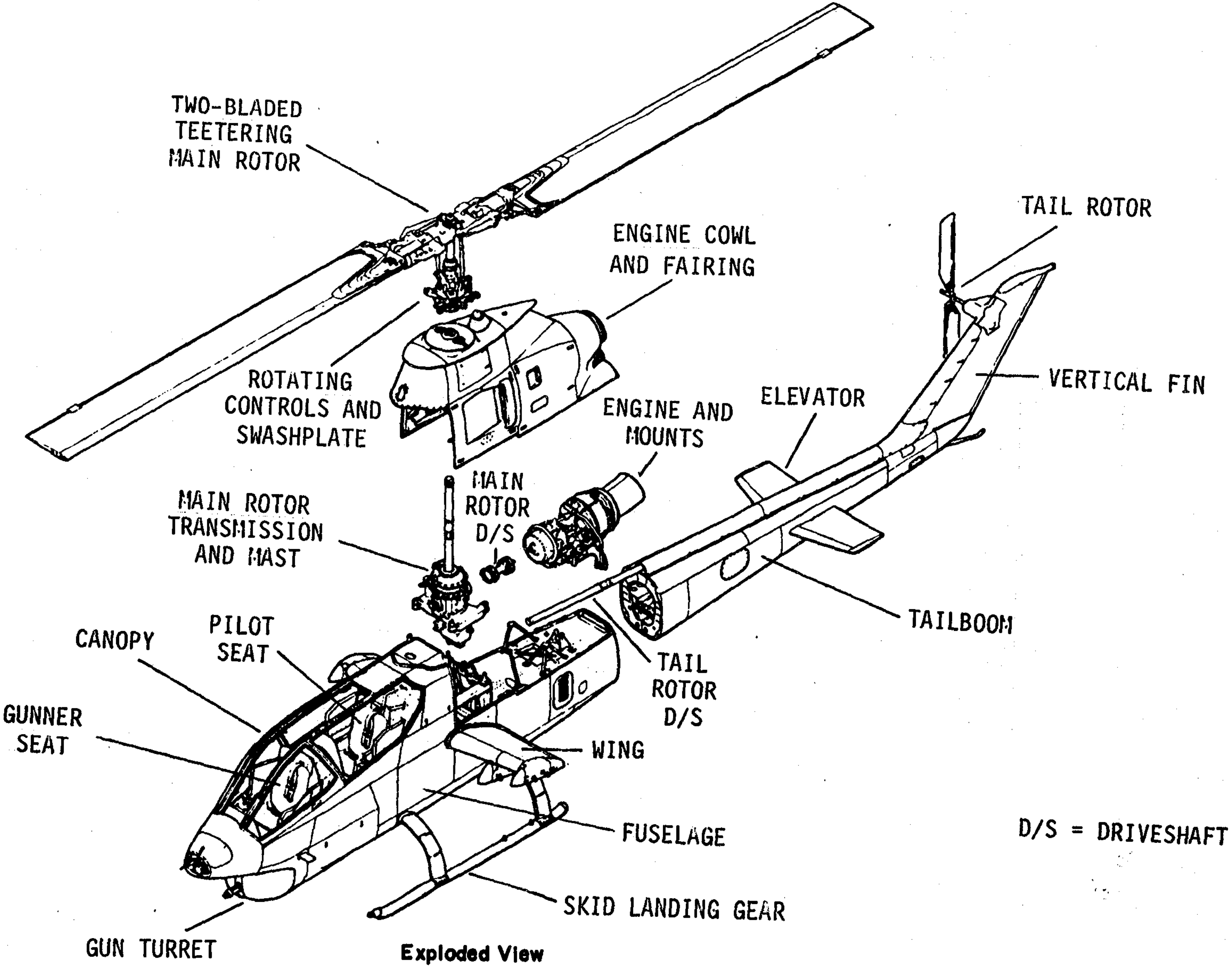
TWO-BLADED TEETERING MAIN ROTOR
TAIL ROTOR
ENGINE COWL AND FAIRING
ROTATING CONTROLS AND SWASHPLATE
VERTICAL FIN
ELEVATOR
ENGINE AND MOUNTS
MAIN ROTOR D/S
MAIN ROTOR TRANSMISSION AND MAST
TAILBOOM
CANOPY
PILOT SEAT
TAIL ROTOR D/S
GUNNER SEAT
WING
FUSELAGE
D/S = DRIVESHAFT
SKID LANDING GEAR
GUN TURRET

Exploded View

AIRFRAME STRUCTURE DESCRIPTION

The actual structure for the latest production configuration of the AH-1G helicopter (identified as FY71 AH-1G ship number 21123) is described in this section. The descriptions are intended to be brief with a liberal use of figures to identify the basic structure used in the analysis.

The areas of the airframe structure in the order they are discussed are:

1. The fuselage
2. The wings and carry-through structure
3. The tailboom and vertical fin

AIRFRAME STRUCTURE DESCRIPTION

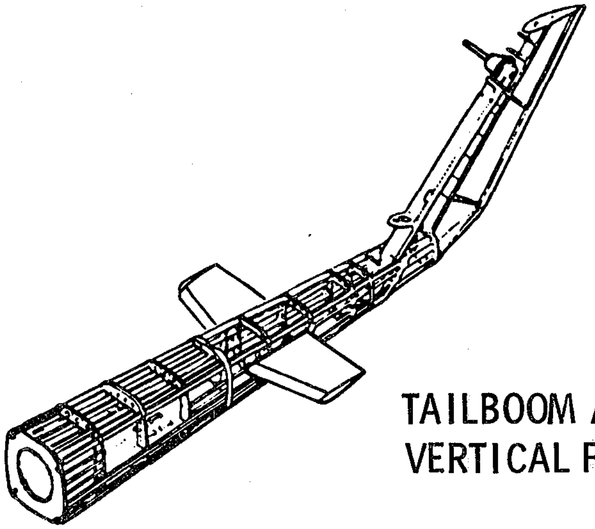

TAILBOOM AND
VERTICAL FIN

FUSELAGE

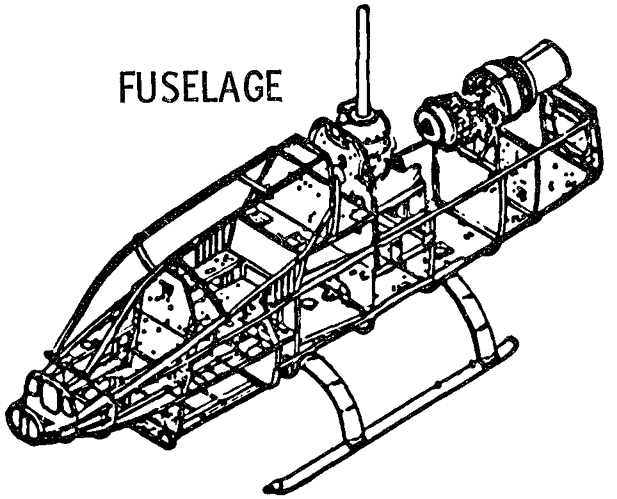

WINGS AND
CARRY THROUGH

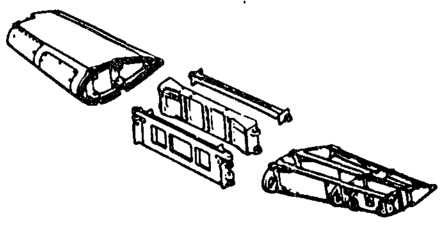

BENDING SECTIONS OF THE AH-1G FUSELAGE STRUCTURE

The fuselage structure with panels removed is illustrated in the figure below. The section cuts between bulkheads show the basic structure used in the stiffness modeling. Structure assumed not effective in the stiffness of the fuselage follows:

1. The canopy
2. Cowling around the engine and main rotor pylon
3. Access panels at contour (FS 61.25 to 213.94)
4. Doors on the ammo bay (FS 93 to 138.7)
5. Top access door on the nose (FS 33-46)
6. Drive shaft connection of the engine to the main transmission

These assumptions are based on experience with the AH-1G structure and on results from the testing and analysis of the AH-1J helicopter (similar to the AH-1G).

The structure is built around the main beams running the length of the fuselage (FS 61 to 300). The beams are made up of vertical webs and upper and lower caps. The left-hand main beam is shown by the shaded area in the figure. The main beams give the primary vertical bending stiffness in the fuselage structure and differential bending of the main beams provides torsional stiffness in the open sections of the forward fuselage (FS 61 to 138).

The main beams are tied together by the lower horizontal floors (FS 46 to 138, WL 46; FS 93 to 138, WL 55; FS 138 to 300, WL 35.97), the forward fuel cell cover (FS 152 to 186, WL 77), and the engine deck (FS 213 to 300, WL 65) to give the fuselage lateral stiffness. The torsion sections are closed in the forward fuel cell area (FS 148.5 to 186) and the aft fuselage (FS 213 to 300), but open on top of the main beams in the main rotor pylon and wing area (FS 186 to 213).

The ammo shelf (FS 93 to 138, WL 27) does not significantly affect the vertical or lateral bending stiffness of the fuselage structure, but does influence the torsional stiffness because of the shear tie at the FS 93 bulkhead.

BENDING SECTIONS OF THE AH-1G FUSELAGE STRUCTURE

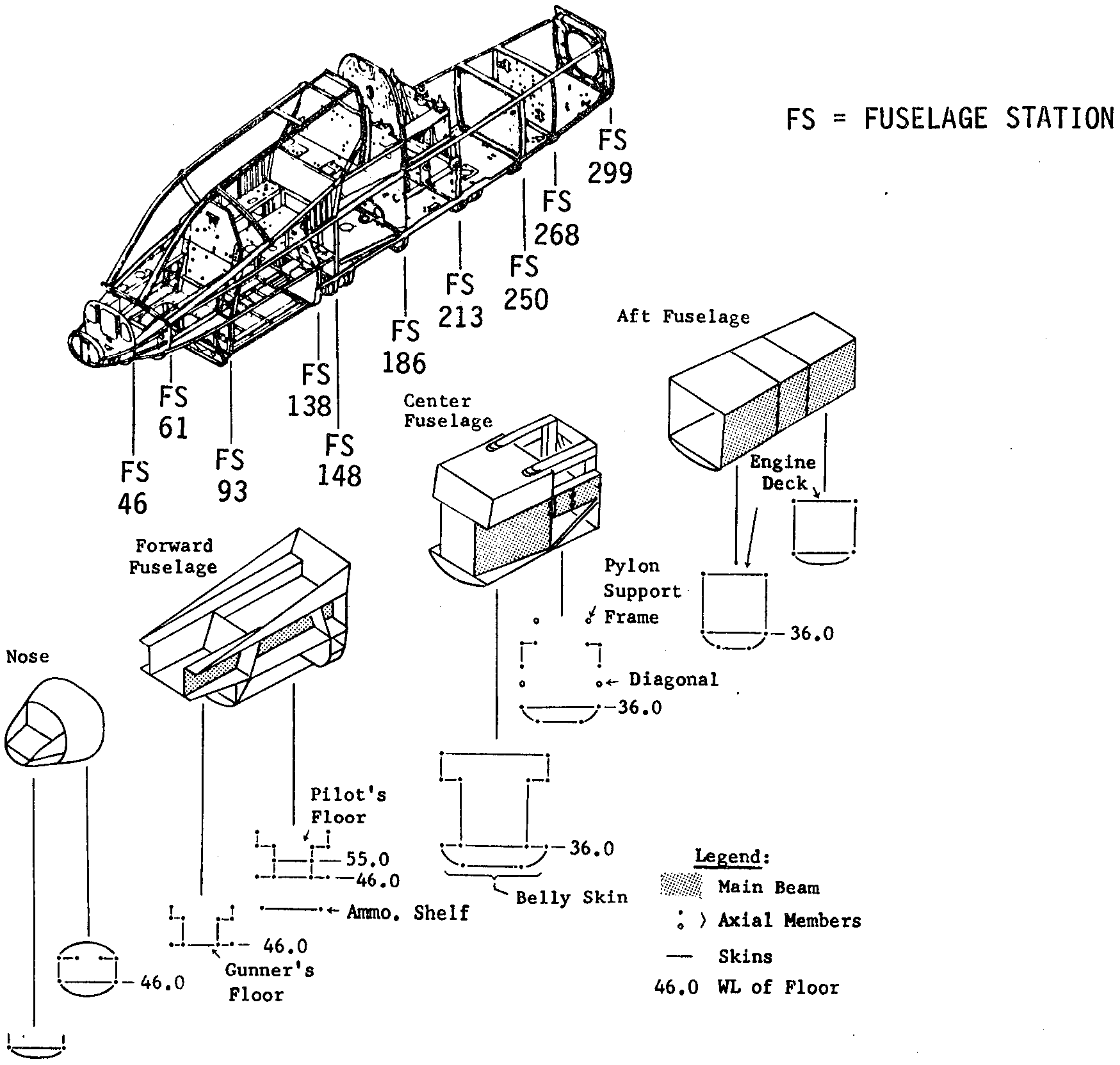
FS = FUSELAGE STATION
FS 46
FS 61
FS 93
FS 138
FS 148
FS 186
FS 213
FS 250
FS 268
FS 299
Nose
46.0
Forward Fuselage
Pilot's Floor
55.0
46.0
Ammo. Shelf
46.0
Gunner's Floor
Center Fuselage
Pylon Support Frame
Diagonal
36.0
36.0
Belly Skin
Aft Fuselage
Engine Deck
36.0
Legend:
▨ Main Beam
⁚ ⟩ Axial Members
— Skins
46.0 WL of Floor

GUN TURRET ATTACHMENT FITTINGS

The XM-28 gun turret shown in the figure is mounted under the gunner's floor (FS 61.25 to 93). Four fittings distribute the recoil loads into the main beams.

GUN TURRET ATTACHMENT FITTINGS

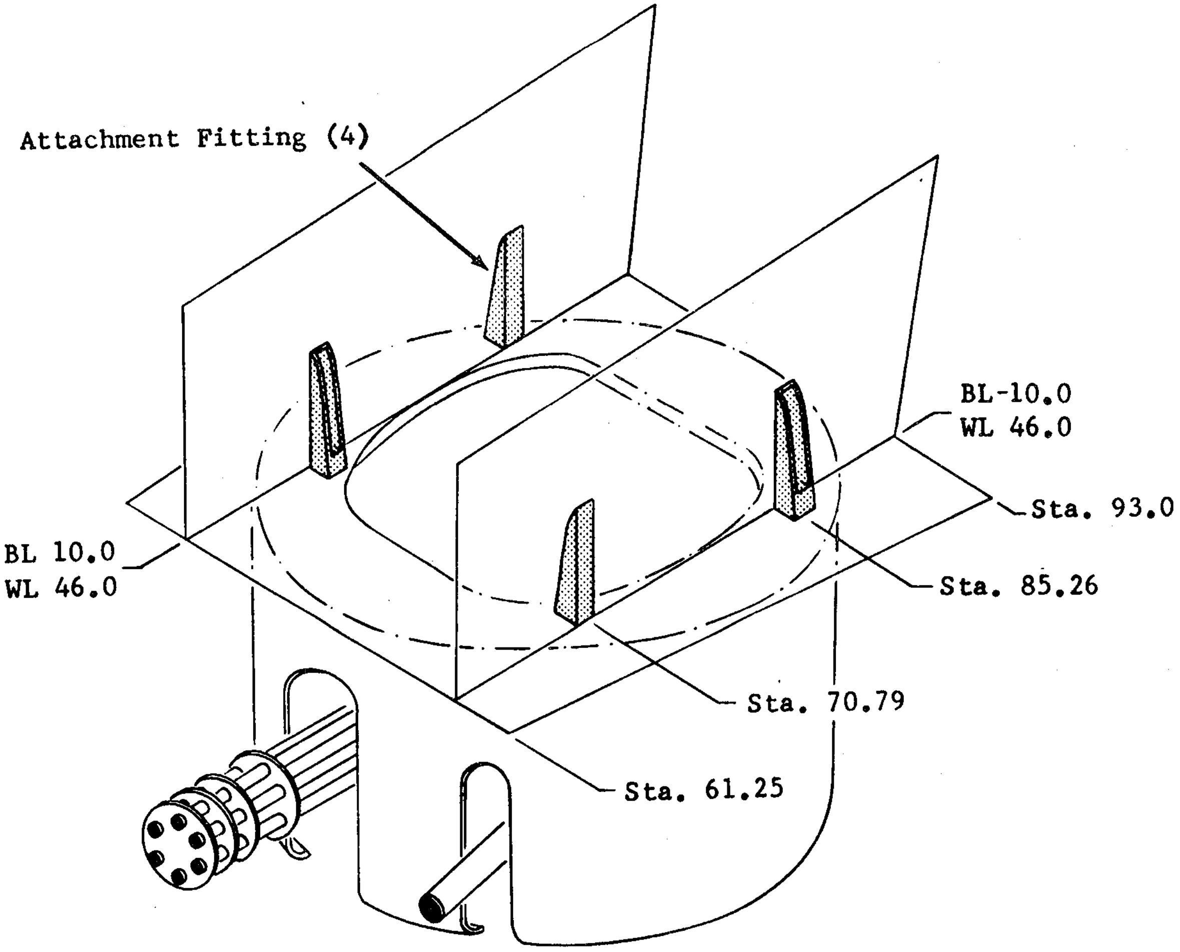
Attachment Fitting (4)
BL-10.0
WL 46.0
Sta. 93.0
BL 10.0
WL 46.0
Sta. 85.26
Sta. 70.79
Sta. 61.25

XM-28 Dual Gun Turret System

MAIN ROTOR PYLON MOUNTS AND LIFT LINK

The main rotor pylon located at FS 200 above WL 65 provides the structural tie between the main rotor and the fuselage. It is attached to the fuselage through five elastomeric mounts and a lift link. This lift link is the primary vertical load path and is pinned to the center wing carry through beam or "lift beam." The elastomeric mounts are designed to produce low pylon rocking frequencies to isolate the main rotor inplane vibratory loads from the fuselage and to react the main rotor torque.

MAIN ROTOR PYLON MOUNTS AND LIFT LINK

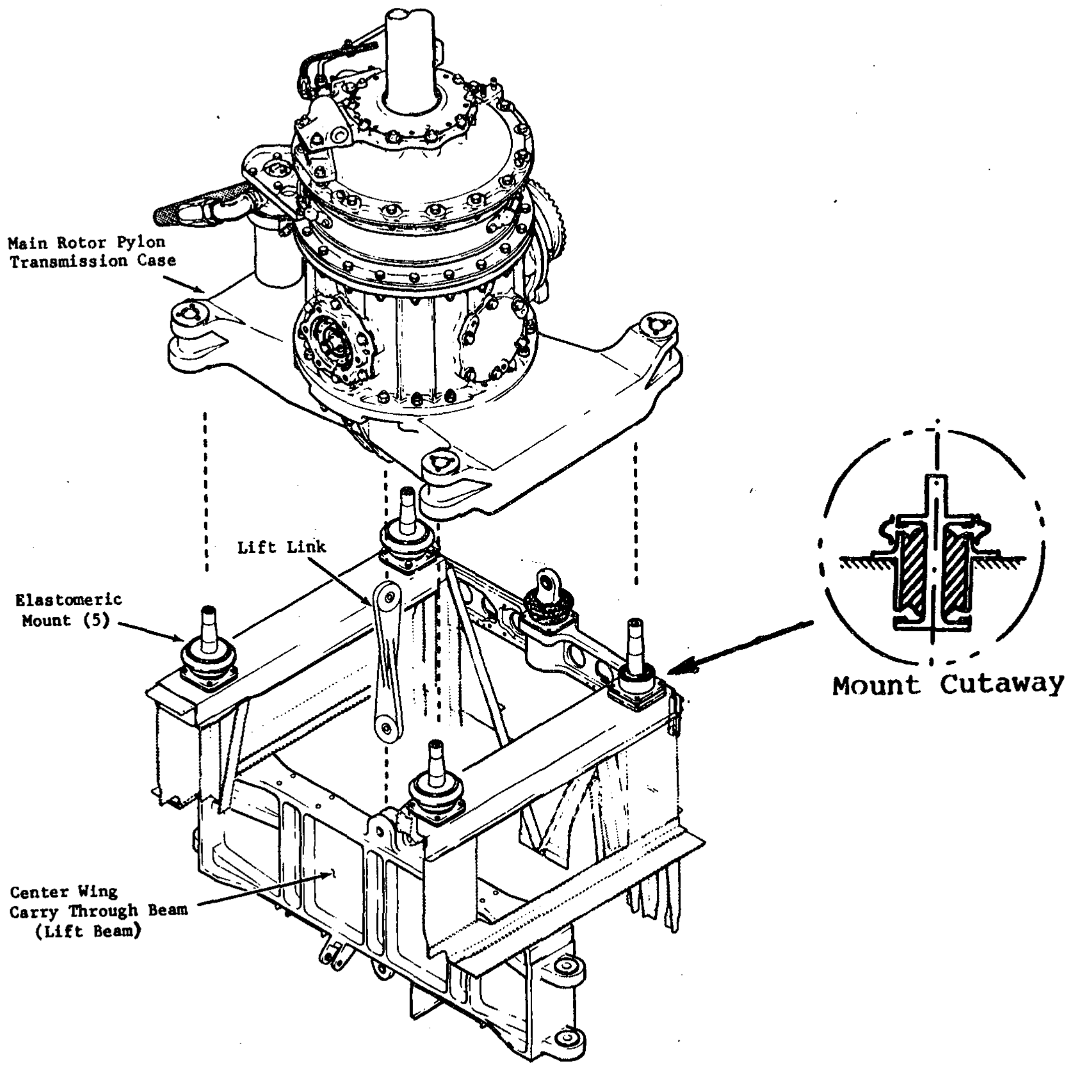
Main Rotor Pylon Transmission Case
Lift Link
Elastomeric Mount (5)
Center Wing Carry Through Beam (Lift Beam)
Mount Cutaway

ENGINE MOUNTS

The engine mounting on the WL 65 deck of the fuselage (FS 228 to 268) is shown in the figure. The mounting is statically determinant with a single strut at the forward left-hand mounting pad, a tripod at the aft left-hand mounting pad, and a bipod at the right-hand aft mounting pad.

ENGINE MOUNTS

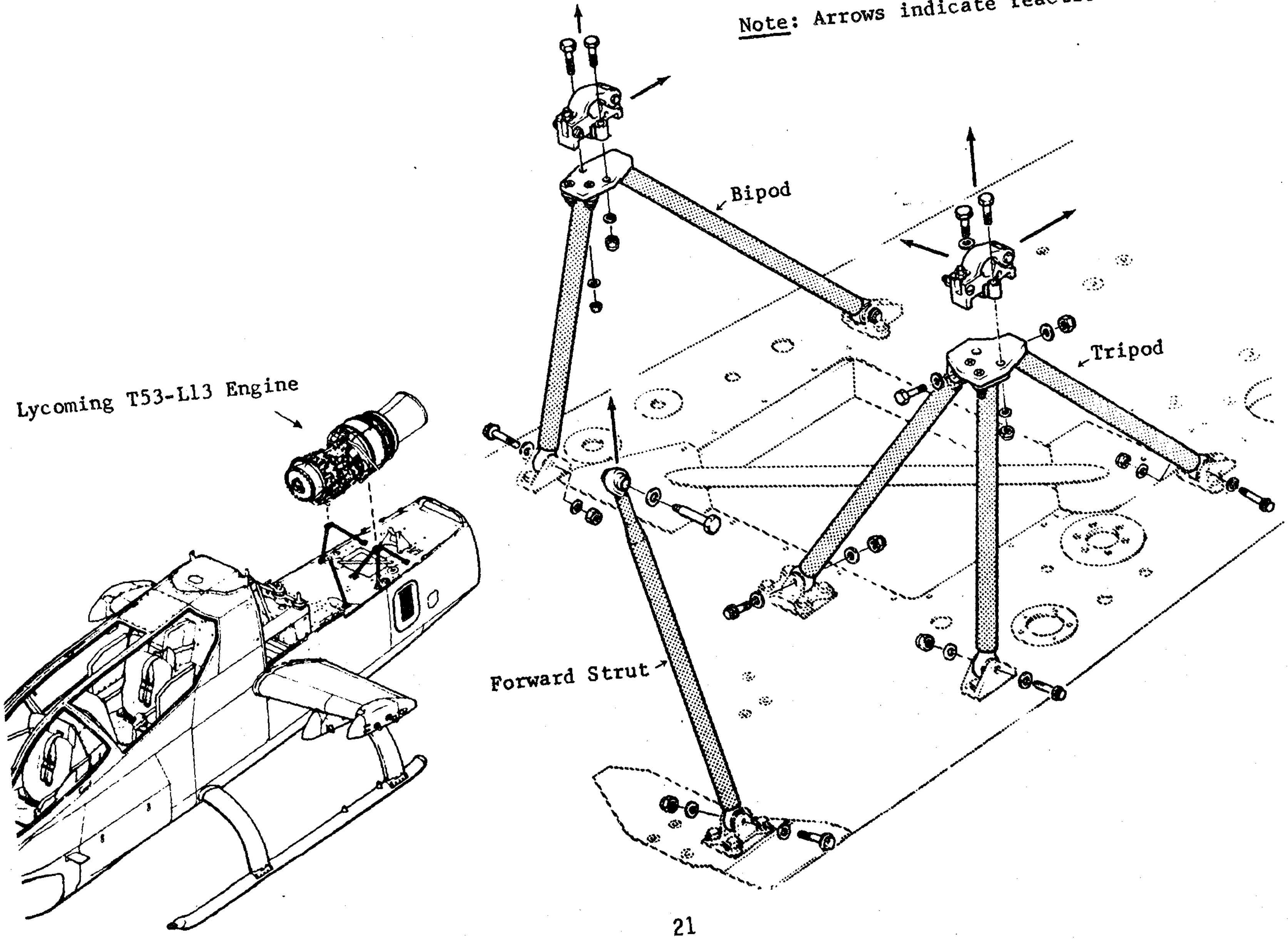
Bipod
Tripod
Lycoming T53-L13 Engine
Forward Strut

Note: Arrows indicate reactions.

SKID LANDING GEAR

The landing gear connected to the fuselage at FS 152 and 223, is shown in the figure. It consists of two energy absorbing cross tubes and skids. The skid gear is attached to the fuselage with pinned connections on the cross tubes at BL ±13.5.

SKID LANDING GEAR

Note: Arrows indicate attachment points to the fuselage.

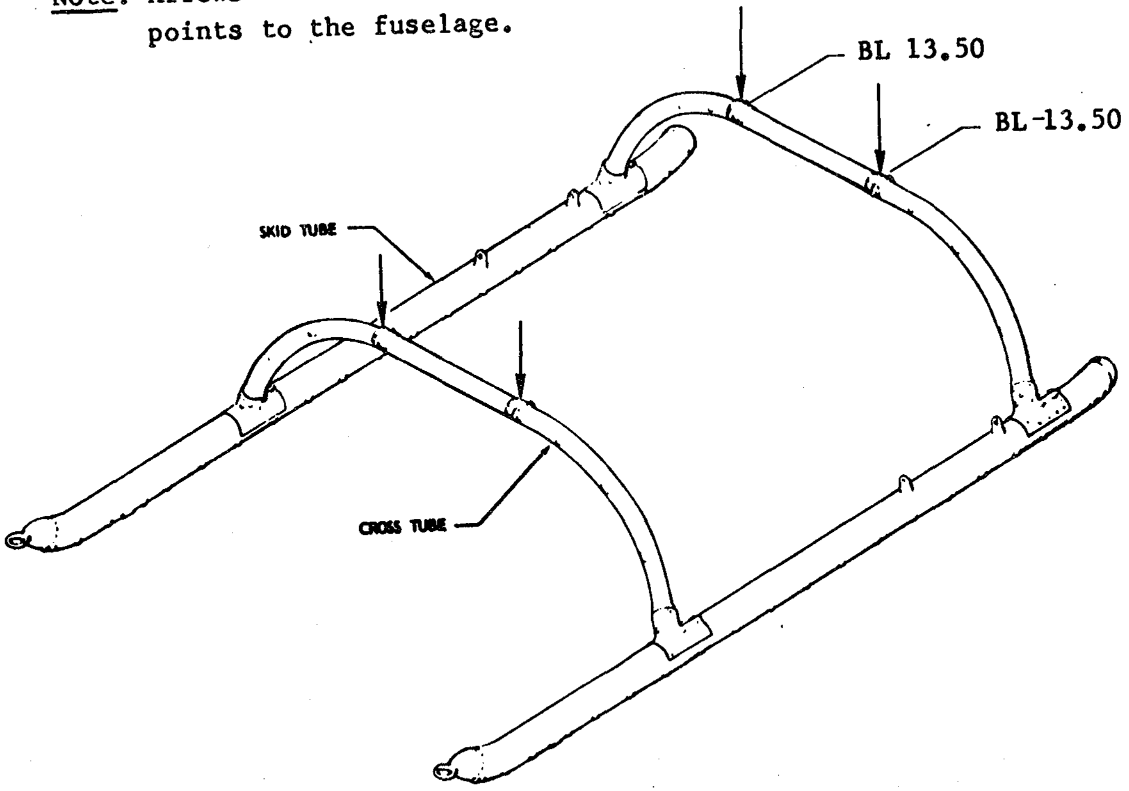
BL 13.50
BL -13.50
SKID TUBE
CROSS TUBE

WING AND CARRY-THROUGH STRUCTURE

The wings on the AH-1G are designed primarily as stores supports, not as aerodynamic lifting surfaces. The stores attachment points are at BL 42.5 and 60.0.

The wing is a two-cell box structure having aluminum skins, three spars, and three ribs. The carry through consists of three beams that are attached to the three wing spars by pinned connections at the fuselage contour. The forward carry through beam is attached to the FS 186.25 bulkhead. The center carry through beam or "lift beam" is attached at the fuselage contour and is pin connected in the center to the lift link. The aft spar carry through is attached to the FS 213.94 bulkhead.

WING AND CARRY-THROUGH STRUCTURE

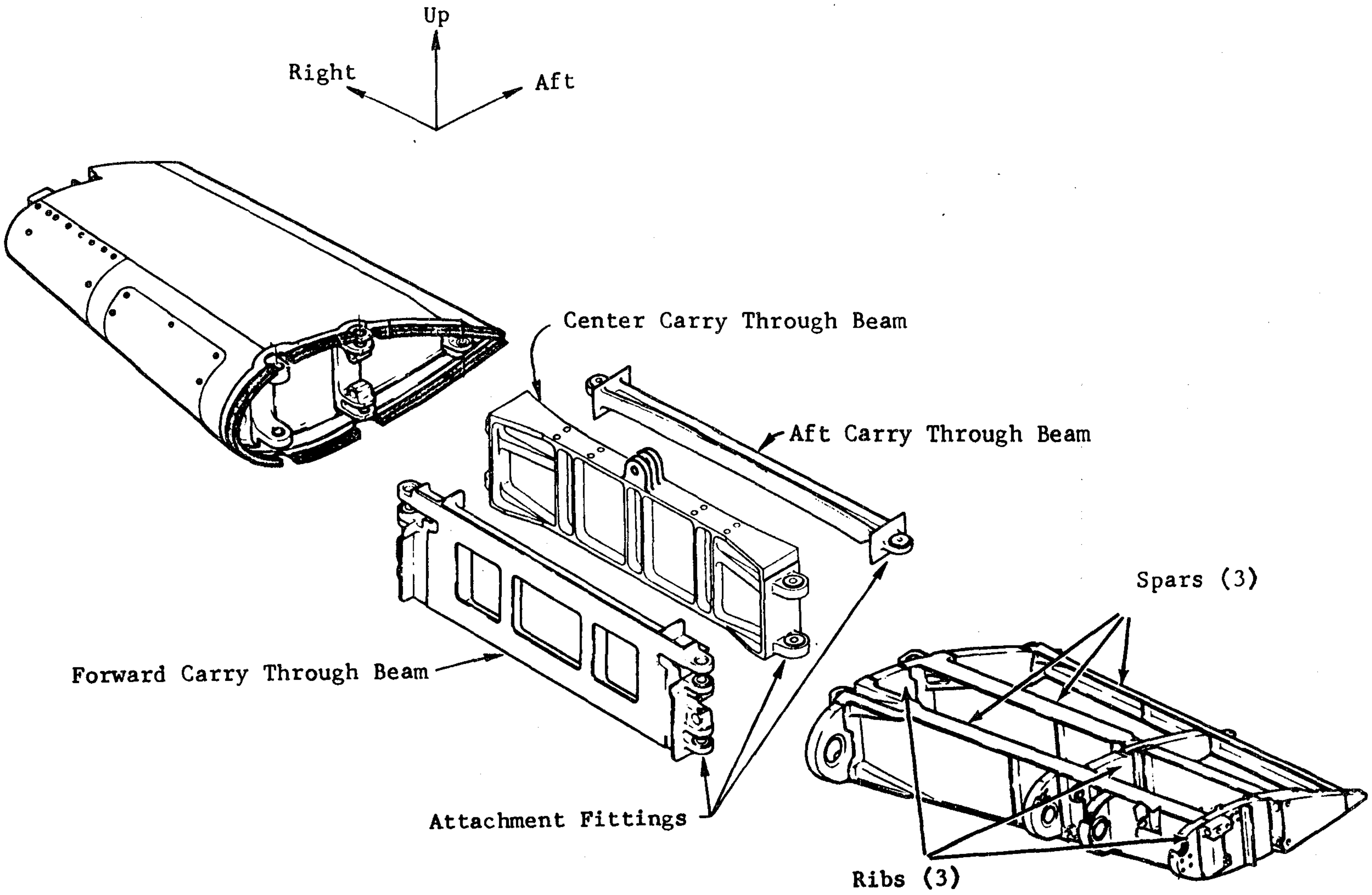
Up
Right
Aft
Center Carry Through Beam
Aft Carry Through Beam
Spars (3)
Forward Carry Through Beam
Attachment Fittings
Ribs (3)

TAILBOOM AND VERTICAL FIN

The tailboom and vertical fin structure are shown in the figure. The tailboom is bolted to the fuselage at FS 299 by means of four attachment fittings located at the four main longerons of the tailboom and the four main beam caps of the fuselage.

The tailboom is of semimonocoque construction having aluminum skins, stringers, and longerons. The longerons and stringers are supported by bulkhead frames spaced down the length of the boom.

The vertical fin has a two-cell cambered airfoil section with two spars and a trailing edge strip. The hinged tail rotor drive shaft cover on the front of the fin is assumed nonstructural as well as the top portion of the fin which extends above the 90 degree gearbox. The 90 degree gearbox and the tail rotor mast provide the connection between the tail rotor and the top of the vertical fin structure. The tail rotor mast is supported on bearings inside the gearbox and the gearbox is bolted to the top of the fin.

TAILBOOM AND VERTICAL FIN

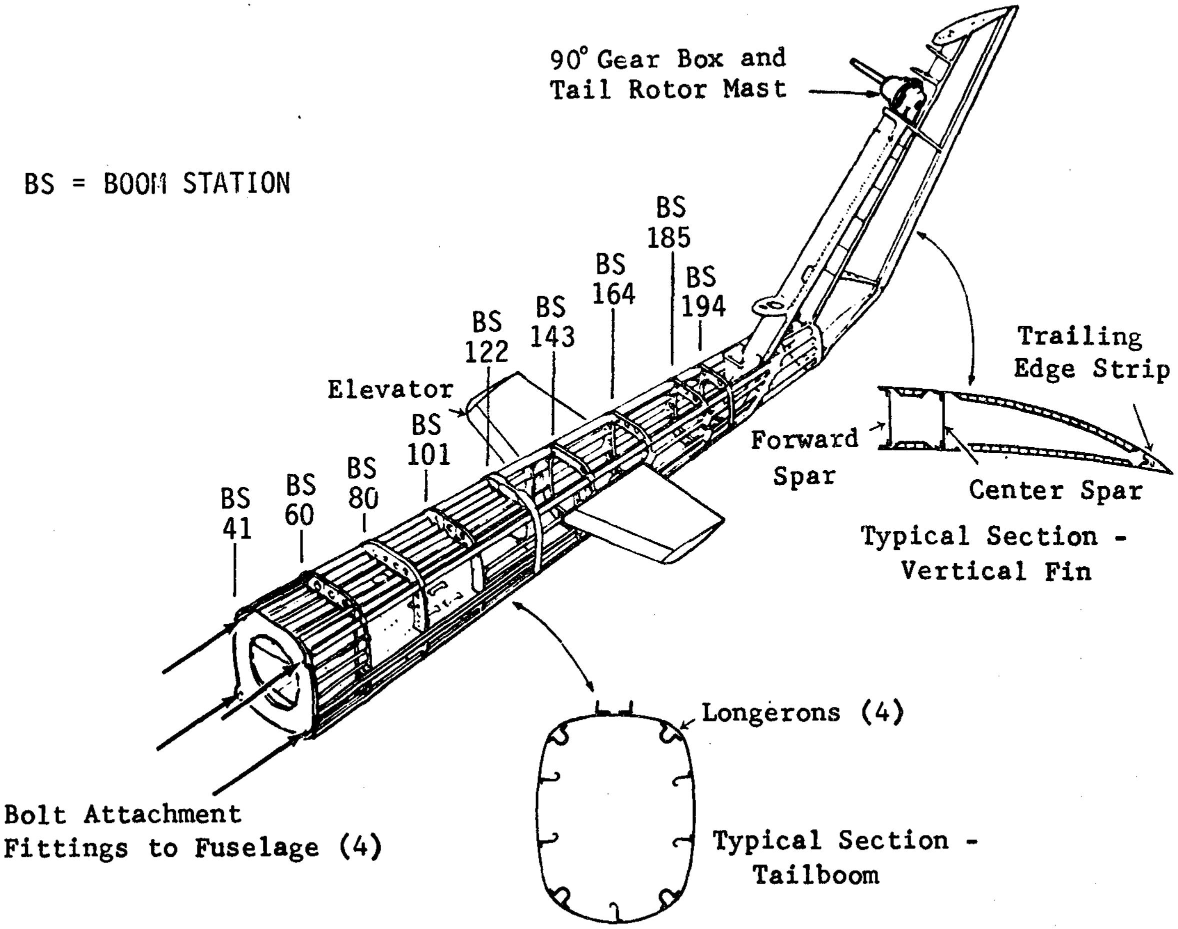
90° Gear Box and
Tail Rotor Mast
BS = BOOM STATION
BS 185
BS 164
BS 194
BS 143
BS 122
Elevator
BS 101
BS 80
BS 60
BS 41
Trailing Edge Strip
Forward Spar
Center Spar
Typical Section - Vertical Fin
Longerons (4)
Typical Section - Tailboom
Bolt Attachment Fittings to Fuselage (4)

ELEVATOR STRUCTURE

The movable elevator is connected to the tailboom by pitch bearings at BS 140.35. The elevator and carry-through structure consist of a single tubular spar. Four ribs covered by a sheet skin making up each elevator surface are connected to the spar.

ELEVATOR STRUCTURE

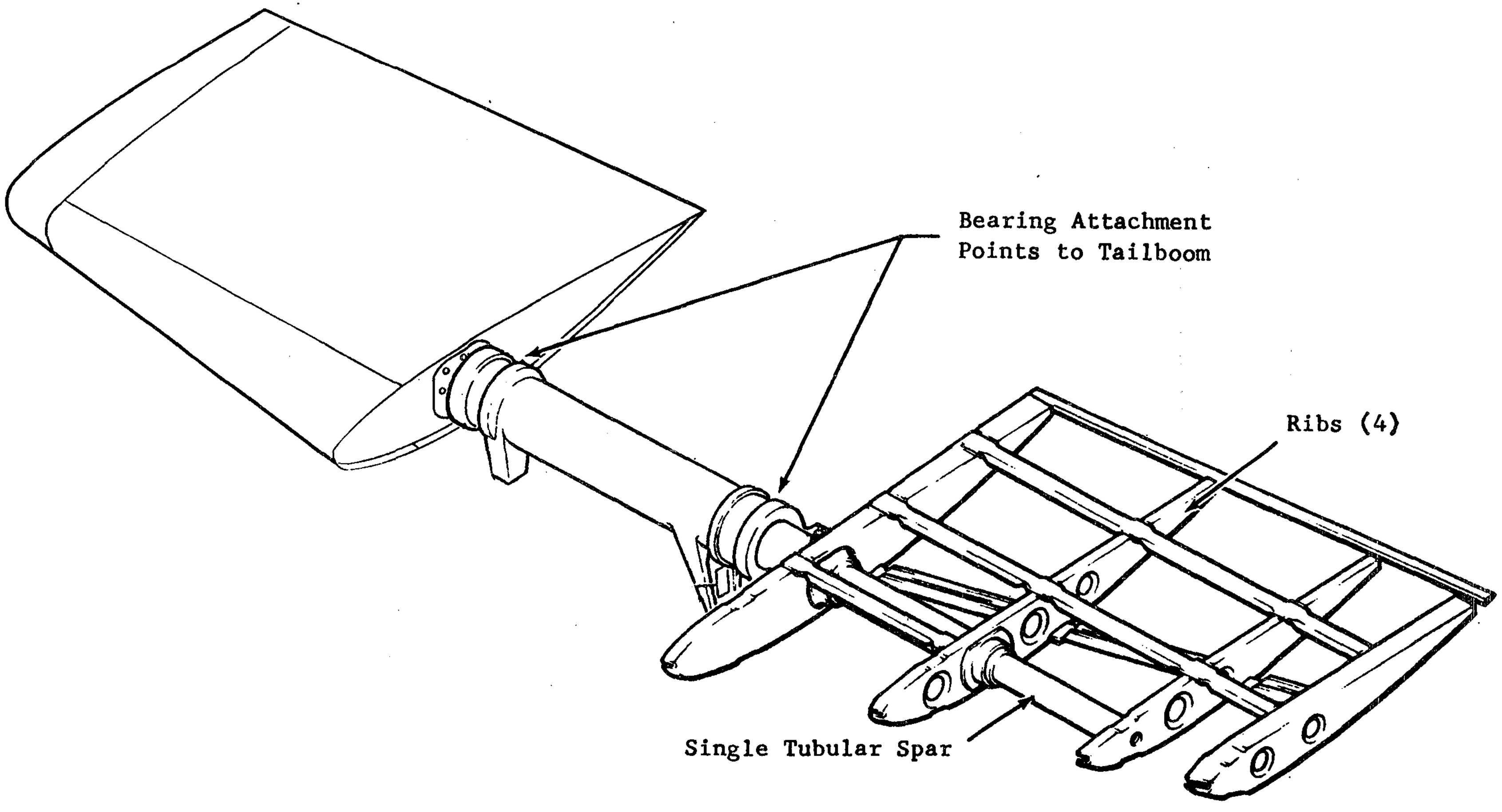
Bearing Attachment
Points to Tailboom
Ribs (4)
Single Tubular Spar

MODELING PHILOSOPHY

The objectives in the modeling are to preserve the low frequency (below 30 Hz) vibration modes of the AH-1G airframe and to predict structural deflections when firing the XM-28 gun turret and wing stores.

To meet these objectives it is important that the stiffness of the structure be accurately modeled. This means that much of the stress analysis documentation on the AH-1G cannot be used. The structure documented in stress analysis reports often does not include such things as

1. Effective stiffness areas of axial members (usually minimum areas are used)
2. Doublers
3. Angles or flanges tied to primary structure caps or axial members and used for attaching nonstructural fairings, cowlings, covers, etc.

The sections effective in the stiffness of the fuselage structure could be derived only by referring directly to the design drawings rather than using stress reports. The tailboom sections, however, are taken directly from an AH-1G stress report with all skins effective in the stiffness calculations.

It is difficult to explain all the judgments made in the stiffness idealization of the structure because the basis for each of the judgments often depends on the artistic skill of the modeler and what has been found to work from past experience; an example would be determining how fine the model must be so that an adequate representation is achieved without causing excessive loss of numerical accuracy due to unnecessary computations. However, some guidelines and techniques generally used in the modeling and requiring some explanation are discussed.

MODELING PHILOSOPHY (continued)

1. In the built-up modeling of the fuselage, grid points are located at the intersection of panels. This is done since the axial members (rods) are generally easier to relocate to the grid point than shear panels or membranes.

2. In bending sections, such as the main beams, relocating rods with centroids offset from the grid point is done by calculating an effective area that preserves the area moment of inertia of the beam about its neutral axis.

3. In sections of the fuselage where the offset of the rod centroid affects both lateral and vertical bending stiffness, the effective rod area is calculated to preserve the vertical bending stiffness. The vertical stiffness which directly affects the vertical vibration of the crew as well as the vertical and pitch vibration of the wing stores is considered more critical than the lateral. Also, preserving the torsional stiffness (primarily differential vertical bending of the main beams) in the open sections of the forward fuselage is important for the structural response to lateral firing of the XM-28 gun turret.

4. When modeling bulkheads, where preserving the bending stiffness in the plane of the bulkhead is not significant in the overall airframe bending stiffness, axial members around the periphery were relocated to the grid points with no change in area.

5. For caps or axial members with varying cross sectional areas between grid points, uniform effective rod areas were used to represent an equivalent axial stiffness.

6. When modeling panels with rods and shear panels, effective rod areas are calculated to preserve either the inplane bending inertia or the total cross sectional area of the panel, or both. The methods used for calculating the rod areas are described later.

7. When modeling panels where it is important to represent the inplane bending stiffness adequately, shear panels surrounded by rods are used instead of quadrilateral membranes. The shear panel elements in NASTRAN contribute no significant inplane bending stiffness and react only shears. The inplane bending stiffness of the panel is represented by the surrounding rods. The quadrilateral membrane element, on the other hand, can be considerably too stiff for inplane bending unless many elements are used. For quadrilateral membranes, at least three elements should be used across the width of a beam or spar web and, as a general rule, the aspect ratio of the element should be kept less than 2.0. Triangular membranes are used where geometry prohibits the use of quadrilateral membranes.

8. The inner skins of joggled sandwich panels are added to the outer skin without considering the offset. The skin in the joggled portion is assumed not effective.

In determining the undamped free vibration modes of the helicopter airframe structure, the weight distribution must be modeled properly as well as the stiffness distribution. The distribution of the hundreds of weight items in the helicopter to the grid points of the finite element model can be a very tedious operation; therefore, the distribution of most of the weight items is done automatically by an in-house computer program. Large weight items that significantly affect the low frequency vibration modes of the airframe are distributed separately by the modeler. These large weight items include the gun turret, main and tail rotors, main transmission, engine, and useful weights such as the crew, fuel, ammunition, and stores. A more detailed discussion of the distribution of weights is included in the Weights Modeling section.

MODELING PHILOSOPHY (concluded)

After idealizing the structure into a stiffness model and distributing the weights to grid points, constraints are applied to the unreduced NASTRAN model to reduce the number of degrees of freedom to an acceptable analysis size for the Givens eigenvalue solution. Constraints and partitioning techniques applied to the model are summarized below.

1. SPCs are applied, removing degrees of freedom having no stiffness.
2. MPC equations representing rigid elements, pin connections, etc. remove the dependent degrees of freedom of the equations from the model.
3. Guyan Reduction performed via OMIT cards condenses out degrees of freedom with zero inertia properties or whose inertia properties can be rationally redistributed to others.

After reducing the degrees of freedom sufficiently, the Givens or Tridiagonal method of eigenvalue extraction is used to compute the natural vibration modes and frequencies of the airframe. The Givens method, which extracts all the eigenvalues of the analysis set, requires a reduction to about 250 degrees of freedom for efficient run times.

The Inverse Power eigenvalue extraction method does not require the Guyan Reduction procedure; however, it operates on an analysis size six to ten times larger than Givens and extracts only one mode at a time. The time spent in Guyan Reduction, which is performed only once in an analysis, becomes comparatively small when several modes are required; the AH-1G airframe model has more than 40 modes below 50 Hz.

A problem, however, lies in the reduction of the large system to the smaller without significant loss in accuracy of the dynamic characteristics of the model. Guidelines for using the Guyan Reduction technique in the modeling are discussed later.

MODELING PHILOSOPHY

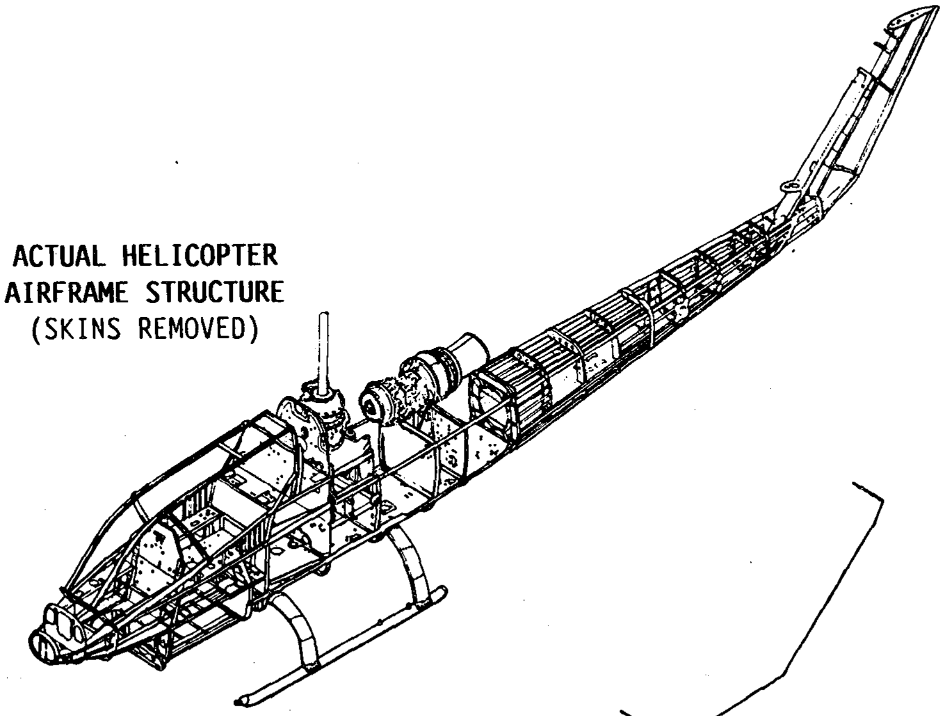

ACTUAL HELICOPTER
AIRFRAME STRUCTURE
(SKINS REMOVED)

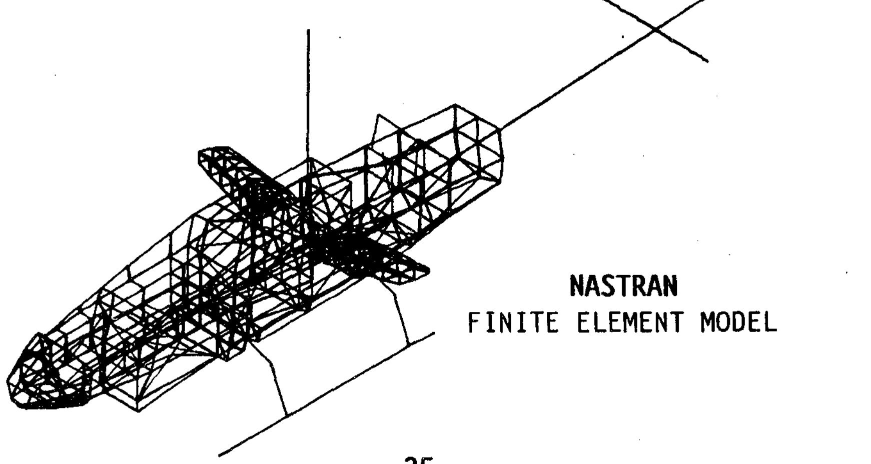

NASTRAN
FINITE ELEMENT MODEL

MATH MODEL IDEALIZATION

The emphasis in the idealization is on developing a model adequately representing the low frequency vibration modes of the airframe with the fewest degrees of freedom possible. Representation of the fuselage and wing structures in the areas of the XM-28 gun turret and the wing stores is given special attention. The gun turret and stores themselves are represented as rigid masses, as are the main and tail rotors, the engine, and useful weight items such as the crew, fuel, and ammunition.

MATH MODEL IDEALIZATION

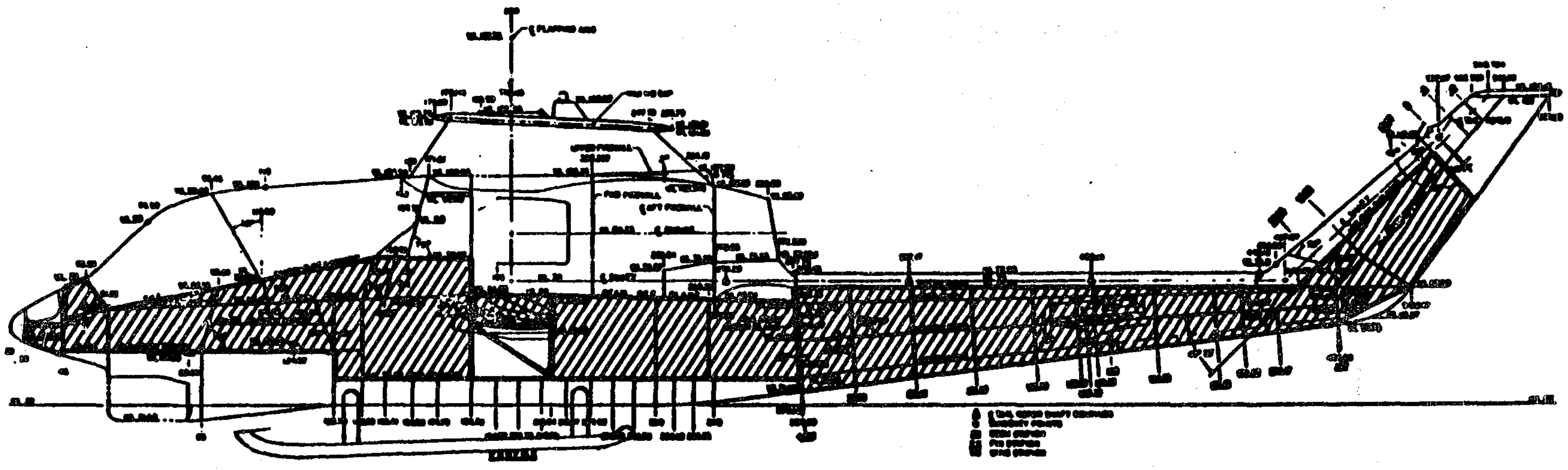

- PRIMARY STRUCTURE IN NASTRAN MODEL ▨
- REPRESENTED AS LUMPED MASSES IN FEM:
  - DOOR AND ACCESS PANELS
  - FAIRINGS, CANOPY, COWLING, SECONDARY STRUCTURE, COVERS
  - COMPONENTS (ENGINES, STORES, ARMAMENT, CREW, FUEL, AVIONICS, INSTRUMENT PANELS, SHAFTING, TRANSMISSION, GEARBOXES)

MATH MODEL IDEALIZATION

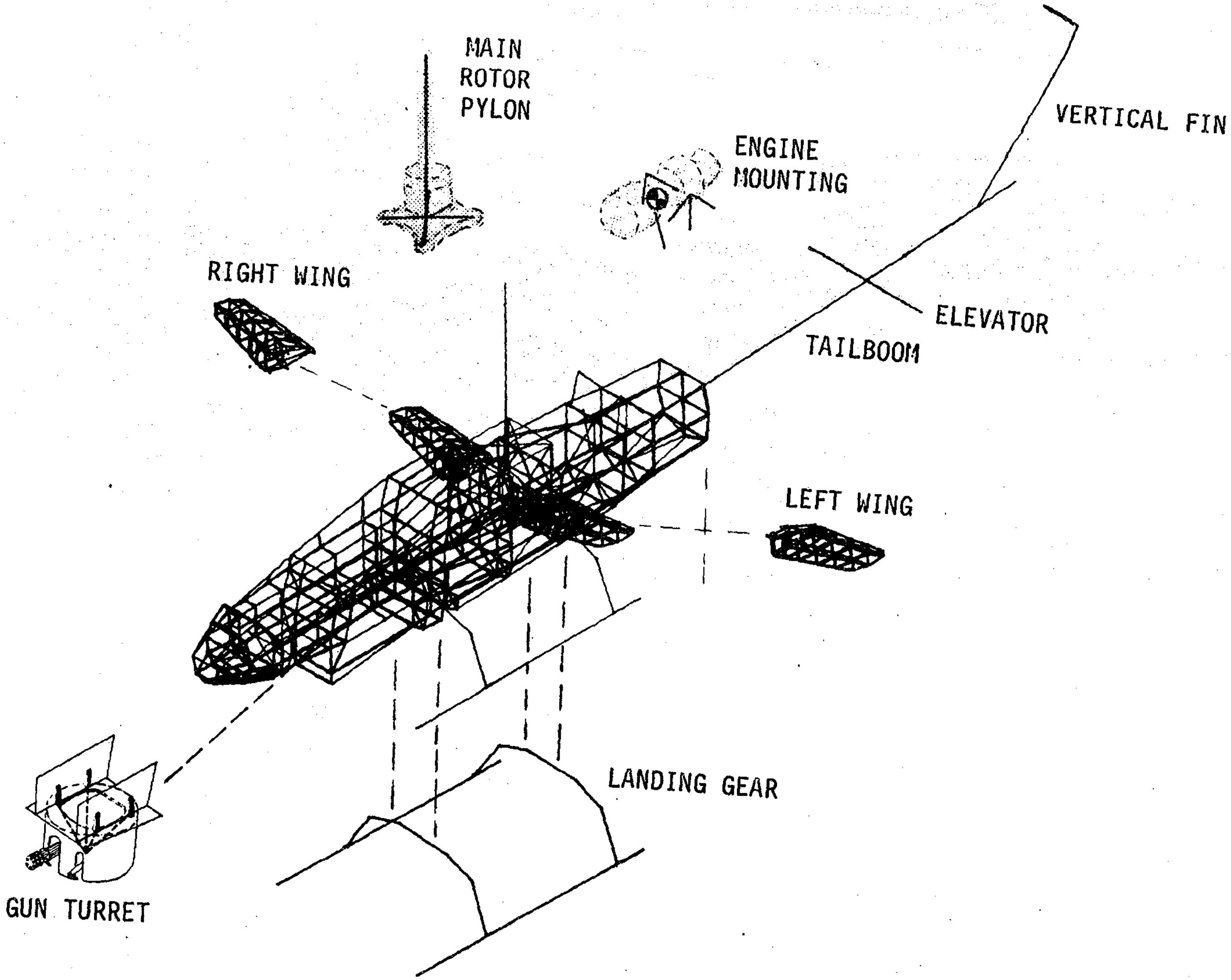
MAIN
ROTOR
PYLON
ENGINE
MOUNTING
VERTICAL FIN
RIGHT WING
ELEVATOR
TAILBOOM
LEFT WING
LANDING GEAR
GUN TURRET

FUSELAGE IDEALIZATION

The fuselage is a built-up idealization using primarily rods and shear panels in the bending sections. Instead of using an elastic line or "beam" representation, build-up modeling is used because of the complex structure in the forward and center fuselage areas. The forward fuselage has open sections making it difficult to calculate the elastic axis and torsional stiffness properties important in determining the structural response to lateral gunfiring. In the center fuselage, where the wing carry through, pylon support, and fuselage structures intersect, built-up modeling is required to represent the complex redundant structure. The primary fuselage bending structure is modeled with rods and shear panels. The belly structure is also modeled with rods and shear panels except where triangular membranes are required due to geometry. The nose structure skins are modeled with membranes, and bulkheads are modeled with membranes surrounded by rods. MPC equations representing rigid elements are used to tie the landing gear, tailboom, and gun turret mass to the fuselage. Bar elements are used only for the pylon support structure.

FUSELAGE IDEALIZATION

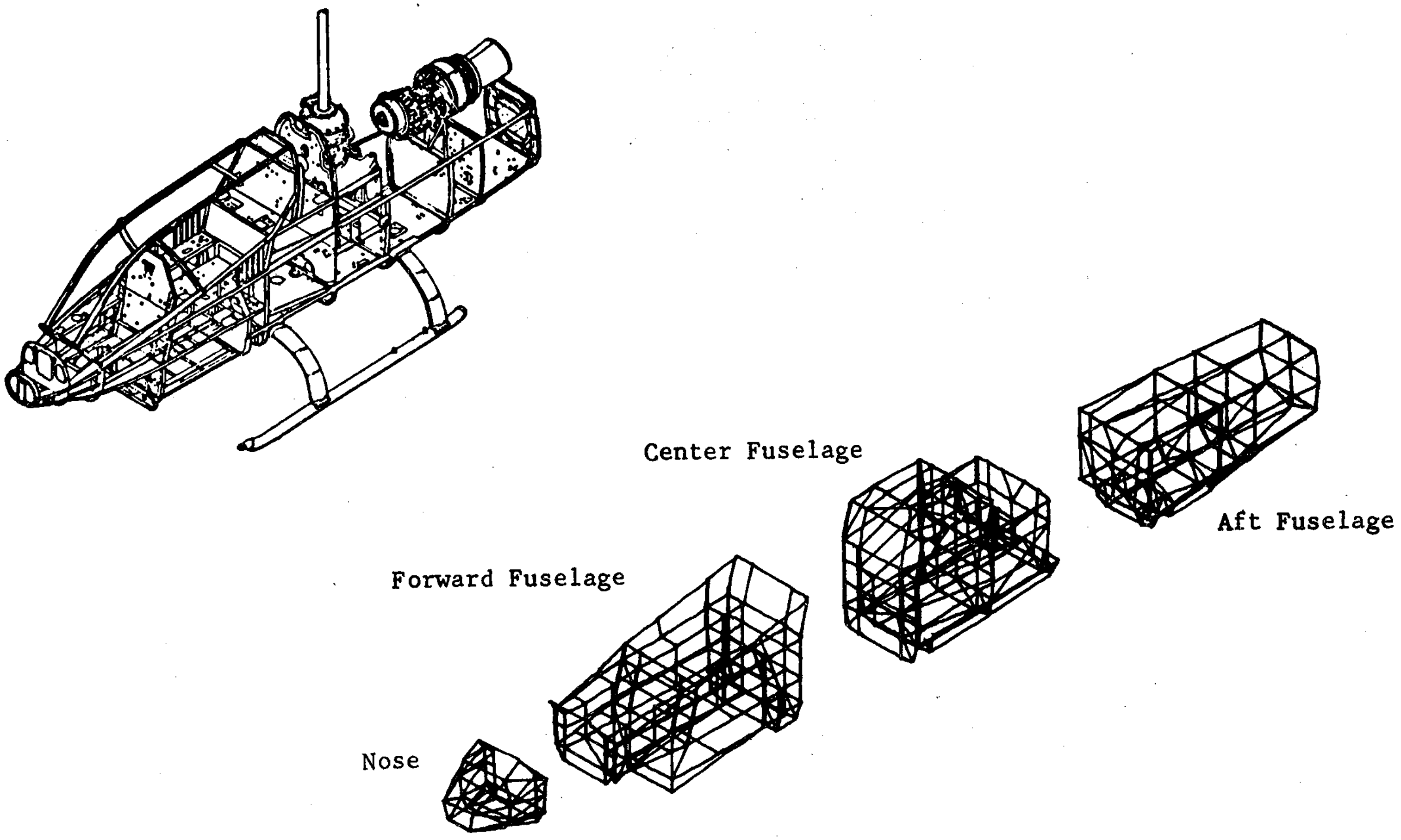
Center Fuselage
Aft Fuselage
Forward Fuselage
Nose

TURRET IDEALIZATION

The XM-28 gun turret is idealized as a rigid body mass. MPC equations are used to rigidly connect the turret cg grid point to the support fitting grids. The attachment angles are modeled with rod elements which transfer the turret inertia loads and/or gunfire loads into the fuselage main beams.

TURRET IDEALIZATION

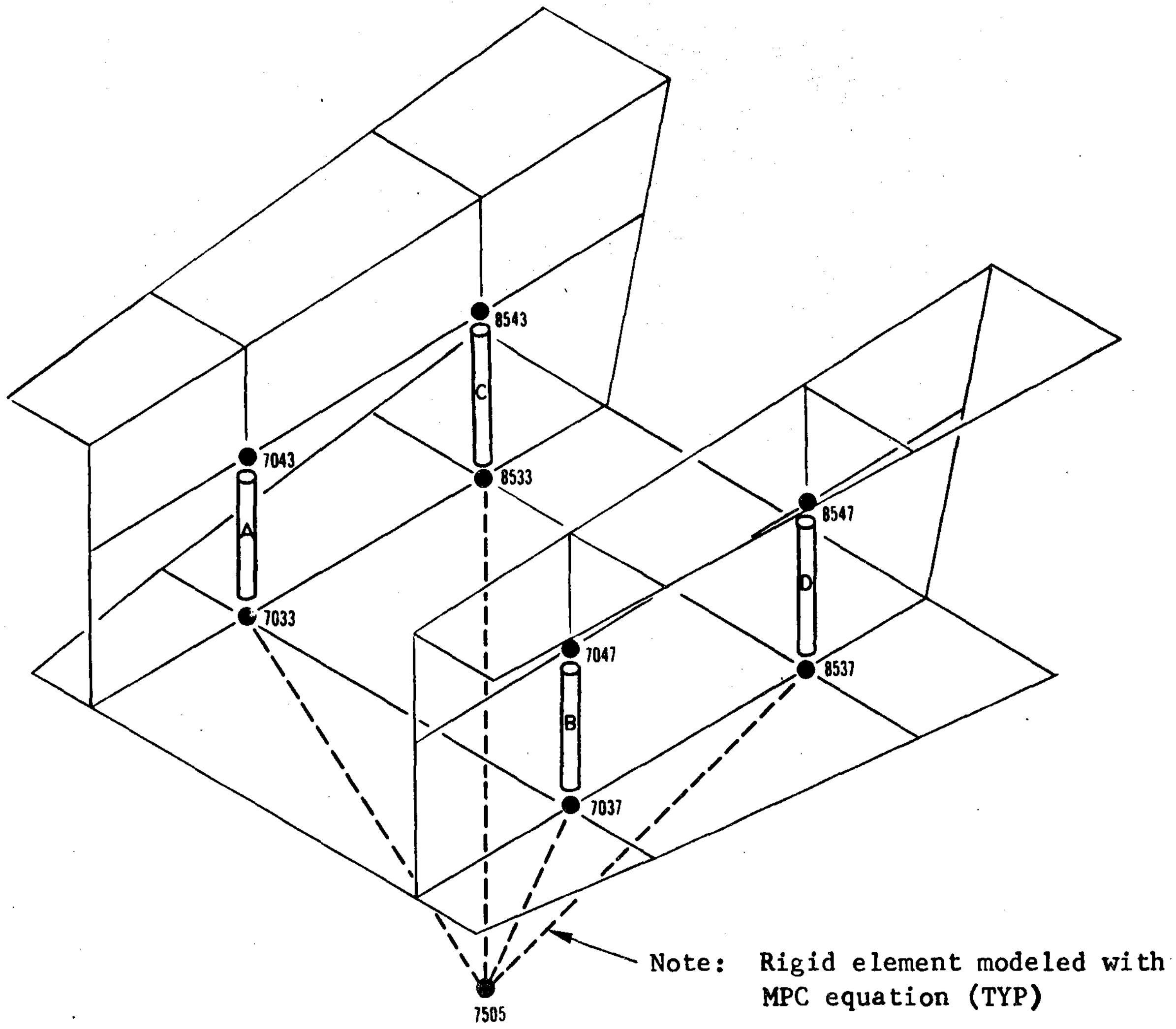
8543
C
7043
8533
A
8547
D
7033
7047
8537
B
7037
7505

Note: Rigid element modeled with MPC equation (TYP)

MAIN ROTOR PYLON IDEALIZATION

The main rotor pylon (transmission and mast) is modeled as an elastic line using bar elements. The mast is pinned to the transmission case at mast bearing locations. The elastomeric pylon mounts are modeled with scalar spring elements, and MPC equations are used to tie the transmission elastic line to the mount locations. The lift link is represented with a bar, pinned and rigidly offset from grid points on the transmission and lift beam.

MAIN ROTOR PYLON IDEALIZATION

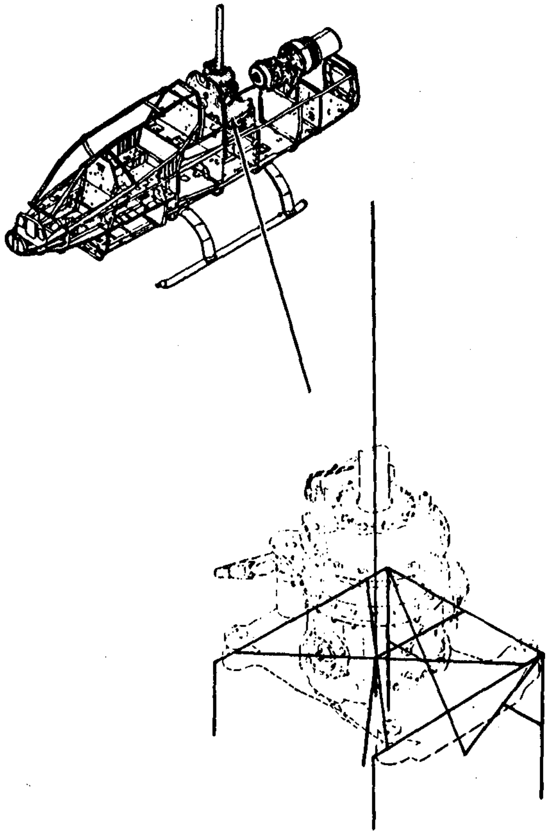

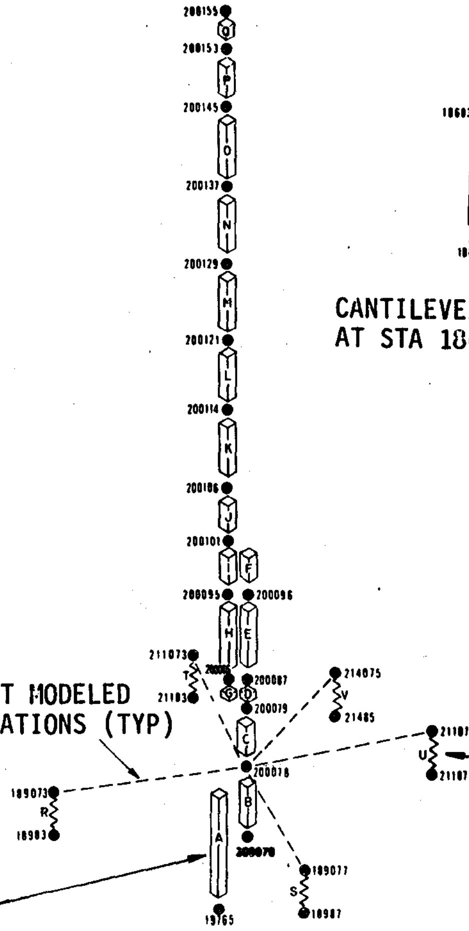
200155
Q
200153
P
200145
O
200137
N
200129
M
200121
L
200114
K
200106
J
200101
I
F
200095
200096
H
E
211073
T
200087
214075
V
21103
D
G
200079
21485
C
211017
U
21107
200078
189073
R
18903
B
A
200070
189077
S
18987
19765

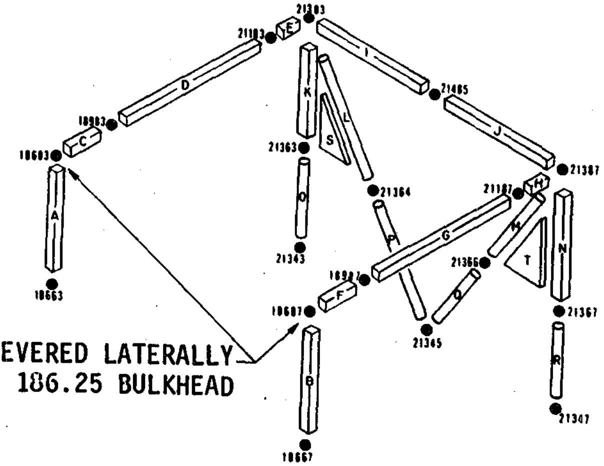
21303
21103
E
I
D
21485
K
L
J
18903
C
S
18603
21363
21364
21387
A
O
21107
H
P
G
M
N
21343
21366
T
18663
18907
F
Q
18607
21367
21345
B
R
18667
21347

CANTILEVERED LATERALLY
AT STA 186.25 BULKHEAD

RIGID ELEMENT MODELED
WITH MPC EQUATIONS (TYP)

SOFT ELASTOMERIC MOUNTS (5)
MODELED AS SPRINGS

STIFF VERTICAL LIFT LINK
MODELED AS PIN-ENDED BAR

ENGINE IDEALIZATION

Because rigid elements were unavailable in NASTRAN at the time of the modeling effort, the engine mounts were modeled with rods and tied to the rigid engine cg with MPC equations. The bottom attachments of the mounts were related to motions of the plane of the engine deck by MPC equations.

ENGINE IDEALIZATION

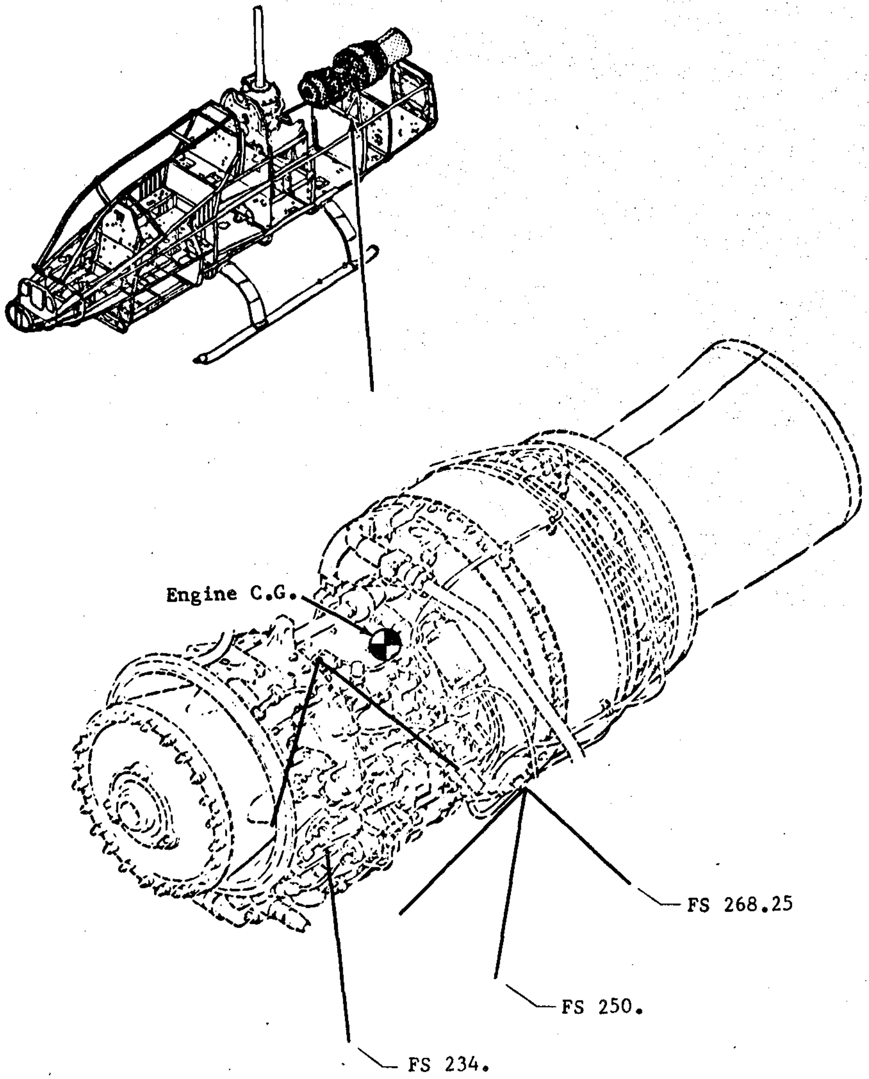
Engine C.G.
FS 268.25
FS 250.
FS 234.

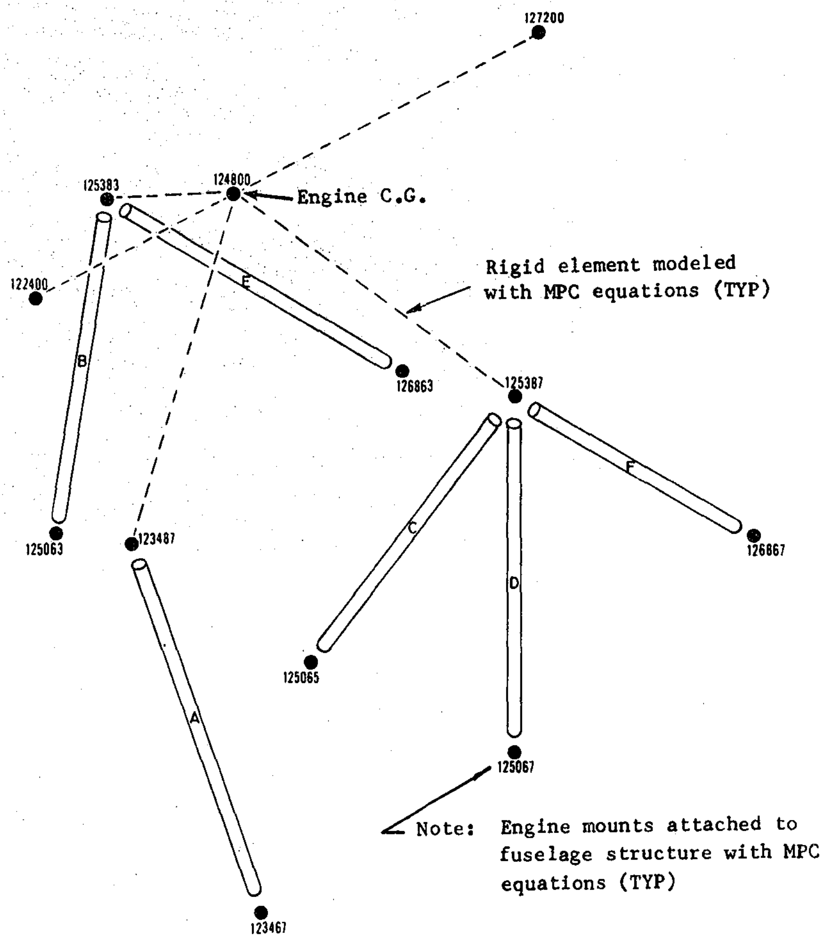
127200
125383
124800
Engine C.G.
122400
E
B
126863
125387
F
C
D
125063
123487
126867
A
125065
125067
123467

Rigid element modeled with MPC equations (TYP)

Note: Engine mounts attached to fuselage structure with MPC equations (TYP)

LANDING GEAR IDEALIZATION

The landing gear is modeled with bar elements representing the cross tubes and skid tubes. The cross tubes are tied to the fuselage with MPC equations.

LANDING GEAR IDEALIZATION

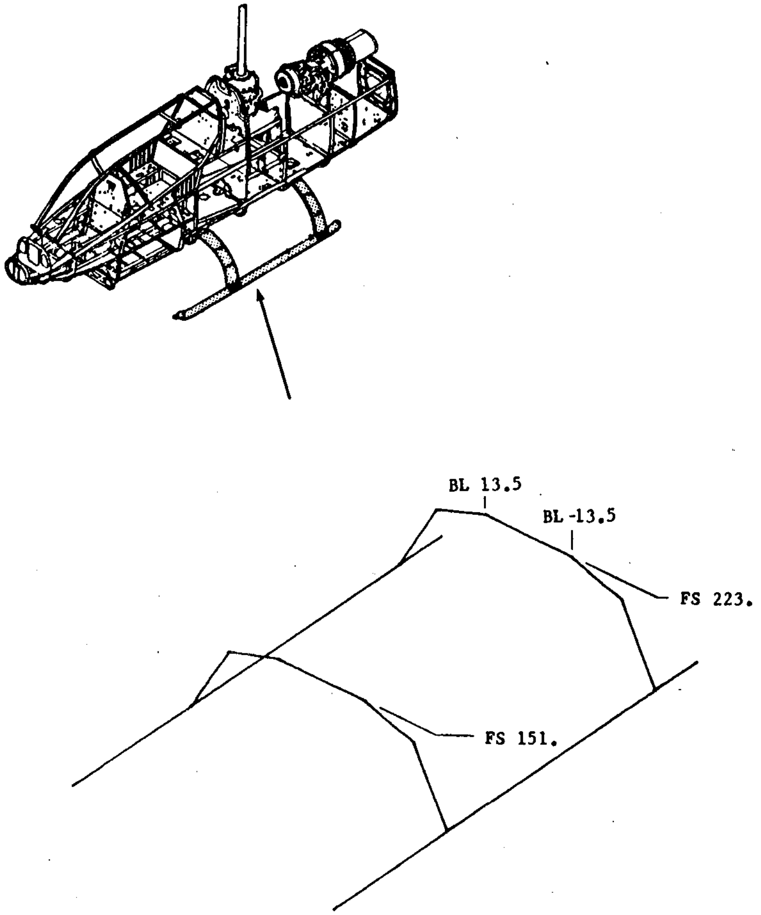
BL 13.5
BL -13.5
FS 223.
FS 151.

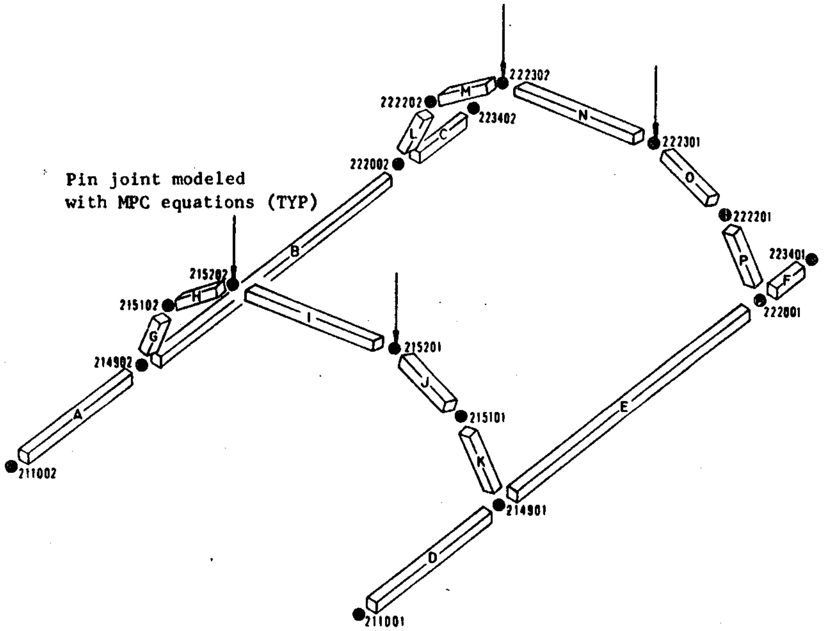
Pin joint modeled
with MPC equations (TYP)
222302
222202
223402
222002
222301
222201
223401
222001
215202
215102
214902
215201
215101
214901
211002
211001
A
B
C
D
E
F
G
H
I
J
K
L
M
N
O
P

WINGS AND CARRY-THROUGH IDEALIZATION

The wings and carry-through are built-up idealizations because of the complex interface between these structures involving pinned connections at the fuselage contour. The wing spar caps, carry through beam caps and attachment lugs are modeled with bars and the spar and beam webs with shear panels and rods. The wing skins are represented by quadrilateral membranes which preserve the beamwise (vertical) bending and torsional stiffness but are somewhat too stiff in chordwise (fore-and-aft) bending. The pinned connections at the attachment lugs are modeled with MPC equations.

WING AND CARRY-THROUGH IDEALIZATION

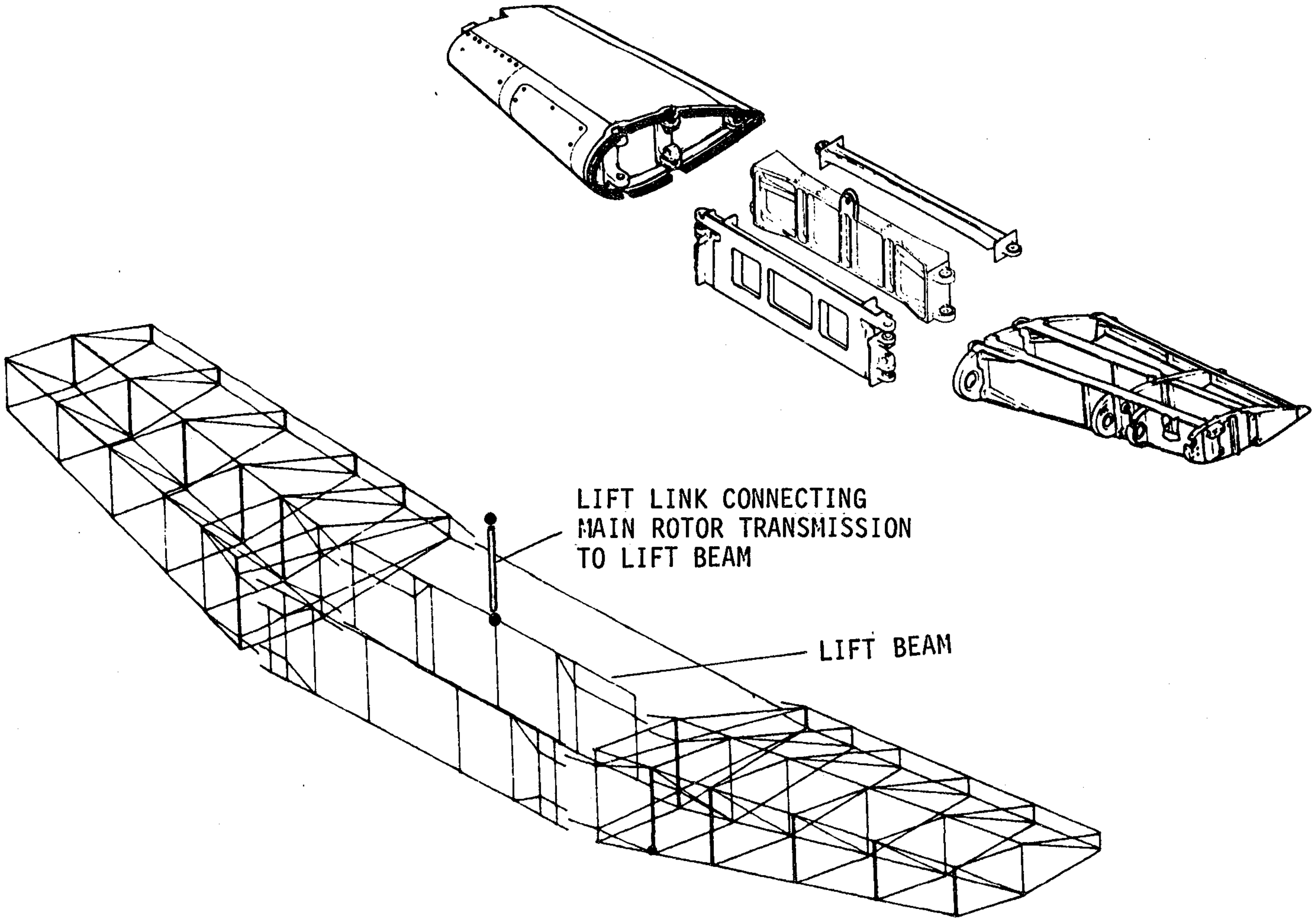
LIFT LINK CONNECTING MAIN ROTOR TRANSMISSION TO LIFT BEAM
LIFT BEAM

TAILBOOM AND VERTICAL FIN IDEALIZATION

The tailboom and vertical fin are modeled as elastic lines using bar elements with calculated bending and torsional stiffness properties. The elastic axis is assumed to be on the geometric center of the tailboom and along the center spar of the vertical fin. In the stiffness calculations, all skins are assumed effective. The change in bending section properties for the tailboom under severe maneuver conditions is also calculated and shown in the Stiffness Modeling section. By using an elastic line model, the bending stiffness changes for maneuver conditions can easily be incorporated by changing only the nine bar property cards representing the tailboom. The effective skin for the vertical fin having sandwich panels will not change for maneuver conditions.

TAILBOOM AND VERTICAL FIN IDEALIZATION

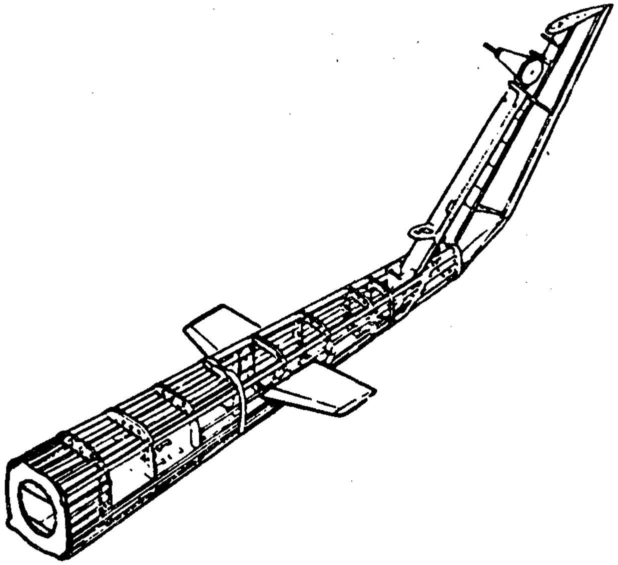

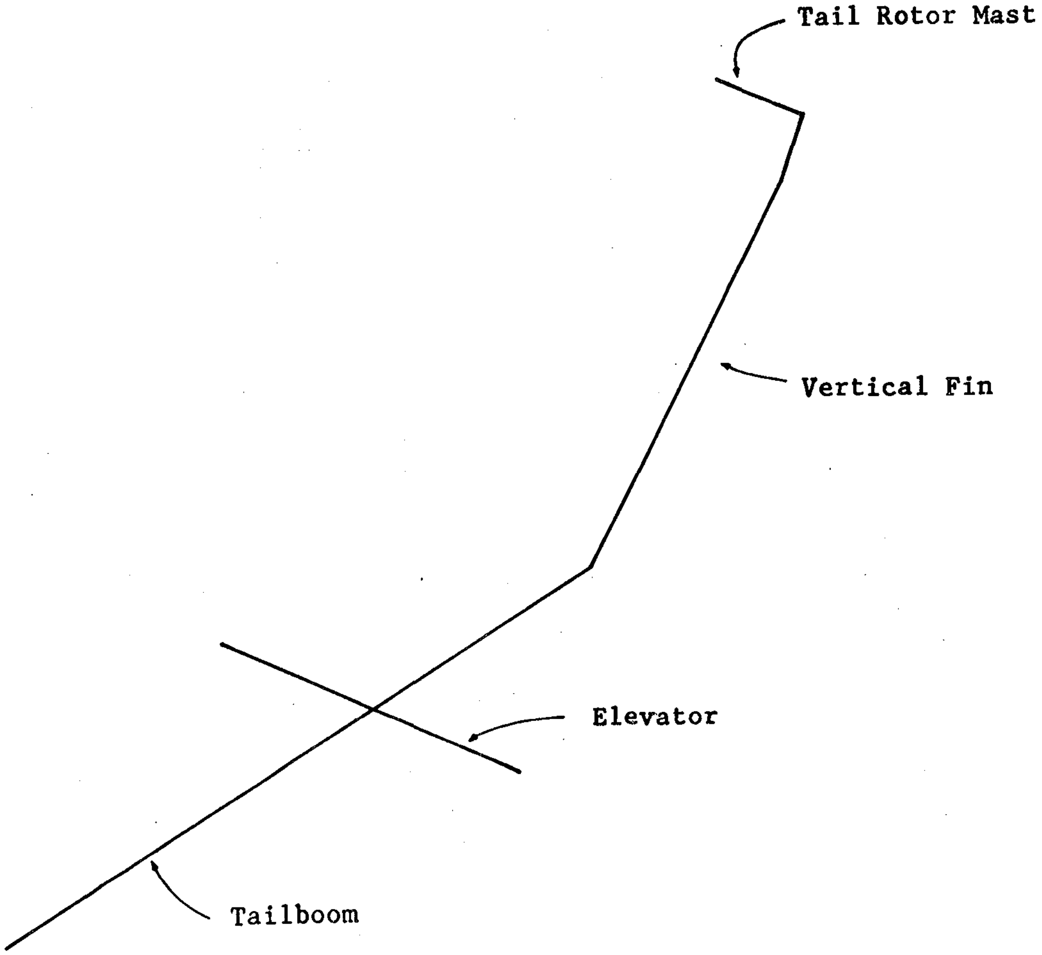
Tail Rotor Mast
Vertical Fin
Elevator
Tailboom

TAILBOOM MODELING

Computer program SFCR02 calculates the bending stiffness section properties for a given shear and bending moment distribution due to flight maneuver loads. The tailboom, constructed of longerons, stringers, and aluminum skin, has some skin width on either side of the axial members effective in reacting bending loads. All of the skin is assumed effective when the axial member is in tension and the amount of effective skin decreases as the compressive load in the member increases.

The program determines the section properties, unsymmetrical bending stresses, element loads, and shear flows for a single cell torque box. Section properties are computed from the input geometry data defining the skin contour and centroids of axial members (stringers and longerons). This includes neutral axis location, shear center location, moments of inertia about the neutral axes, maximum and minimum moments of inertia, angle to principal axis, and torsional stiffness. The skin area is lumped at the centroid of the axial members in the neutral axis and moment of inertia calculations which would result in the bending stiffness being slightly low since the skin area should be acting at contour. Bending moments are computed at the neutral axis and torsion is computed at the reference axis for the first iteration. Bending stresses are computed by use of the standard unsymmetrical bending equation:

$$f_b = \frac{M'_y I_{yz} - M'_z I_y}{I_y I_z - I_{yz}^2} \cdot Y + \frac{M'_z I_{yz} - M'_y I_z}{I_y I_z - I_{yz}^2} \cdot Z'$$

Element loads are then computed at this station. The same process is repeated at the next station aft.

TAILBOOM MODELING (concluded)

Using the previously calculated stress levels, an effective skin width, W, on either side of each axial element is found by using the following equation:

$$W = .85t \frac{E_c}{f_c}$$

where E_c = 10.5 x 10^6 psi (entire structure based on aluminum)

f_c = computed compression stress

t = skin thickness in equivalent aluminum

This equation is based on flat sheets and should be conservative for the curved tailboom skin resulting in the bending stiffness calculations being low. A limit of W equals one-half of the arc length between axial elements is applied to this equation. If f_b is tension (+) then W equals one-half the arc length. New areas are computed for each element and section properties and bending stresses are calculated. New effective skin widths are found, based on the new stress levels, and compared with the previous widths. If a five percent difference is evident, the process continues up to a maximum of ten iterations.

TAILBOOM MODELING

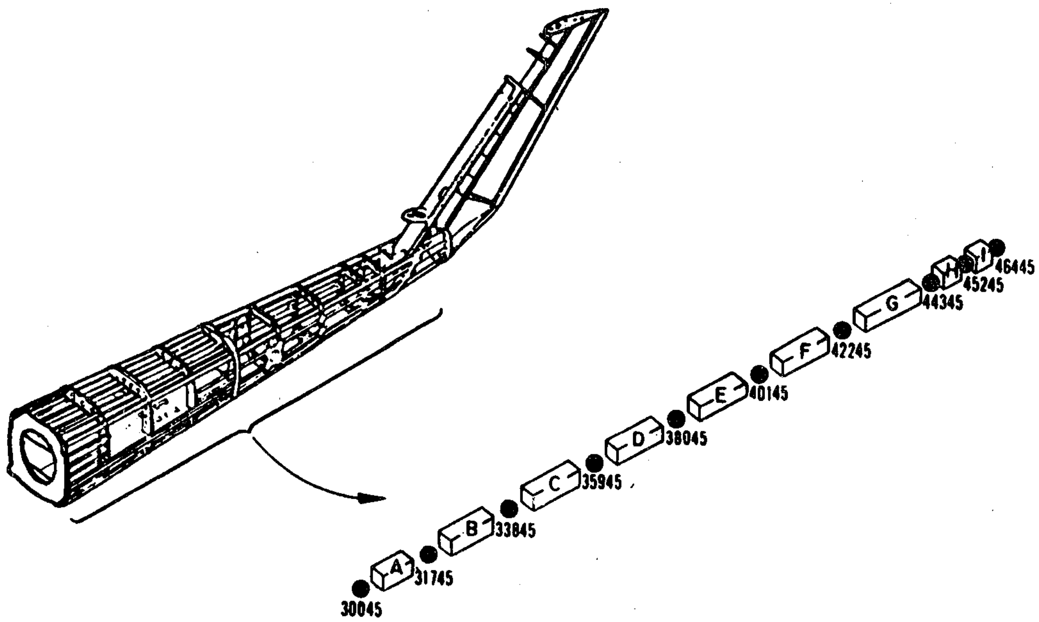
A
B
C
D
E
F
G
H
I
30045
31745
33845
35945
38045
40145
42245
44345
45245
46445

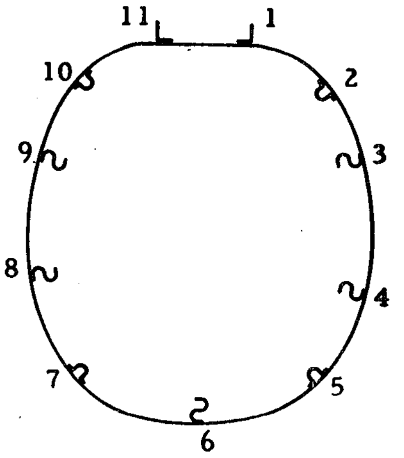
11
1
10
2
9
3
8
4
7
5
6

ELEMENT NUMBER	AREA	Z'	Y'
1	0.0	19.074	3.887
2	0.6602	13.274	12.278
3	0.0	5.174	14.128
4	0.0	3.276	14.108
5	0.8990	-11.476	12.078
6	0.0	-16.576	0.452
7	0.8200	-11.476	-11.422
8	0.0	-3.276	-13.452
9	0.0	5.174	-13.472
10	0.8259	13.274	-11.622
11	0.0	19.194	-3.262

SECTION PROPERTIES

AREA = 3.2052
IY = 488.25
IZ = 449.22
J = 995.51

ELEVATOR IDEALIZATION

The elevator is modeled with bars and is pin connected to the tailboom at the bearing locations (Grids 40143 and 40147). Rigid bars are used to tie the tailboom elastic line to the bearing supports.

ELEVATOR IDEALIZATION

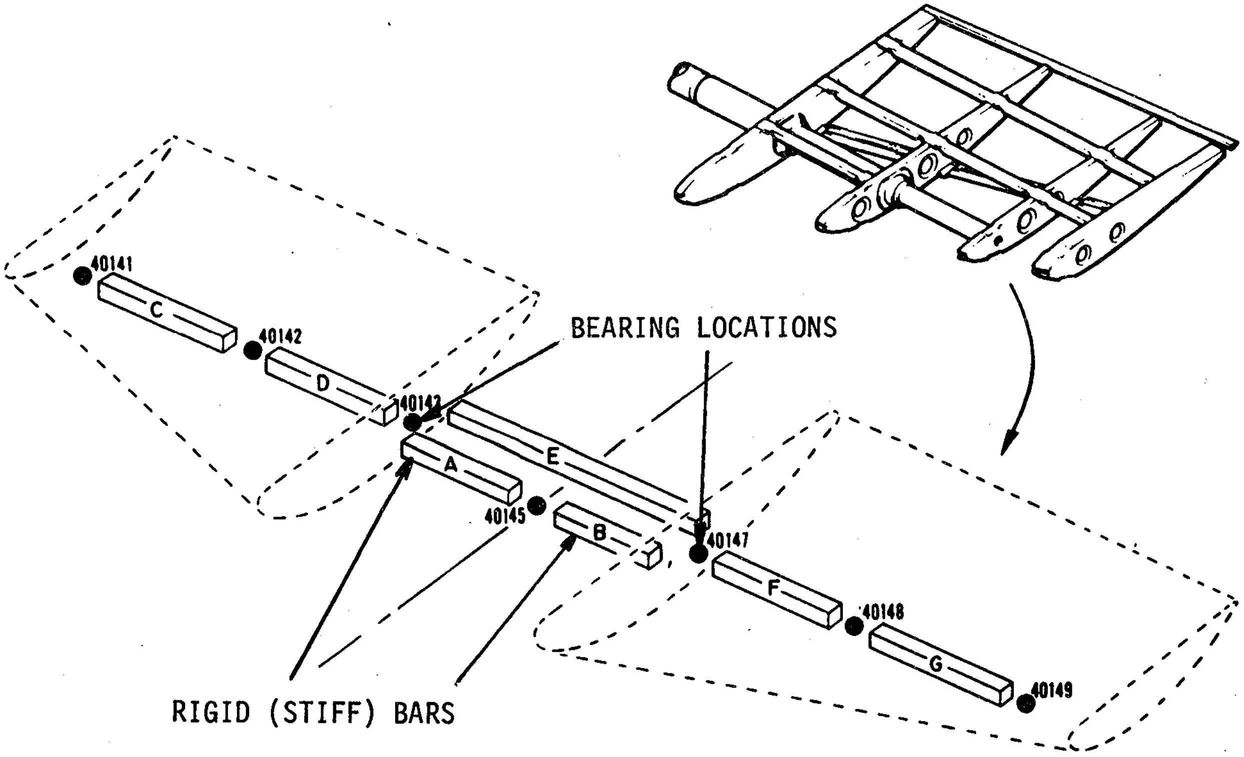
40141
C
40142
D
40142
BEARING LOCATIONS
E
A
40145
B
40147
F
40148
G
40149
RIGID (STIFF) BARS

TAIL ROTOR IDEALIZATION

The tail rotor mast is modeled with bars and pinned at the bearing supports in the 90 degree gearbox. Rigid bars are used to tie the fin elastic line to the bearing supports.

TAIL ROTOR IDEALIZATION

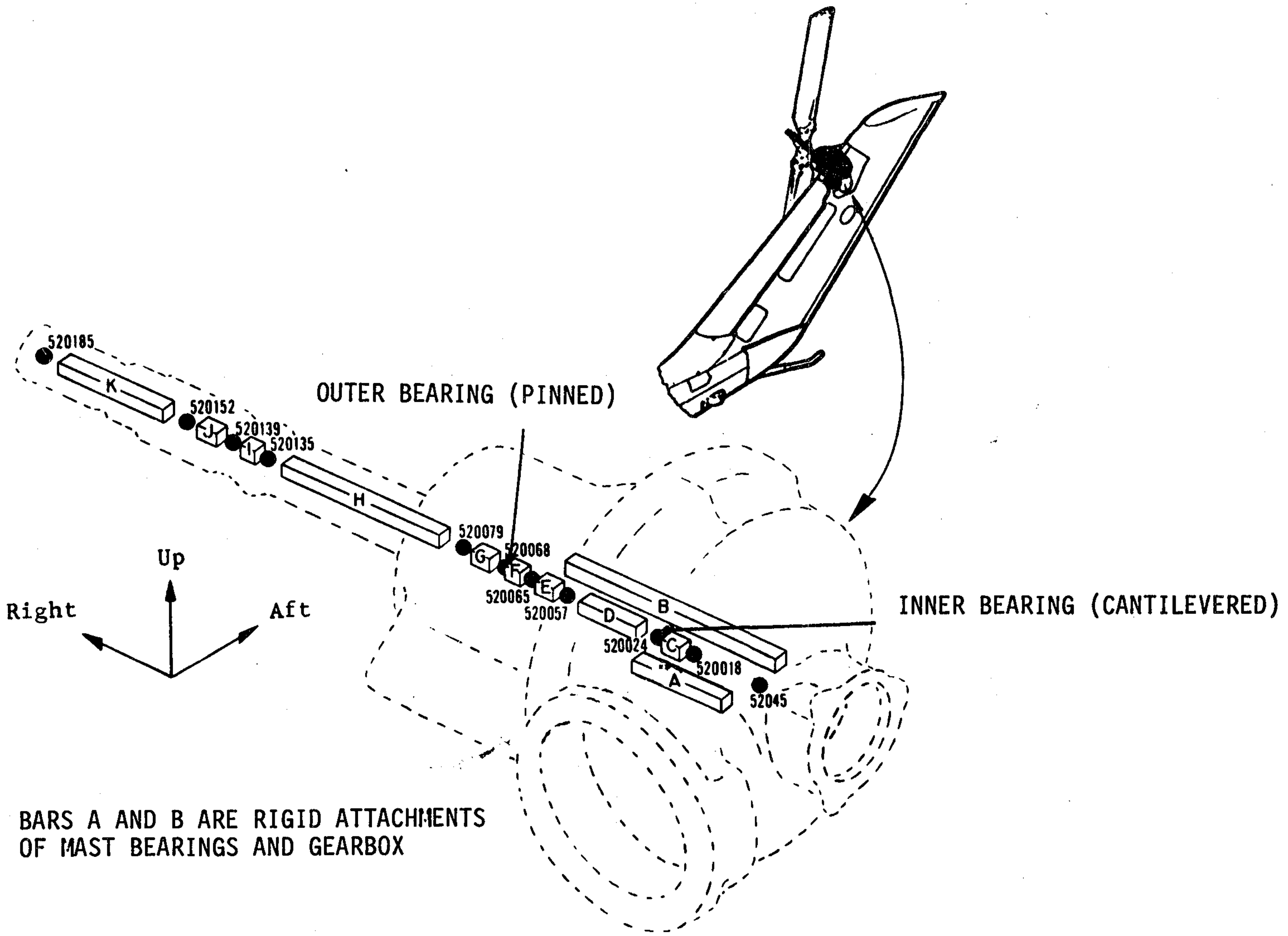
520185
K
520152
J
520139
I
520135
H
OUTER BEARING (PINNED)
520079
G
520068
F
520065
E
520057
D
B
INNER BEARING (CANTILEVERED)
520024
C
520018
A
52045
Up
Right
Aft

BARS A AND B ARE RIGID ATTACHMENTS
OF MAST BEARINGS AND GEARBOX

MODELING DOCUMENTATION REPORT

A complete description of the AH-1G NASTRAN model is contained in the documentation report of Reference 3. The report contains descriptions of the stiffness modeling by breaking down the NASTRAN model from the complete final assembly, to major assembly, then subassembly, and finally the detail part of the model containing the grid point degree of freedom and element data tables. The mass modeling is then described including the automatic distribution of weight empty items and manual distribution of large useful weight items. In addition to descriptions of the mass and stiffness modeling, the input data listing is annotated so that the user can easily relate the NASTRAN input data to the actual structure. There is also a grid point and element cross reference index to locate where these data are described in the report. Finally, a sample normal modes run and plots are included. Examples of the NASTRAN modeling documentation report are given on the following pages.

MODELING DOCUMENTATION REPORT

- STIFFNESS MODELING
  - FINAL ASSEMBLY
  - MAJOR ASSEMBLY
  - SUBASSEMBLY
  - DETAIL (INCLUDING GRID POINT AND ELEMENT DATA TABLES)
- WEIGHTS MODELING
- ANNOTATED INPUT DATA LISTING
- NORMAL MODES SAMPLE RUN

STIFFNESS MODELING - FINAL ASSEMBLY

The stiffness model is described in detail by drawings and sketches organized in a manner similar to the design drawings for the helicopter, however, depicting the finite element model instead of the actual structure. The drawings describing the stiffness model are organized as follows:

> FINAL ASSEMBLY - includes a NASTRAN plot of the complete airframe model showing the major assemblies of the model: fuselage, wings and carry-through, and tailboom and vertical fin.

STIFFNESS MODELING
FINAL ASSEMBLY

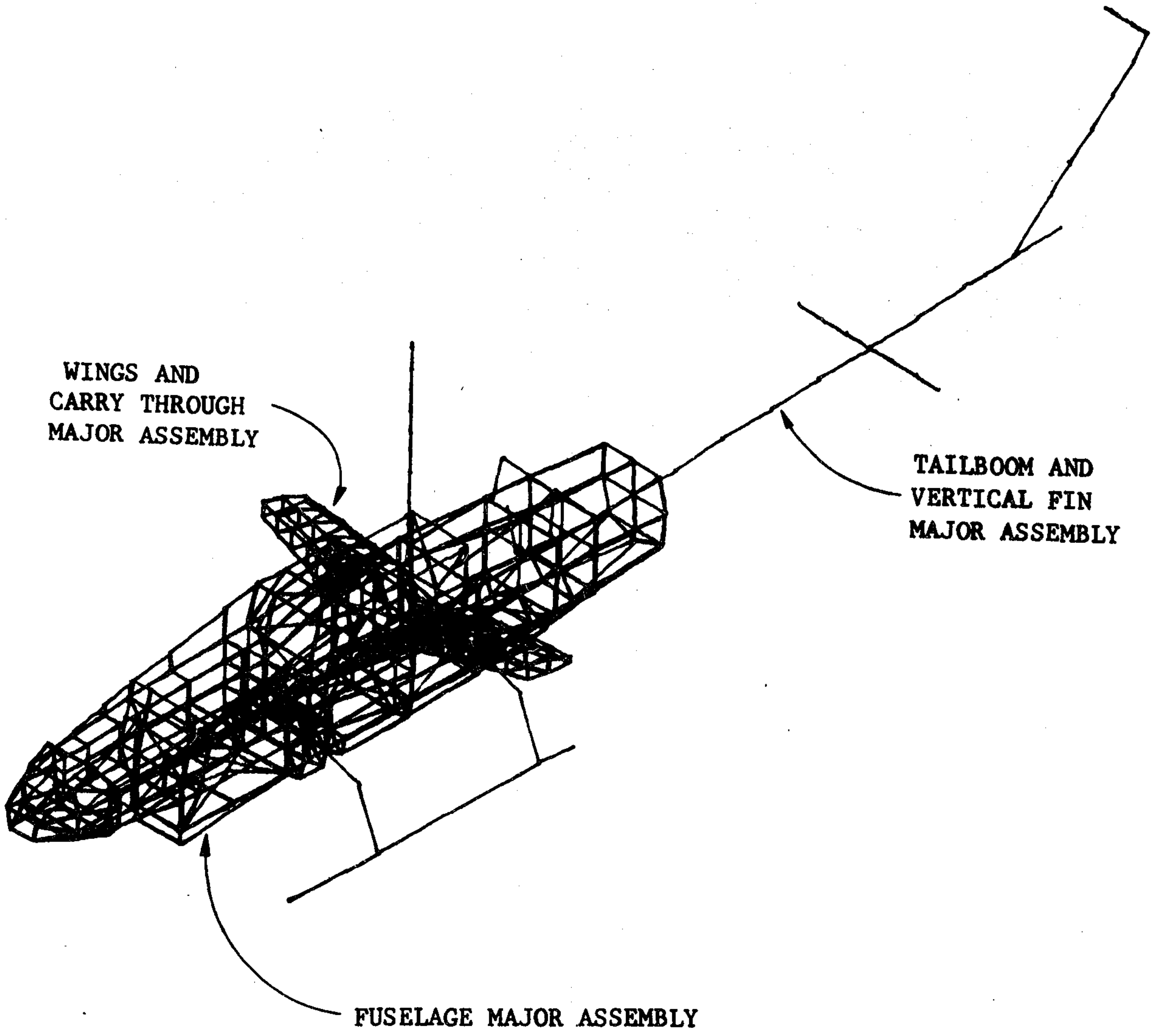
WINGS AND CARRY THROUGH MAJOR ASSEMBLY
TAILBOOM AND VERTICAL FIN MAJOR ASSEMBLY
FUSELAGE MAJOR ASSEMBLY

STIFFNESS MODELING - FUSELAGE MAJOR ASSEMBLY

MAJOR ASSEMBLY - includes a NASTRAN plot of the major assembly with subassemblies identified; also included is an illustration of the actual structure represented by the major assembly.

STIFFNESS MODELING
FUSELAGE MAJOR ASSEMBLY

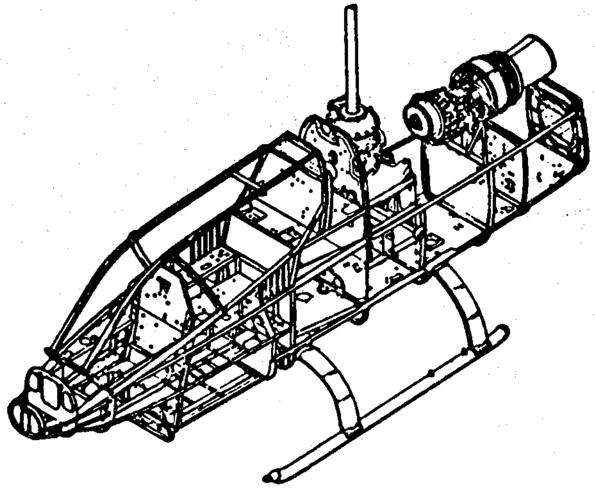

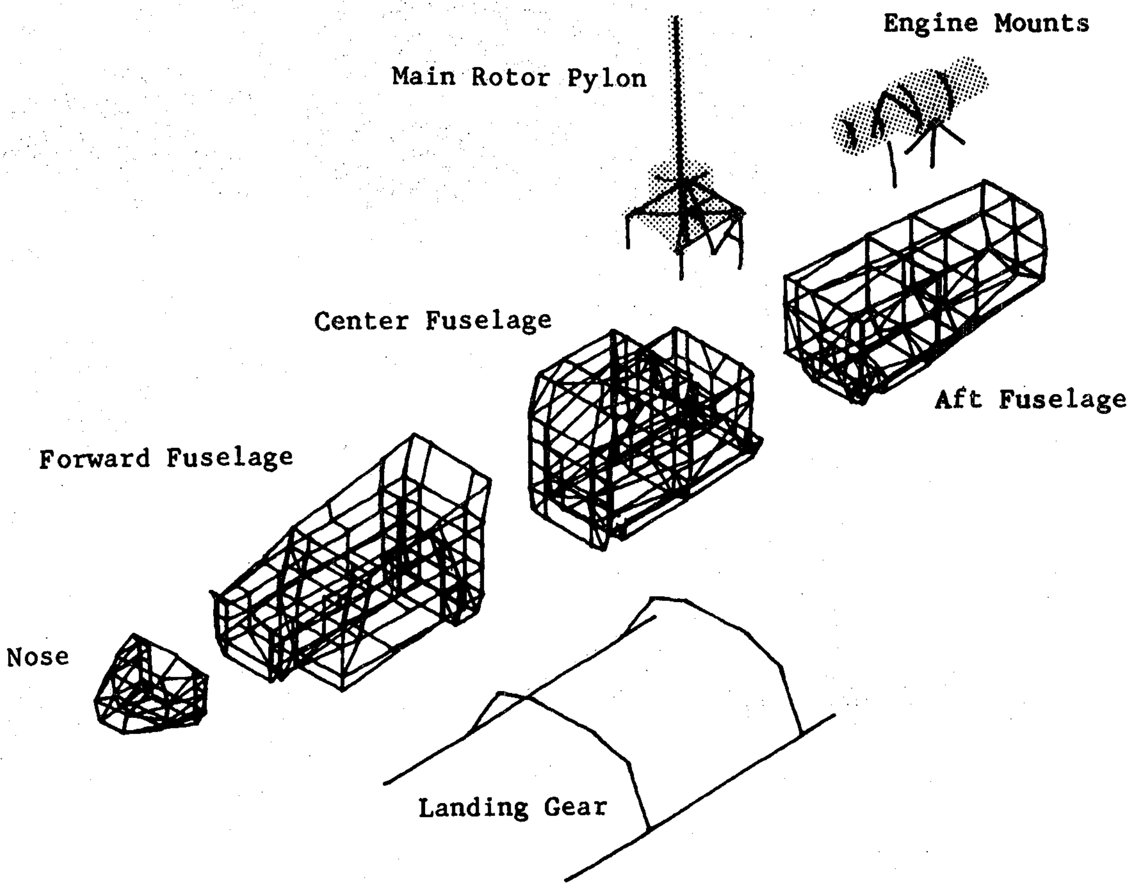
Engine Mounts
Main Rotor Pylon
Center Fuselage
Aft Fuselage
Forward Fuselage
Nose
Landing Gear

STIFFNESS MODELING - FORWARD FUSELAGE SUBASSEMBLY

SUBASSEMBLY - includes a NASTRAN plot showing the location of the subassembly in the actual structure and is used for reference in locating the detail drawings.

STIFFNESS MODELING
FORWARD FUSELAGE SUBASSEMBLY

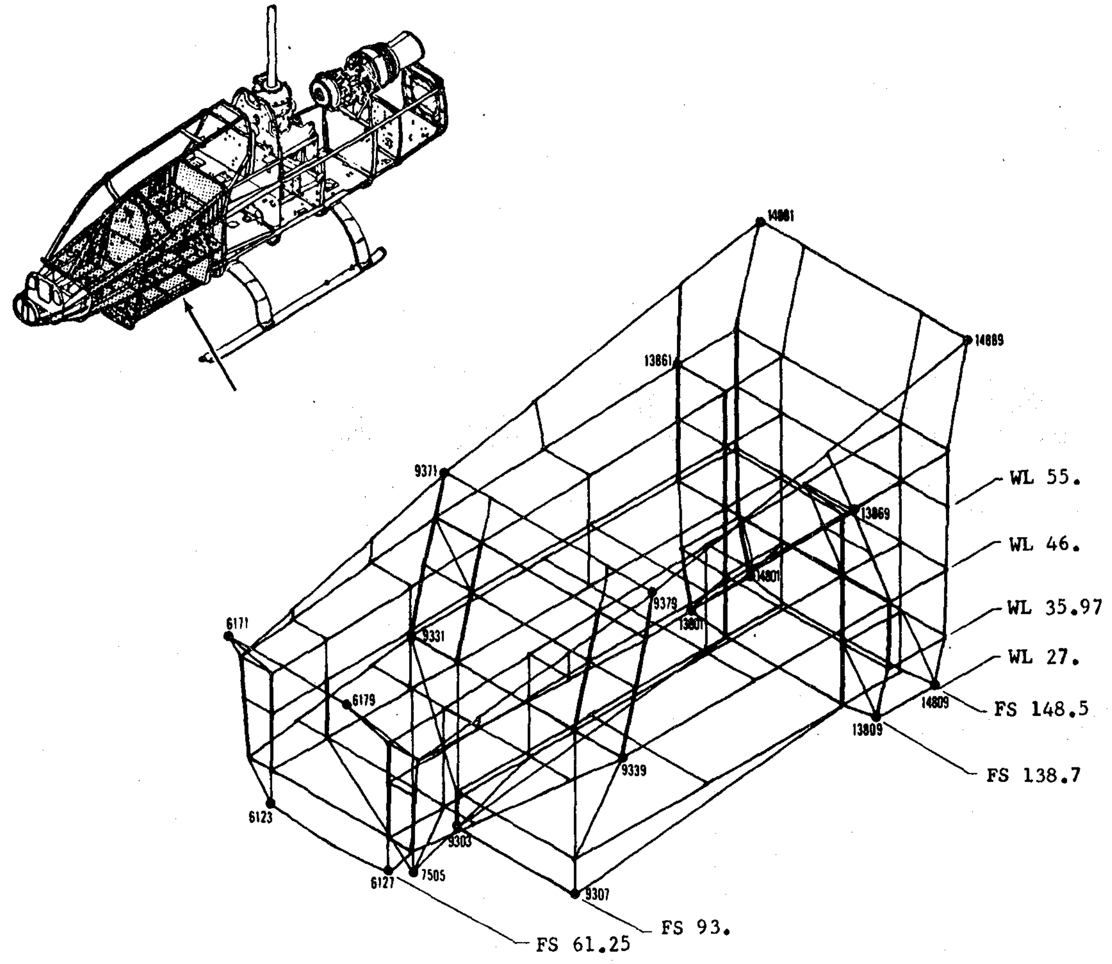
14861
14889
13861
9371
13869
14801
9379
13801
6171
9331
6179
14809
13809
9339
6123
9303
6127
7505
9307
WL 55.
WL 46.
WL 35.97
WL 27.
FS 148.5
FS 138.7
FS 93.
FS 61.25

STIFFNESS MODELING - DETAIL

DETAIL - refers to a subassembly drawing and includes a symbolized sketch of structural elements and grid points in the model followed by tabular listings of the element properties, grid points, and constraints.

Notes are located on the detail drawing or after the data tables to explain modeling techniques that are not clear or need special explanation beyond that given in the tables.

The detail drawings and corresponding data tables provide information about each structural element in the model and constraints at each grid point. The drawings show grid points and structural elements for a local area of the model. The elements are marked with letters referring to one or more specific elements in the following element data tables. In addition to the element data tables, grid point tables provide information about constraints or reduction of specific degrees of freedom.

STIFFNESS MODELING DETAIL

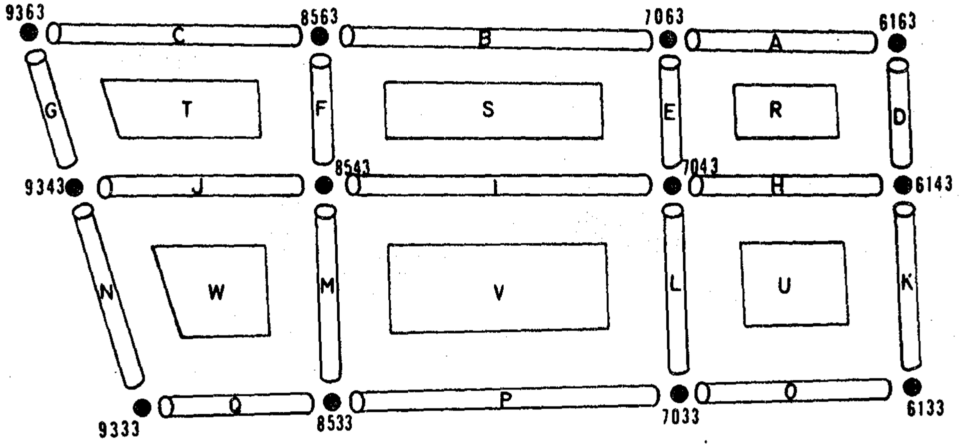
9363
C
8563
B
7063
A
6163
G
T
F
S
E
R
D
8543
7043
9343
J
I
H
6143
N
W
M
V
L
U
K
9333
Q
8533
P
7033
O
6133

View looking inboard

STIFFNESS MODELING - GRID POINT DATA TABLE

The grid point tables include information about SPCs, MPCs, and OMITs for the degrees of freedom at the grid points shown on the detail drawing.

Rules for Single Point Constraints (SPC)

The rules for using single point constraints in the modeling are:

A - elimination of degrees of freedom with zero stiffness

B - representation of boundary conditions

Rule B is not used in the modeling of the free helicopter airframe modes. In order to use rule A for eliminating degrees of freedom that are not aligned with the basic coordinate system, a coordinate system is defined in the direction that the constraint is applied.

When applying rule A, it is important that the structure is not actually constrained by the SPC. As a check on this, the SPC reactions are printed out in the Normal Modes NASTRAN run and checked to ensure that they are negligible.

Rules for Multi-Point Constraints (MPC)

Two common rules for using multi-point constraint equations in the modeling are:

A - representation of rigid bar or rod elements

B - representation of pin connections between parts of the structure

The rule refers to the dependent coordinate in the MPC equation.

STIFFNESS MODELING - GRID POINT DATA TABLE (concluded)

Rules for Guyan Reduction (OMIT)

The Guyan Reduction technique is used to condense the degrees of freedom down to a practical size for the Givens eigenvalue solution. Degrees of freedom are omitted that have negligible inertia properties or whose inertia properties can be rationally redistributed to others. The rules used for omitting degrees of freedom are:

A - the inertia properties are negligible

B - for a relatively uniform mass distribution uniform omitting is used which preserves the distribution

C - for structure such as panels where relative inplane deflections are insignificant many of the inplane degrees of freedom are omitted

D - knowledge of the mode shapes of importance and the relative stiffness in certain areas of the structure

Use of rule D depends on knowledge of the relative stiffness and significant mode shapes of the structure. Degrees of freedom in low response areas of a particular mode will not develop inertia loads as large as high response areas and can be omitted without a significant effect on that mode. Degrees of freedom may also be omitted in high stiffness areas where relative deflections are small and inertia loads redistributed to degrees of freedom not omitted will still give accurate results.

STIFFNESS MODELING
GRID POINT DATA TABLE

GRID POINT DATA

GRID POINT	SPC		MPC		OMIT	
	D.O.F.	RULE	D.O.F.	RULE	D.O.F.	RULE
6133	456	AAA	-	-	23	CC
6143	456	AAA	-	-	12	DC
6163	456	AAA	-	-	123	DCC
7033	456	AAA	123	AAA	-	-
7043	2456	AAAA	-	-	1	D
7063	456	AAA	-	-	23	CC
8533	456	AAA	123	AAA	-	-
8543	2456	AAAA	-	-	1	D
8563	456	AAA	-	-	13	DC
9333	456	AAA	-	-	1	D
9343	456	AAA	-	-	123	DCC
9363	456	AAA	-	-	2	C

STIFFNESS MODELING - ROD ELEMENT DATA TABLE

Rod element tables include the CONROD element identification number (ID), a type, the actual cross sectional area, offsets of the area centroid from the grid point, and the final area used in the model. The types of rod elements are the following:

1. Cap - axial load carrying member in a beam or spar
2. R/SP1, R/SP2, R/SP3 - rod used with a shear panel
3. Doubler
4. Frame - used primarily around bulkheads
5. Fitting - used for the gun turret attachment fittings

Shear panels surrounded by rods are used extensively in the modeling. Since the shear panels can only react shear loads in the plane of the panel, rods are required to react inplane bending and axial loads. Three types of modeling are used to calculate the rod areas surrounding the shear panel:

1. R/SP1 - is used when a beam web is represented with three rods and two shear panels. The rod areas are calculated to preserve the area, cg, and moment of inertia of the web as follows:

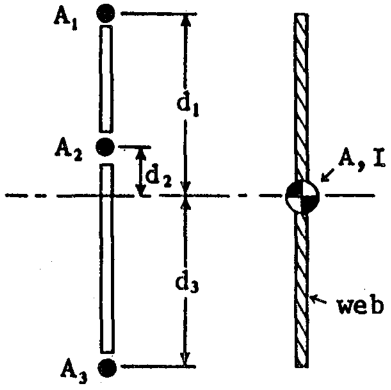

$$\begin{Bmatrix} A_1 \\ A_2 \\ A_3 \end{Bmatrix} = \begin{bmatrix} 1 & 1 & 1 \\ d_1 & d_2 & d_3 \\ d_1^2 & d_2^2 & d_3^2 \end{bmatrix}^{-1} \begin{Bmatrix} A \\ 0 \\ I \end{Bmatrix}$$

2. R/SP2 - The shear panel cross sectional area is lumped at the rods to preserve the axial stiffness of the panel.

3. R/SP3 - The inplane bending moment of inertia of the shear panel or $1/12th^3$ is preserved by giving the rods an area of 1/6th.

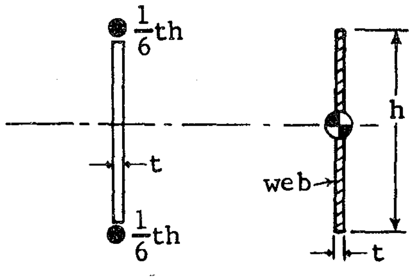

Note that two different types of modeling are often used on one panel.

STIFFNESS MODELING
ROD ELEMENT DATA TABLE

ROD ELEMENT DATA

LETTER DESIGNATION	NASTRAN EID	TYPE	ACTUAL AREA (in.^{2})	OFFSETS FROM GRIDPOINT		FINAL AREA (in.^{2})
				Z	Y	
I	1290973	R/SP2	.256	-	-	.256
	1290993	R/SP2	.289	-	-	.289
	1294913	R/SP2	.155	-	-	.155
	1294931	R/SP2	.176	-	-	.176
J	1291373	Doubler	.047	1.12	0.0	.054
	1290995	R/SP2	.289	-	-	.289
	1294933	R/SP2	.176	-	-	.176
K	1580044	Cap	.370	0.34	0.0	.344
	1290254	Doubler	.057	1.12	0.0	.046
	1290961	R/SP1	.079	-	-	.079
	1294901	R/SP1	.030	-	-	.030
L	1580045	Cap	.370	0.34	0.0	.347
	1291971	Doubler	.057	1.12	0.0	.044
	1290981	R/SP1	.077	-	-	.077
	1294921	R/SP1	.028	-	-	.028

STIFFNESS MODELING - SHEAR PANEL/MEMBRANE ELEMENT DATA TABLE

The shear panel and membrane element tables include CSHEAR, CTRMEM, and CQDMEM element IDs, type, and thickness. The types used are the following:

1. Inner skin
2. Outer skin
3. Interior skin (or doubler)
4. Bulkhead

for sandwich panels

5. Web
6. Skin

STIFFNESS MODELING
SHEAR PANEL/MEMBRANE ELEMENT DATA TABLE

SHEAR PANEL/MEMBRANE ELEMENT DATA

Letter Designation	NASTRAN EID	Type	Thickness (IN.)
R	1292091	Inner Skin	.025
	1291832	Outer Skin	.016
S	1292093	Inner Skin	.025
	1290412	Interior Skin	.016
	1291592	Interior Skin	.016
	1291834	Outer Skin	.016
T	1292095	Inner Skin	.025
	1291836	Outer Skin	.016
U	1292090	Inner Skin	.025
	1291831	Outer Skin	.016
V	1292092	Inner Skin	.025
	1290411	Interior Skin	.016
	1291591	Interior Skin	.016
	1291833	Outer Skin	.016
W	1292094	Inner Skin	.025
	1291835	Outer Skin	.016

STIFFNESS MODELING - BAR ELEMENT DATA TABLE

The bar element tables include the CBAR element ID, cross sectional area, area moments of inertia, and torsional stiffness constant. References to notes following the tables are used to indicate bar offsets or pin flags.

STIFFNESS MODELING
BAR ELEMENT DATA TABLE

CBAR ELEMENT DATA

LETTER DESIGNATION	NASTRAN EID	SECTION PROPERTIES			
		AREA (in.^{2})	INERTIA-PLANE 1 (in.^{4})	INERTIA-PLANE 2 (in.^{4})	TORSION (in.^{4})
A	1070321	2.100	13.035	6.442	0.0
B	1070311	2.100	13.035	6.442	0.0
C	1210611	0.643	0.342	2.081	0.0
D	1210612	0.643	0.342	2.081	0.0
E	1210613	0.643	0.342	2.081	0.0
F	1210211	0.643	0.342	2.081	0.0
G	1210212	0.643	0.342	2.081	0.0
H	1210213	0.643	0.342	2.081	0.0
I [1]	3440011	1.405	2.216	0.0	0.0
J [2]	3440012	1.405	2.216	0.0	0.0
K	1210101	1.643	5.770	5.205	0.0
N	1210091	1.643	5.770	5.205	0.0

NOTES -

[1] Offsets at End A: x=0.56 in., y=0.0 in., z=-2.96 in.
Offsets at End B: x=0.0 in., y=0.0 in., z=-2.96 in.

[2] Offsets at End A: x=0.0 in., y=0.0 in., z=-2.96 in.
Offsets at End B: x=0.56 in., y=0.0 in., z=-2.96 in.

STIFFNESS MODELING - SCALAR SPRING ELEMENT DATA TABLE

The scalar spring element tables include the CELAS2 element ID, the direction of the element, and spring rate.

STIFFNESS MODELING
SCALAR SPRING ELEMENT DATA TABLE

SPRING ELEMENT DATA

LETTER DESIGNATION	NASTRAN EID	COORDINATE	SPRING RATE (lb/in.)
R	189831	1	28125
	189832	2	28125
	189833	3	4500
S	189871	1	28125
	189872	2	28125
	189873	3	4500
T	211831	1	28125
	211832	2	28125
	211833	3	4500
U	211871	1	28125
	211872	2	28125
	211873	3	4500
V	214853	3	20000

WEIGHTS MODELING

The program SDSN02 computes the distribution of helicopter weight items to grid points in the model and generates NASTRAN concentrated mass data in the form of CONM2 cards. Using the program involves first dividing the helicopter into regions or boxes. Data defining these regions along with the GRID data from the model and the detailed weights tape are input to SDSN02. The center of gravity of all the weight items that lie within each region is computed and the total region weight is distributed to the selected or specified grid points in the region. The weights distributed to each grid point are summed for all regions and resulting weights are punched on CONM2 cards. The flow of the program is shown schematically in the figure.

The formula for distributing the total region weight to the j^{th} grid point in the region is given below.

$$W_j = \frac{W_r/L_j}{\sum_{i=1}^{n} (1/L_i)}$$

where:

W_r = region weight

L_j = distance from region cg to grid point j

L_i = distance from region cg to grid point i

n = number of grid points in the region

This formula preserves the total weight of the region and distributes the weight to each grid point based on its proximity to the cg, i.e., the closer the grid point, the larger the weight. The formula does not necessarily preserve the cg of the region. However, this is not considered to be a problem provided the regions are kept small and are chosen to include a balanced set of grid points within the region.

The detailed weights tape for the FY71 Model AH-1G used in the modeling is being kept on permanent file at BHT. The tape is identified as follows: Weights Group Data File for the Model 209 (AH-1G) sorted by AN (Army/Navy) Code - File Number SDSN01-F10.

Because of the model size, the AH-1G NASTRAN dynamic model is divided into three major sections, each requiring a separate SDSN02 data deck.

1. Fuselage excluding wings and main rotor pylon

2. Tailboom and wings

3. Main rotor pylon

The fuselage section includes the built-up fuselage structure (Station 28 to 300) and skid landing gear and is divided into 194 regions. The engine and XM-28 gun turret weights are not processed with SDSN02. The tailboom and wings section consists of 48 regions encompassing the tailboom, vertical fin, elevator, tail rotor mast, and wings. The main rotor pylon section has 16 regions and includes the rotating controls, main transmission, and mast.

WEIGHTS MODELING

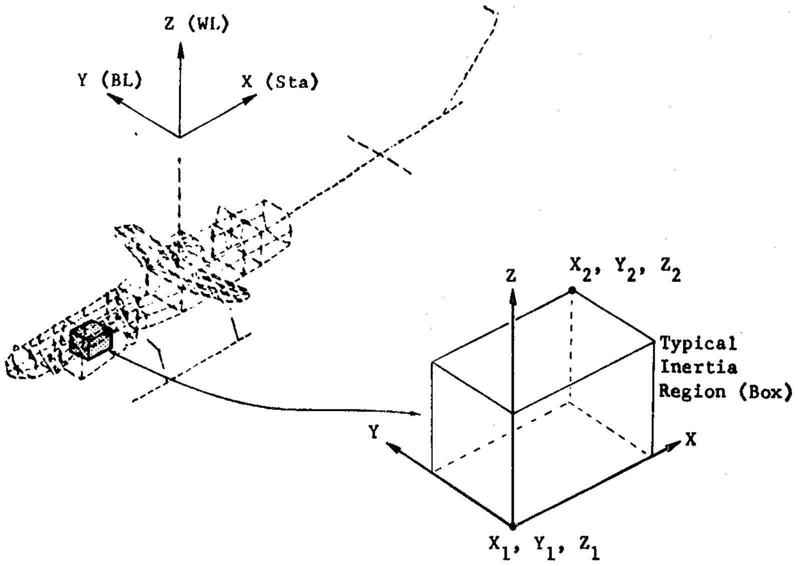
Z (WL)
Y (BL)
X (Sta)
Z
X_2, Y_2, Z_2
Typical Inertia Region (Box)
Y
X
X_1, Y_1, Z_1

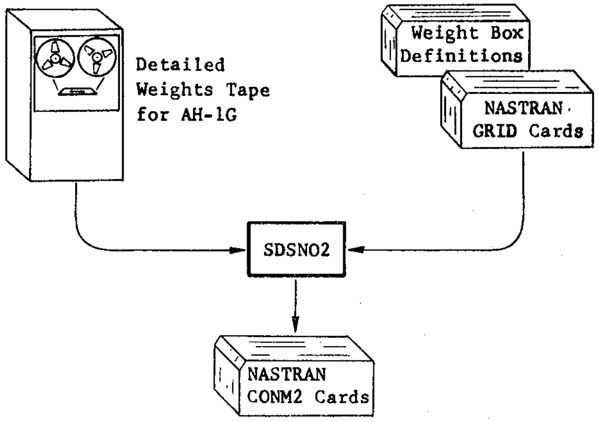
Detailed Weights Tape for AH-1G

Weight Box Definitions

NASTRAN GRID Cards

SDSNO2

NASTRAN CONM2 Cards

LARGE MASS AND USEFUL LOAD MODELING

Weight items on the helicopter that are not automatically distributed by the weights program are the following:

1. Lycoming T53-L13 engine
2. XM-28 gun turret
3. Main rotor and tail rotor
4. Useful weights

Lycoming T53-L13 Engine

The engine weight items and corresponding Army/Navy (AN) code number are listed below.

Engine (AN 24051) = 530.00 lb
Starter-generator (AN 27225) = 48.00 lb
Residual fluid (AN 24061) = 5.00 lb
One-half drive shaft (AN 30051) = 1.55 lb
Transmitter dual tachometer (AN 32054) = 0.80 lb

Total engine weight = 585.35 lb

The weight moments of inertia about the cg of the engine are given below.

$I_{roll} = 17{,}800 \ (\text{lb-in}^2)$

$I_{pitch} = 109{,}500 \ (\text{lb-in}^2)$

$I_{yaw} = 94{,}300 \ (\text{lb-in}^2)$

The total weight and inertias of the engine are lumped at grid point 124800 located at the engine cg (Station 248, WL 86, and BL 0). This grid point is tied rigidly to the elastic engine mounts by MPC equations.

XM-28 Gun Turret

The weight items included in the gun turret system are listed below:

Turret fluid (AN 38051)	=	1.00 lb
Turret (AN 38051)	=	124.50 lb
Turret closure, right side (AN 38051)	=	2.30 lb
Turret closure, left side (AN 38051)	=	2.30 lb
Turret rub strip (AN 38051)	=	0.10 lb
Launcher (AN 38061)	=	40.80 lb
Cradle (AN 38061)	=	10.30 lb
Gearbox and motor (AN 38061)	=	9.10 lb
Minigun (AN 38061)	=	48.30 lb
Cable (AN 38061)	=	1.00 lb
Gearbox (AN 38061)	=	1.50 lb
Motor (AN 38061)	=	7.70 lb
Feed tray (AN 38061)	=	4.50 lb
Total gun turret weight	=	253.4 lb

The total weight of the gun turret system represented as a rigid body is concentrated at grid point 7505 located at the turret cg (Station 75.5, WL 29, and BL 0). Grid point 7505 is tied to the turret attachment fittings on the fuselage by MPC equations. Moments due to turret rigid body motions are represented by the cg offset from the fuselage structure.

Main Rotor and Tail Rotor

The weights of the main rotor and tail rotor are given below:

Blade inertia weights (AN 2486)	=	110.0 lb
Blade assembly (AN 2546)	=	348.0 lb
Hub assembly (AN 3041-3501)	=	489.5 lb
Total main rotor weight	=	947.5 lb

Tail rotor blades (AN 8105)	=	14.3 lb
Tail rotor hub (AN 8206)	=	16.5 lb
Total tail rotor weight	=	30.8 lb

LARGE MASS AND USEFUL LOAD MODELING (continued)

The main rotor weight is lumped at grid point 200153 located at the rotor cg (Station 200, WL 153, and BL 0). The tail rotor blade weight is lumped at its cg location at grid point 520152 (Station 520.67, WL 118.27, and BL 15.19), and the tail rotor hub weight is lumped at its cg location at grid point 520139 (Station 520.67, WL 118.27, and BL 13.88). Rotor flapping inertias are not included with the rotor weights because of the Bell teetering hinge rotor system which does not transfer flapping moments to the airframe.

Useful Weight Items

The weight items discussed up to this point, including the weight distributed automatically and those previously mentioned in this section, constitute the empty weight items of the helicopter. The total empty weight of the AH-1G is 5760 lb.

The Basic Mission configuration was selected as a representative flyable weight configuration to be used in the modeling. The useful loads for this configuration total 3173 lb and include crew, fuel, wing stores, and ammo. This gives a Basic Mission gross weight of 8933 lb.

The Basic Mission total weight, cg, and inertias from the grid point weight generator table in NASTRAN are compared with actual weights tape data below.

Parameter	NASTRAN	Weights Tape
Center of gravity - station (in)	193.2	193.9
WL (in)	69.4	71.4
BL (in)	.001	0.
Total weight (lb)	8914.15	8930.77
Roll inertia (lb-in^2)	13.41 x 10^6	13.49 x 10^6
Pitch inertia (lb-in^2)	62.14 x 10^6	61.64 x 10^6
Yaw inertia (lb-in^2)	53.78 x 10^6	53.06 x 10^6

The discrepancy of about 19 lb in the total weight comes from the portion of the empty weights generated by the computer program and is possibly due to accumulated error resulting from processing the thousands of weight items and distributing them to the grid points.

LARGE MASS AND USEFUL LOAD MODELING (concluded)

Grid points associated with the crew, fuel, and ammo are located at their respective cgs and each is tied to the fuselage by four rods as shown in the figure. This is done to represent the inertia loads distributed into the structure for these particular weight items. For example, the inertia loads due to the weight of the pilot are distributed into the bulkhead at Station 148.50 through the seat support structure. The rods properly distribute loads and moments into the bulkhead caused by fore-and-aft, lateral, and vertical accelerations of the weight cg offset forward of the bulkhead.

The wing stores consisting of smoke grenades and XM-157A rockets are offset from grid points at the left and right wing tip ribs, grid points 65929 and 75929. MPC equations are used to distribute moments into the wing structure due to the weight offsets.

The NASTRAN data deck listing and normal modes run have included the Basic Mission useful weights; however, the useful weights can be readily changed to another weight configuration. The useful weights are all grouped together in one section of the unsorted Bulk Data deck. In addition, all the CONM2 cards representing Basic Mission useful loads have comments in field 10 indicating the weight configuration. These cards can then be easily located and removed and another set of useful load cards inserted. The useful load data cards for the 9500 lb gross weight HOG II configuration which has a heavier wing stores loading than the Basic Mission are included after the Bulk Data deck and can be interchanged with the Basic Mission cards if the user desires.

LARGE MASS AND USEFUL LOAD MODELING

NOTE: Elements A through X are CONRODs.

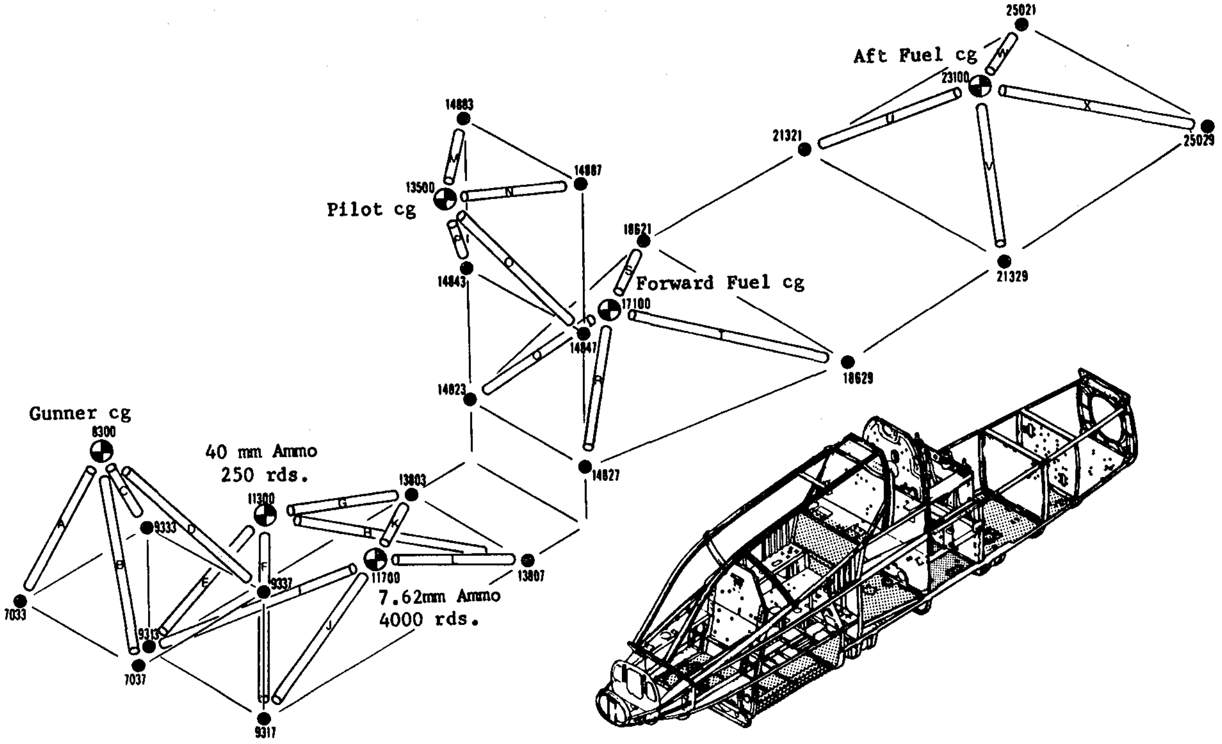
25021
Aft Fuel cg
23100
21321
25029
14883
14887
13500
Pilot cg
18621
14843
Forward Fuel cg
17100
21329
14847
18629
14823
Gunner cg
8300
40 mm Ammo
250 rds.
13803
14827
11300
9333
11700
13807
9337
7.62mm Ammo
4000 rds.
7033
9313
7037
9317
A
B
C
D
E
F
G
H
I
J
K
L
M
N
O
P
Q
R
S
T
U
V
W
X

NASTRAN VIBRATION MODEL OF THE AH-1G HELICOPTER AIRFRAME

The complete model consists of structural elements from the NASTRAN library such as scalar springs, rods, bars, shear panels, and triangular and quadrilateral membranes. There was no use of General Elements, substructuring, or DMAPing in the model. Symmetry could not be used because of unsymmetrical sections in the fuselage and the tail rotor offset to the right side. The table below shows the degrees of freedom before and after constraints and partitioning were applied.

Stiffness Matrix	Degrees of Freedom	Description
K_{gg}	2940	Unreduced size
K_{nn}	2699	After applying MPC equations
K_{ff}	1714	After applying SPCs
K_{aa}	241	After partitioning with OMITs
$K_{\ell\ell}$	235	After applying free body SUPORTs

NASTRAN VIBRATION MODEL OF THE AH-1G HELICOPTER AIRFRAME

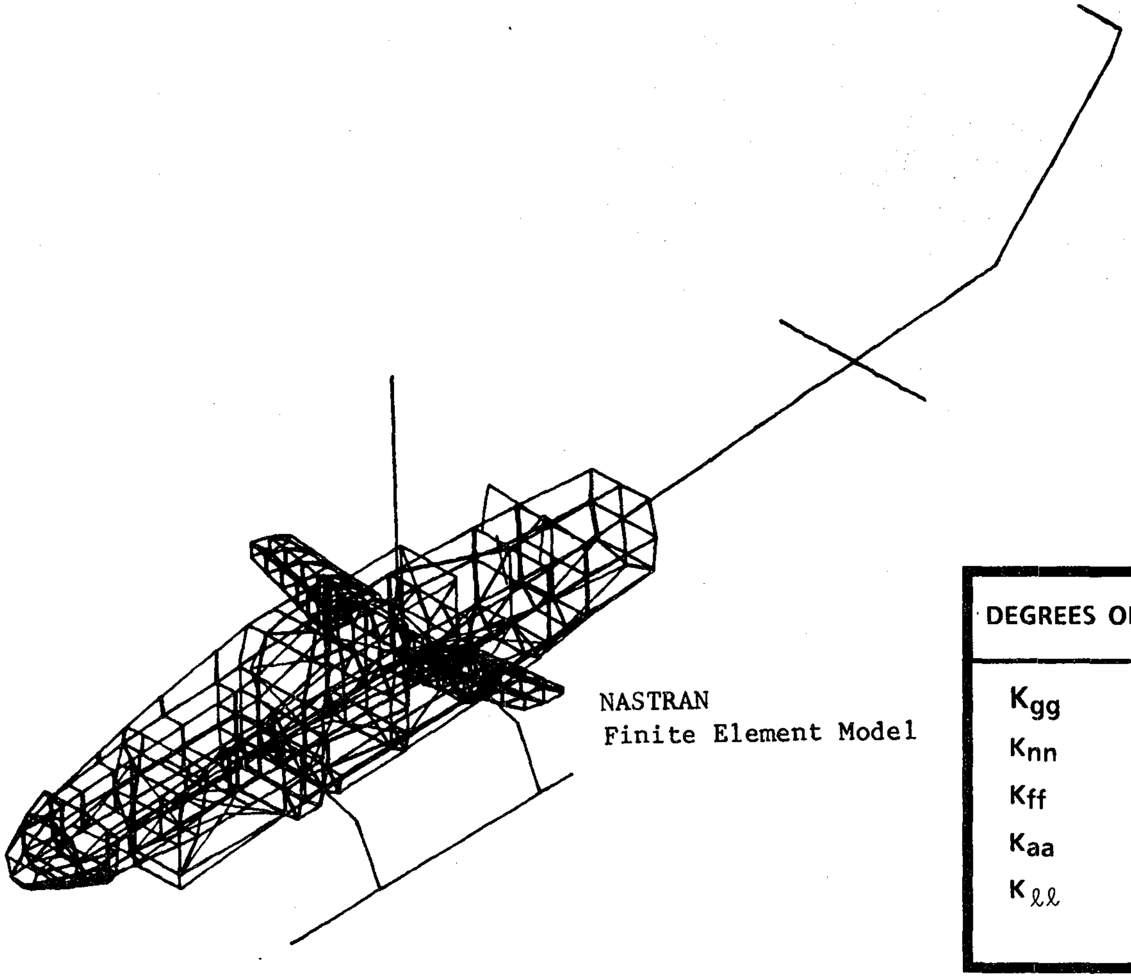

NASTRAN
Finite Element Model

DEGREES OF FREEDOM		ELEMENTS	
K_{gg}	2940	BAR	197
K_{nn}	2699	ROD	2012
K_{ff}	1714	SHEAR	340
K_{aa}	241	QDMEM	160
$K_{\ell\ell}$	235	TRMEM	243
		ELAS2	13

ANNOTATED INPUT DATA LISTING

The unsorted bulk data is organized in a manner which should allow quick and easy reference to the NASTRAN model. Special ID numbering conventions are used in the modeling which should allow the user to easily identify and locate grid points and structural elements. The outline below shows the organization of the bulk data and should provide additional aid in referring to the model.

ANNOTATED INPUT DATA LISTING (SAMPLE)

```
                I N P U T   B U L K   D A T A   D E C K   E C H O
.   1   ..  2   ..  3   ..  4   ..  5   ..  6   ..  7   ..  8   ..  9   ..  10  .
$ * * * * * * * * * * * * * * * * * * * * * * * * * * * * * * * * * * * * * * *
$                               GRID POINT DATA
$                                    BEGIN
$ * * * * * * * * * * * * * * * * * * * * * * * * * * * * * * * * * * * * * * *
$
$
$                              NOSE SUBASSEMBLY
$                                    * * *
$
$                             STA  33.00 BULKHEAD
$                               209-030-580-057
$
GRID     3331   0        33.00    4.90   49.60  0          456
GRID     3339   0        33.00   -4.90   49.60  0          456
GRID     3341   0        33.00    6.95   56.85  0          456
GRID     3349   0        33.00   -6.95   56.85  0          456
$
$                             STA  46.00 BULKHEAD
$                               209-030-582-053
$
GRID     4631   0        46.00   11.46   49.60  0          456
GRID     4633   0        46.00    9.07   46.00  0          456
GRID     4637   0        46.00   -9.07   46.00  0          456
GRID     4639   0        46.00  -11.46   49.60  0          456
GRID     4641   0        46.00   12.34   57.00  0          456
GRID     4649   0        46.00  -12.34   57.00  0          456
GRID     4661   0        46.00    9.70   65.00  0          456
GRID     4669   0        46.00   -9.70   65.00  0          456
$
$                        FORWARD FUSELAGE SUBASSEMBLY
$                                    * * *
$
$                             STA  61.25 BULKHEAD
$                               209-030-101-001
$                               209-030-510-007
$
GRID     6123   0        61.25   10.00   40.91  0          456
GRID     6127   0        61.25  -10.00   40.91  0          456
GRID     6131   0        61.25   13.82   46.00  0          456
GRID     6133   0        61.25   10.00   46.00  0          456
GRID     6137   0        61.25  -10.00   46.00  0          456
GRID     6139   0        61.25  -13.82   46.00  0          456
GRID     6141   0        61.25   14.54   54.16  0          456
GRID     6143   0        61.25   10.00   54.16  0          456
GRID     6147   0        61.25  -10.00   54.16  0          456
GRID     6149   0        61.25  -14.54   54.16  0          456
GRID     6161   0        61.25   15.06   60.00  0          456
GRID     6163   0        61.25   10.00   60.00  0          456
GRID     6167   0        61.25  -10.00   60.00  0          456
GRID     6169   0        61.25  -15.06   60.00  0          456
GRID     6171   0        53.95   10.00   69.42  0          456
GRID     6179   0        53.95  -10.00   69.42  0          456
$
$                         STA  70.79 PSEUDO-BULKHEAD
$                        FORWARD TURRET ATTACH POINTS
$
GRID     7031   0        70.79   15.04   46.00  0         3456
GRID     7033   0        70.79   10.00   46.00  0          456
```

SAMPLE NORMAL MODES RUN

```
                                           R E A L   E I G E N V A L U E S
  MODE    EXTRACTION     EIGENVALUE           RADIAN              CYCLIC           GENERALIZED         GENERALIZED
   NO.       ORDER                           FREQUENCY           FREQUENCY             MASS              STIFFNESS

     1        236      0.0                 0.0                 0.0                 1.190112E+00        0.0
     2        235      0.0                 0.0                 0.0                 2.016131E+00        0.0
     3        234      0.0                 0.0                 0.0                 5.918257E+00        0.0
     4        233      0.0                 0.0                 0.0                 6.543401E+00        0.0
     5        232      0.0                 0.0                 0.0                 8.660554E+00        0.0
     6        231      0.0                 0.0                 0.0                 9.656038E+00        0.0
     7        230      3.521150E+02        1.876472E+01        2.986499E+00        3.992990E+00        1.405991E+03
     8        229      5.898723E+02        2.428729E+01        3.865442E+00        3.124393E+00        1.842992E+03
     9        228      2.000551E+03        4.472752E+01        7.118607E+00        4.378621E-01        8.759656E+02
    10        227      2.502017E+03        5.002017E+01        7.960958E+00        6.119395E-01        1.531083E+03
    11        226      8.383637E+03        9.156221E+01        1.457258E+01        2.720276E-01        2.280581E+03
    12        225      1.014475E+04        1.007212E+02        1.603027E+01        1.259047E+00        1.277271E+04
    13        224      1.170949E+04        1.082104E+02        1.722221E+01        8.391414E-01        9.825914E+03
    14        223      1.247148E+04        1.116758E+02        1.777374E+01        5.719226E-01        7.132719E+03
    15        222      1.464762E+04        1.210274E+02        1.926210E+01        6.061330E-01        8.878406E+03
    16        221      1.552996E+04        1.246193E+02        1.983377E+01        3.217663E-01        4.997020E+03
    17        220      1.888009E+04        1.374048E+02        2.186865E+01        1.164402E+00        2.198401E+04
    18        219      2.167299E+04        1.472175E+02        2.343039E+01        2.507871E-01        5.435305E+03
    19        218      2.496716E+04        1.580100E+02        2.514807E+01        5.954853E-01        1.486757E+04
    20        217      2.583294E+04        1.607263E+02        2.558038E+01        3.391594E-01        8.761480E+03
    21        216      2.776841E+04        1.666386E+02        2.652135E+01        1.121486E+00        3.114187E+04
    22        215      2.901755E+04        1.703454E+02        2.711131E+01        4.637750E-01        1.345762E+04
    23        214      3.343495E+04        1.828523E+02        2.910184E+01        2.207931E-01        7.382203E+03
    24        213      4.104958E+04        2.026070E+02        3.224590E+01        2.804956E+00        1.151422E+05
    25        212      4.556135E+04        2.134510E+02        3.397179E+01        8.255469E-01        3.761303E+04
    26        211      5.953663E+04        2.440013E+02        3.883400E+01        2.721863E+00        1.620505E+05
    27        210      6.385187E+04        2.526893E+02        4.021674E+01        8.329037E-01        5.318246E+04
    28        209      7.150406E+04        2.674023E+02        4.255840E+01        2.538875E-01        1.815399E+04
    29        208      8.557487E+04        2.925317E+02        4.655786E+01        1.072490E-01        9.177820E+03
    30        207      8.999481E+04        2.999915E+02        4.774512E+01        3.399632E-02        3.059492E+03
    31        206      9.049456E+04        3.008232E+02        4.787750E+01        0.0                 0.0
    32        205      1.005236E+05        3.170547E+02        5.046082E+01        0.0                 0.0
    33        204      1.052026E+05        3.243494E+02        5.162180E+01        0.0                 0.0
    34        203      1.107091E+05        3.327297E+02        5.295558E+01        0.0                 0.0
    35        202      1.141998E+05        3.379346E+02        5.378395E+01        0.0                 0.0
    36        201      1.154878E+05        3.398350E+02        5.408641E+01        0.0                 0.0
    37        200      1.191757E+05        3.452185E+02        5.494322E+01        0.0                 0.0
    38        199      1.224386E+05        3.499124E+02        5.569028E+01        0.0                 0.0
    39        198      1.253923E+05        3.541077E+02        5.635799E+01        0.0                 0.0
    40        197      1.328343E+05        3.644644E+02        5.800630E+01        0.0                 0.0
    41        196      1.358285E+05        3.685491E+02        5.865640E+01        0.0                 0.0
    42        195      1.429330E+05        3.780647E+02        6.017087E+01        0.0                 0.0
    43        194      1.490204E+05        3.860315E+02        6.143881E+01        0.0                 0.0
    44        193      1.530297E+05        3.911902E+02        6.225984E+01        0.0                 0.0
    45        192      1.633219E+05        4.041311E+02        6.431946E+01        0.0                 0.0
    46        191      1.731186E+05        4.160782E+02        6.622041E+01        0.0                 0.0
    47        190      1.748829E+05        4.181899E+02        6.655699E+01        0.0                 0.0
    48        189      1.832999E+05        4.281355E+02        6.813988E+01        0.0                 0.0
    49        188      1.937251E+05        4.401421E+02        7.005078E+01        0.0                 0.0
    50        187      2.177544E+05        4.666416E+02        7.426831E+01        0.0                 0.0
    51        186      2.224951E+05        4.716938E+02        7.507240E+01        0.0                 0.0
    52        185      2.310052E+05        4.806299E+02        7.649461E+01        0.0                 0.0
    53        184      2.390831E+05        4.889612E+02        7.782059E+01        0.0                 0.0
    54        183      2.566749E+05        5.066309E+02        8.063280E+01        0.0                 0.0
    55        182      2.689586E+05        5.186121E+02        8.253967E+01        0.0                 0.0
    56        181      2.869623E+05        5.356887E+02        8.525751E+01        0.0                 0.0
    57        180      2.950417E+05        5.431775E+02        8.644939E+01        0.0                 0.0
    58        179      3.276893E+05        5.724417E+02        9.110692E+01        0.0                 0.0
```

SAMPLE NORMAL MODE PLOTS

Sample normal mode plots from the NASTRAN normal modes analysis (Rigid Format 3) are shown in the figure. Only the elastic modes below 10 Hz are shown with many structural elements deleted for clarity.

SAMPLE NORMAL MODE PLOTS

Main Rotor Pylon Fore-and-Aft Rocking Mode (Pylon Pitch)

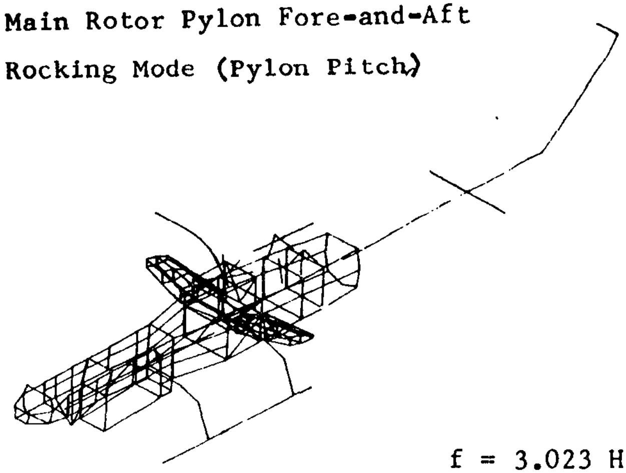

f = 3.023 Hz

Main Rotor Pylon Lateral Rocking Mode (Pylon Roll)

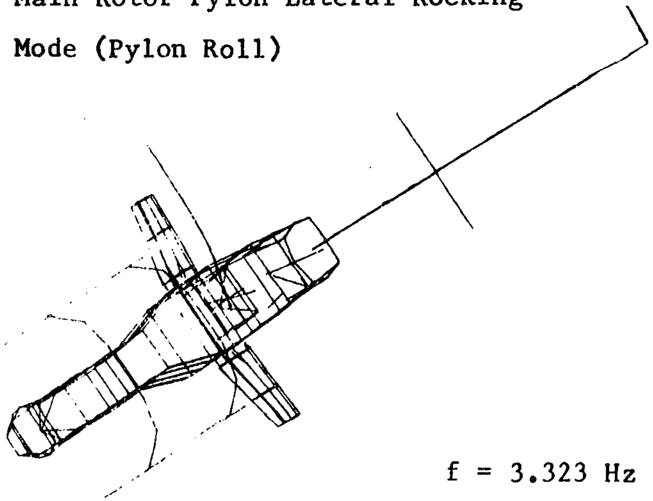

f = 3.323 Hz

First Fuselage Lateral Bending Mode

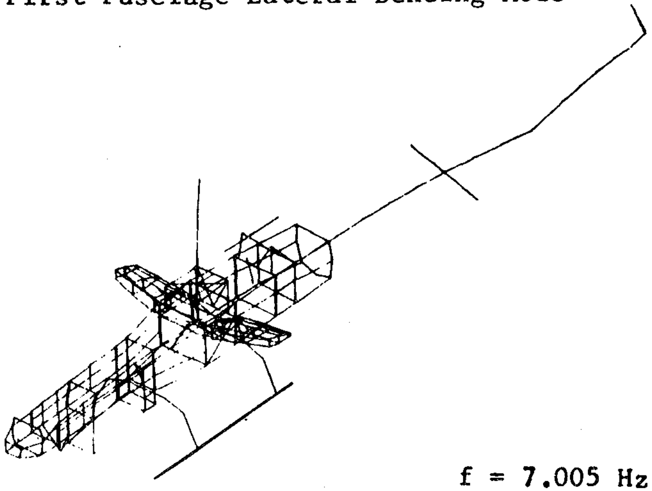

f = 7.005 Hz

First Fuselage Vertical Bending Mode

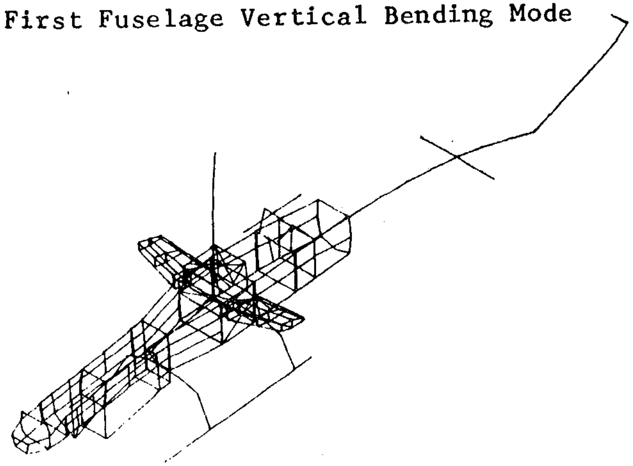

f = 7.910 Hz

3. STATIC TESTING

NASTRAN MODEL COMPARISON WITH STATIC TESTS

The purpose of the study was to provide test data for evaluating the stiffness representation of a mathematical model of the BHT AH-1G helicopter airframe. The math model (Ref. 3) was developed and analyzed using the NASTRAN structural analysis computer program.

Data from static tests was used for comparison with the math model. Two sets of tests were conducted:

1. Static fuselage and wing load-deflection tests performed at the Rock Island Arsenal (1976 - Ref. 4).

2. Static tailboom load-deflection tests conducted at BHT (1975 - Refs. 1 and 5).

Static tests of the fuselage and tailboom were conducted to verify the stiffness representation of the NASTRAN model.

In general, the results of the comparisons show good agreement between the NASTRAN analysis and test. Problems encountered during the test data reduction and subsequent correlation are discussed.

NASTRAN MODEL COMPARISON WITH STATIC TESTS

1. FUSELAGE STATIC LOAD-DEFLECTION TESTS
2. TAILBOOM STATIC LOAD-DEFLECTION TESTS

} VERIFY STIFFNESS MODELING

AH-1G FUSELAGE IN ROCK ISLAND ARSENAL SIMULATOR

Static load-deflection tests of the AH-1G fuselage and wings were conducted at Rock Island Arsenal. The purpose of the tests was to determine the stiffnesses of the fuselage and wing structures.

The test article was AH-1G ship number 15048. The fuselage had fire damage in the area under the main rotor pylon (FS 186 - FS 213). The damaged structure was repaired with stiffened sheet resulting in good structural integrity. Although the stiffness was not identical, it was fairly representative of the original fuselage. The repair changes were well documented so that the NASTRAN math model could be changed accordingly so that there was a direct correspondence between the test article and the math model. The side contour panels (FS 61 - FS 186) that are not used in the NASTRAN model were removed and the side doors of the ammo compartment (FS 93 - FS 138) were propped open during the tests for compatibility between test and analysis.

AH-1G FUSELAGE IN ROCK ISLAND ARSENAL SIMULATOR

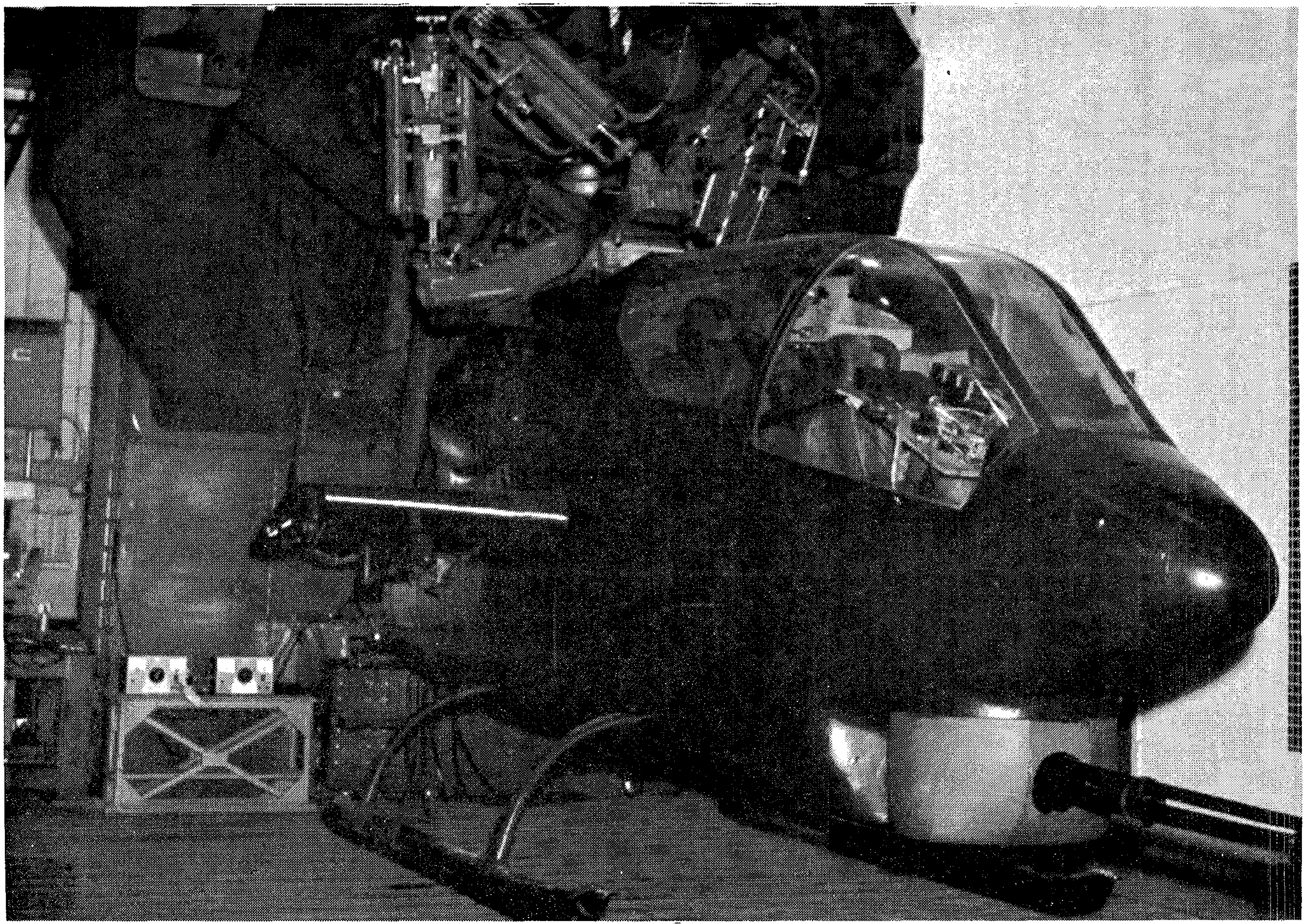

AH-1G FUSELAGE STATIC TEST SETUP

In the fuselage load-deflection tests, the stiffness of the entire fuselage was determined for each direction of loading, i.e., vertical, lateral, and torsion. The mounting location chosen for the fuselage was the four bolt attachment points at the tailboom junction. The location for the applied load was chosen at the nose of the fuselage where a loading fixture could be mounted at the gun turret attachment points. The figure shows the fuselage positioned on the base mounting plate with load cells at each of the four mounting locations. Linear variable differential transformers (LVDTs) were used for deflection measurements. These were located at several stations along the fuselage and at the four base attachment points where measurements were taken with respect to ground.

There were three separate fuselage load-deflection tests conducted: vertical, torsion, and lateral. A maximum applied load of 1000 lb was used for the vertical and lateral tests and a maximum torque of 20,000 in-lb was used for the torsion test. The fuselage was rotated 90 degrees about its roll axis and the wings were removed for the lateral load-deflection test.

Because of some instrumentation location problems, the lateral fuselage test was rerun using dial indicators for measuring deflections. For this test the ammo doors were closed to see if there was any stiffening from the doors.

AH-1G FUSELAGE STATIC TEST SETUP

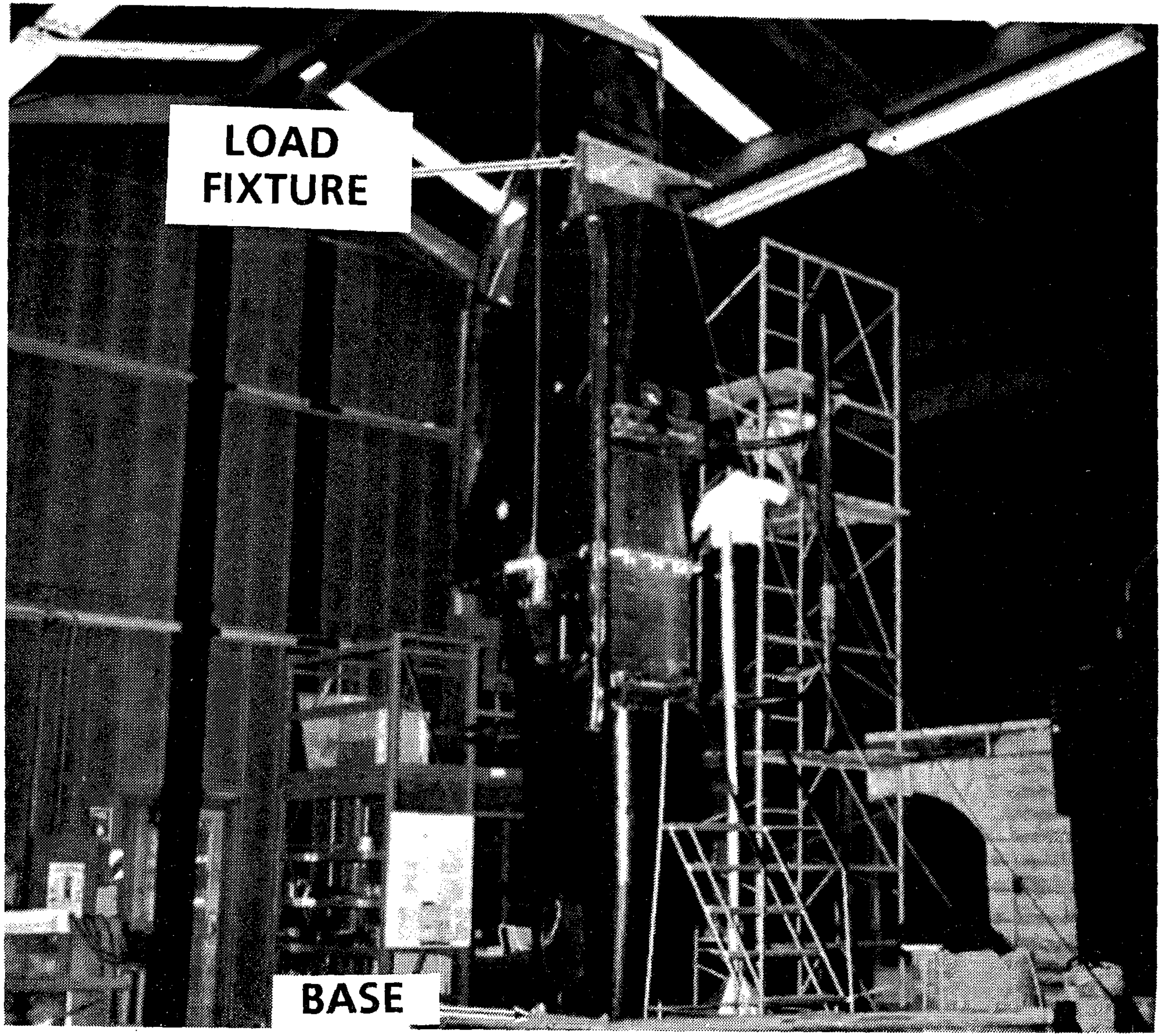

LOAD
FIXTURE
BASE

WING TEST SETUP

For the wing load-deflection tests, the wings were left attached to the fuselage. The fuselage mounting for the fuselage vertical and torsion tests was used for the wing tests. An instrumentation fixture was developed to allow measurement of wing deflections relative to the fuselage at the wing root. Wing elastic deflections could then be measured directly. This would eliminate having to calculate wing deflections from measurements taken with respect to ground which would also include fuselage and base deflections.

Two wing load-deflection tests were conducted: beamwise (vertical) and torsion. Wing loads were applied through a fixture at each wing tip. A maximum beamwise downward load of 1000 lb was used at each wing tip. The wing torsion load was intended to be a 20,000 in-lb torque applied equally and in opposite directions at each wing tip. However, the left wing upward load was made twice the other three applied loads by mistake. The maximum load was then 800 lb at all locations but the left upward load which was 1600 lb. This resulted in a maximum torque of 19,200 in-lb (800 lb loads with a 24 inch couple arm) applied to the right wing tip and a 28,800 in-lb countertorque and 800 lb chordwise shear applied to the left wing tip.

WING TEST SETUP

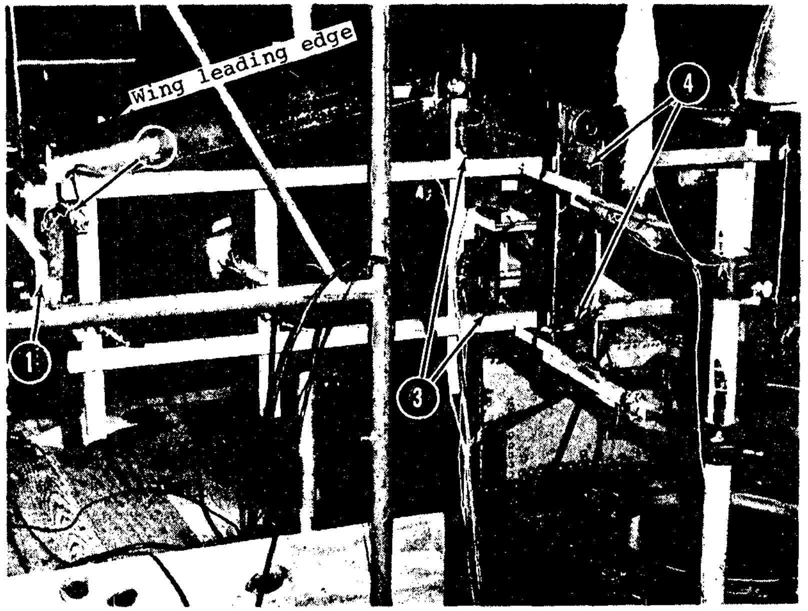
Wing leading edge
1
3
4

1 Load fixture
2 Typical LVDT
3 Instrumentation fixture
4 Instrumentation fixture clamped to fuselage structure

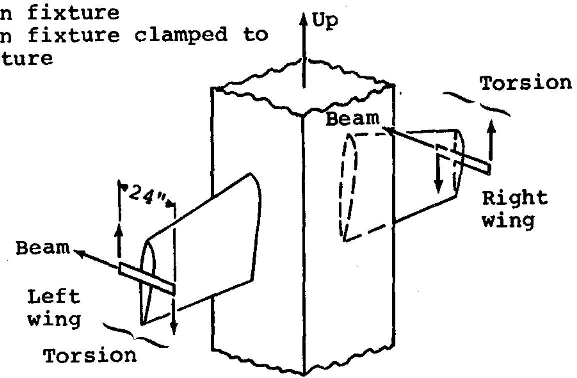
Up
Torsion
Beam
Right wing
24"
Beam
Left wing
Torsion

Wing load application

FUSELAGE STATIC TEST SETUP

The signals from the LVDT measuring devices and load transducers were recorded on tape as the tests were being run. Load versus deflection plots were obtained by playing the recorded data through an automated data reduction system at the Ware Simulation Center at the Rock Island Arsenal.

Data was taken for three or more cycles of loading for each test. The absolute deflections at maximum load for all load conditions were then averaged. Following this, corrections were made for deflections due to rotation of the base of the fuselage with respect to ground.

Base rotations were accounted for in the following manner. Deflections were measured on the fuselage structure at the four corners of the base. Deformations of the support structure, load cells and fuselage attachment fittings were accounted for in the measurements. Rotations were calculated using the pairs of deflections on the left hand and right hand sides for the vertical test and the pairs of deflections on the upper and lower sides for the lateral test.

FUSELAGE STATIC TEST SETUP

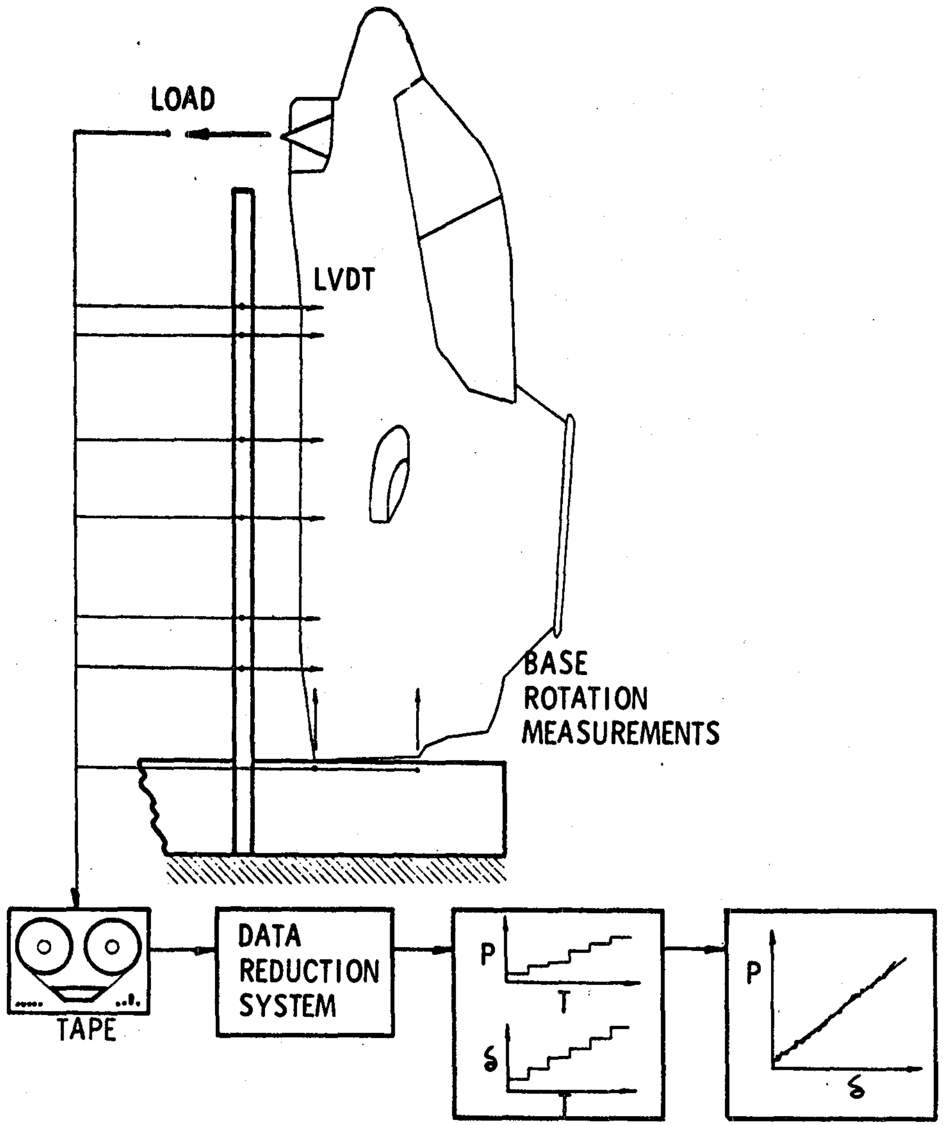
LOAD
LVDT
BASE
ROTATION
MEASUREMENTS
TAPE
DATA
REDUCTION
SYSTEM
P
T
δ
P
δ

FUSELAGE VERTICAL LOAD-DEFLECTION COMPARISON

1. NASTRAN results are stiffer than the test results (about 15 percent stiffer at FS 93). NASTRAN results at FS 61 are about 25 percent stiffer than test.

2. The deflection shape is in good agreement between NASTRAN and test except in the nose area between FS 61 and FS 93 where the test is softer.

3. There may be a steady translation of the base since the deflections from test do not project to a zero deflection at FS 300. However, this could be due to the difficulty in measuring the much smaller deflections near the base.

4. Possible explanations for the NASTRAN results being stiffer than test are:

   a. The actual structure is not as stiff as the idealized NASTRAN model indicates

   b. The stiffness of the load fixture, modeled as rigid in NASTRAN, is affecting the deflections between FS 61 and FS 93

   c. The side panels and ammo doors that were removed during the test were included in the NASTRAN model and effect the structure as follows:

      - panels considered fully effective in NASTRAN and add stability/stiffness

      - panel effectiveness may have compensated for stiffness loss in cutout areas

   d. Errors in instrumentation and loading calibration or in the data reduction

   e. That the fuselage structure of ship number 15048 being from a 1968 model helicopter may be "looser" than a new structure.

FUSELAGE VERTICAL LOAD-DEFLECTION COMPARISON

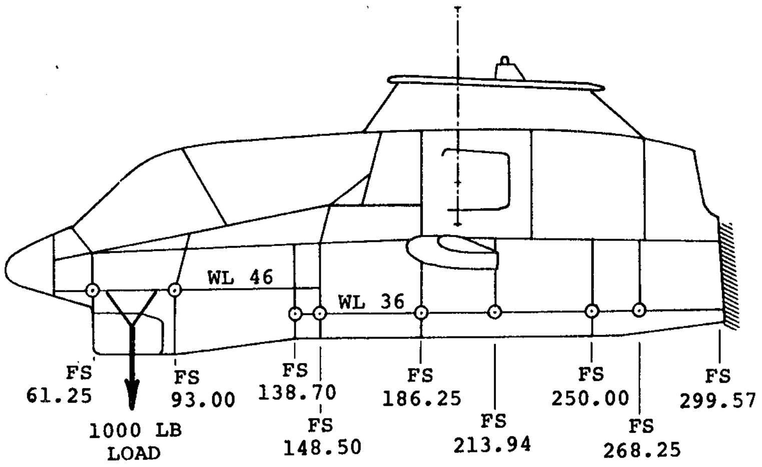
WL 46
WL 36
FS 61.25
FS 93.00
FS 138.70
FS 148.50
FS 186.25
FS 213.94
FS 250.00
FS 268.25
FS 299.57
1000 LB LOAD

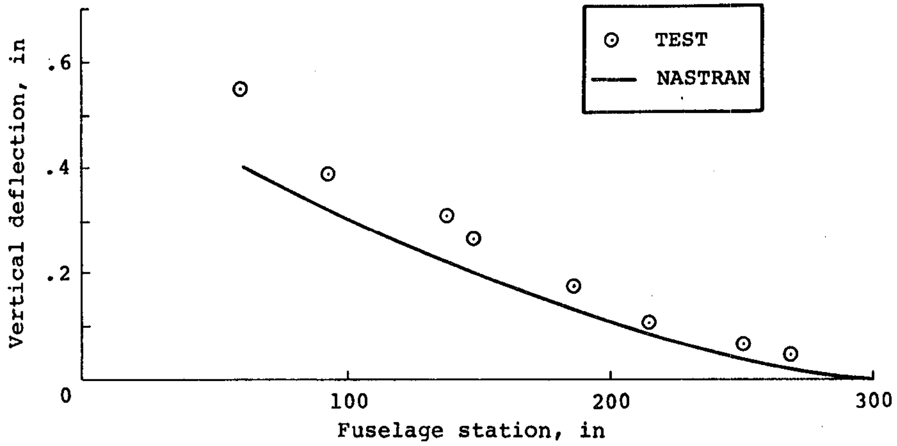

FUSELAGE TORSION LOAD-DEFLECTION COMPARISON

1. It was found after initial comparisons of the data that the NASTRAN model was much stiffer in the forward fuselage than test. In an attempt at improving the correlation, the ammo bay structure (FS 93 - FS 138) was removed in the NASTRAN model. This modification was warranted since the shelf is free on both sides except for hinged doors which were propped open during the test. The correlation was found to improve with the shelf removed.

2. With the ammo bay removed, the NASTRAN results are about 10 to 15 percent stiffer than test.

3. The deflection shapes are in good agreement.

4. Possible explanations for the NASTRAN results being stiffer are the same as those discussed for the vertical test.

FUSELAGE TORSION
LOAD-DEFLECTION COMPARISON

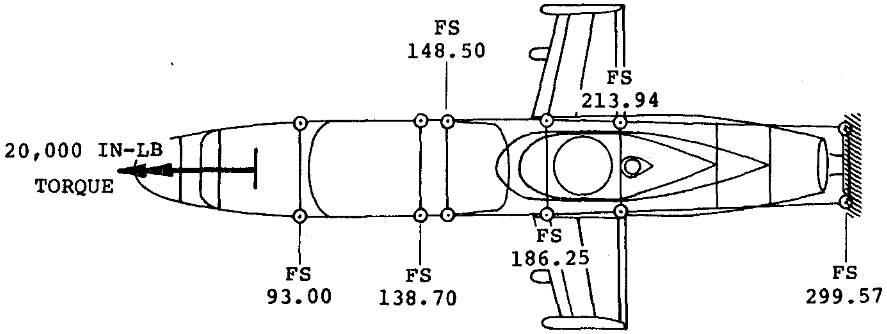
FS
148.50
FS
213.94
20,000 IN-LB
TORQUE
FS
186.25
FS
93.00
FS
138.70
FS
299.57

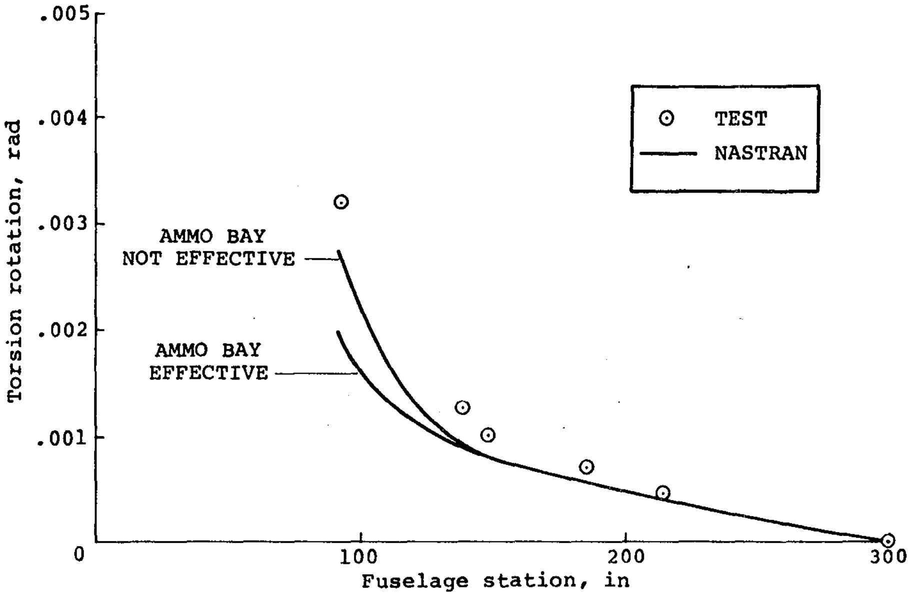

FUSELAGE LATERAL LOAD-DEFLECTION COMPARISON

1. At FS 93, the NASTRAN results are between 5 and 25 percent stiffer than test. The large spread in the test data is due to the variation in base rotations used in the calculations. Using the average test value, the correlation is similar to that of the previous vertical and torsion tests.

2. As mentioned in the discussion of the test procedure, the lateral test was rerun with dial indicators instead of LVDTs. The deflections measured with the dial indicators are about 15 percent lower than the other test and agree very well with the NASTRAN results.

FUSELAGE LATERAL LOAD-DEFLECTION COMPARISON

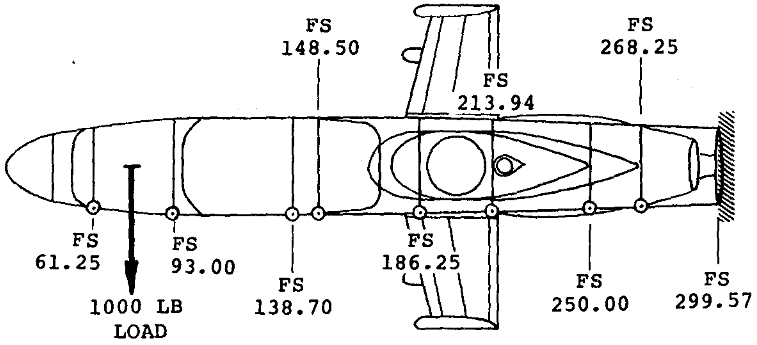
FS 148.50
FS 213.94
FS 268.25
FS 61.25
FS 93.00
FS 138.70
FS 186.25
FS 250.00
FS 299.57
1000 LB LOAD

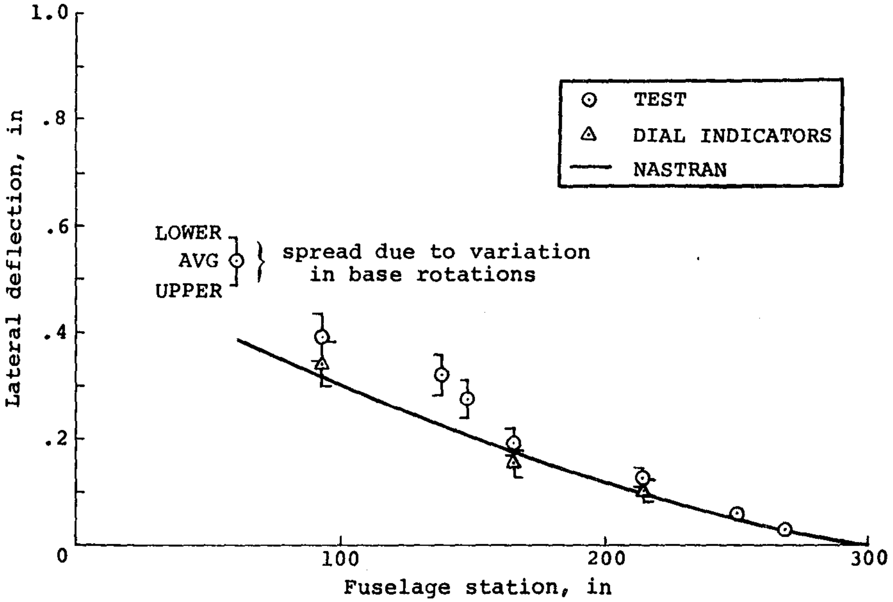

WING LOAD-DEFLECTION COMPARISON

Wing Beamwise Comparison

The correlation of the wing tests with NASTRAN was not expected to be good for two reasons. The first is the complicated joint between the wing and the fuselage which tended to be sloppy and could be affected by such things as the fit and torque of the bolts tying the wing and fuselage together. The second reason was the order of the maximum deflections to be measured was considerably lower than for the fuselage test. Such factors as possible joint sloppiness or deflections of the fuselage where the instrumentation fixture was attached could strongly affect the measurements.

1. The agreement between NASTRAN and test is better than expected with the NASTRAN deflection at the tip of the wing being about 15 percent stiffer than test.
2. There appears to be very little bending in the wing with most of the deflection due to rotation of the wing attachment joint (WS 18 - WS 20).

Wing Torsion Comparison

1. The NASTRAN results are about 15 percent softer than test.
2. There appears to be a steady shift in the test data which could be due to warping of the fuselage structure where the instrumentation fixture is attached. This could cause warping and bending deflections in the fixture that could affect the measurements.
3. If the rotation at the wing root (WS 21) is corrected to agree with the NASTRAN curve at the wing root, the wing tip would show NASTRAN about 15 percent stiffer than test which is similar to that of the previous tests.

WING LOAD-DEFLECTION COMPARISON

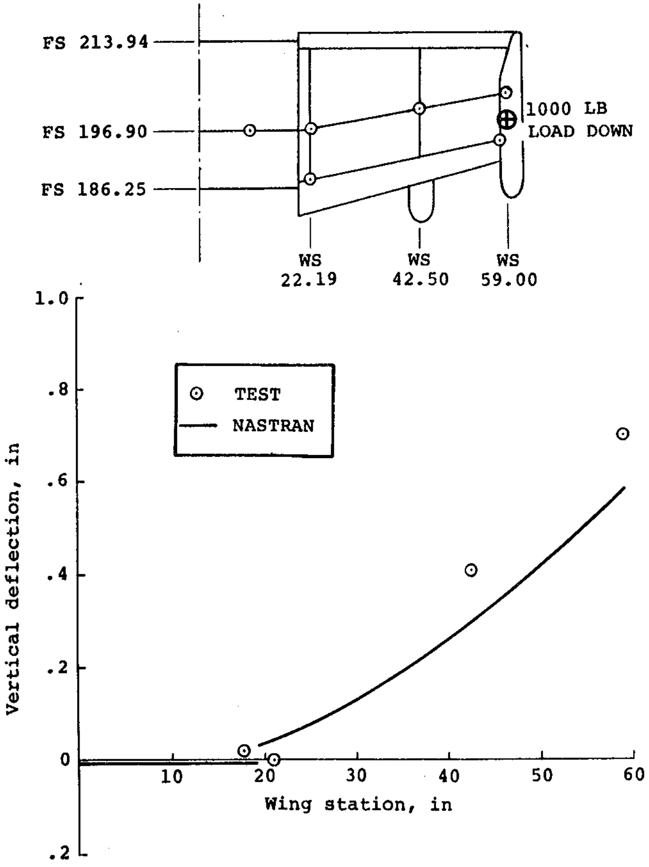

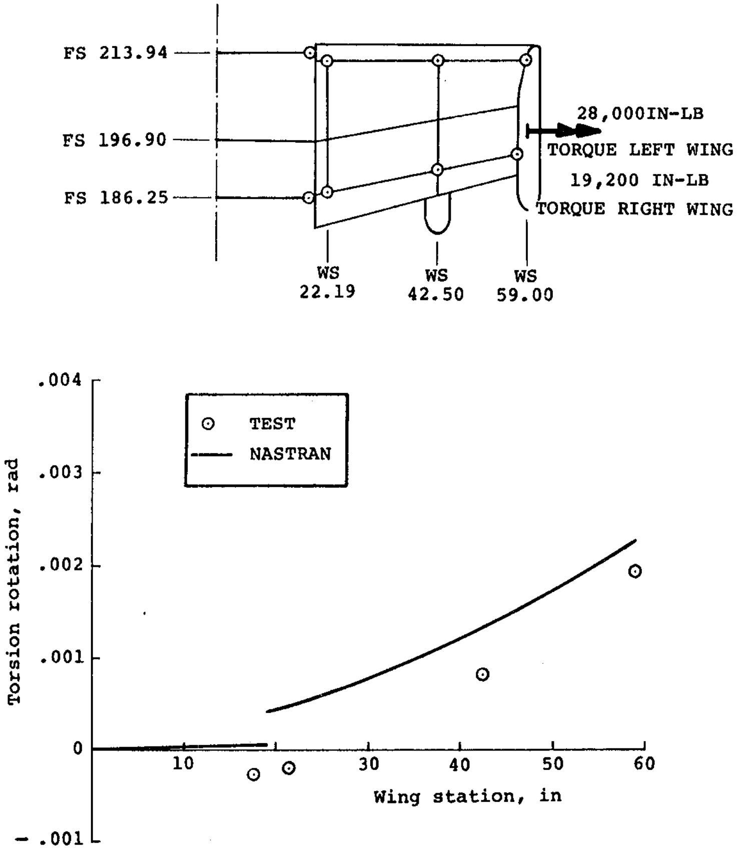

TAILBOOM STATIC TEST

The static load-deflection tests of the tailboom and vertical fin were conducted by the Mechanical Test Lab at Bell Helicopter Textron. The purpose of the tests was to validate the stiffness representation of the tailboom and vertical fin structure used in the NASTRAN math model.

The test article was the tailboom from the helicopter at Rock Island Arsenal that was used for the fuselage static testing, AH-1G ship number 15048. The basic structure of the tailboom was in good condition with only minor preparation, such as replacing fasteners for access doors, having to be done before testing.

The tailboom was mounted to a base fixture at the four fuselage attachment points at BS 41.32 for the tailboom and vertical fin loading conditions. Structure deflections up to 1.0 inch were measured with dial indicators. Deflections expected to be greater than 1.0 inch were measured with tube scales which were attached to the structure through a string and pulley arrangement. The small base rotation and translation deflections were measured electrically with strain-leaf indicators which were small cantilevers with strain-gaged flexures.

Three loading conditions were used in the tailboom testing: vertical, lateral, and torsion. The instrumentation for measuring base deflection and structure deflections was attached to a framework built around the tailboom and base and attached to ground.

The load fixture for the tailboom tests was located at BS 227. The maximum load for the vertical and lateral tests was 1000 lb. The maximum torque for the tailboom torsion test was 40,000 in-lb.

TAILBOOM STATIC TEST

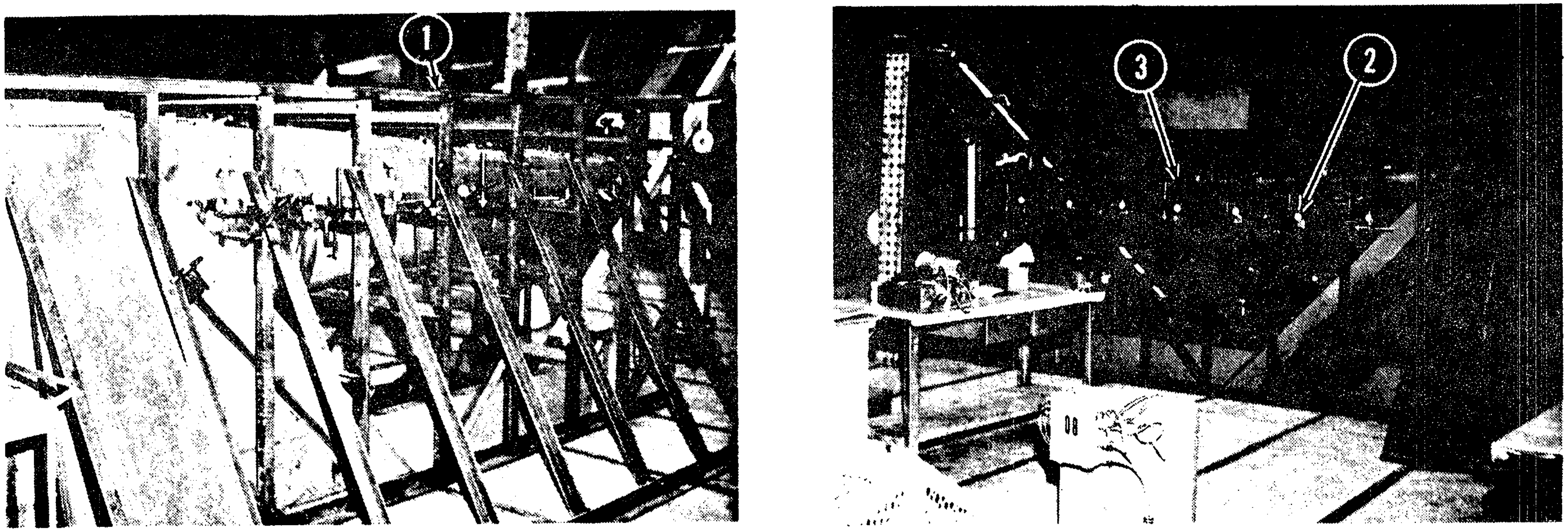

1 Indicator support fixture
2 Typical dial indicator (set for vertical deflection measurement
3 Tailboom installation

TAILBOOM VERTICAL LOAD-DEFLECTION COMPARISON

1. There is fairly good agreement between the NASTRAN and test results with NASTRAN being slightly softer - about 4 percent when compared to the average deflections at the aft end (BS 206). There were significant differences in the base rotations measured on the left hand and right hand sides which resulted in about a 14 percent variation in the deflections.

2. The curve shapes agree well, NASTRAN being slightly softer at the aft end of the tailboom.

TAILBOOM VERTICAL LOAD-DEFLECTION COMPARISON

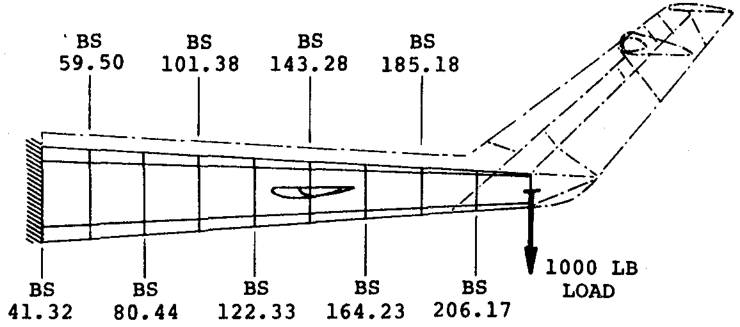
BS 59.50
BS 101.38
BS 143.28
BS 185.18
BS 41.32
BS 80.44
BS 122.33
BS 164.23
BS 206.17
1000 LB LOAD

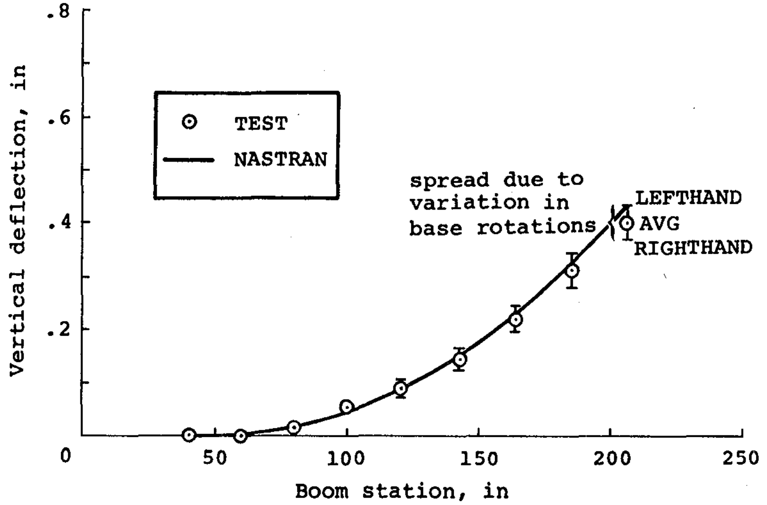

TAILBOOM LATERAL LOAD-DEFLECTION COMPARISON

1. As with the vertical loading, there is good agreement between NASTRAN and test results with NASTRAN slightly softer at the aft end of the tailboom (about 7 percent).
2. Again the curve shapes agree well, NASTRAN being slightly softer in the aft end.

TAILBOOM LATERAL LOAD-DEFLECTION COMPARISON

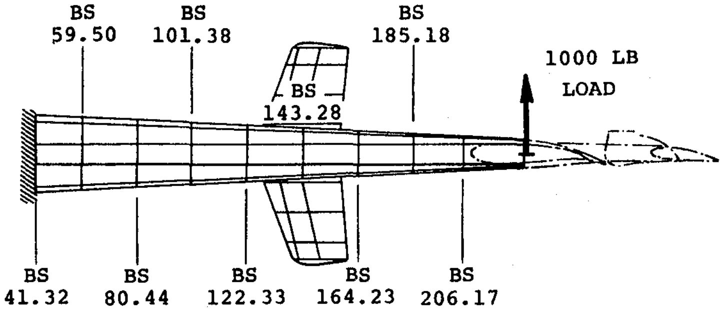
BS 59.50
BS 101.38
BS 143.28
BS 185.18
1000 LB LOAD
BS 41.32
BS 80.44
BS 122.33
BS 164.23
BS 206.17

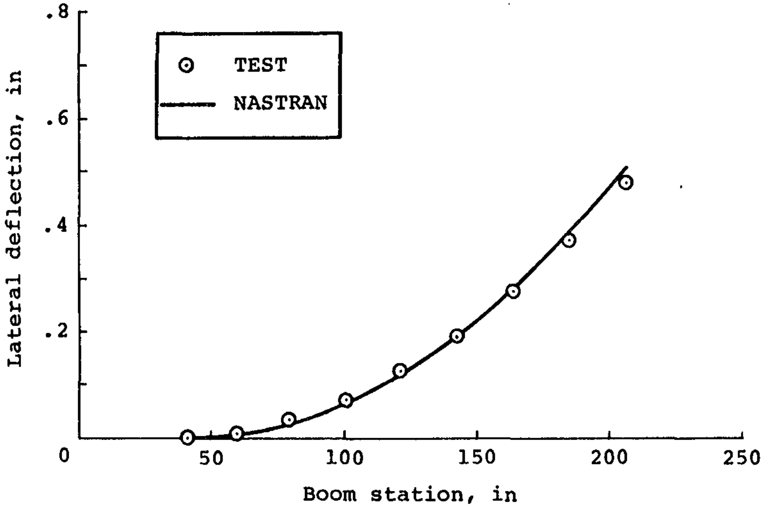

TAILBOOM TORSION LOAD-DEFLECTION COMPARISON

1. There is good agreement except at the aft end of the tailboom (BS 206). There was a large variation in the test data at that location as indicated by the band of measured rotations in the figure. Test varies from 19 to 45 percent stiffer than NASTRAN with the average being about 28 percent stiffer at BS 206.

2. The curve shapes agree well except for the BS 206 location.

TAILBOOM TORSION LOAD-DEFLECTION COMPARISON

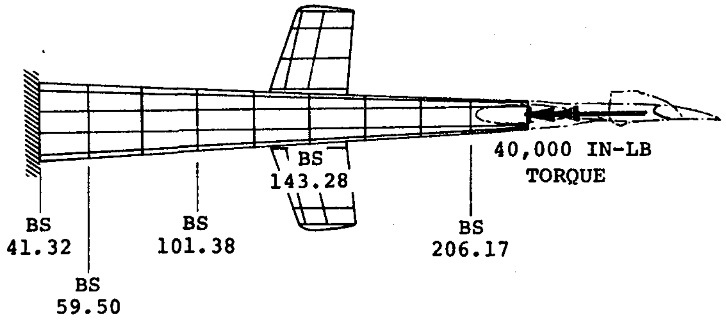
40,000 IN-LB
TORQUE
BS
41.32
BS
59.50
BS
101.38
BS
143.28
BS
206.17

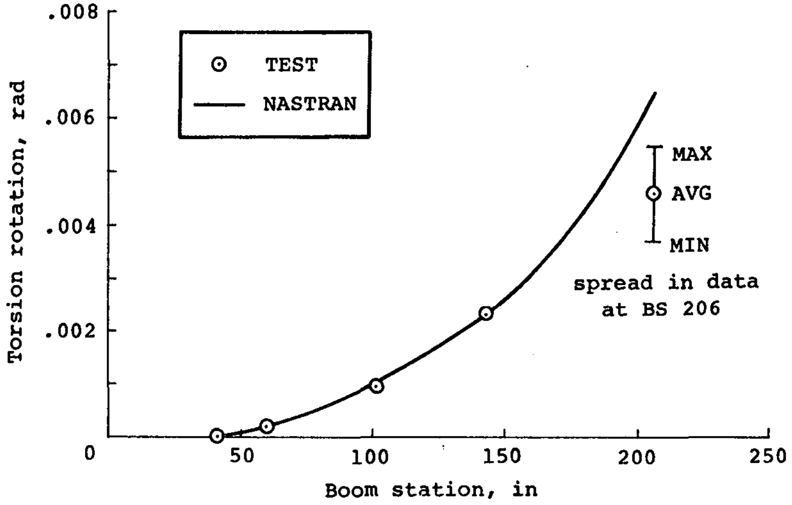

VERTICAL FIN STATIC TEST

Three loading conditions were used in the vertical fin testing: lateral, torsion, and chordwise. An instrumentation fixture was used for the vertical fin tests so that elastic deflection of the fin could be measured with respect to the base of the fin. Testing of the fin was not as extensive as the tailboom and only two sets of measurements were taken along the fin for each load condition.

Vertical fin loads were applied through the tail rotor gearbox and mast in the lateral, torsion, and chordwise directions. Maximum lateral and chordwise loads were 500 lb. The maximum fin torsion load was 13,000 in-lb.

VERTICAL FIN STATIC TEST

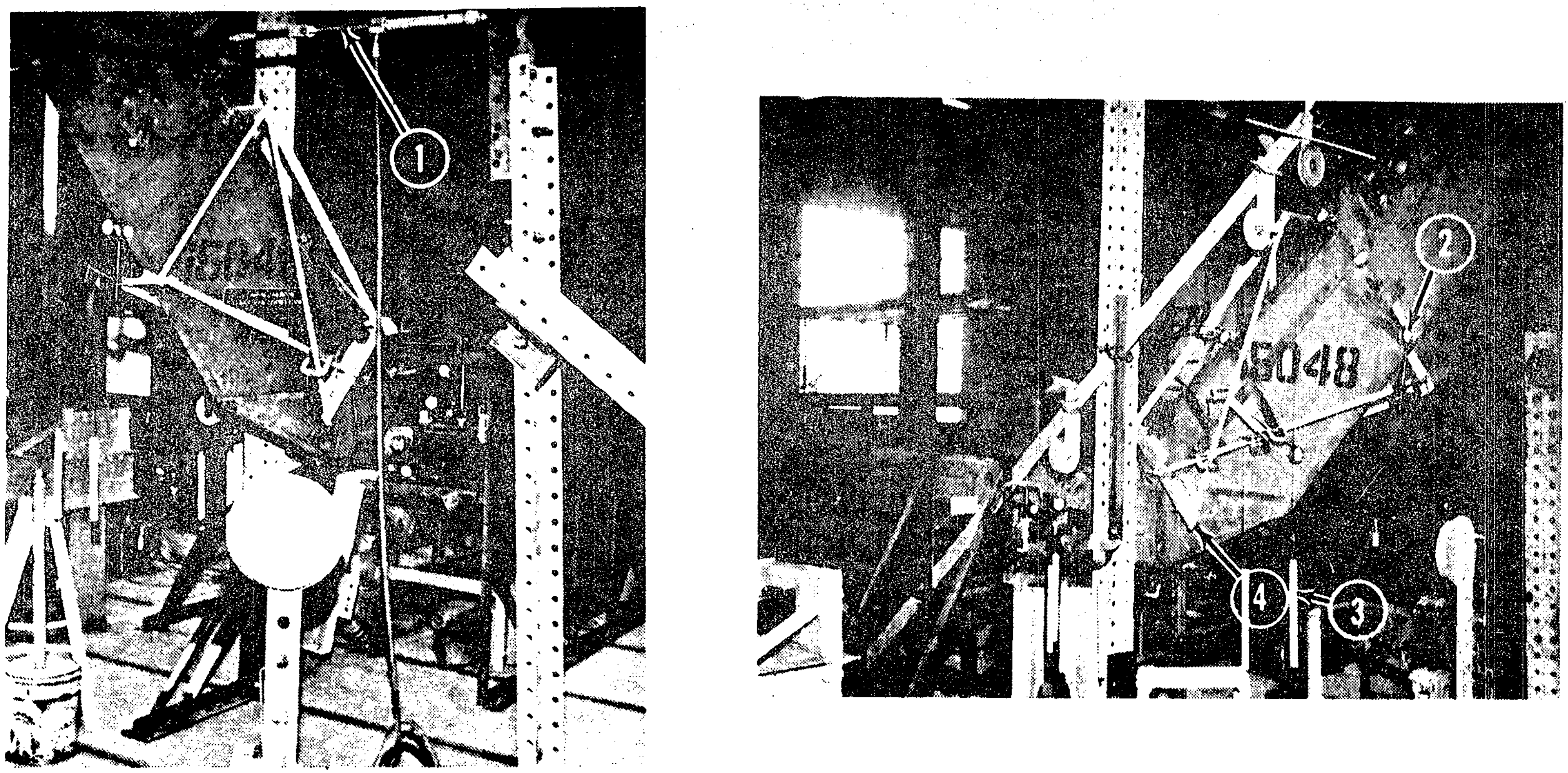

1 Hydraulic cylinder for applying load
2 Typical dial indicator - measures relative deflection
3 Tube scale - measures total deflection
4 Base for dial indicator fixture

FIN LOAD-DEFLECTION COMPARISON

Vertical Fin Lateral Load-Deflection Comparison

1. Deflections measured relative to the base of the fin are about 25 percent lower than NASTRAN.

2. There is good agreement when comparing the total deflections of the fin with respect to the tailboom base (NASTRAN results are about 3 percent softer than test).

3. The relative fin bending deflections are only about 10 percent of the total deflections at the top of the fin.

Vertical Fin Torsion Torque-Rotation Comparison

1. The test is considerably stiffer than NASTRAN (about 35 percent) for the torsional rotations of the fin.

Vertical Fin Chordwise Load-Deflection Comparison

1. The test gets stiffer towards the top of the fin when compared to NASTRAN. Test is about 20 percent stiffer at FNS 10.

2. The total vertical deflections with respect to the tailboom base show better agreement with test. Test was about 10 percent stiffer than NASTRAN.

FIN LOAD-DEFLECTION COMPARISON

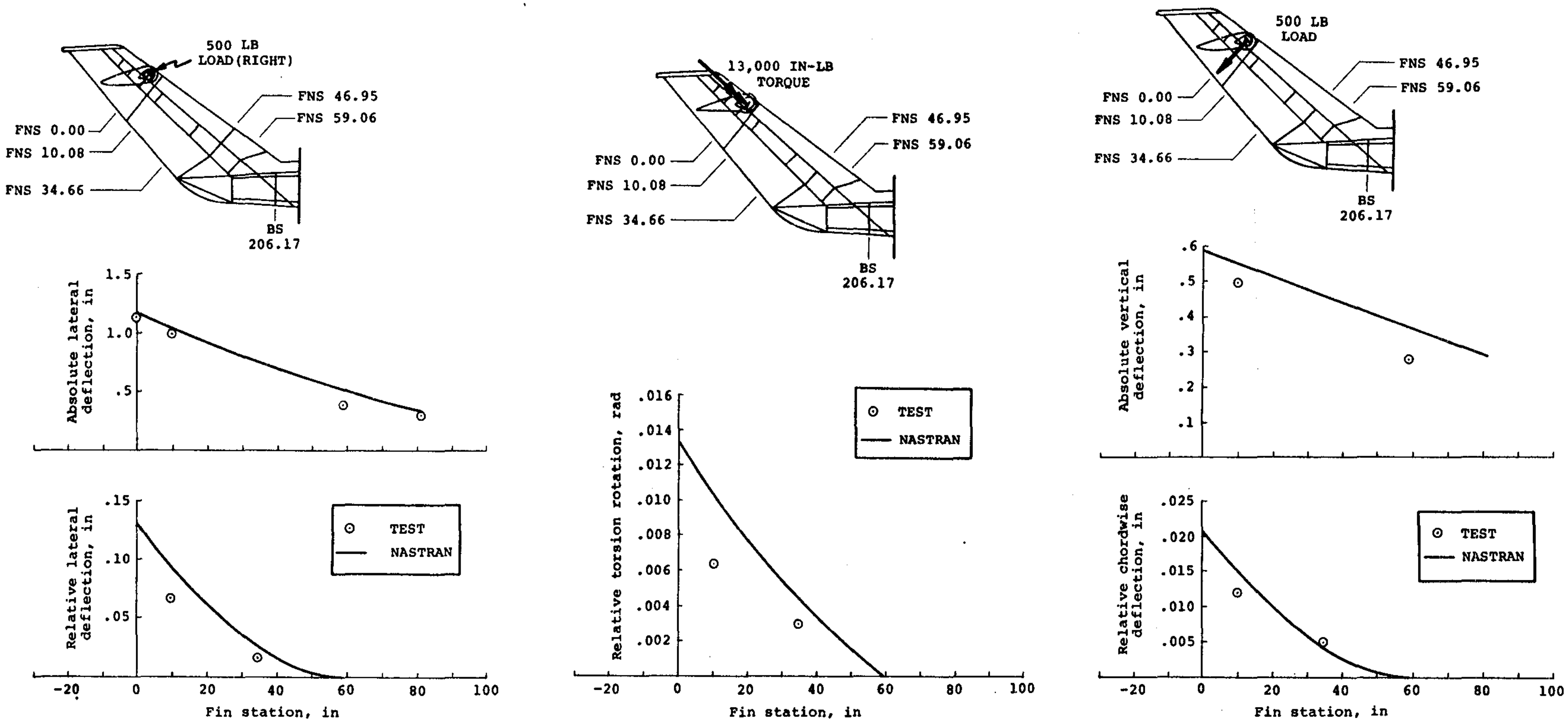

CONCLUSIONS - STATIC TESTING

For most of the fuselage static test comparisons, the NASTRAN results were about 15 percent stiffer than test. However, one of the tests (lateral) was rerun using two different methods of measuring deflections, LVDTs, and dial indicators. The dial indicators showed much better agreement with the NASTRAN analysis. The conclusion then is that the analysis is between 0 and 15 percent stiff.

For the tailboom static tests, the NASTRAN analysis, using fully effective skin for the representation of the semimonocoque sheet-stringer tailboom, showed good agreement with test. The analysis was generally about 0 to 5 percent softer than the average test values.

CONCLUSIONS - STATIC TESTING

- FUSELAGE STATIC TEST
  - NASTRAN UP TO 15% STIFFER THAN TEST
  - 15% DISCREPANCY IN MEASUREMENTS (LVDT VS DIAL INDICATORS)
- TAILBOOM STATIC TEST
  - NASTRAN UP TO 5% SOFTER THAN TEST
  - 100% EFFECTIVE SKIN USED ON TAILBOOM

4. GROUND VIBRATION TESTING

NASTRAN MODEL COMPARISON WITH GVT

The purpose of the study was to provide test data for evaluating a mathematical vibration model of the BHT AH-1G helicopter airframe. The math model was developed and analyzed using the NASTRAN structural analysis computer program.

Data from two independent dynamic tests were used for comparison with the math model as listed below:

1. Airframe vibration tests also conducted at BHT but under another contract, Army Contract DAAJ02-73-C-0105 (1975 - Ref. 5).
2. Airframe vibration tests conducted at Kaman Aerospace Corporation (KAC) (1980 - Refs. 6 and 7).

Dynamic test data was obtained from shake tests of the airframe and was used to evaluate the NASTRAN model for representing the low frequency (below 30 Hz) vibration response of the airframe. Since dynamic response must be calculated, both stiffness and mass modeling techniques are required. Stiffness modeling can be correlated directly from static load-deflection test data, but mass modeling can be correlated only indirectly with shake test data which contains both stiffness and mass effects. Good correlation between analytical and test results for both static and dynamic tests implies that both stiffness and mass modeling are correct. If only static test correlation is good, then the error should be in the mass modeling.

In general, the results of the comparisons show good agreement between the NASTRAN analysis and test. Problems encountered during the test data reduction and subsequent correlation are discussed.

NASTRAN MODEL COMPARISON WITH GVT

1. AIRFRAME GROUND VIBRATION TEST
    - a. BHT OPERATIONAL LOADS SURVEY (OLS)
    - b. KAC GROUND VIBRATION TESTS

COMPARE FREQUENCY RESPONSE TO EVALUATE MASS AND STIFFNESS MODELING UP TO 30 HZ

GROUND VIBRATION TEST (GVT) COMPARISONS

Correlation with shake tests was done to evaluate the NASTRAN model in light of the assumptions made, i.e., an elastic structural model aimed at representing the low frequency (below 30 Hz) vibration response of the airframe. Test results were obtained from shake tests conducted at BHT as a part of Army contract DAAJ02-73-C-0105 and at Kaman Aerospace Corporation (KAC) as a part of Army contract DAAJ02-77-C-0027.

The BHT shake testing was conducted on an AH-1G helicopter, ship number 28391. The helicopter was configured with clean wings (no stores) and with 325 lb rocket pods at the inboard store stations on the stub wings. These particular stores were chosen to be consistent with a flight test program done under contract DAAJ02-73-C-0105. The configuration with stores was tested in order to evaluate the effect of wing stores on airframe vibration.

The KAC shake testing was conducted on a U.S. Army AH-1G airframe, ship number 15683. The aircraft was tested with main rotor hub and blades removed. A substitute hub, weighing 230 lb, was used to suspend the airframe. Four configurations were tested, including three gross weights and two cg locations for the heaviest configuration. One clean wing and two wing store configurations were represented. The KAC vibration test comparisons are presented in the section following the BHT vibration test section.

Different values of modal damping were used in the NASTRAN analysis to determine an appropriate value for the comparison with test data. The criteria used for evaluating the amount of damping to be used was that the response near resonances should be higher than test results while trying to maintain a shape of the curve that was representative of the test curve. This is considered to be a conservative but representative method of determining the airframe vibration response analytically. In the response valleys, however, this approach would be unconservative since more damping generally increases the response in these areas. In a design analysis the effects of both low (up to 2 percent) and high (up to 5 percent) values of damping of the airframe structure modes should be considered; the low values of damping for evaluating near resonance responses and higher values of damping for evaluating response in the valleys.

The method of comparison between the shake tests and the NASTRAN analysis was to overlay frequency response data or forced response mode shape data for the same boundary conditions, applied force and response locations for test and analysis and comment on their agreement.

GROUND VIBRATION TEST (GVT) COMPARISONS

- SINUSOIDAL VIBRATION TESTING OF AH-1G
  - BELL HELICOPTER TEXTRON (OLS)
  - KAMAN AEROSPACE CORPORATION (KAC)
- FREQUENCY RESPONSE
- DAMPING EFFECTS

BHT AIRFRAME SINUSOIDAL VIBRATION TEST

The AH-1G helicopter was suspended from the main rotor hub by a long cable and soft bungee (the bungee was removed for the lateral and fore-and-aft hub shakes). The suspension system was intended to support the helicopter in a way that would allow free vibration of the airframe in the manner that it would vibrate in flight. The vertical mode of the helicopter on the suspension system with bungee was below 1.3 Hz and should not affect the airframe vibration response at higher frequencies (4 Hz and above). The main and tail rotors were replaced with dummy hubs that were ballasted to represent the rotor weights. Two helicopter weight configurations were tested: clean wing and inboard wing stores.

The shake tests were run with a single sinusoidal applied force and sweeping frequency from 2 to 40 Hz. NASTRAN frequency response results were used as a guide in the testing.

After a frequency sweep was completed, forced response mode shape data was obtained by dwelling at frequency response peaks. Response was measured by accelerometers distributed along the airframe. The excitation force was measured by transducers located between the airframe and the shaker.

Shaker locations and the suspension of the helicopter for the vertical and lateral tail shake tests and for the main rotor hub shake tests are shown in the figure. Note that the bungee is used for the vertical hub shake but the stiff cable alone is used for the lateral and longitudinal hub shake tests. This minimizes the effect of the suspension system on hub vibration when shaking horizontally at the hub. It was assumed that vertical response when shaking horizontally at the hub is not significant; otherwise the stiff cable suspension could affect the response.

Vertical and lateral excitations applied to the tail of the airframe were the principal shake tests used for evaluation of the NASTRAN model. However, comparisons with shake tests where the force is applied to the main rotor hub were also made. The structural dynamics characteristics of the soft-mounted pylon that depend on its loading or mounting nonlinearities were expected to cause significant discrepancies between the test results and NASTRAN math model results since the math model does not include effects of large motions (differential stiffening or "pendulum" stiffening) or material nonlinearities in the elastomeric mounts. Shaking at the main rotor hub through the pylon would then result in an excitation to the airframe structure that is not as well defined as it would be when shaking at the tail. However, shaking at the hub is of interest in determining in-flight airframe vibration response. The exciting force from the main rotor is at the hub and one would like to know the transfer function between the excitation at the hub and response at locations on the airframe.

BHT AIRFRAME SINUSOIDAL VIBRATION TEST

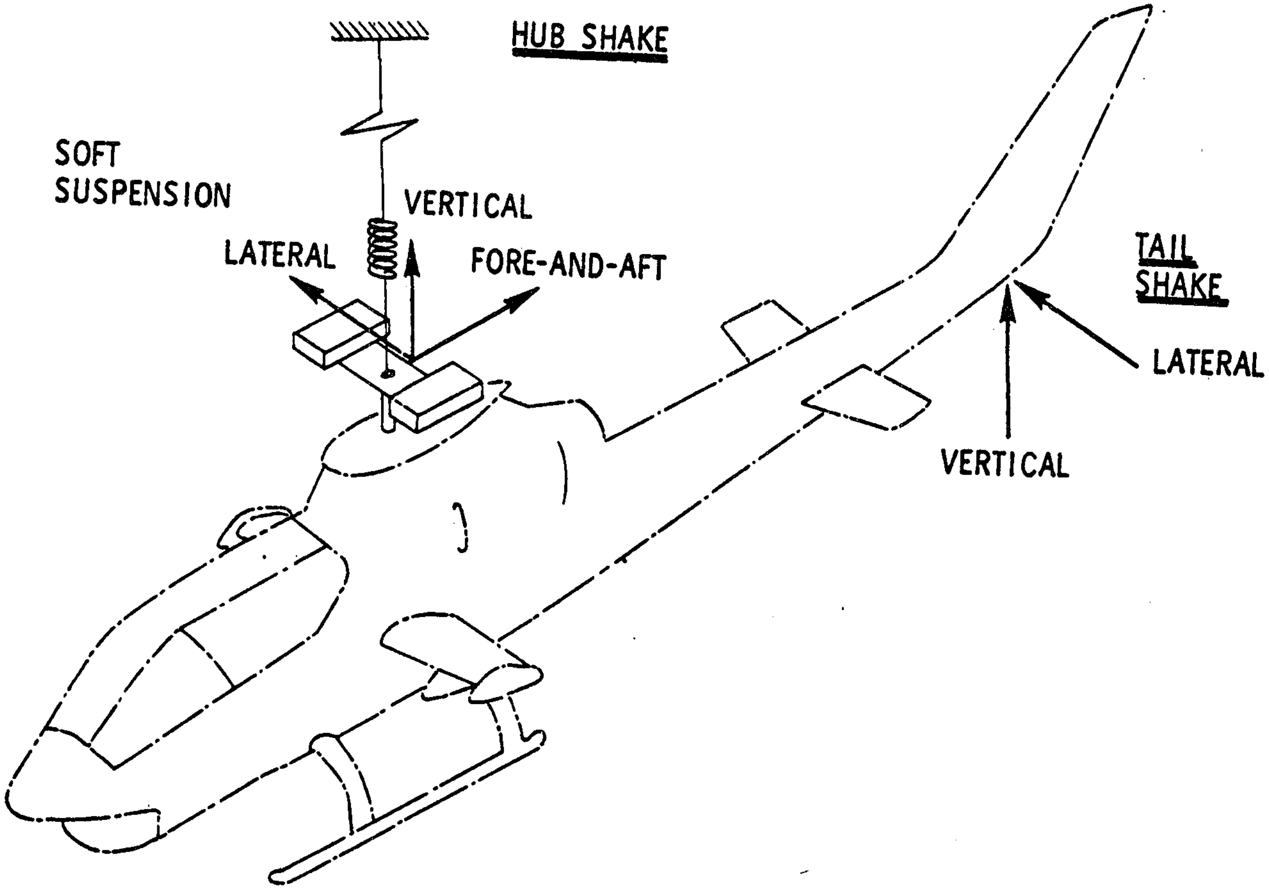
HUB SHAKE
SOFT SUSPENSION
VERTICAL
LATERAL
FORE-AND-AFT
TAIL SHAKE
LATERAL
VERTICAL

BHT VIBRATION TEST SETUP

Accelerometer and force transducer data were reduced on-site to monitor the testing and off-site to obtain complete results for correlation with the NASTRAN analysis.

The on-site data reduction was used to monitor the testing and check the digital data reduction technique. Frequency response plots were made for a few accelerometers. These plots along with a mode shape meter were used to locate frequencies upon which to dwell for taking forced response mode shape data.

The mode shape meter visually displays the relative response of several accelerometers along the airframe and allows quick identification of modes without having to guess or feel the structure by hand. No data were recorded from the mode shape meter.

The off-site data reduction procedure was used to generate the test data used for correlation. This procedure involved digitizing the on-board analog FM tapes on which the accelerometer and force transducer signals were recorded and then digitally analyzing the data to generate frequency response (magnitude and phase) plots and forced response mode shape plots. These plots were then used directly for comparison with the NASTRAN analysis.

Frequency response plots from the on-site system were compared to the off-site digital data reduction system to verify the digital technique. Plots for response locations at the nose, tail, and hub (hub shakes only) were compared and showed that the shape of the frequency response magnitudes were always in good agreement, but there was sometimes a steady shift between the two curves. Since the magnitudes were plotted on logarithmic scale this indicated the difference was a constant multiplying factor which could have occurred in calibration of the digital data. No shifts occurred in the tail shake test data, but a few shifts did occur in the hub shake test data.

BHT VIBRATION TEST SETUP

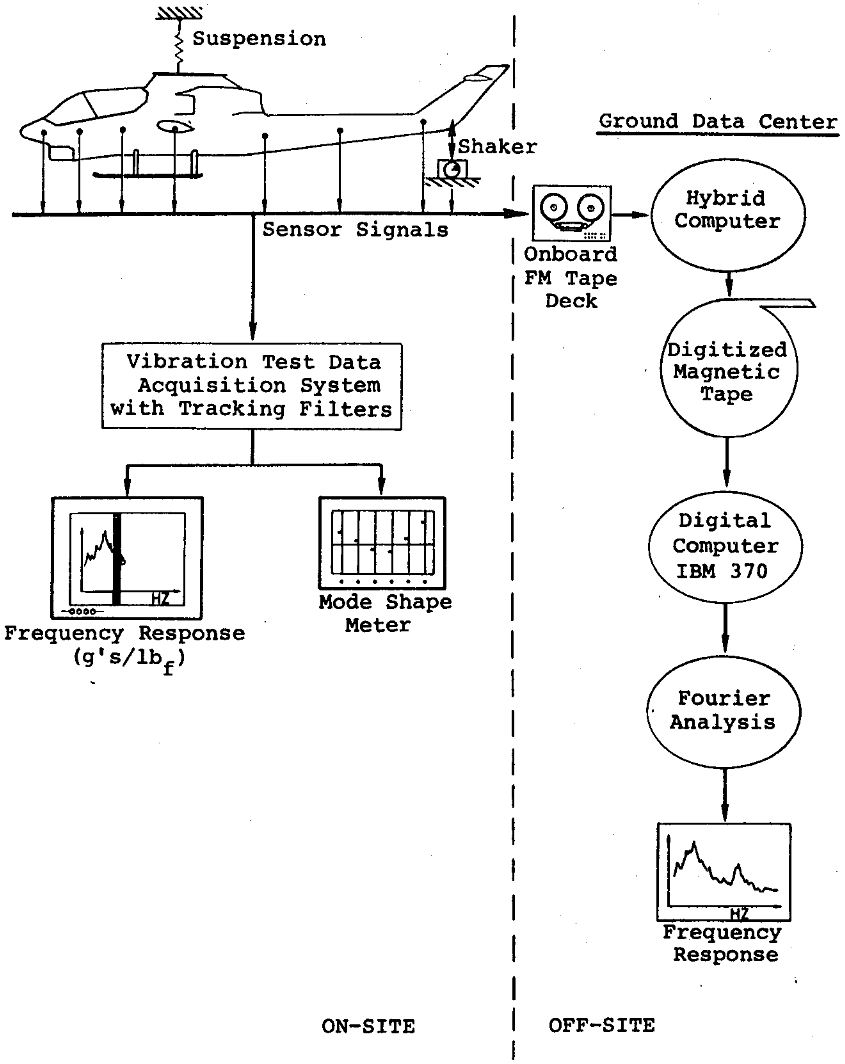
Suspension
Shaker
Sensor Signals
Ground Data Center
Onboard FM Tape Deck
Hybrid Computer
Digitized Magnetic Tape
Digital Computer IBM 370
Fourier Analysis
Vibration Test Data Acquisition System with Tracking Filters
HZ
Frequency Response (g's/lb_f)
Mode Shape Meter
HZ
Frequency Response
ON-SITE
OFF-SITE

BHT SHAKE TEST ACCELEROMETER LOCATIONS

Accelerometers were used for measuring vibration response of the airframe. Accelerometer locations were selected to correspond as closely as possible to grid point locations in the NASTRAN model to facilitate correlation.

BHT SHAKE TEST ACCELEROMETER LOCATIONS

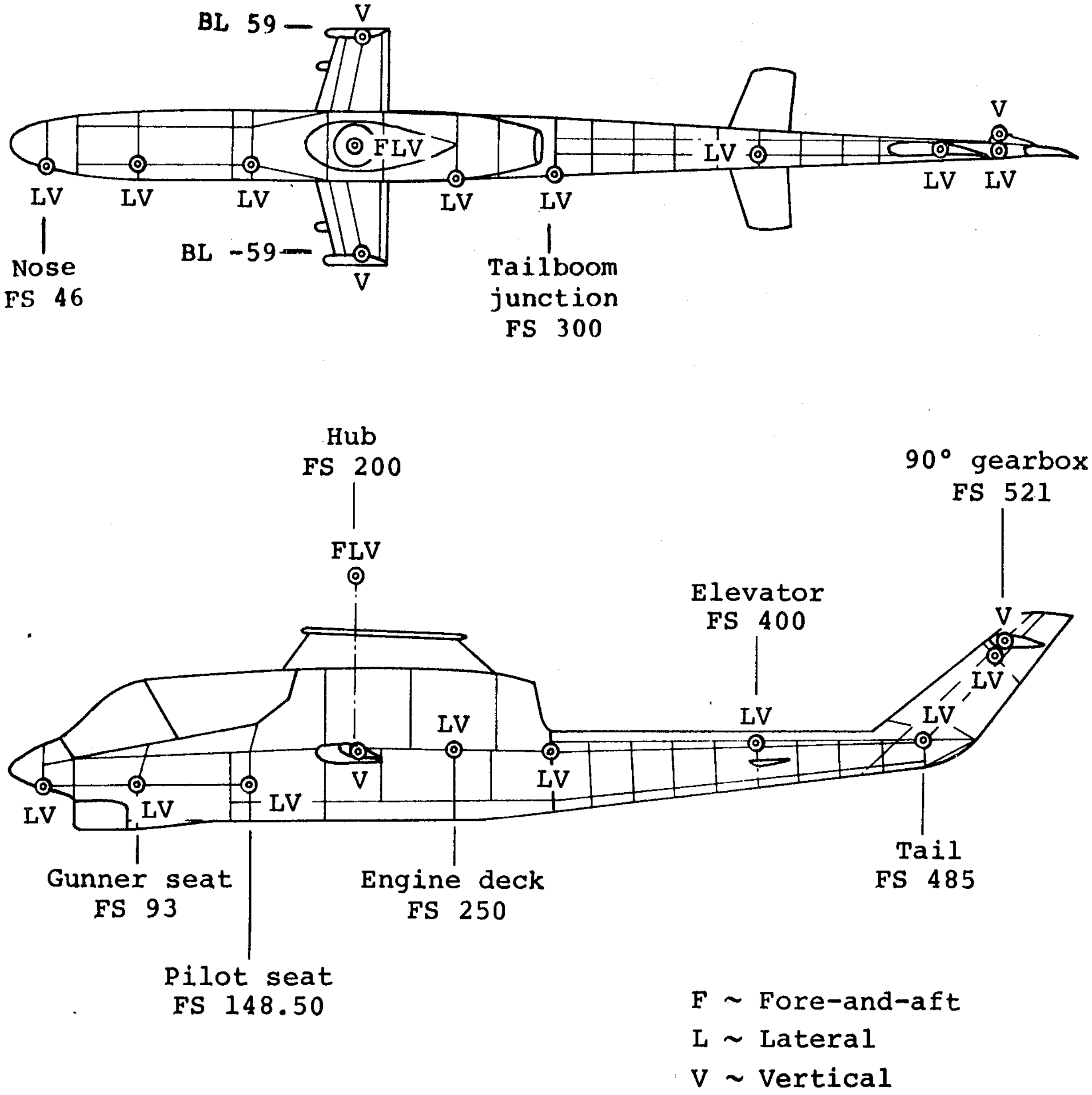
BL 59
V
FLV
V
LV
LV
LV
LV
LV
LV
LV
LV
Nose
FS 46
BL -59
V
Tailboom
junction
FS 300
Hub
FS 200
FLV
90° gearbox
FS 521
Elevator
FS 400
V
LV
LV
LV
LV
V
LV
LV
LV
LV
Tail
FS 485
Gunner seat
FS 93
Engine deck
FS 250
Pilot seat
FS 148.50
F ~ Fore-and-aft
L ~ Lateral
V ~ Vertical

BHT FREQUENCY RESPONSE COMPARISON - VERTICAL

Vertical Tail Shake - Clean Wing

1. Response amplitudes, shape and peaks agree well through main rotor four-per-rev (21.6 Hz). At higher frequencies, the measured forward responses (farthest from excitation) are reduced while the aft response points (nearest the excitation) remain high. Attenuation of the force by the intervening structure between the excitation point and the forward response locations is suspected.

2. The NASTRAN pylon fore-and-aft rocking mode at 3 Hz is lower than test (about 4 Hz). This is probably due to "pendulum" stiffening (differential stiffness) of the pylon caused by suspending the helicopter at the hub in a gravity field. This effect is not represented in the NASTRAN model.

Vertical Tail Shake - With Stores

1. As in the clean wing configuration, test and analysis responses agree well.

2. The wing stores do not have a big effect on the response. The lowest NASTRAN wing frequency is calculated to be at 21.5 Hz and does not show up strongly in the NASTRAN or test curves. There is a store mode (probably a store sway mode) with weak response in a valley at about 11 Hz on the test curve. This mode shows up much stronger in the lateral shake test. The NASTRAN model had the stores rigidly attached to the wing and would not represent this mode.

Hub Vertical Shake

1. Except for the 1st vertical bending mode, the test data is relatively flat and does not show as much response as NASTRAN.

2. The test curves look rather rough and "noisy."

3. The suspension system, excitation apparatus, or dummy hub might be affecting the response. An instrumentation or data reduction problem or some transient dynamics in the pylon system is suspected.

Hub Longitudinal Shake

1. The NASTRAN response is relatively flat compared to the test data because the dynamics of the cable suspension system are not represented in the math model.

BHT FREQUENCY RESPONSE COMPARISON - VERTICAL

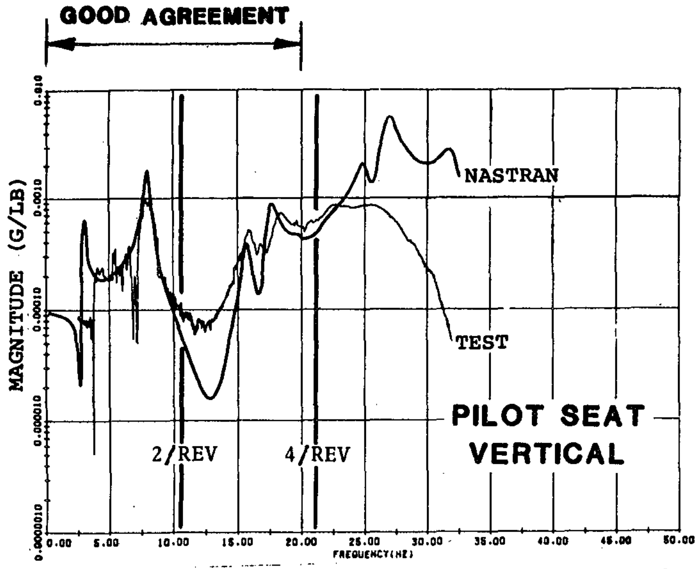

TAIL VERTICAL SHAKE - CLEAN WING

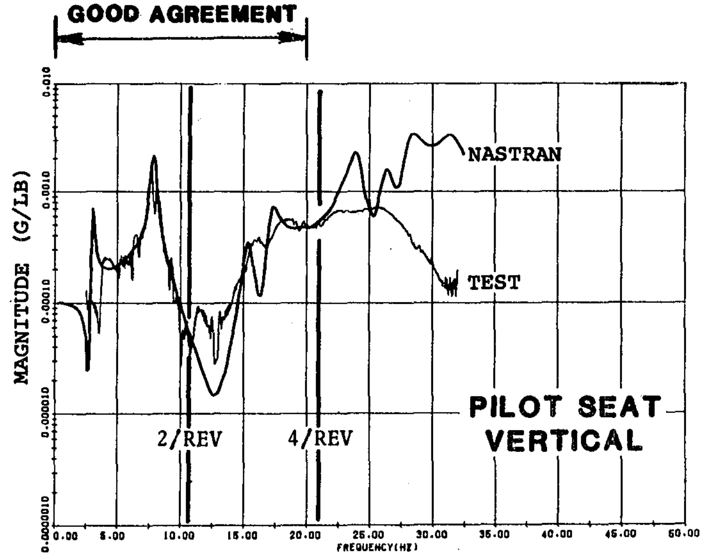

TAIL VERTICAL SHAKE - WING STORES

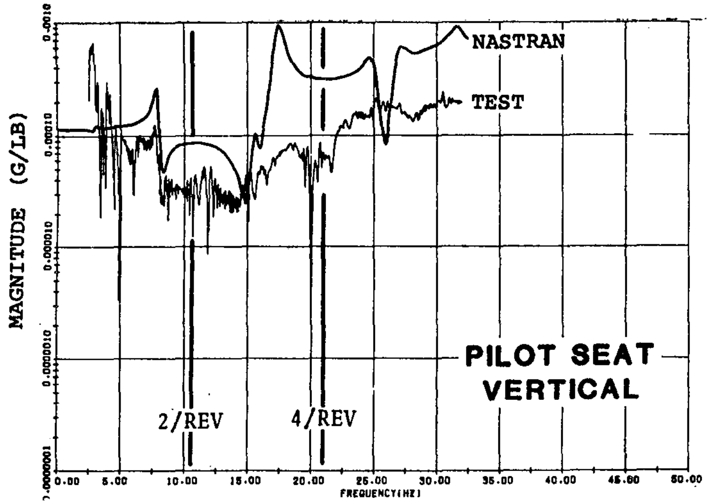

HUB VERTICAL SHAKE - CLEAN WING

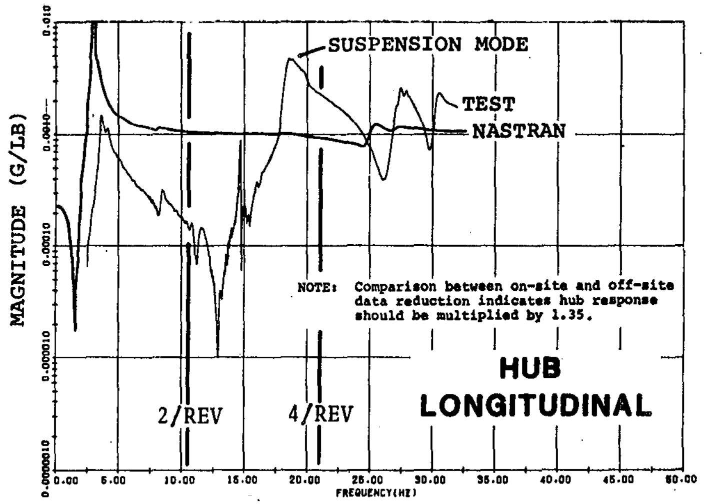

NOTE: Comparison between on-site and off-site data reduction indicates hub response should be multiplied by 1.35.

HUB LONGITUDINAL SHAKE - CLEAN WING

BHT FREQUENCY RESPONSE COMPARISON - LATERAL

Lateral Tail Shake - Clean Wing

1. Response amplitudes and shape agree well except in the area of the fuselage torsion/wing yaw mode which amplifies the NASTRAN response in the 20 to 25 Hz range. This mode is suspected to be a weak mode at 22.5 Hz that appears to be highly damped on the test curve.

Lateral Tail Shake - With Stores

1. The store mode mentioned in the vertical tail shake comparison shows up strong at 11 Hz and would not be represented in the NASTRAN model.

2. Except for the store mode at 11 Hz, curves agree well.

Hub Lateral Shake

1. The pylon roll mode is at 5 Hz for the test compared to 4 Hz calculated by NASTRAN. The difference is probably due to "pendulum" stiffening effects on the soft-mounted pylon not represented in the NASTRAN model.

2. The lateral hub response test curves show a very strong mode at 19 Hz that is not in the NASTRAN model. This is probably a suspension mode or a mode of the dummy hub, neither of which is modeled in NASTRAN.

3. The airframe response amplitudes apparently agree well but it is probably just a coincidence. The effect of the pylon dynamics were expected to cause force attenuation and result in a highly damped looking response of the airframe at higher frequencies. That the high airframe response amplitudes agree fairly well with NASTRAN in the 15 to 25 Hz range could be due to the effect of the high hub response at 19 Hz cancelling the effect of force attenuation through the pylon.

BHT FREQUENCY RESPONSE COMPARISON - LATERAL

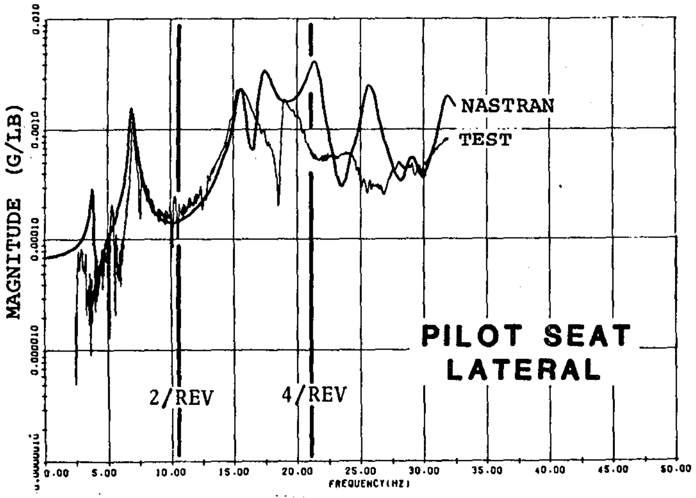

TAIL LATERAL SHAKE – CLEAN WING

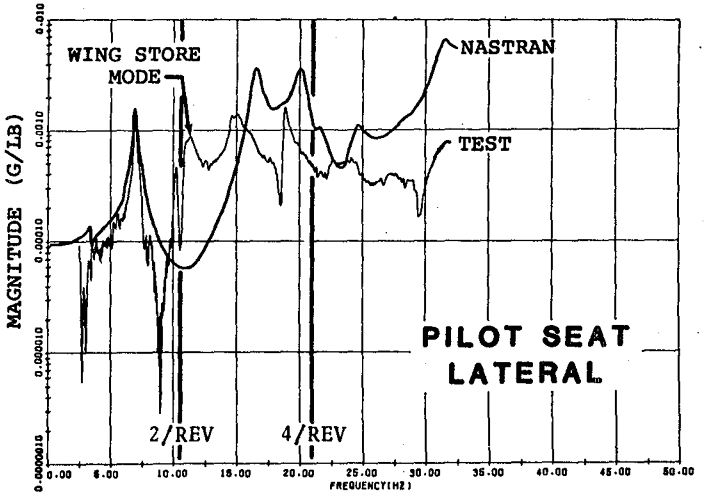

TAIL LATERAL SHAKE – WING STORES

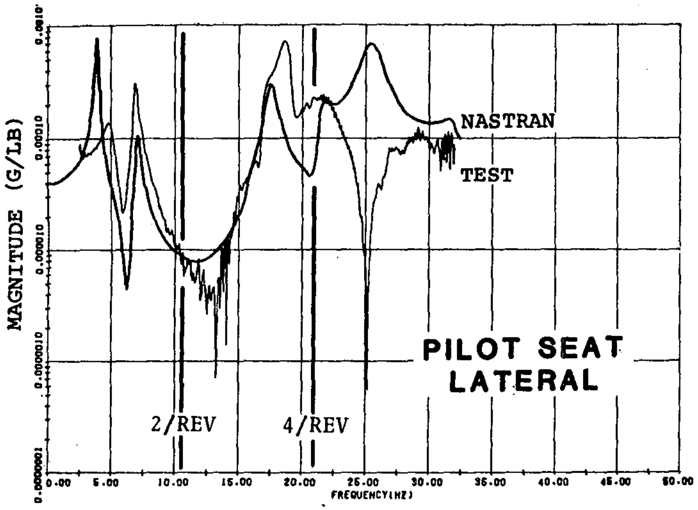

HUB LATERAL SHAKE – CLEAN WING

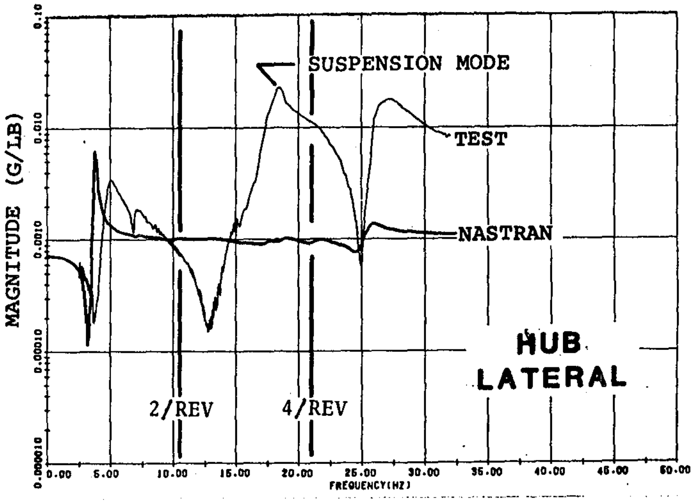

HUB LATERAL SHAKE – CLEAN WING

BHT NATURAL FREQUENCY COMPARISON

A comparison of the natural frequencies obtained from the BHT shake test measured modal response and NASTRAN fuselage FEM calculated modal response is made in this figure. The frequencies are in good agreement up to four-per-rev (21.6 Hz). This is consistent with the agreement in the transfer functions shown in the previous two figures.

BHT NATURAL FREQUENCY COMPARISON

VERTICAL TAIL SHAKE - CLEAN WING

MODE	TEST	NASTRAN
MAIN ROTOR PYLON FORE AND AFT ROCKING (PYLON PITCH)	3.9	3.0
FIRST FUSELAGE VERTICAL BENDING	8.0	8.0
FUSELAGE TORSION	15.5	15.7
SECOND FUSELAGE VERTICAL BENDING	18.0	17.5
THIRD FUSELAGE VERTICAL BENDING	-	25.0

LATERAL TAIL SHAKE - CLEAN WING

MODE	TEST	NASTRAN
FIRST FUSELAGE LATERAL BENDING	7.1	7.2
FUSELAGE TORSION	15.5	15.7
SECOND FUSELAGE LATERAL BENDING	18.9	17.5
FUSELAGE ROLL / ENGINE LATERAL	-	18.8
FUSELAGE TORSION / WING YAW	-	21.5
MAIN ROTOR MAST LATERAL BENDING	-	25.3
THIRD FUSELAGE LATERAL BENDING	24.4	25.8

BHT FORCED RESPONSE MODE SHAPE COMPARISON

When comparing frequency response results, the frequency placement of peaks, overall amplitudes of response, and curve shape representation of the test curve by the NASTRAN analysis were primarily considered. The phase relationship was sometimes useful in locating resonances but was more difficult to compare than magnitudes and was often jumping back and forth between ±180 degrees.

Forced response mode shapes were helpful in finding correspondence between peaks of the test and NASTRAN curves. Sample comparisons of forced response mode shapes for the lateral and vertical tail shake of the clean wing configuration are shown in the figure. The NASTRAN forced response mode shape was determined by normalizing everything with respect to the tail when the tail response was maximum for comparison with the BHT test data.

BHT FORCED RESPONSE MODE SHAPE COMPARISON

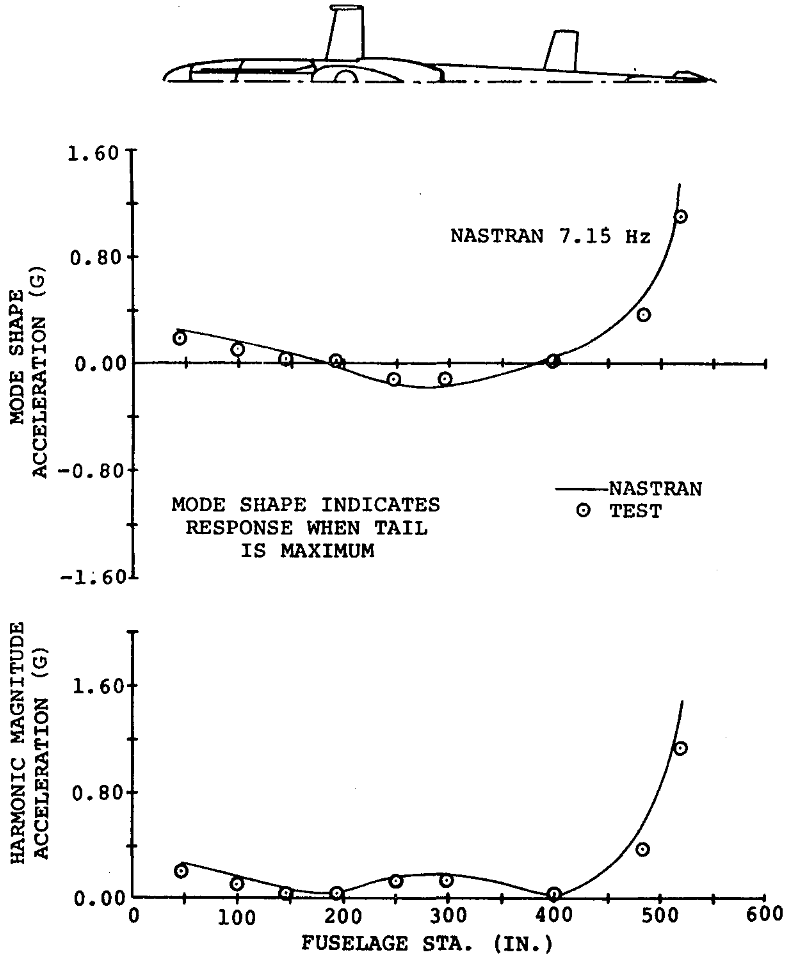

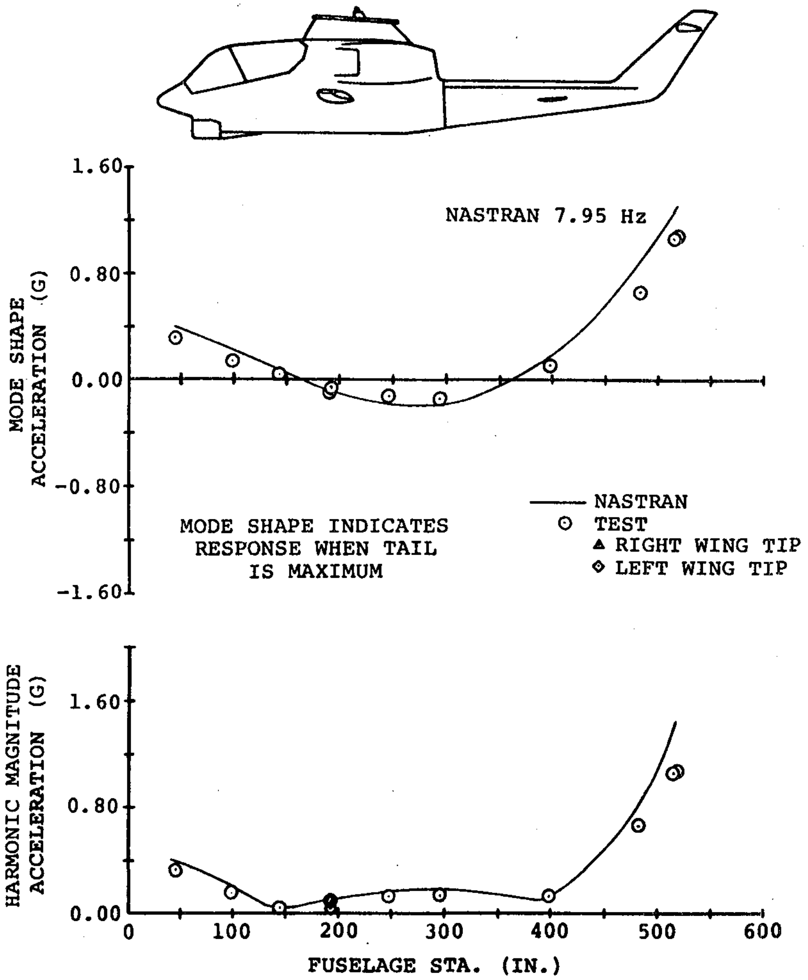

KAMAN SINUSOIDAL GROUND VIBRATION TEST COMPARISON

This section contains a brief description of AH-1G ground vibration tests conducted by Kaman Aerospace Corporation (KAC) and comparisons of the KAC test data with previous ground vibration tests done at Bell Helicopter under the U.S. Army's Operational Load Survey (OLS) program (Ref. 1) and the dynamic NASTRAN FEM of the AH-1G (Ref. 3). This work was undertaken as part of NASA contract NAS1-17496 to provide for a more complete assessment of the AH-1G NASTRAN vibrations model idealization through comparisons with other well documented ground vibration test data.

Frequency response (0 - 30 Hz), natural frequencies and mode shapes for three gross weight (GW) configurations of U.S. Army AH-1G ship number 15683 were conducted:

1. Low GW (clean wing), 7730 lb., cg Sta. 196.3
2. Mean GW (outboard wing stores), 8350 lb., cg Sta. 196.3
3. High GW (outboard and inboard wing stores), 8780 lb., cg Sta. 196.3

Comparisons of response amplitude versus frequency for the low GW configuration are given in this section. Both the KAC test data along with the OLS data are presented for direct comparison. In addition, forced response mode shapes at natural frequencies are presented. Appendix A contains amplitude and phase comparisons between the KAC test data and the NASTRAN analysis for all three gross weight configurations. Natural frequency comparisons between NASTRAN and the KAC test data for major modes are also tabulated in Appendix A.

KAMAN SINUSOIDAL GROUND VIBRATION TEST COMPARISON

- VIBRATION TEST SETUP
- FREQUENCY RESPONSE COMPARISON - NASTRAN VS TEST
  - RESPONSE AMPLITUDE VS FREQUENCY, 0 - 30 HZ
  - KAMAN AND OLS TEST COMPARISONS
  - CLEAN WING (LOW GW) CONFIGURATION
- NATURAL FREQUENCY COMPARISON
- MODE SHAPE COMPARISONS
- CONCLUSIONS
- APPENDIX - FREQUENCY RESPONSE (AMP & PHASE) COMPARISONS FOR LOW, MEAN, AND HIGH GW CONFIGURATIONS

KAC AIRFRAME SINUSOIDAL VIBRATION TEST

The Kaman Aerospace Corporation (KAC) shake testing was done in their full size test rig. The suspension and shake test system were designed to perform both single point excitation (calibration and ground vibration testing) and multi-point excitations (ground flying testing). The information and correlation efforts reported here are only for ground vibration single point excitation at the tail rotor gearbox in the lateral direction (FS 521) and at the tail skid location in the vertical direction (FS 485). Eight accelerometers were used to acquire the measured data.

Extensive work was done by KAC to assess the accuracy of the results for frequency domain transfer function measurements. Several excitations were performed at each shaker location to determine the global natural frequency and damping parameters of the test vehicle. The magnitude of the excitation force was chosen to avoid response nonlinearities and residual mode effects. The excitation was achieved by applying pure sine wave signals to the electromagnetic shaker and varying the frequency of the sine waves over the range spanned by the desired bandwidth.

After a frequency sweep was completed, forced response mode shape data was obtained by dwelling at frequency response peaks. The forced response mode shape data was measured by accelerometers distributed throughout the airframe. The excitation force was measured by transducers located between the airframe and the shaker.

KAC AIRFRAME SINUSOIDAL VIBRATION TEST

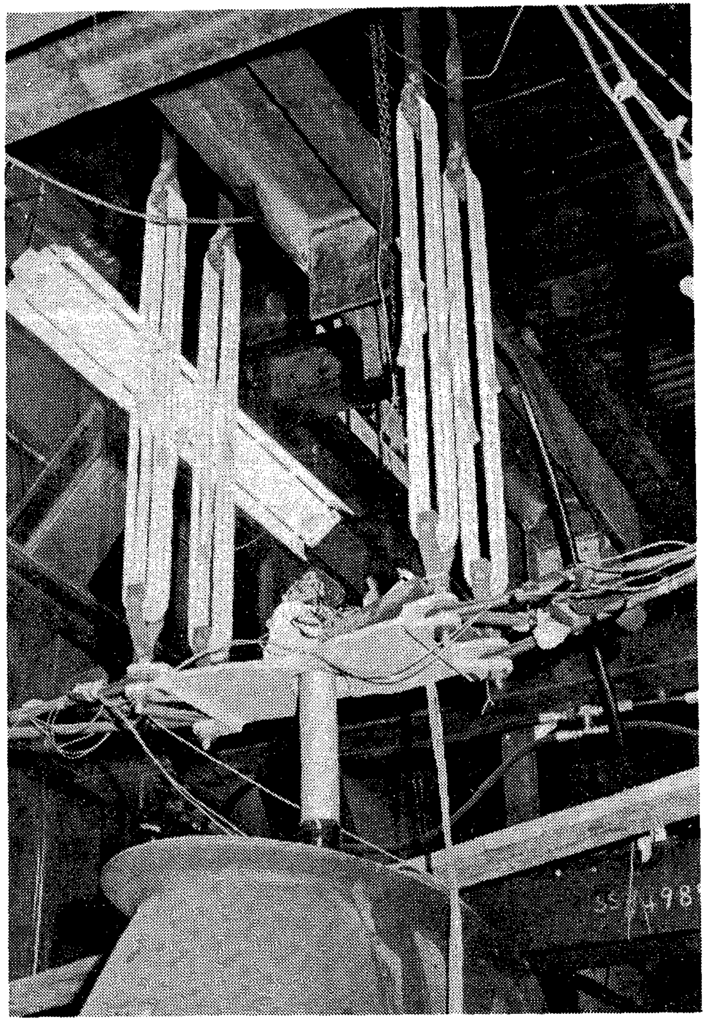

Suspension System

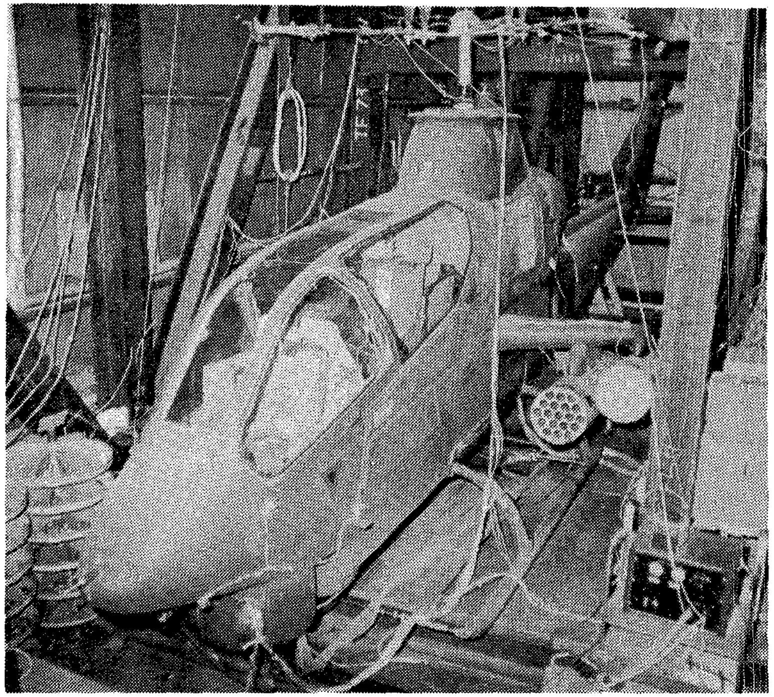

AH-1G Test Article

KAC AIRFRAME SINUSOIDAL VIBRATION TEST SETUP

Accelerometer and force transducer data were reduced on-site to monitor the testing and off-site to obtain complete results for correlation with the NASTRAN analysis.

Details of the shake test fixture and calibration testing are given in Reference 7. The helicopter was suspended as a free body by soft rubber bungee chords. The figure shows a configuration with the shaker positioned for vertical excitation at the tail and the response accelerometer at the horizontal stabilizer station. Signals for driving the electromagnetic shaker originate from the signal generator. A gage installed at the point of force application generates voltage signals proportional to the applied force. These signals are input to the dual channel signal analyzer along with the accelerometer voltage signals which are proportional to the response acceleration.

The signal analyzer samples the time domain force and response signals, digitizes them and computes the real-time Fourier transforms of the data. The analyzer also computes a least squares estimate, between the force and response inputs, of the frequency domain resultant transfer functions. The functions computed by the analyzer were stored on cassette tapes for off-site data retrieval, reduction and analysis. The time domain signals from the force and response transducers were passed from the digital signal analyzer to the oscilloscope for on-site monitoring.

The frequency counter provided a means to precisely measure the frequencies of harmonic signals whenever needed.

KAC AIRFRAME SINUSOIDAL VIBRATION TEST SETUP

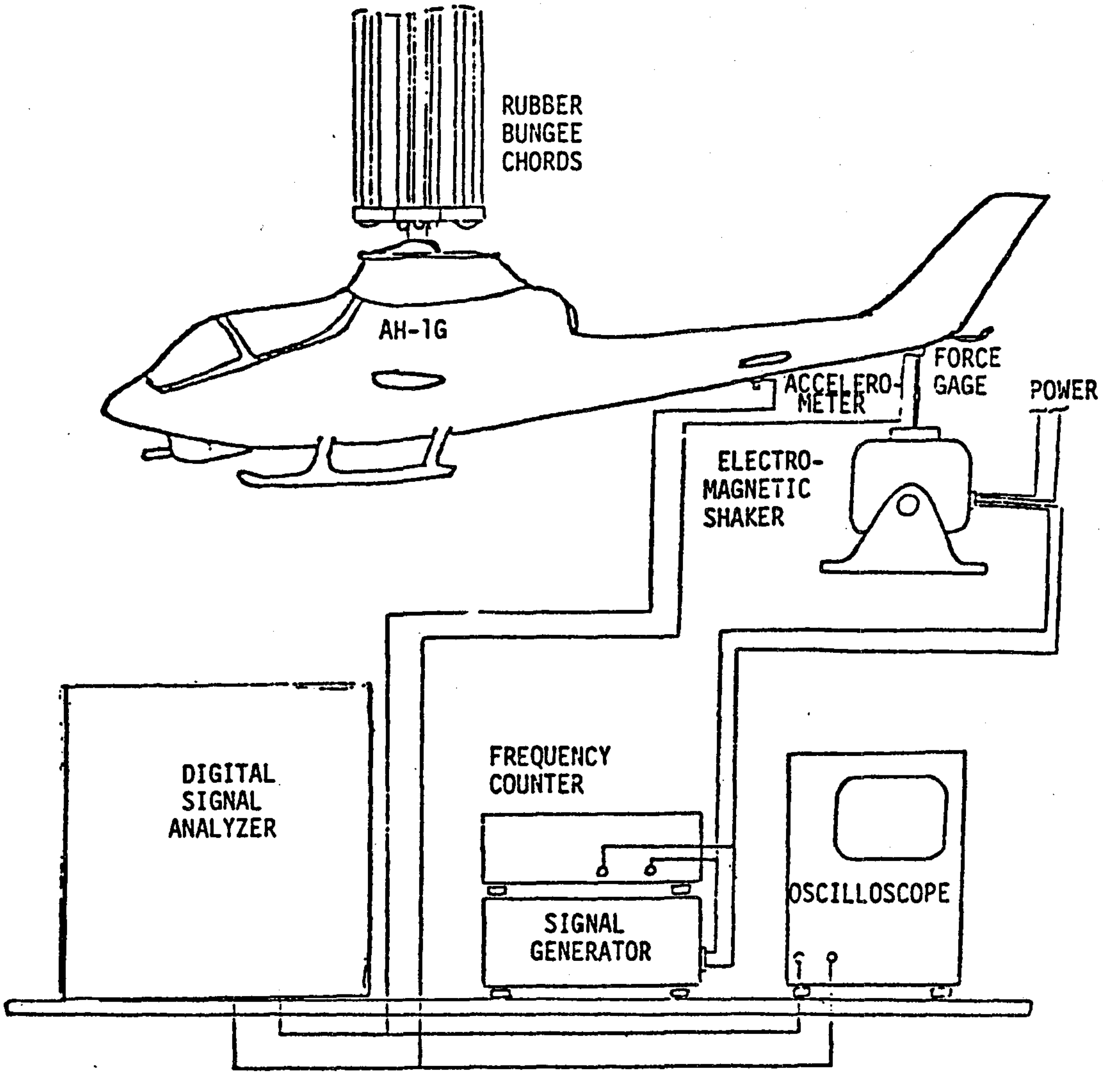
RUBBER
BUNGEE
CHORDS
AH-1G
ACCELERO-
METER
FORCE
GAGE
POWER
ELECTRO-
MAGNETIC
SHAKER
DIGITAL
SIGNAL
ANALYZER
FREQUENCY
COUNTER
SIGNAL
GENERATOR
OSCILLOSCOPE

KAMAN SHAKE TEST ACCELEROMETER LOCATIONS

Kaman Aerospace Corporation had eight transducers on the AH-1G test vehicle which read continuous data for calibrating the system. These accelerometers were used to obtain structural mobilities or transfer functions, system damping and natural frequency global parameters. Their locations are shown on the figure below. A table is shown here relating the test accelerometers to the closest existing NASTRAN grid points.

KAC ACCELEROMETER	NASTRAN GRID	DIRECTION	LOCATION
1. Y46L	4637	Lat.	Nose, Sta. 46
2. Z50	3339	Vert.	Nose, Sta. 50
3. Z195B	19765	Vert.	C.G., Sta. 195
4. Z202L	75921	Vert.	LH Wing Tip, Sta. 202
5. Z202R	65921	Vert.	RH Wing Tip, Sta. 202
6. Z400	40145	Vert.	Elevator, Sta. 400
7. Z485	48845	Vert.	End of Tailboom, Sta. 485
8. Y521	520079	Lat.	Tail Rotor Gearbox, Sta. 521

The relative small number of KAC frequency response points and directions recorded limits the availability of response plots for direct comparison between KAC and OLS test data. Five locations are comparable for vertical excitation at the tail skid and only three locations can be compared for lateral excitation on the tail fin.

KAMAN SHAKE TEST ACCELEROMETER LOCATIONS

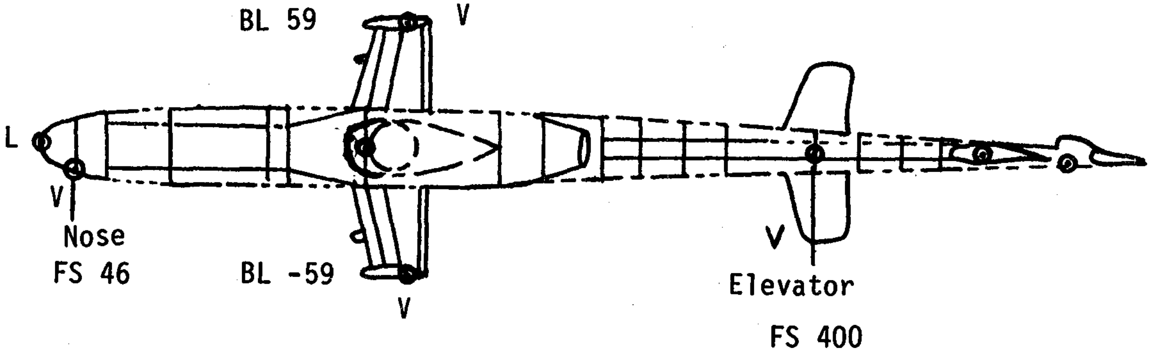
BL 59
V
L
V
Nose
FS 46
BL -59
V
V
Elevator
FS 400

L	Lateral
V	Vertical
FS	Fuselage Station
WL	Waterline
BL	Buttline

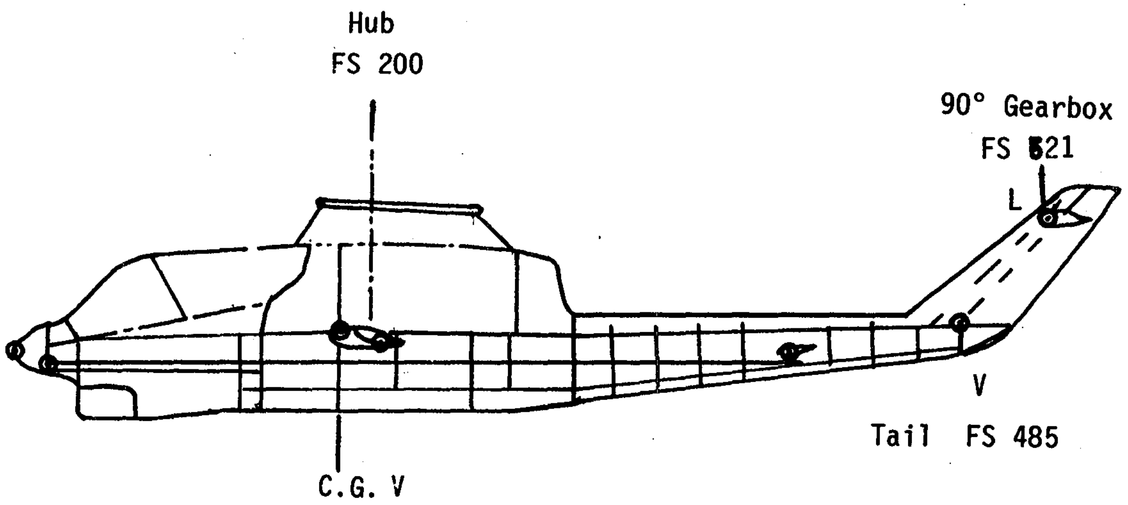
Hub
FS 200
90° Gearbox
FS 521
L
V
Tail FS 485
C.G. V

NASTRAN VIBRATIONS MODEL MODIFICATIONS NEEDED TO SIMULATE THE KAC TEST CONFIGURATIONS

The AH-1G NASTRAN finite element vibrations model documented in Reference 3, which was used for comparison with the OLS data, was also used for comparison with the KAC test data. However, several changes had to be made to the weight distribution so that the model represented the various KAC test vehicle configurations. The changes are documented in the figure below.

NASTRAN VIBRATIONS MODEL MODIFICATIONS NEEDED TO SIMULATE THE KAC TEST CONFIGURATIONS

	LB		
Original NASTRAN AH-1G Model	8933	**Kaman AH-1G NASTRAN Configuration**	
WEIGHT DELETED		WEIGHT ADDED	LB
Gun Turret (XM-28)	89	Test Instrumentation	195
40-MM Drum/Pallet	75	M200 A/1 Inboard Rocket Pod/Rockets (Both Wings)	1058
40-MM Grenades (250 rounds)	190	Inboard Pylon Assembly (Both Wings)	62
7.62-MM Mamee Drum	63	M200 A/1 Outboard Pod/Rockets (Both Wings)	770
7.62-MM Ammunition (4000 rounds)	260	Main Rotor Hub	231
Forward Fuel	780	Turret Ballast	150
Aft Fuel	830	Gun Sight Ballast	25
Pilot	200	Pilot	230
Gunner	200	Gunner	180
Main Rotor Hub	490	Fuel	933
Main Rotor Blades	458	Instrumentation (wiring, transducers, etc)	100
XM-157A Pod (Both Wings)	114		3934
M-151/XM 429 Rockets (Both Wings)	292		
Smoke Grenades (Both Wings)	80		
	4121		

8933 - 4121 + 3934 = 8746 lb

KAC NASTRAN FEM NORMAL MODES RESULTS

The normal modes analysis results for the AH-1G NASTRAN vibrations model modified to represent the KAC test vehicle low gross weight configuration are listed below. The listing includes the natural frequency and generalized mass and stiffness values for the first 30 modes that were used in the frequency response calculation. To adequately represent the 0 - 30 Hz frequency response range of interest, modes through 50 Hz were used in the analysis. A constant value of .04 structural damping (2% critical) was used in the comparisons.

REAL EIGENVALUES

MODE NO.	EXTRACTION ORDER	EIGENVALUE	RADIAN FREQUENCY	CYCLIC FREQUENCY	GENERALIZED MASS	GENERALIZED STIFFNESS
1	238	0.0	0.0	0.0	1.225741E+00	0.0
2	237	0.0	0.0	0.0	1.656425E+00	0.0
3	236	0.0	0.0	0.0	3.027740E+00	0.0
4	235	0.0	0.0	0.0	8.077121E+00	0.0
5	234	0.0	0.0	0.0	4.123577E+00	0.0
6	233	0.0	0.0	0.0	1.432602E+01	0.0
7	232	9.668289E+02	3.109387E+01	4.948743E+00	1.505954E+00	1.456000E+03
8	231	1.038057E+03	3.221889E+01	5.127795E+00	8.470825E-01	8.793198E+02
9	230	1.994172E+03	4.465616E+01	7.107248E+00	4.732642E-01	9.437700E+02
10	229	2.447704E+03	4.947427E+01	7.874075E+00	6.722036E-01	1.645355E+03
11	228	8.363559E+03	9.145250E+01	1.455512E+01	2.716014E-01	2.271554E+03
12	227	9.571668E+03	9.783490E+01	1.557091E+01	1.447545E+00	1.385542E+04
13	226	1.177961E+04	1.085339E+02	1.727370E+01	1.693212E+00	1.994537E+04
14	225	1.187316E+04	1.089641E+02	1.734216E+01	8.739576E-01	1.037664E+04
15	224	1.391411E+04	1.179581E+02	1.877361E+01	3.505436E-01	4.877500E+03
16	223	1.551888E+04	1.245748E+02	1.982669E+01	3.235099E-01	5.020512E+03
17	222	1.746543E+04	1.321568E+02	2.103340E+01	1.451831E+00	2.535684E+04
18	221	2.167644E+04	1.472292E+02	2.343225E+01	2.519270E-01	5.460879E+03
19	220	2.530038E+04	1.590609E+02	2.531532E+01	1.004838E+00	2.542278E+04
20	219	2.559145E+04	1.599733E+02	2.546053E+01	1.978270E-01	5.062676E+03
21	218	2.665452E+04	1.632621E+02	2.598396E+01	1.391972E+00	3.710234E+04
22	217	2.916418E+04	1.707752E+02	2.717972E+01	8.112777E-01	2.366025E+04
23	216	3.316361E+04	1.821088E+02	2.898351E+01	2.068470E-01	6.859789E+03
24	215	3.975609E+04	1.993893E+02	3.173378E+01	1.619993E+00	6.440460E+04
25	214	4.667631E+04	2.160470E+02	3.438495E+01	7.242365E-01	3.380469E+04
26	213	5.736561E+04	2.395112E+02	3.811938E+01	1.014321E+00	5.818716E+04
27	212	6.784875E+04	2.604780E+02	4.145636E+01	5.285847E-01	3.586381E+04
28	211	7.050631E+04	2.655303E+02	4.226045E+01	2.683509E-01	1.892043E+04
29	210	8.364212E+04	2.892095E+02	4.602911E+01	1.822141E-01	1.524078E+04
30	209	8.691900E+04	2.948203E+02	4.692210E+01	1.565797E-01	1.360975E+04

KAC NASTRAN FEM NORMAL MODES RESULTS

MODE		NATURAL FREQUENCY HERTZ
1-6	Rigid Body Modes	----
7	Main Rotor Pylon Lateral Rocking (Pylon Roll)	4.949
8	Main Rotor Pylon Fore-and-Aft Rocking (Pylon Pitch)	5.128
9	First Fuselage Lateral Bending	7.107
10	First Fuselage Vertical Bending	7.874
11	Skid	14.555
12	First Fuselage Torsion	15.571
13	Second Fuselage Lateral Bending	17.274
14	Second Fuselage Vertical Bending	17.342
15	Fuselage Roll/Engine Lateral	19.273
16	Skid	19.827
17	Fuselage Torsion/Wing Yaw	21.034
18	Skid	23.432
19	Third Fuselage Vertical Bending	25.315
20	Skid	25.461
21	Main Rotor Mast Lateral Bending	25.984
22	Main Rotor Mast Fore-and Aft Bending	27.180
23	Skid	28.984
24	Third Fuselage Lateral	31.734
25	Fuselage Torsion	34.385

KAMAN VS OLS TEST DATA - VERTICAL

The frequency response comparisons of KAC and OLS test data for a vertical load applied at the tail skid location are presented for the following response locations and directions:

KAC	NASTRAN GRID	OLS
NOSE V	3339, V (KAC) 9339, V (OLS)	GUNNER V
LEFT WING TIP V	75921 V	LEFT WING TIP V
RIGHT WING TIP V	65921 V	RIGHT WING TIP V
ELEVATOR V	40145 V	ELEVATOR V
AFT TAILBOOM V	46445 V	AFT TAILBOOM V

V = Vertical response

The reader should note the differences in scale of the KAC and OLS plots. The 2-per-rev and 4-per-rev labels should help for comparison. The reason for these differences is that the two comparisons were done approximately 10 years apart during separate contractural arrangements. However, a fairly comprehensive comparison can be made from these plots to evaluate the test data.

The results from both tests are remarkably similar. They exhibit the same trends in response amplitudes, shape and peaks. The NASTRAN calculations agree well with test through main rotor four-per-rev (21.6 Hz) but the agreement degrades for higher frequencies. At the higher frequencies, the trends suggest that the measured forward responses (farthest from excitation) are reduced while the aft response points (nearest the excitation) remain high. Attenuation of the force by the intervening structure is suspected.

KAMAN VS OLS TEST DATA - VERTICAL

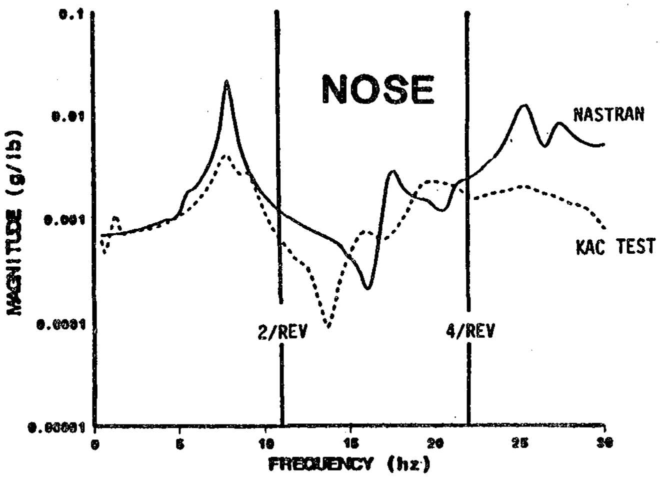

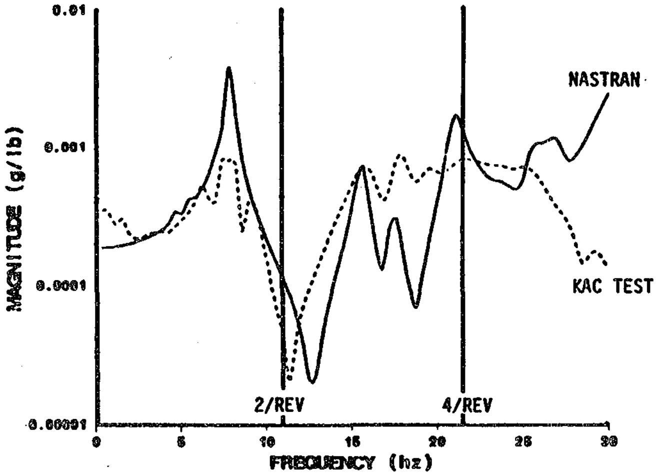

LEFT WING TIP

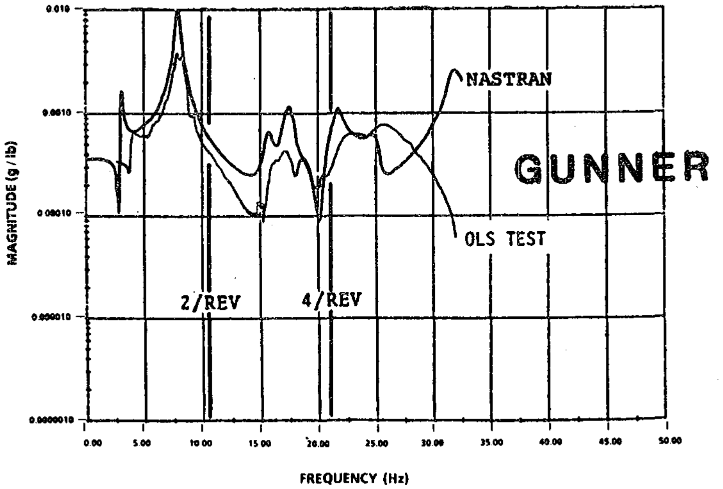

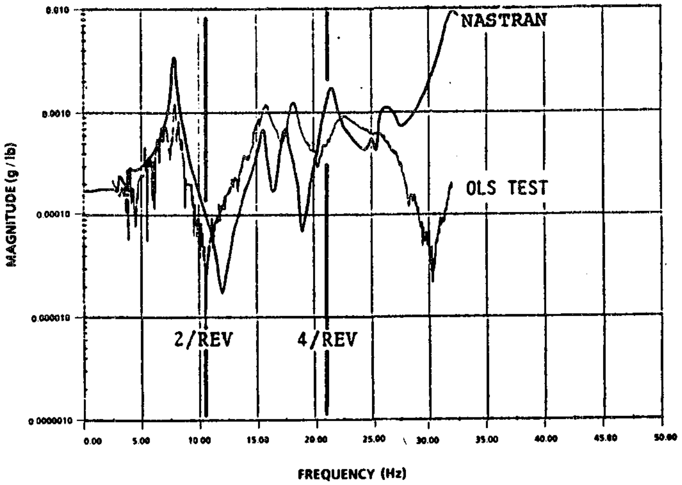

KAMAN VS OLS TEST DATA - VERTICAL

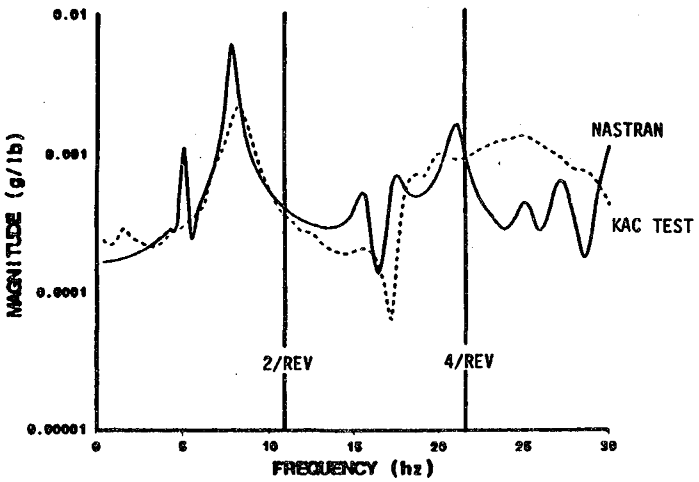

RIGHT WING TIP

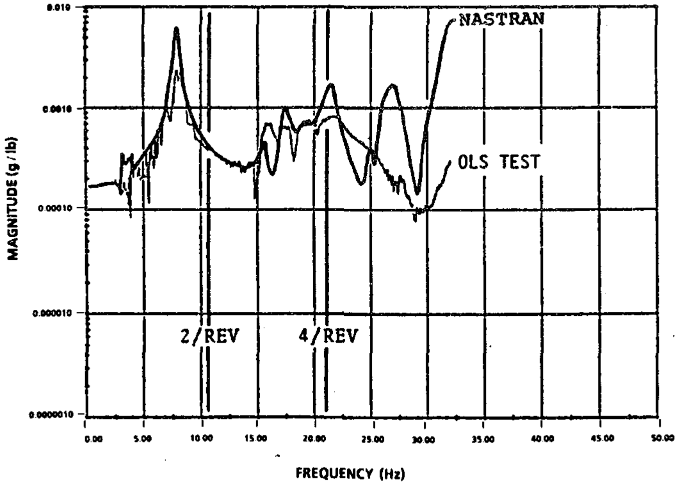

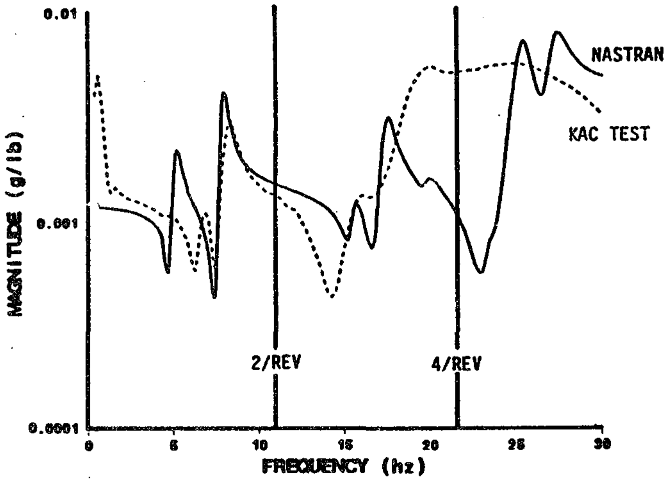

ELEVATOR

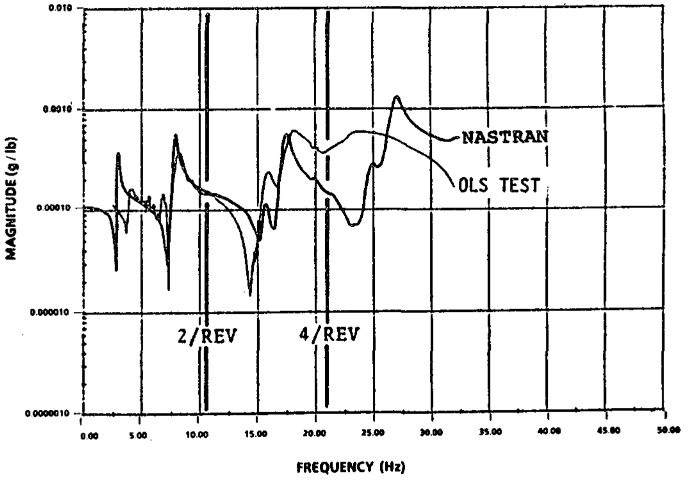

KAMAN VS OLS TEST DATA - VERTICAL

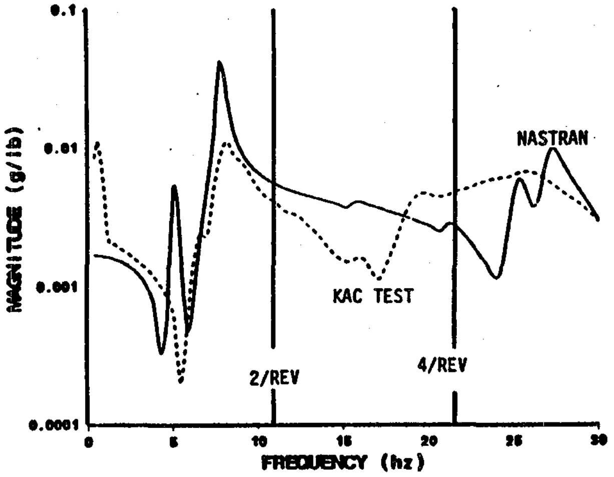

AFT TAIL

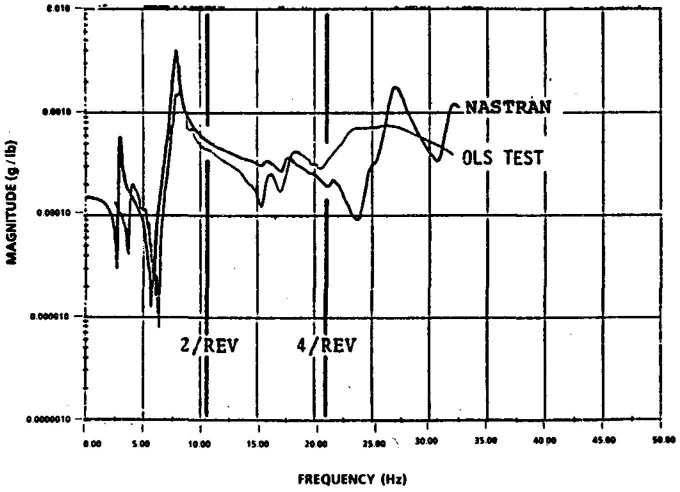

KAMAN VS OLS TEST DATA - LATERAL

The frequency response comparisons of KAC and OLS test data for a lateral excitation applied at the vertical tail fin are presented for the following response locations and directions:

KAC	NASTRAN GRID	OLS
LEFT WING TIP V	75921 V	LEFT WING TIP V
RIGHT WING TIP V	65921 V	RIGHT WING TIP V
TAIL ROTOR GEARBOX L	520079, L (KAC) 52045, L (OLS)	TAIL FIN L

V = Vertical response
L = Lateral response

The response trends for the KAC and OLS test data comparisons are very similar. Both test data groups measure lower amplitude vertical wing tip response in the area of the first fuselage vertical bending mode which amplifies the NASTRAN response in the 5 - 10 Hz range. The lateral response of both cases shows good agreement for the vertical tail fin locations. One significant difference appears in these plots. The KAC test data and NASTRAN calculated response agree better for frequencies greater than four-per-rev (21.6 Hz) than do the OLS data and NASTRAN comparisons.

KAMAN VS OLS TEST DATA - LATERAL

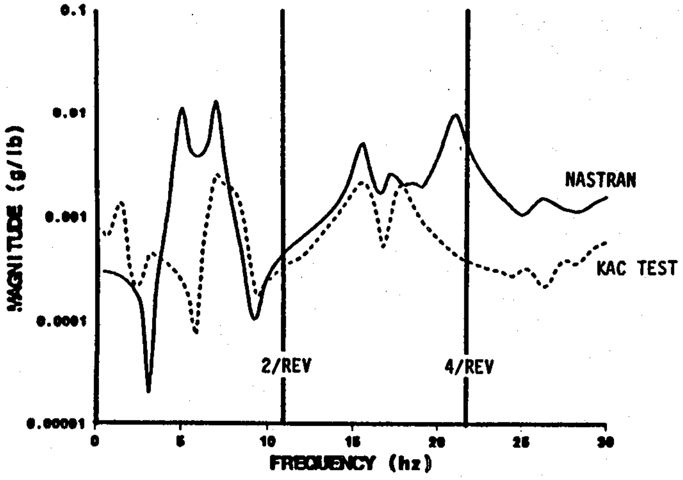

LEFT WING TIP

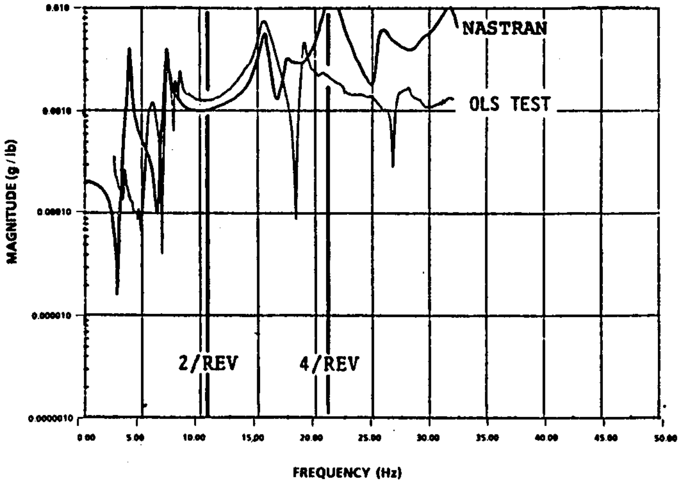

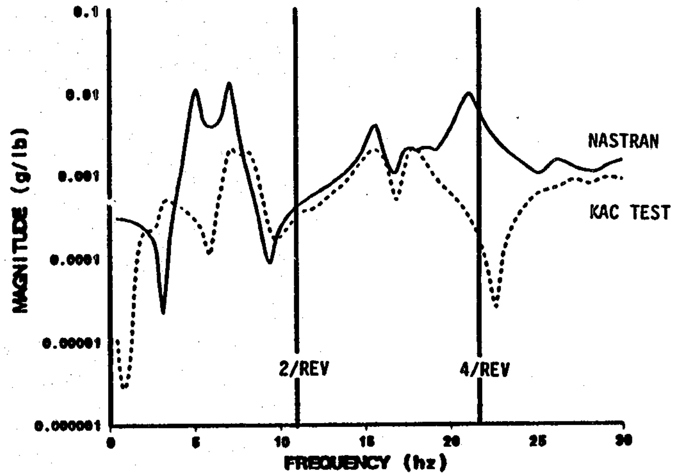

RIGHT WING TIP

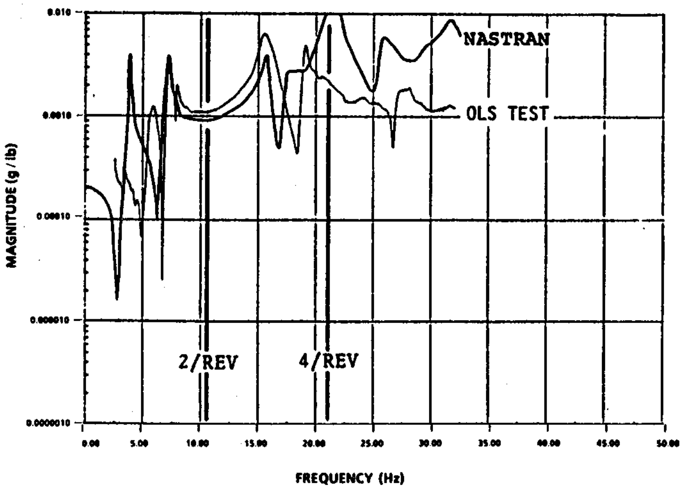

KAMAN VS OLS TEST DATA - LATERAL

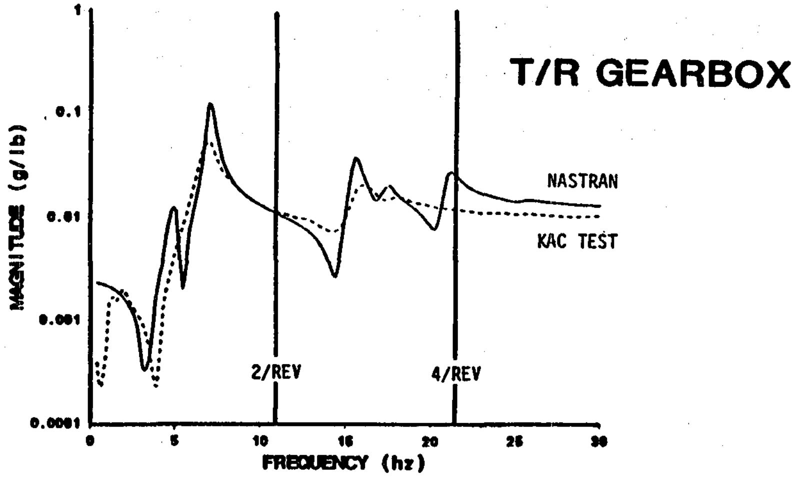
T/R GEARBOX

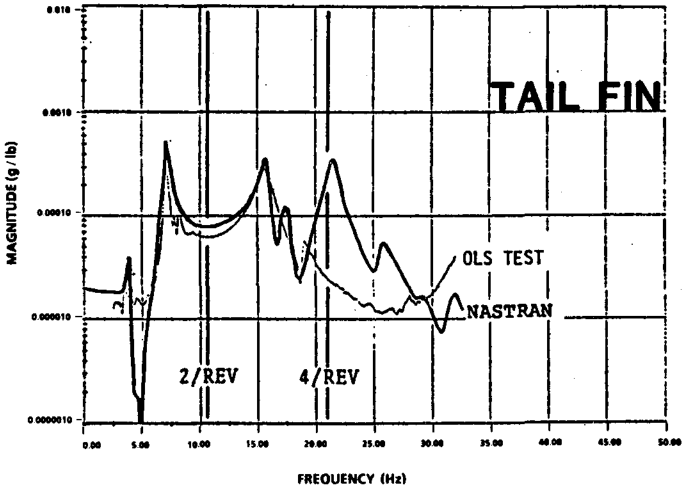
TAIL FIN

KAC NATURAL FREQUENCY COMPARISON

Comparison of the natural frequencies obtained from the Kaman and OLS measured modal responses with those calculated from a NASTRAN analysis are shown in the figure. The close proximity of these values corroborates the good agreement exhibited up to four-per-rev (21.6 Hz) in the frequency response comparisons shown previously. The NASTRAN FEM(s) used in the Kaman and OLS comparisons differ only in the placement of certain useful weight items which varied in the two test configurations.

One important point to note here is the significant variance of measured natural frequencies which appears in some of the Kaman test data comparisons. However, the KAC frequency response data comparisons shown earlier suggest better agreement in mode placement than indicated by this table. The process of selecting the natural frequencies for test used by Kaman included a selection of frequencies at ±.25 Hz on either side of the indicated natural frequency for use in a matrix differencing method for determining peak effects (Ref. 6).

KAC NATURAL FREQUENCY COMPARISON

VERTICAL TAIL SHAKE - CLEAN WING

MODE	Kaman - Low GW		NASTRAN (Hz)		OLS - 35A (Hz)
	Damping	Freq (Hz)	KAC	OLS	
Fore-aft Pylon	-	-	5.13	3.00	3.90
First Vertical Bending	0.07	7.19*	7.87	8.00	8.00
Fuselage Torsion	0.10	16.44*	15.57	15.70	15.50
Second Vertical Bending	0.09	17.71	17.34	17.50	18.00

LATERAL TAIL SHAKE - CLEAN WING

MODE	Kaman - Low GW		NASTRAN (Hz)		OLS - 35A (Hz)
	Damping	Freq (Hz)	KAC	OLS	
Lateral Pylon	-	-	4.95	-	-
First Lateral Bending	0.05	7.51*	7.11	7.15	7.10
Fuselage Torsion	0.17	14.66*	15.57	15.70	15.50
Second Lateral Bending	0.10	17.36	17.27	17.50	18.90
Third Lateral Bending	-	-	-	25.80	24.40

*See explanation of KAC natural frequency placement in text.

KAC MODE SHAPE IDENTIFICATION

The AH-1G test vehicle is characterized by nonproportional damping as a result of the elastomeric isolators and nonstructural access panels. Due to the nature of this damping, the test data exhibits complex modes. Conversion of the complex orthonormal modes measured during the test to real orthonormal modes is required because the NASTRAN fuselage FEM can only predict real mode shapes. The technique implemented for conversion of the complex modes to real modes was judgemental and based on the choice of a reference phase angle. From a review of the test data, the complex axis system was rotated 45° to accommodate the transformation from complex modes to real modes (Ref. 6, pgs 36-37). The real normal modes were obtained from the real orthonormal modes from test by normalizing to the maximum response point and directly compared with the NASTRAN real modal output.

In comparison, the BHT conversion process (see page 156) was similar except that the tail was used as the reference point for normalization of the data for all cases. The phase angle obtained for maximum tail response served as the reference phase angle. Any response within ±90 degrees was considered as positive amplitude (covering a 180° arc) and any response outside this sector was plotted as a negative amplitude similar to the transformation technique from complex to real modes used by KAC.

KAC MODE SHAPE IDENTIFICATION

COMPLEX → REAL

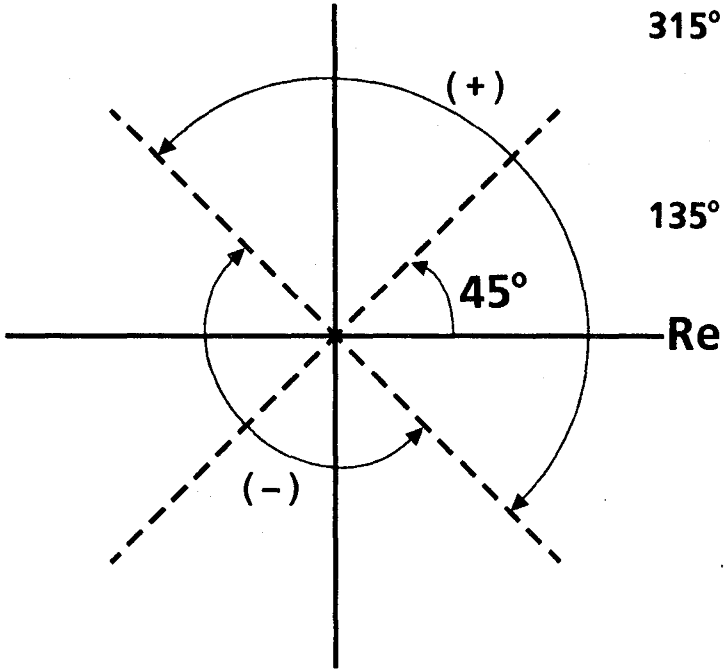

$315^\circ \leq \theta_j \leq 135^\circ \quad \Psi_j = +\sqrt{a_j^2 + b_j^2}$

$135^\circ \leq \theta_j \leq 315^\circ \quad \Psi_j = -\sqrt{a_j^2 + b_j^2}$

Ψ_{jk} = JTH MODAL ELEMENT OF KTH COMPLEX MODE, Ψ

KAMAN MODE SHAPE TRANSDUCER LOCATIONS

The Kaman accelerometer locations and corresponding NASTRAN grid points were chosen to be representative of the centerline motion for the aircraft. The mode shape data represents the real orthonormalized modes as described on the previous page. The following steps were done to perform the correlation:

1. Choose desired test and corresponding NASTRAN grid points
2. Plot Kaman mode shapes
3. Identify NASTRAN mode shapes
4. Overlay corresponding mode shapes

The locations of the grid points are shown below. Correlation plots follow on succeeding pages.

KAMAN MODE SHAPE TRANSDUCER LOCATIONS

VERTICAL RESPONSE

LOCATION	NASTRAN GRID PT	FS	KAMAN ACCELEROMETER ID	FS
NOSE	3339	33	Z50	39
GUNNER	9339	93	Z90L	101
PILOT	13861	139	Z140R	134
C.G.	200070	196*	Z200	196*
AFT FAIRING	25049	250	Z260L	266
TAILBOOM	33845	339	Z340	342
ELEVATOR	40145	401	Z400	400
FIN, BOTTOM	46445	464	Z460	477
FIN, TOP	52045	521	Z540	545

*LOW GW CONFIGURATION

LATERAL RESPONSE

LOCATION	NASTRAN GRID PT	FS	KAMAN ACCELEROMETER ID	FS
NOSE	4639	46	Y50	40
GUNNER	9339	93	Y90	103
PILOT	13861	139	Y140	138
AFT FUEL	21825	219	Y220B	212
TAILBOOM JUNCTION	29945	300	Y300	300
TAILBOOM	38045	380	Y380	379
ELEVATOR	44345	443	Y440	448
FIN, BOTTOM	48845	489	Y490	489
FIN, TOP	52045	521	Y517	518

KAC MODE SHAPE COMPARISON - VERTICAL

The results of the forced response mode shape comparisons for vertical excitation at the tail skid location are shown in the figure for the first three vertical bending modes. It should be noted that above 10 Hz the agreement between test and analysis ranges from fair to poor.

KAC MODE SHAPE COMPARISON - VERTICAL

FIRST VERTICAL

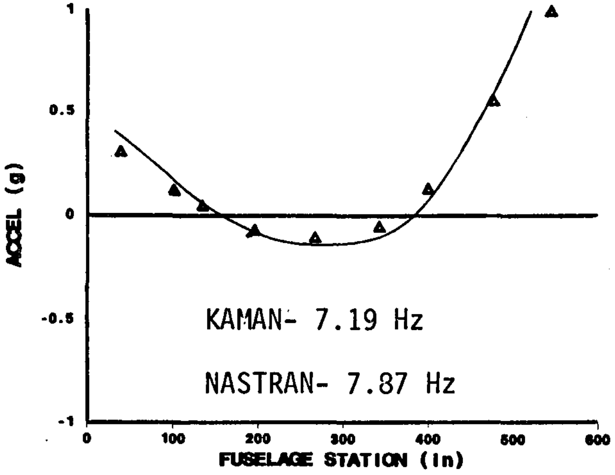

KAMAN- 7.19 Hz

NASTRAN- 7.87 Hz

SECOND VERTICAL

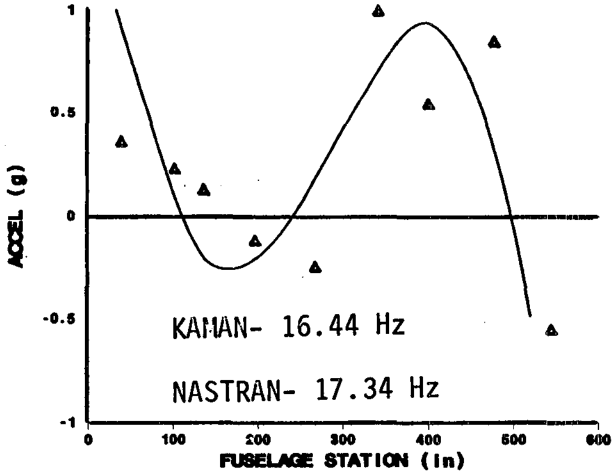

KAMAN- 16.44 Hz

NASTRAN- 17.34 Hz

LEGEND

—— NASTRAN

△ Test

THIRD VERTICAL

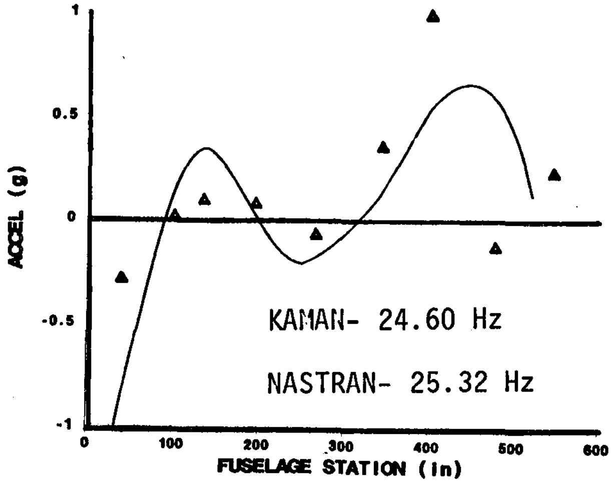

KAMAN- 24.60 Hz

NASTRAN- 25.32 Hz

KAC MODE SHAPE COMPARISON - LATERAL

The results of the forced response mode shape comparison for lateral excitation at the vertical tail fin are shown in the figure for the first three lateral bending modes. It should be noted that above 10 Hz the agreement between test and analysis ranges from fair to poor.

KAC MODE SHAPE COMPARISON - LATERAL

FIRST LATERAL

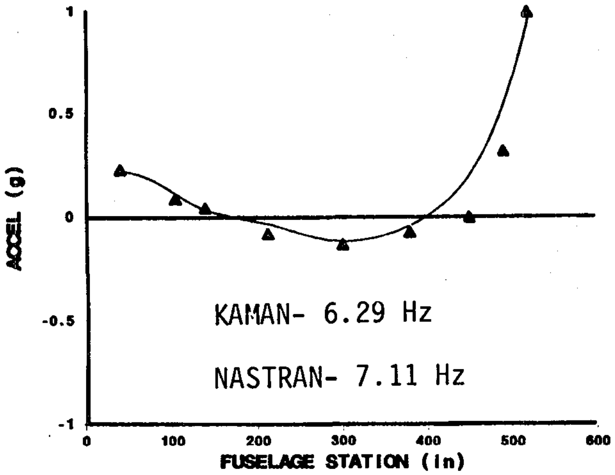

KAMAN- 6.29 Hz

NASTRAN- 7.11 Hz

SECOND LATERAL

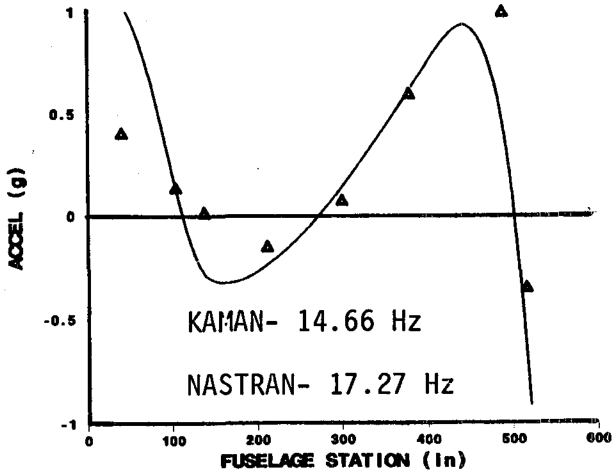

KAMAN- 14.66 Hz

NASTRAN- 17.27 Hz

LEGEND

―――― NASTRAN

▲ Test

THIRD LATERAL

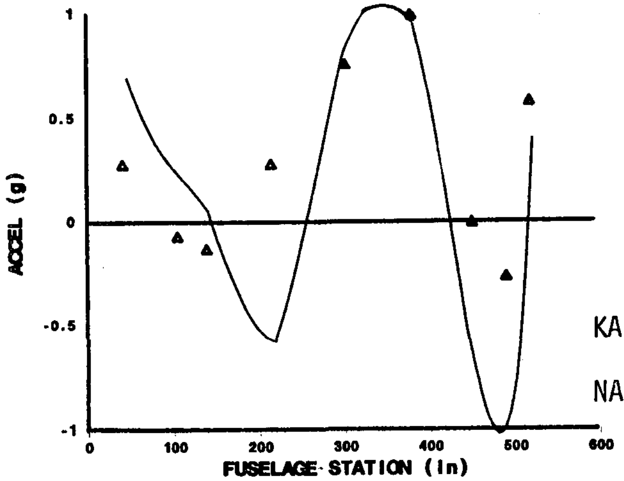

KAMAN- 32.42 Hz

NASTRAN- 31.73 Hz

COMMENTS ON THE EFFECT OF DAMPING ON FREQUENCY RESPONSE

It was found early in the study that using zero damping in the NASTRAN response analysis gave results that were difficult to interpret. Every mode of the structure would show up on the frequency response curves because of slight coupling that occurs due to structure and mass asymmeteries. It became a problem to determine whether the response of a particular mode was significant to the shape of the frequency response curve. The conclusion drawn from comparing NASTRAN response with 0 percent and 2 percent viscous modal damping is that some amount of damping, say 1 to 2 percent, is needed to obtain reasonable frequency response results from analysis.

As would be expected, the effects of increased damping shown by these comparisons are:

1. The frequency response curve shows unimportant mode responses have been smoothed out
2. The response near a resonance is lowered
3. The responses in the low response areas of "valleys" are raised

After comparing the NASTRAN results using different amounts of damping with test, it was concluded that using a constant 2 percent modal damping would result in a representative shape of the frequency response curve. Also, this was slightly lower value of damping than test and would therefore be conservative (higher) in high response or resonance areas of the frequency range. Attempts at determining modal damping from the test frequency response curves using a "half power point" technique indicated about 2 to 3 percent constant modal damping with greater values at some of the higher frequencies. A linear damping increase was also applied to determine its effect on frequency response. This technique increased damping linearly with frequency since observation of test data showed a flatter response in high frequency ranges.

COMMENTS ON THE EFFECT OF DAMPING ON FREQUENCY RESPONSE

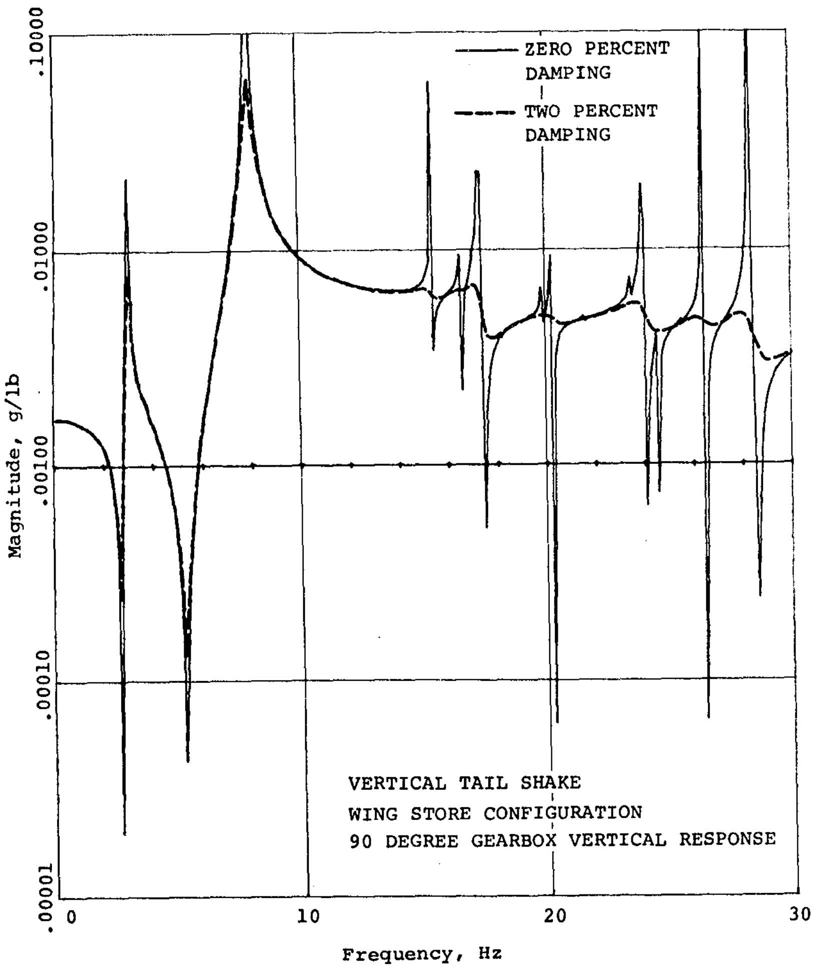

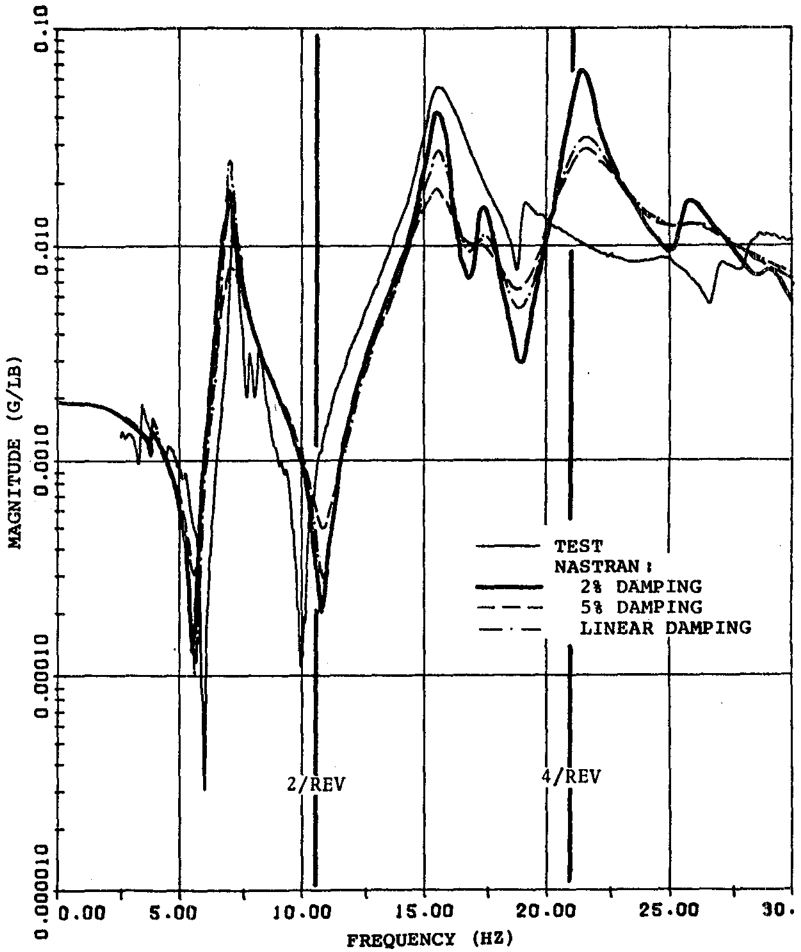

CONCLUSIONS - GVT

The vibration shake tests with excitation at the tail of the airframe were the principal tests used in the evaluation of the vibration analysis. The NASTRAN frequency response characteristics agreed well with these tests in overall amplitudes, forced response mode shapes, peak responses, and general curve shape through four-per-rev using both the BHT and KAC test data. Above four-per-rev, correlation is fair to poor. The vibration response comparisons show that modes involving certain difficult components (such as pylon and wing stores) have discrepancies. These discrepancies are expected, however, because of the simplified "stick" modeling of the pylon and the lumped-mass wing-store models in the FEM. Also, significant dynamic response differences showed up between NASTRAN and test for the BHT hub shake test and were believed to be associated with pylon dynamics not represented in the math model and the suspension system and dummy main rotor hub that were used for the test.

The effects of damping on the comparison of frequency response characteristics were considered in the analysis. Although a constant 2 percent viscous modal damping was used in most of the comparisons, it is felt that damping should be varied in a design analysis to see its effect in both the high response (resonance) and low response (antiresonance) frequency ranges. The damping coefficients measured in the KAC tests ranged from 2.5 to 9 percent critical damping.

CONCLUSIONS - GVT

NASTRAN FEM COMPARISONS WITH GVT DATA

- FREQUENCY RESPONSE AGREEMENT GOOD ≤ 20 HZ (4p)
- INCONSISTENT TRENDS ABOVE 20 HZ
- INDEPENDENT TEST SOURCES SHOWED VERY SIMILAR RESULTS
- IMPORTANT AIRFRAME VIBRATION MODES AND NATURAL FREQUENCIES SHOWED GOOD AGREEMENT ≤ 20 HZ (4p), SOME DISCREPANCIES IN KAC NATURAL FREQUENCY MEASUREMENTS
- DIFFICULT COMPONENTS SUCH AS PYLON MODES (<5 HZ) AND WING STORE CONFIGURATIONS (APPENDIX A) PRESENT SPECIAL MODELING PROBLEMS AND NEED FURTHER WORK
- NONPROPORTIONAL (NONLINEAR) DAMPING EFFECTS DIFFICULT TO QUANTIFY
- GVT COMPARISONS ESSENTIALLY VERIFY THE CAPABILITIES OF THE NASTRAN FEM AS AN ADEQUATE REPRESENTATION OF THE AH-1G VIBRATION CHARACTERISTICS UP TO 20 HZ, BUT INADEQUATE FOR HIGHER FREQUENCY RANGES

5. FLIGHT VIBRATION TESTING

FLIGHT VIBRATION CORRELATION

The flight test data used for correlation of the NASTRAN analysis was taken under the AH-1G operational load survey, Eustis Contract DAAJ02-73-C-0105.

Level flight vibration data were selected for one configuration: clean wing at aft cg. The clean wing configuration used was Flight 35A which was 3768 kg (8300 lb) gross weight at aft cg.

Level flight vibration data were taken at six airspeeds for Flight 35A. The airspeeds flown were the following:

	Airspeed (knots)					
Configuration	1	2	3	4	5	6
35A clean wing at aft cg	67	85	101	114	128	142

Measured hub accelerations and boost cylinder control loads were used as excitation in the NASTRAN analysis.

FLIGHT VIBRATION CORRELATION

- FLIGHT TEST DATA FROM AH-1G OLS (EUSTIS CONTRACT DAAJ02-73-C-0105)
- COMPARE 2, 4 AND 6/REV LEVEL FLIGHT VIBRATION
- AIRSPEEDS 60 TO 140 KT RANGE
- CLEAN WING GROSS WEIGHT CONFIGURATION
- MAIN ROTOR EXCITATION
  - MEASURED HUB ACCELERATIONS
  - 2/REV CONTROL LOADS

APPLIED EXCITATION

Locations of the hub accelerations and boost cylinder control loads that were instrumented in test are shown. Two-, four-, and six-per-rev hub accelerations and corresponding boost cylinder loads are tabulated on the following pages.

Two-per-rev is the predominant excitation frequency of the BHT two-bladed rotor. The loads are higher and, consequently, the response is normally higher than the four- and six-per-rev harmonics. The loads increase with airspeed and coupling between the inplane and vertical response becomes more significant. Large percentage errors in low response levels are not considered essential if fatigue damage and annoying vibration environments are to be assessed.

APPLIED EXCITATION

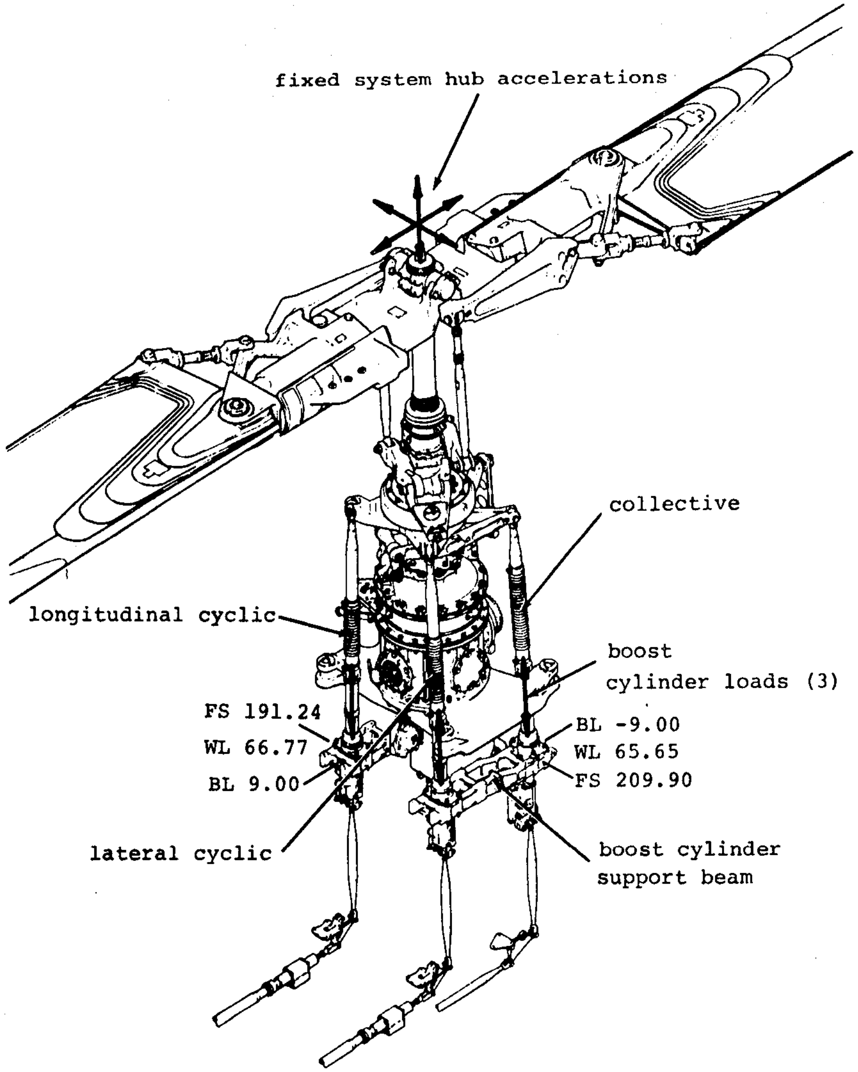
fixed system hub accelerations
collective
longitudinal cyclic
boost
cylinder loads (3)
FS 191.24
WL 66.77
BL 9.00
BL -9.00
WL 65.65
FS 209.90
lateral cyclic
boost cylinder
support beam

TWO-PER-REV HUB ACCELERATIONS

GROSS WEIGHT CONFIGURATION TRUE AIRSPEED	TWO-PER-REV HUB ACCELERATIONS					
	LONGITUDINAL		LATERAL		VERTICAL	
	AMP (G)	PHASE (DEG)	AMP (G)	PHASE (DEG)	AMP (G)	PHASE (DEG)
FLIGHT 35A - CLEAN WING - AFT CG - 3768 KG (8300 LB)						
67 KT	0.839	217.2	0.763	121.1	0.057	30.7
85 KT	0.968	224.5	0.863	122.3	0.055	32.6
101 KT	1.014	227.3	1.026	126.1	0.057	30.8
114 KT	1.281	215.6	1,284	120.1	0.043	31.4
128 KT	1.538	208.8	1.557	110.7	0.051	20.7
142 KT	2.063	216.1	2.193	118.4	0.039	48.7

TWO-PER-REV BOOST CYLINDER LOADS

GROSS WEIGHT CONFIGURATION TRUE AIRSPEED	TWO-PER-REV BOOST CYLINDER LOADS					
	LONGITUDINAL CYCLIC		LATERAL CYCLIC		COLLECTIVE	
	AMP (N) (LB)	PHASE (DEG)	AMP (N) (LB)	PHASE (DEG)	AMP (N) (LB)	PHASE (DEG)
FLIGHT 35A - CLEAN WING - AFT CG - 3768 KG (8300 LB)						
67 KT	1499 (337)	37.2	2197 (494)	132.1	1308 (294)	308.1
85 KT	1526 (343)	56.6	2531 (569)	159.5	1681 (378)	333.9
101 KT	1788 (402)	87.8	2598 (584)	196.5	2491 (560)	0.9
114 KT	1984 (446)	167.2	2816 (633)	264.2	3487 (784)	77.1
128 KT	2393 (538)	225.3	3149 (708)	312.9	4088 (919)	139.3
142 KT	3167 (712)	343.6	3536 (795)	69.8	4270 (960)	263.1

FOUR-PER-REV HUB ACCELERATIONS

GROSS WEIGHT CONFIGURATION TRUE AIRSPEED	FOUR-PER-REV HUB ACCELERATIONS					
	LONGITUDINAL		LATERAL		VERTICAL	
	AMP (G)	PHASE (DEG)	AMP (G)	PHASE (DEG)	AMP (G)	PHASE (DEG)
FLIGHT 35A - CLEAN WING - AFT CG - 3768 KG (8300 LB)						
67 KT	0.304	156.4	0.245	47.1	0.041	216.2
85 KT	0.269	92.3	0.373	28.2	0.021	102.5
101 KT	0.498	130.8	0.494	57.6	0.076	125.2
114 KT	0.753	160.6	0.431	67.6	0.074	128.5
128 KT	0.950	154.9	0.418	41.0	0.090	69.8
142 KT	1.193	168.8	0.867	43.9	0.077	59.0

FOUR-PER-REV BOOST CYLINDER LOADS

GROSS WEIGHT CONFIGURATION TRUE AIRSPEED	FOUR-PER-REV BOOST CYLINDER LOADS					
	LONGITUDINAL CYCLIC		LATERAL CYCLIC		COLLECTIVE	
	AMP (N) (LB)	PHASE (DEG)	AMP (N) (LB)	PHASE (DEG)	AMP (N) (LB)	PHASE (DEG)
FLIGHT 35A - CLEAN WING - AFT CG - 3768 KG (8300 LB)						
67 KT	102 (23)	310.1	360 (81)	65.8	142 (32)	299.0
85 KT	351 (79)	5.2	632 (142)	149.3	80 (18)	11.0
101 KT	503 (113)	97.9	703 (158)	238.5	196 (44)	351.6
114 KT	374 (84)	247.7	485 (109)	22.5	311 (70)	144.2
128 KT	383 (86)	347.4	311 (70)	145.4	276 (62)	267.2
142 KT	280 (63)	251.8	236 (53)	115.0	200 (45)	163.8

SIX-PER-REV HUB ACCELERATIONS

GROSS WEIGHT CONFIGURATION TRUE AIRSPEED	SIX-PER-REV HUB ACCELERATIONS					
	LONGITUDINAL		LATERAL		VERTICAL	
	AMP (G)	PHASE (DEG)	AMP (G)	PHASE (DEG)	AMP (G)	PHASE (DEG)
FLIGHT 35A - CLEAN WING - AFT CG - 3768 KG (8300 LB)						
67 KT	0.177	337.5	0.128	307.5	0.063	241.3
85 KT	0.339	23.4	0.256	356.3	0.042	203.2
101 KT	0.263	60.1	0.285	351.3	0.049	145.1
114 KT	0.068	353.2	0.207	301.1	0.035	168.0
128 KT	0.197	7.2	0.387	268.2	0.025	13.0
142 KT	0.210	42.7	0.485	305.9	0.039	15.1

SIX-PER-REV BOOST CYLINDER LOADS

GROSS WEIGHT CONFIGURATION TRUE AIRSPEED	SIX-PER-REV BOOST CYLINDER LOADS					
	LONGITUDINAL CYCLIC		LATERAL CYCLIC		COLLECTIVE	
	AMP (N) (LB)	PHASE (DEG)	AMP (N) (LB)	PHASE (DEG)	AMP (N) (LB)	PHASE (DEG)
FLIGHT 35A - CLEAN WING - AFT CG - 3768 KG (8300 LB)						
67 KT	67 (15)	345.6	196 (44)	334.2	22 (5)	187.4
85 KT	289 (65)	105.8	436 (98)	92.3	62 (14)	207.1
101 KT	463 (104)	177.3	120 (27)	201.3	67 (15)	254.2
114 KT	347 (78)	35.6	93 (21)	252.8	169 (38)	86.1
128 KT	396 (89)	190.6	356 (80)	35.5	205 (46)	271.0
142 KT	222 (50)	229.9	476 (107)	75.0	320 (72)	282.5

ACCELEROMETER LOCATIONS

Airframe accelerations were recorded and harmonically analyzed for comparison with the NASTRAN analysis. Airframe locations of accelerometers used in the flight tests are shown.

ACCELEROMETER LOCATIONS

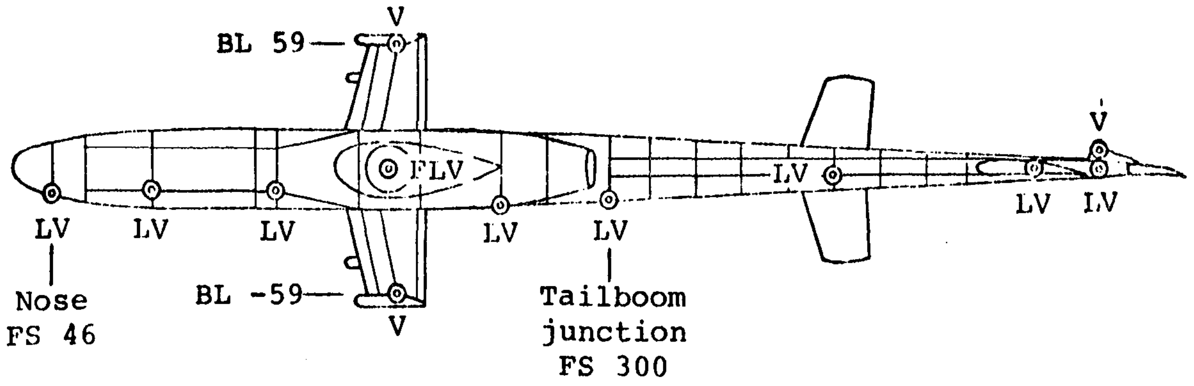
V
BL 59
FLV
LV
V
LV
LV
LV
LV
LV
Nose
FS 46
BL -59
V
LV
Tailboom
junction
FS 300
LV
LV
V

F ~ Fore-and-aft
L ~ Lateral
V ~ Vertical
FS ~ Fuselage station
WL ~ Waterline
BL ~ Buttline

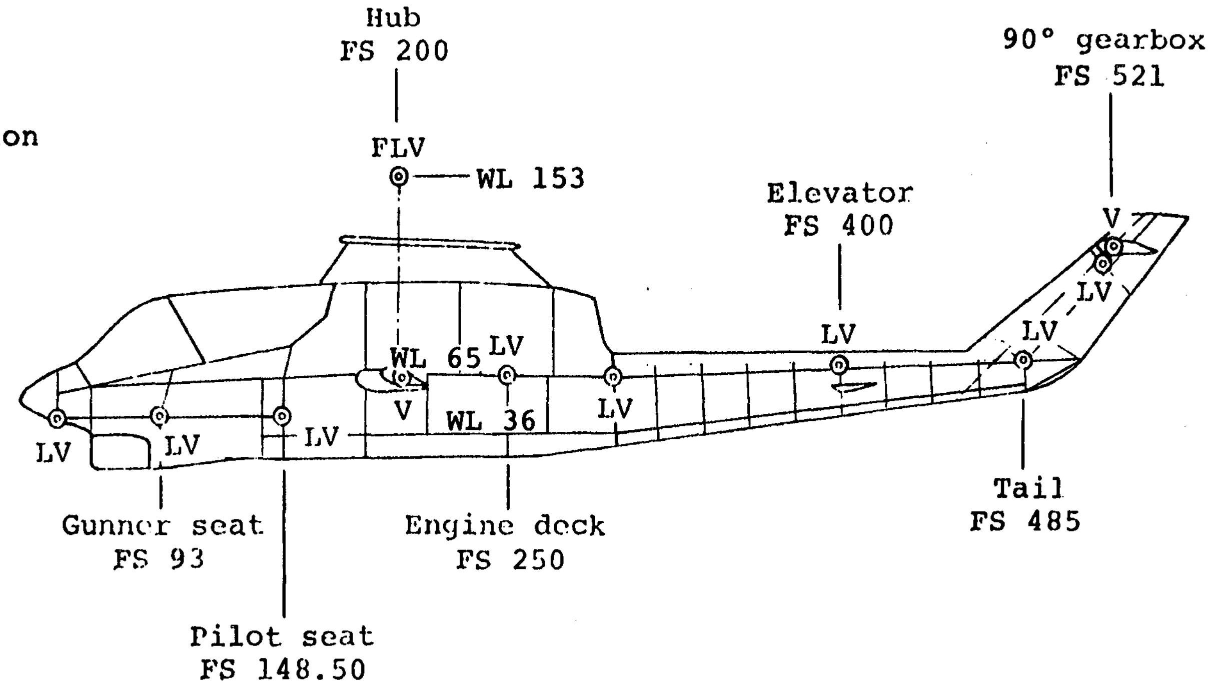
Hub
FS 200
FLV
WL 153
90° gearbox
FS 521
Elevator
FS 400
V
LV
LV
LV
WL 65
LV
V
WL 36
LV
LV
LV
LV
LV
Gunner seat
FS 93
Engine deck
FS 250
Tail
FS 485
Pilot seat
FS 148.50

AH-1G NASTRAN MODEL FORCED RESPONSE ANALYSIS

The model useful weights were changed to correspond to the two configurations that were flown.

Hub accelerations were applied to the NASTRAN model using a large hub mass of 0.454 x 10^7 kg (10^7 lb). The hub mass was excited with the force required to give the mass the measured 'g' acceleration. For example, a force of 4.448 x 10^7 N (10^7 lb) is required to produce a 1-g acceleration of the 0.454 x 10^7 kg (10^7 lb) hub mass. The size of the mass is arbitrary but must be large enough so that it is not influenced by the airframe response, i.e., the response to the applied input force is the only significant response of the hub mass.

The boost cylinder control loads were applied to the NASTRAN model. The boost cylinder support beams were modeled using bar elements. The support beams distribute the control loads to the airframe and should not affect the local structural stiffness.

The two-, four-, and six-per-rev responses were computed using the NASTRAN rigid format 8, Direct Frequency Response Analysis. Two percent viscous damping was used. This was input by setting PARAM G equal to .04. The G parameter is considered as two times the percent critical damping at the natural frequency.

AH-1G NASTRAN MODEL FORCED RESPONSE ANALYSIS

- CORRELATION AT MAIN ROTOR TWO-, FOUR-, AND SIX-PER-REV HARMONICS
- USEFUL WEIGHTS REVISED TO REFLECT FLIGHT TEST CONFIGURATION
- MEASURED MAIN ROTOR HUB ACCELERATIONS USED TO EXCITE NASTRAN MODEL
- MAST AND TRANSMISSION AXIAL STIFFNESS REPRESENTED
- MEASURED BOOST CYLINDER CONTROL LOADS USED AS EXCITATION AT TWO-PER-REV
- DIRECT FREQUENCY RESPONSE RIGID FORMAT SOLUTION SEQUENCE
- 2% CRITICAL DAMPING USED AT ALL HARMONICS

TWO-PER-REV HUB ACCELERATIONS VERSUS AIRSPEED

The vertical hub accelerations were found to be much smaller than the horizontal hub accelerations, about a factor of 40 to 50 at high airspeeds. The difference in hub component accelerations is caused by the stiff vertical load path into the airframe through the mast transmission case and lift link. The pylon rocking motions are reacted by soft elastomeric mounts resulting in the hub being much softer horizontally than vertically.

TWO-PER-REV HUB ACCELERATIONS VERSUS AIRSPEED

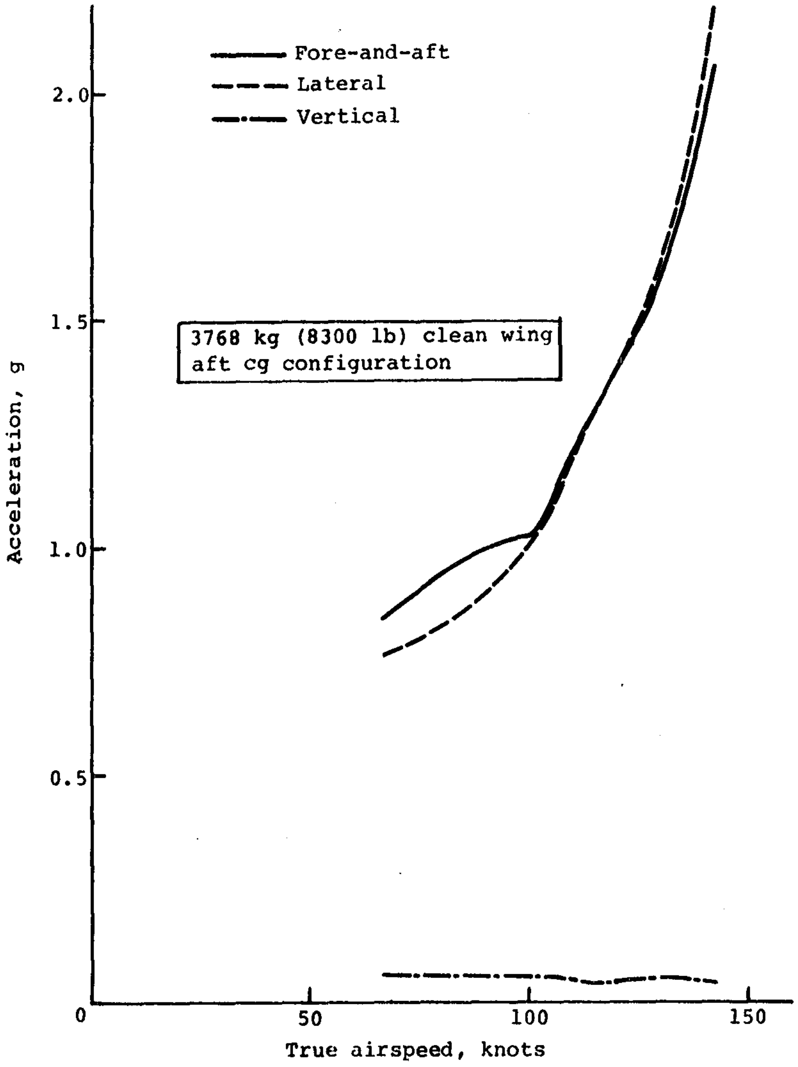

EFFECT OF PYLON VERTICAL STIFFNESS ON TWO-PER-REV VERTICAL RESPONSE

When imposing the hub accelerations on the NASTRAN model, it was found that the vertical stiffness of the pylon was very important to the computed airframe response. The sensitivity of the two-per-rev airframe response to changes in the axial stiffness of the pylon is shown. The low response condition results from the original rigid modeling of the pylon in the vertical direction. The high response condition was for an arbitrarily soft spring rate of 175 x 10^5 N/m (10^5 lb/in) to assess the effect of pylon vertical stiffness. The response difference is more than an order of magnitude. After observing this, it was obvious that axial deformations of the pylon which were originally considered negligible were in fact extremely important to the airframe response.

The sensitivity of the airframe response to the vertical (axial) stiffness of the pylon results from the method of applying hub accelerations which does not limit the load to the pylon. The load applied at the hub comes from the main rotor and will be limited between a cantilevered (highest load) and a free (zero load) boundary condition on the rotor hub. The use of hub shear loads rather than hub accelerations should be a more representative method of applying excitation in the NASTRAN analysis, at least in the vertical direction.

With helicopter isolation systems that provide vertical isolation as well as horizontal, the problem of extreme sensitivity to small deformations is not expected. For these systems, two-per-rev vertical deformations at the hub are the same order of magnitude as the horizontal hub deformations.

EFFECT OF PYLON VERTICAL STIFFNESS ON TWO-PER-REV VERTICAL RESPONSE

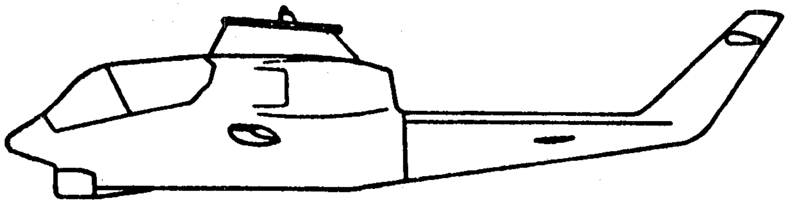

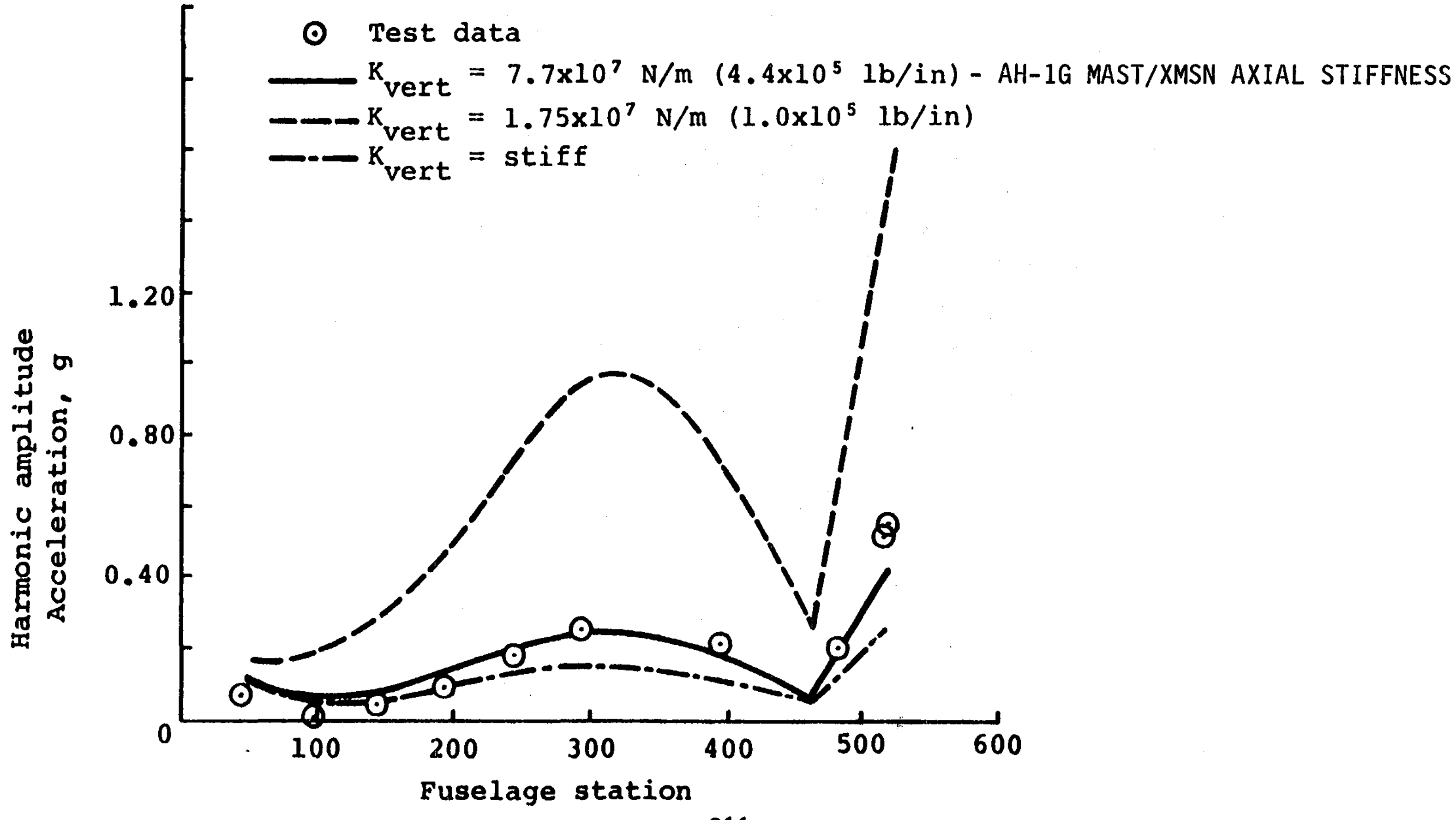
⊙ Test data
—— K_{vert} = 7.7x10⁷ N/m (4.4x10⁵ lb/in) - AH-1G MAST/XMSN AXIAL STIFFNESS
– – – K_{vert} = 1.75x10⁷ N/m (1.0x10⁵ lb/in)
—·— K_{vert} = stiff
Harmonic amplitude
Acceleration, g
0
0.40
0.80
1.20
100
200
300
400
500
600
Fuselage station

VERTICAL STIFFNESS OF MAIN ROTOR PYLON

Calculations of the actual pylon axial stiffness were made. The vertical spring rate that was calculated was 770 x 10^5 N/m (4.4 x 10^5 lb/in). This spring rate includes the stiffness of the mast, thrust bearing, upper transmission case, side case, and lower case. Resulting stiffnesses for the pylon components and a schematic of each is shown in the cutaway sketch. The spring rate was represented in the NASTRAN model by making the axial stiffness of the bar at the top of the mast equal to the calculated pylon spring rate.

For all conditions used in the correlation study, the 770 x 10^5 N/m (4.4 x 10^5 lb/in) spring rate was included.

VERTICAL STIFFNESS OF MAIN ROTOR PYLON

$$\frac{1}{K_{vert}} = \frac{1}{K_m} + \frac{1}{K_t} + \frac{1}{K_u} + \frac{1}{K_s} + \frac{1}{K_l}$$

$$\boxed{\begin{array}{l} K_{vert} = 7.7\text{x}10^7 \text{ N/m} \\ (4.4\text{x}10^5 \text{ lb/in}) \end{array}}$$

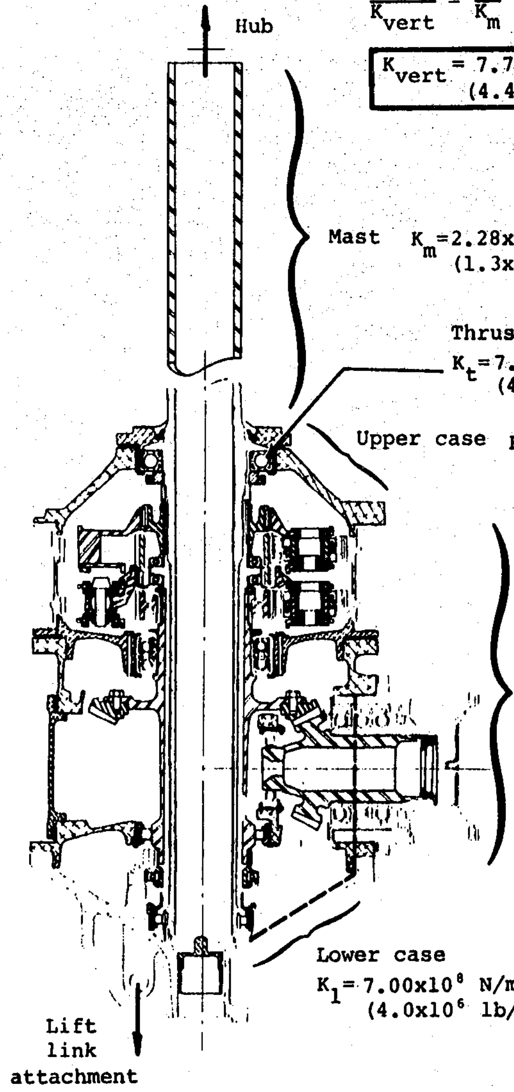

Mast $K_m = 2.28\text{x}10^8$ N/m (1.3x10⁶ lb/in)

Thrust bearing $K_t = 7.00\text{x}10^8$ N/m (4.0x10⁶ lb/in)

Upper case $K_u = 7.00\text{x}10^8$ N/m (4.0x10⁶ lb/in)

Side case $K_s = 2.45\text{x}10^8$ N/m (1.4x10⁶ lb/in)

Lower case $K_l = 7.00\text{x}10^8$ N/m (4.0x10⁶ lb/in)

Transmission and mast cutaway

EFFECT OF PYLON STIFFENING AND DAMPING ON TWO-PER-REV ISOLATION

The pylon was represented as a linear elastic model with scalar springs representing the translational stiffness of the elastomeric mounts. Two percent modal damping was selected for all modes since that value was considered representative of the damping of predominant airframe modes of the helicopter. In the vibration testing, it was found that the natural frequencies and damping of the longitudinal and lateral pylon rocking modes were both higher than the NASTRAN analysis. It was therefore surmised that some known stiffening and damping effects should be incorporated into the pylon model in order to evaluate their influence on two-per-rev airframe vibration. Two-per-rev (10.8 Hz) is the most significant rotor harmonic since it is closest to the pylon rocking modes which are below 5 Hz. Effects of near resonance amplification and damping decrease as the forcing frequency becomes further removed.

The known pylon stiffening and damping effects considered are the following:

1. Pendulum stiffening due to rotor thrust
2. Elastomeric mount cocking (rotational) stiffness, and
3. 10 percent damping of the pylon rocking modes

The pendulum stiffening of the pylon is controlled by the rotor thrust at the hub. When the pylon rocks, the 1g rotor thrust at the hub produces a restoring moment. This effect was analyzed in NASTRAN using a DMAP alter. The alter allowed addition of the differential stiffness matrix from a static load condition with 1g rotor thrust to be added to the structure stiffness matrix. The resulting stiffness matrix was then used to determine the pylon natural frequencies and airframe frequency response using rigid format 11. Format 11 was used instead of format 8 because it provides a more economic analysis scheme during full spectrum frequency response runs through modal representation than the direct analysis scheme of format 8. However, careful selection of the truncated modes used to approximate complete system response is required to achieve accurate response predictions with format 11.

A simplified model was used for the NASTRAN analysis. The elastic pylon model was attached to a rigid body fuselage to evaluate the differential stiffness effect on pylon isolation at two-per-rev. The fuselage was attached to ground by soft springs in order to perform the static analysis. The springs were soft so as not to affect the pylon rocking frequencies. In addition to the pendulum stiffening, measured cocking spring rates of 0.113 x 10^5 N-m/rad (10^5 in-lb/rad) were added to the elastomeric pylon mounts which were represented by only the mount translational spring rates in the airframe model. Also, ten percent viscous modal damping was used in the analysis as indicated from the measured frequency response. This model was then compared to the original pylon model without the stiffening effects and using two percent modal damping. A comparison of pylon rocking frequencies is given below.

Mode	Natural Frequency (Hz)	
	Baseline	Stiffened
Pylon pitch (longitudinal)	3.215	3.308
Pylon roll (lateral)	3.357	3.621

The comparisons of the frequency response of the fuselage cg are shown. Roll response to a lateral hub shear and pitch response to a longitudinal hub shear are presented. Although the responses are shown to be quite different near the pylon rocking frequencies, the responses at two-per-rev do not differ significantly. Therefore, the stiffness and damping effects discussed in this section are not considered significant in the flight vibration correlation and are not included in the NASTRAN airframe analysis.

EFFECT OF PYLON STIFFENING AND DAMPING ON TWO-PER-REV ISOLATION

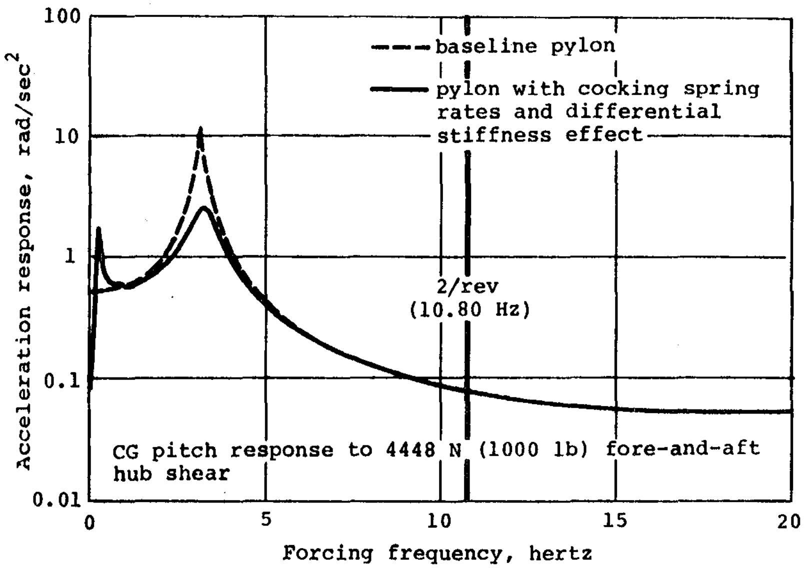

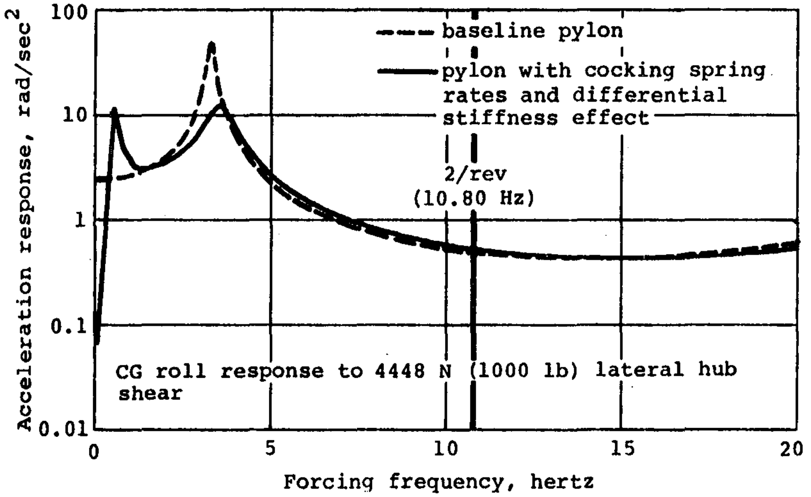

EVALUATION OF RESPONSE

Results of the vibration test comparison indicate the airframe analysis agrees quantitatively well through four-per-rev (21.6 Hz) but differs significantly in the frequency range proximate to four- and six-per-rev. The basis for evaluating the mode shape data, using the "frozen" mode shape when tail response is maximum, is subject to some error in choosing the reference phase angle. Therefore, the amplitudes experienced for these modes are more important than the resulting shapes. The two-per-rev magnitudes and phases at the predominant main rotor excitation frequency of 10.8 Hz have the most significant response and are predicted well. Also, the vertical response levels are predicted more accurately than the lateral. This is important because human tolerance to vertical vibration has a lower threshold level.

Errors in the prediction of higher vibration levels can lead to more critical evaluation of design safety. The effect of the noseboom, downwash impingement, simplified modeling of the elevator, pylon dynamics, structural damping, and elastomeric nonlinearities are typical influences which can cause errors in predicted higher vibration levels.

EVALUATION OF RESPONSE

- AMPLITUDES MORE IMPORTANT THAN MODE SHAPE
- TWO-PER-REV MOST IMPORTANT
  - PREDOMINANT EXCITATION FREQUENCY
  - DISCOMFORT LEVELS MORE CRITICAL THAN THOSE AT HIGHER FREQUENCIES
  - VERTICAL DISCOMFORT LEVELS MORE CRITICAL THAN LATERAL
- ERRORS IN HIGH VIBRATION LEVELS MORE IMPORTANT
- VIBRATION LEVELS BELOW .05 G'S NOT CONSIDERED

HUMAN COMFORT VIBRATION LEVELS

The following graph depicts International Standards Organization (ISO) ride comfort levels used as guidelines to produce a "jet-smooth" vibration environment. The darkly shaded area (dashed lines) represents the ride comfort boundaries of vertical vibration that a human being can tolerate from a few minutes to eight hours. The lightly shaded area (dot matrix) represents these ride comfort intervals for lateral vibration levels. A ride of .05g peak vibrations is the desirable goal for rotorcraft design to obtain a suitable comfort level.

HUMAN COMFORT VIBRATION LEVELS

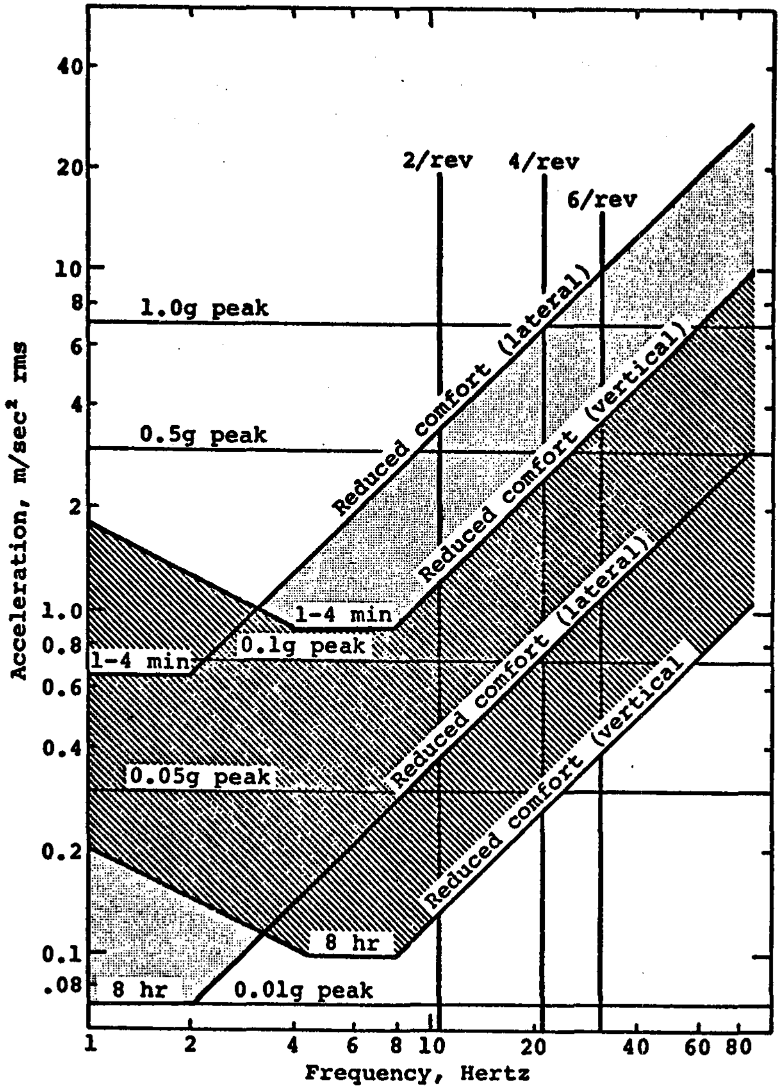

INTERNATIONAL STANDARDS ORGANIZATION, ISO 2631

DISCUSSION OF RESULTS

Sample comparisons between calculated and measured flight vibration responses are presented and possible explanations for poor correlation (large percentage errors) are discussed on the following pages.

DISCUSSION OF RESULTS

- ● VERTICAL RESPONSES
  - TWO-PER-REV
  - FOUR-PER-REV
  - SIX-PER-REV

- ● LATERAL RESPONSES
  - TWO-PER-REV
  - FOUR-PER-REV
  - SIX-PER-REV

TWO-PER-REV VERTICAL RESPONSE

There is general agreement of the harmonic amplitudes between analysis and test. The trends of response with airspeed are consistent with exception of the highest airspeed. In these cases the forward fuselage response predictions are significantly lower than test. The vibratory hub shears in the horizontal directions increase more than the vertical hub shears at the higher airspeeds and the idealized NASTRAN pylon may be isolating pitching moments due to the horizontal shear better than test indicates. Also, the noseboom that was on the test helicopter but not in the NASTRAN analysis may be affecting the nose response.

TWO-PER-REV VERTICAL RESPONSE

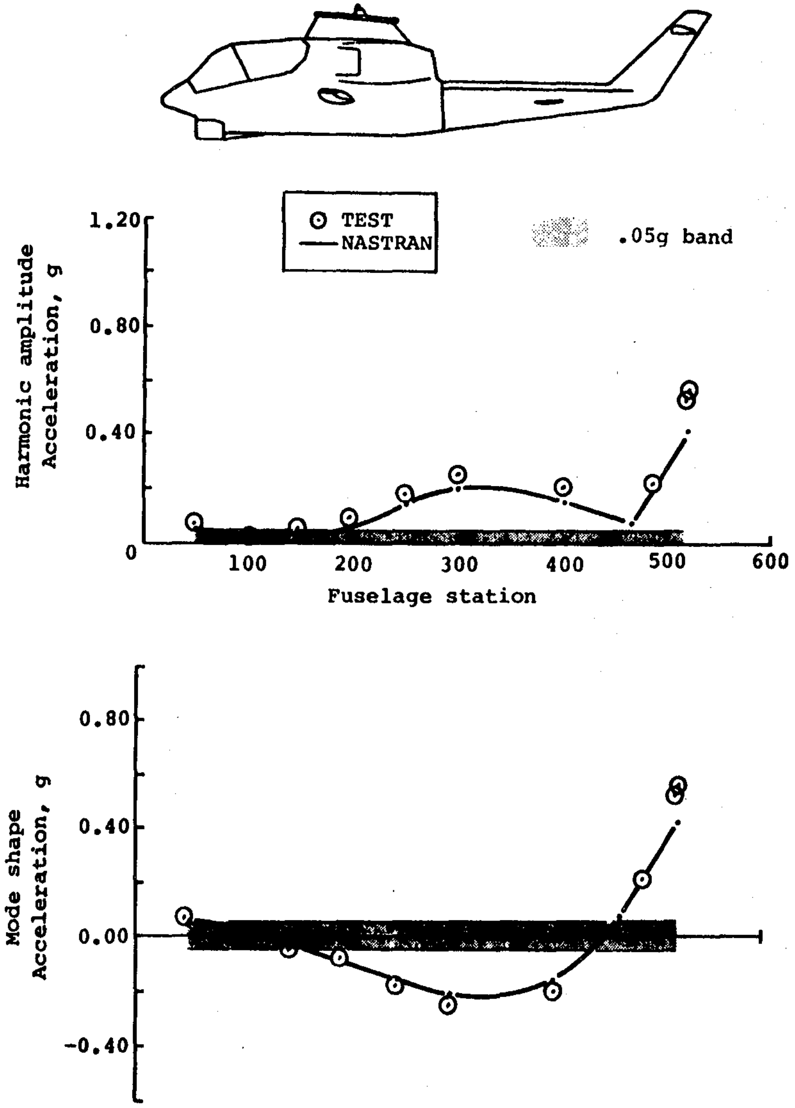

67 KT - CLEAN WING

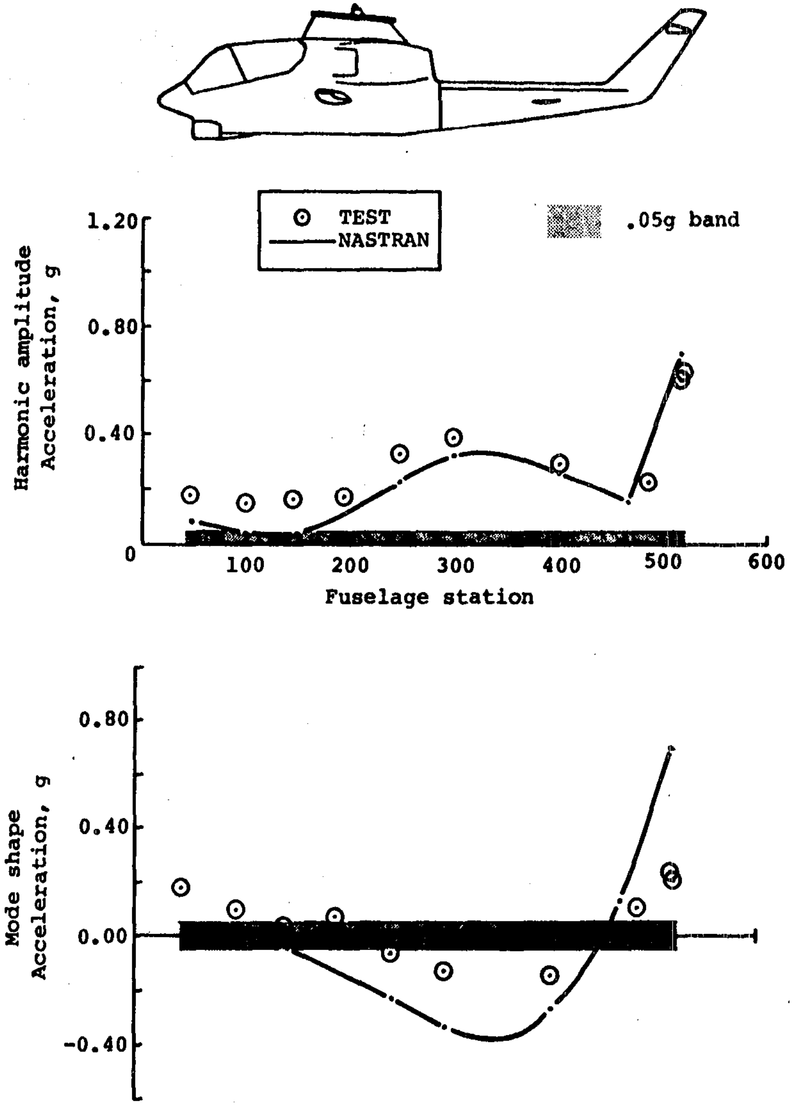

142 KT - CLEAN WING

FOUR-PER-REV VERTICAL RESPONSE

The NASTRAN response is extremely high compared to flight test. The four-per-rev vertical resonance introduced by the big hub mass is a possible source for these large differences. This big hub mass constrains the hub and produces a vertical bounce mode of the fuselage on the pylon axial spring. The resulting vertical hub shear at the top of the mast is 14233 N (3200 lb). The expected vertical load, using the in-flight vertical vibration at the hub and the indicial vertical hub response is 1388 N (312 lb). This ratio of applied vertical load to expected vertical load reduces the response by a factor of ten. The reduced responses agree much better with test. This supports the hypothesis that hub shears instead of hub accelerations are a more practical means of exciting the model in the vertical direction.

NOTE: The expected vertical load was calculated as follows:

Vibration test vertical hub response = 0.000045 g/N
(0.0002 g/lb)

Vertical hub response at 142 knots = 0.077g = 0.75 m/s^2

Rotor weight = 430 kg (947 lb)

Vertical load = [0.077g ÷ 0.000045 g/N]

- [430 kg x 0.75 m/s^2]

= 1388 N (312 lb)

FOUR-PER-REV VERTICAL RESPONSE (concluded)

Assuming that the method for reducing the NASTRAN responses is feasible, the following comments apply. Although the percentage error is not small, the predicted responses are the same order of magnitude as the measured responses with better agreement at the higher airspeeds. The trend with airspeed for the clean wing configuration is poor as indicated by the apparent scatter in the data.

The frequency response data indicates some degradation of correlation near four-per-rev. The method of applying hub excitations introduces an artificial vertical resonance. For these reasons, the lessened degree of correlation at the four-per-rev main rotor harmonic may have been expected. Additional analyses and ground tests appear necessary to confirm these suspected deficiencies.

In general, the four-per-rev response levels are significantly lower than the two-per-rev responses. For purposes of design, these differences between analysis and test may be of little consequence.

FOUR-PER-REV VERTICAL RESPONSE

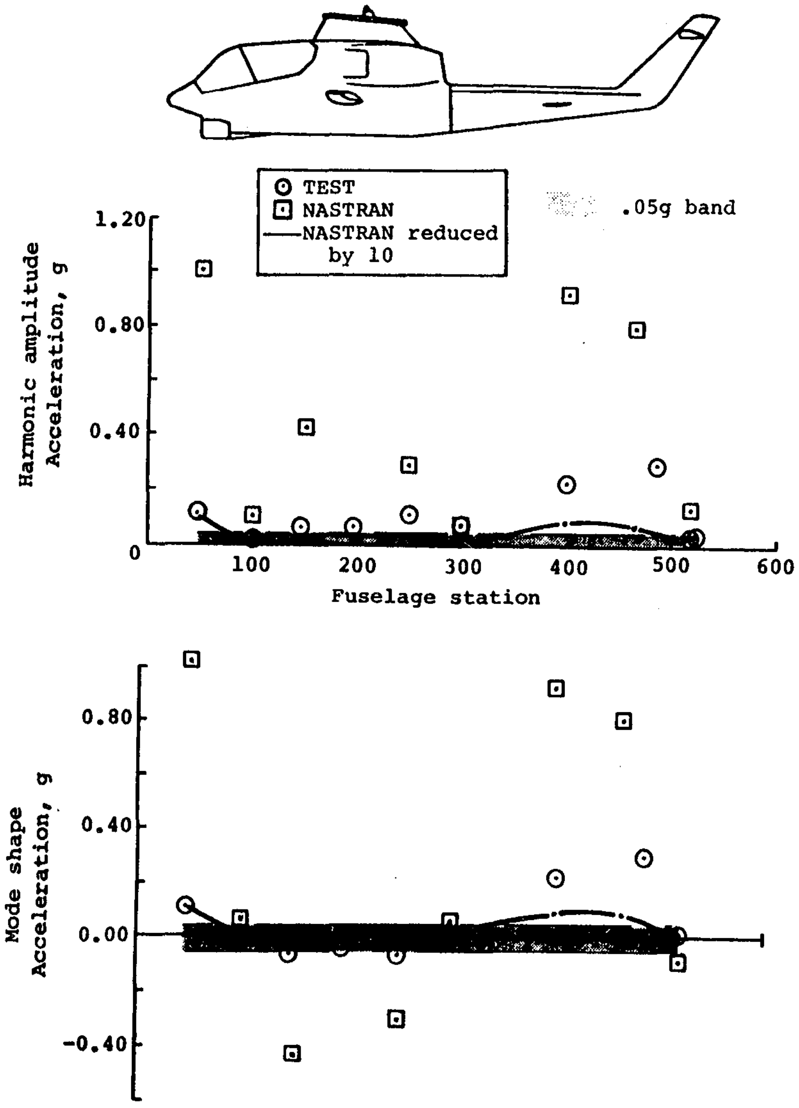

67 KT - CLEAN WING

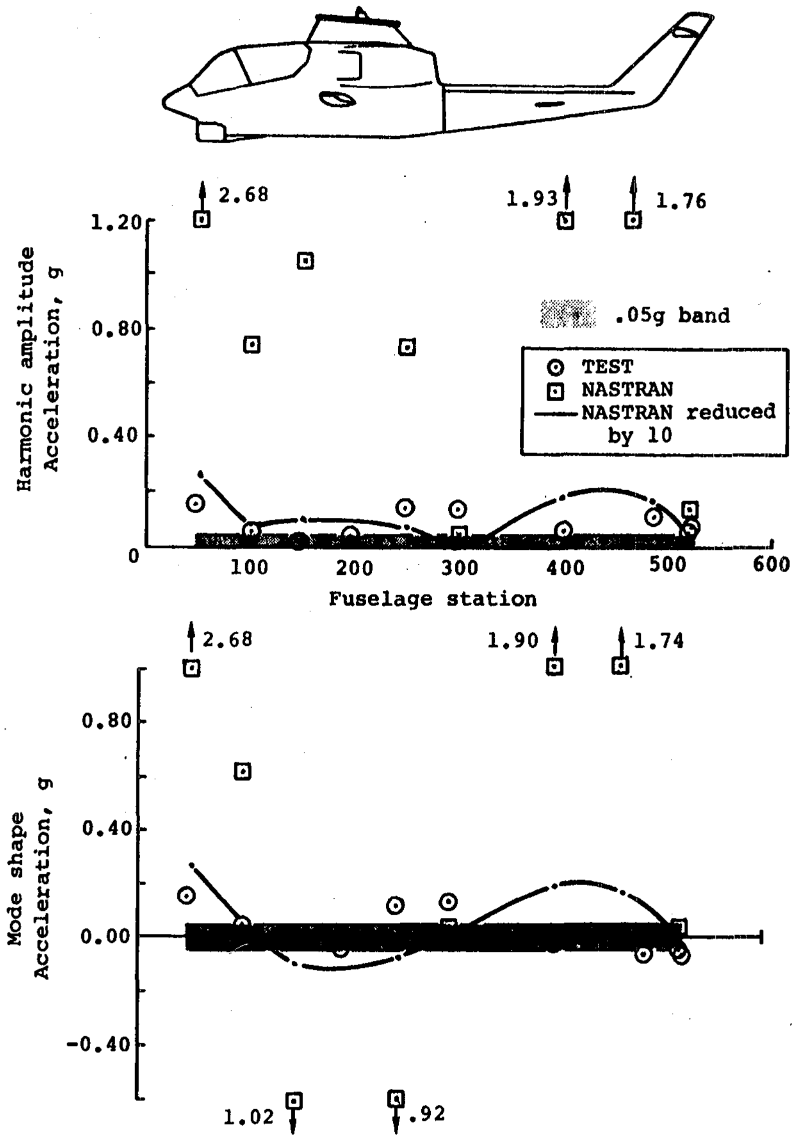

142 KT - CLEAN WING

SIX-PER-REV VERTICAL RESPONSE

The overall predicted response levels are the same order of magnitude as test. The most significant differences occur along the tailboom and the vertical fin. The higher measured elevator response is controlled by the elevator natural frequencies. The NASTRAN elevator model is a simplified elastic line representation with very few degrees of freedom remaining in the analysis after the Guyan reduction. The calculated elevator natural frequencies are 42 Hz for the symmetric bending mode and 47 Hz for the asymmetric bending mode. The test data indicate this mode to be closer to six-per-rev. Improved correlation may be possible by a more detailed representation of the elevator model in NASTRAN.

The frequency response data indicate significant differences at the six-per-rev main rotor harmonic. Consequently, any agreement for this flight vibration correlation study is difficult to assess. The six-per-rev responses are, in general, lower than the two-per-rev responses except along the tailboom. Although the percentage errors are large, the trend in terms of response magnitude was predicted. These differences between analysis and test may not be important for design.

SIX-PER-REV VERTICAL RESPONSE

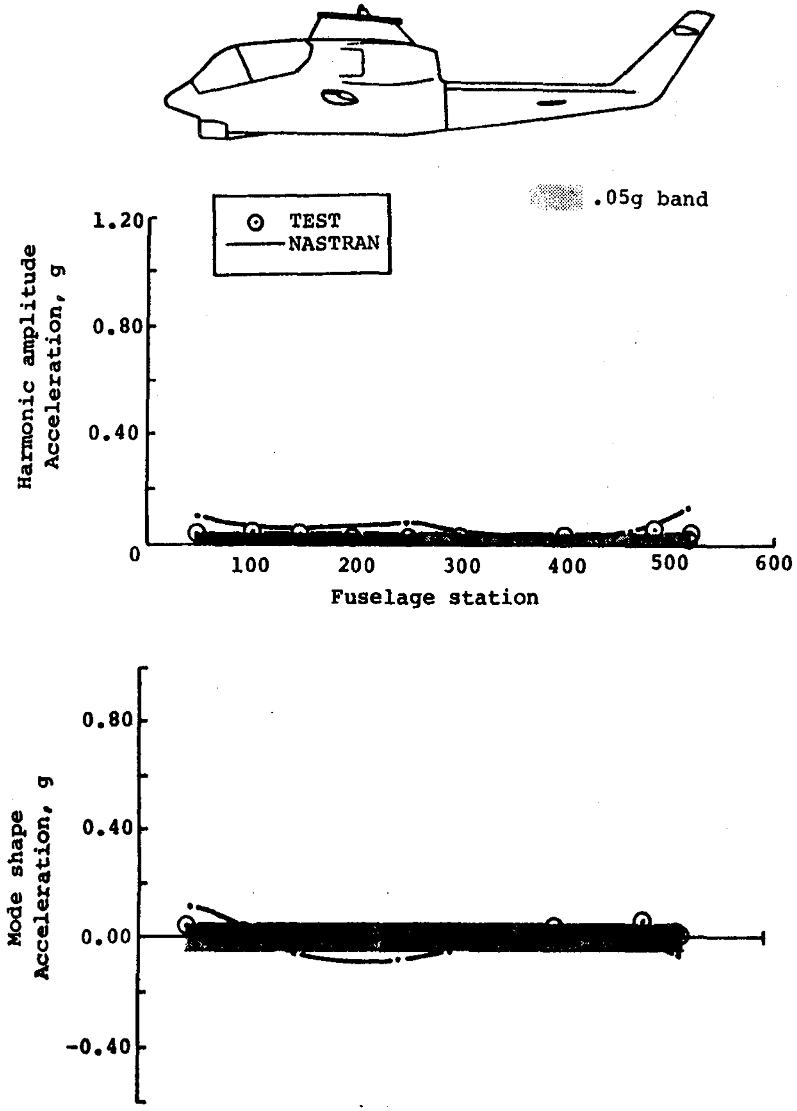

67 KT - CLEAN WING

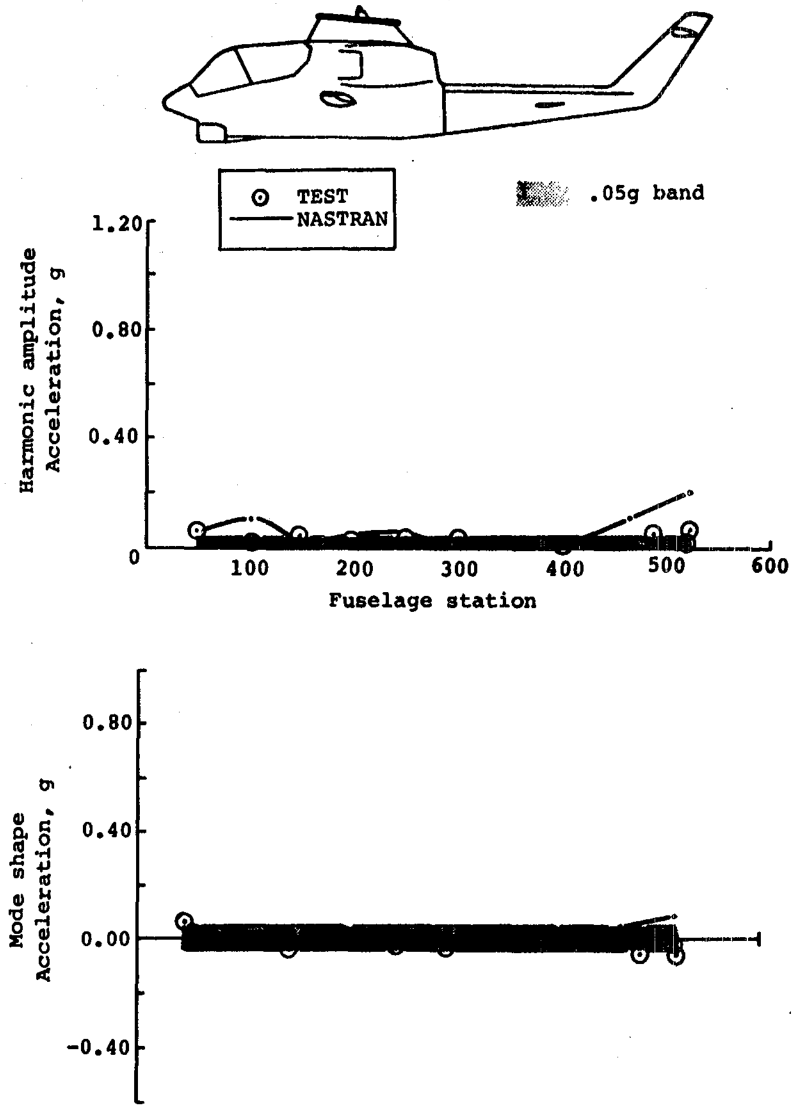

142 KT - CLEAN WING

TWO-PER-REV LATERAL RESPONSE

The correlation between analysis and test is poor, especially at the tail. The predicted responses are considerably lower than test. These significant differences are important in design since NASTRAN underestimates the order of magnitude and trend characteristics necessary to structural fatigue and vibration isolation assessments.

The large differences may result from main rotor downwash exciting the tail fin laterally. In addition, the idealized NASTRAN pylon may be isolating rolling moments due to inplane hub shears better than test indicates.

Frequency response data is insufficient for excitation at the main rotor hub and suspect. Additional analysis and test is necessary to resolve this problem.

TWO-PER-REV LATERAL RESPONSE

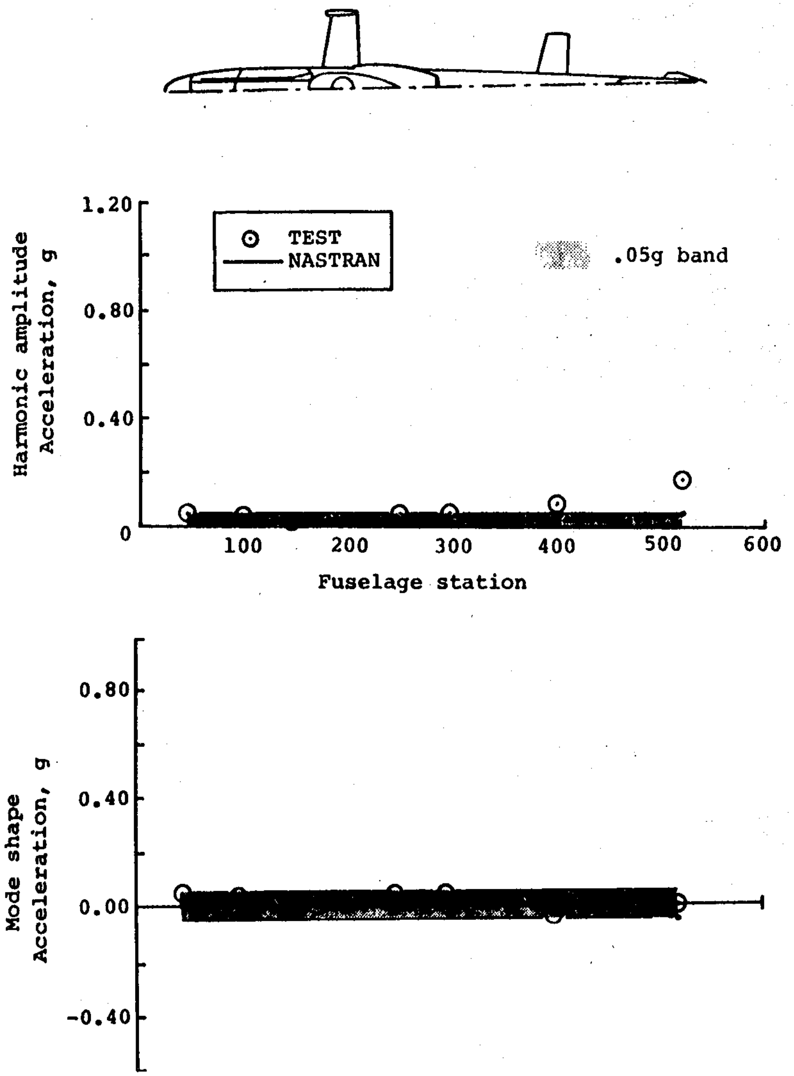

67 KT - CLEAN WING

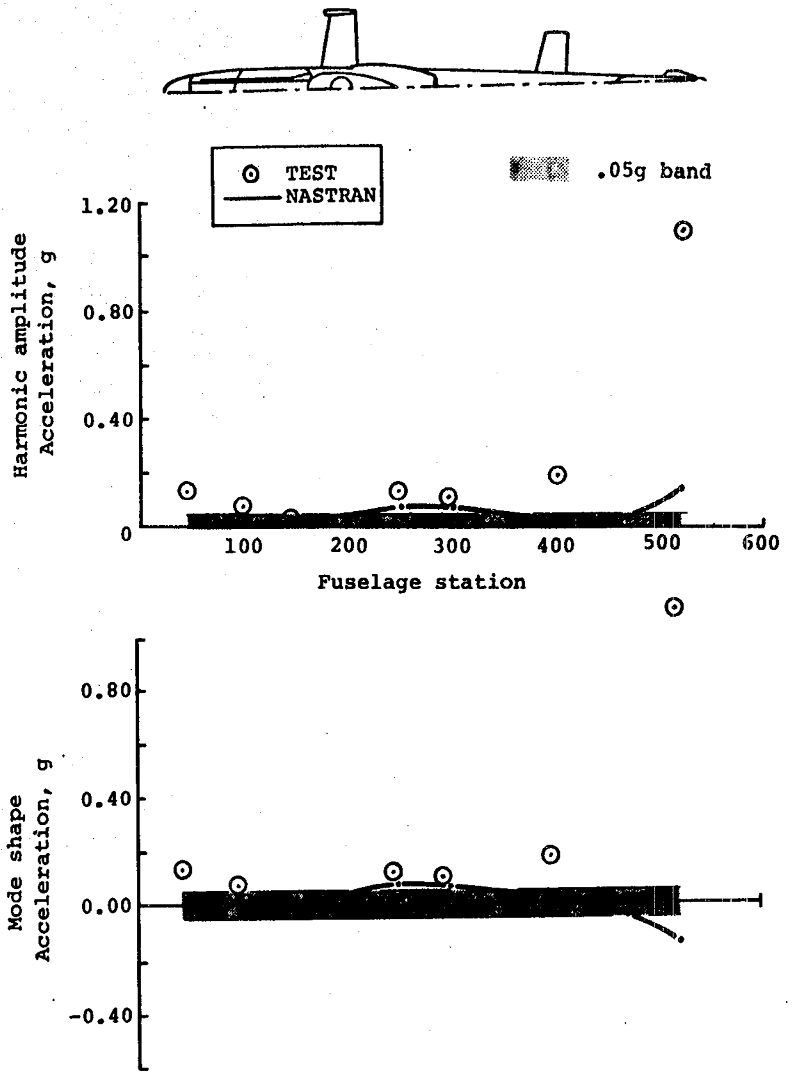

142 KT - CLEAN WING

FOUR-PER-REV LATERAL RESPONSE

While the two-per-rev responses were underestimated, the predicted four-per-rev responses are significantly higher than test. Strong coupling between the lateral response and the artificial vertical pylon bounce mode resonance that was discussed earlier may explain these differences for the clean wing configuration. The data indicate NASTRAN is consistently higher than test. Additional analysis and test is required to properly assess these differences. It is considered an important design requirement to predict low responses as well as high responses if fatigue damage and vibration isolation are to be properly assessed.

FOUR-PER-REV LATERAL RESPONSE

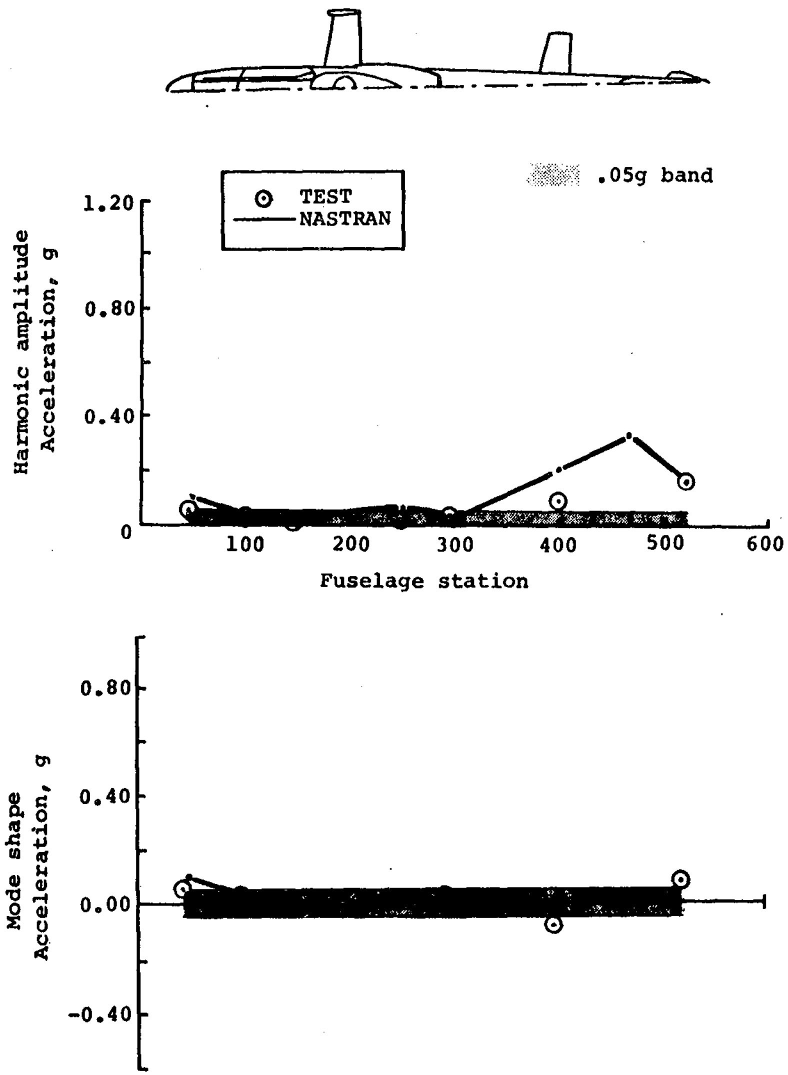

67 KT - CLEAN WING

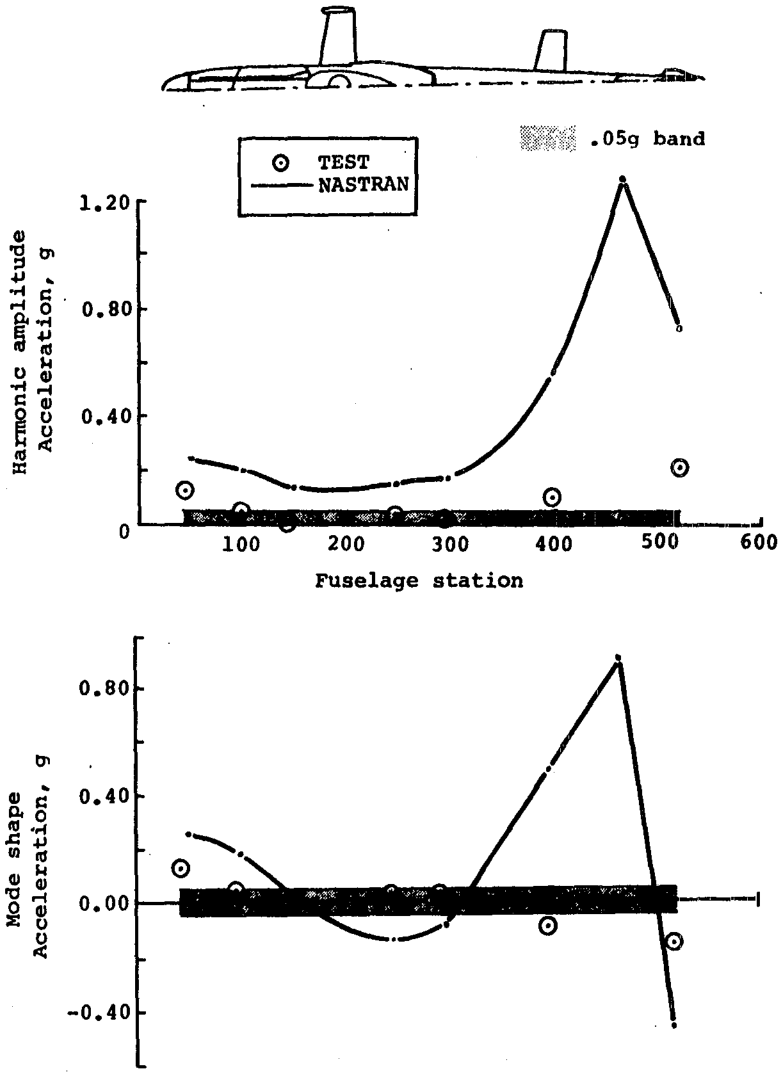

142 KT - CLEAN WING

SIX-PER-REV LATERAL RESPONSE

For the clean wing configuration the predicted responses are generally higher than test except at mid and high airspeeds where the measured elevator and tail responses are higher. An elevator asymmetric mode near six-per-rev is suspected. This mode produces torsion in the tailboom which in turn causes high lateral responses at the tail.

The frequency response data indicate significant differences between NASTRAN and test for six-per-rev. Consequently, any agreement for this main rotor harmonic may be fortuitous.

SIX-PER-REV LATERAL RESPONSE

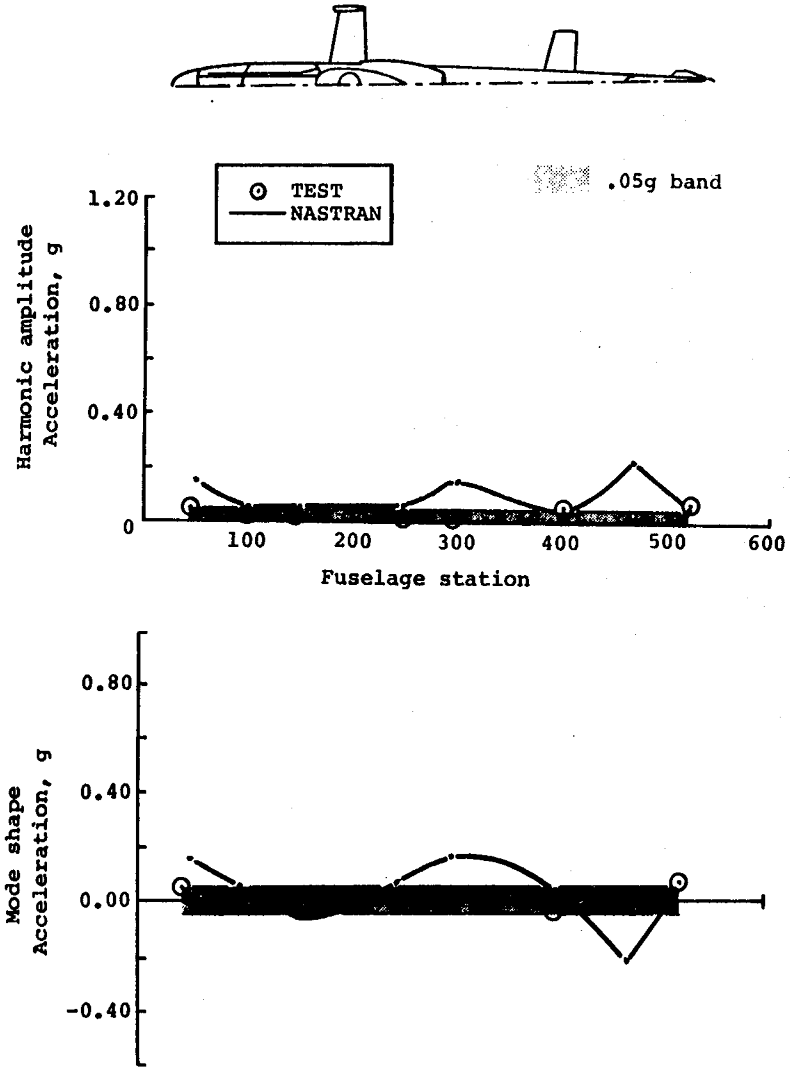

67 KT - CLEAN WING

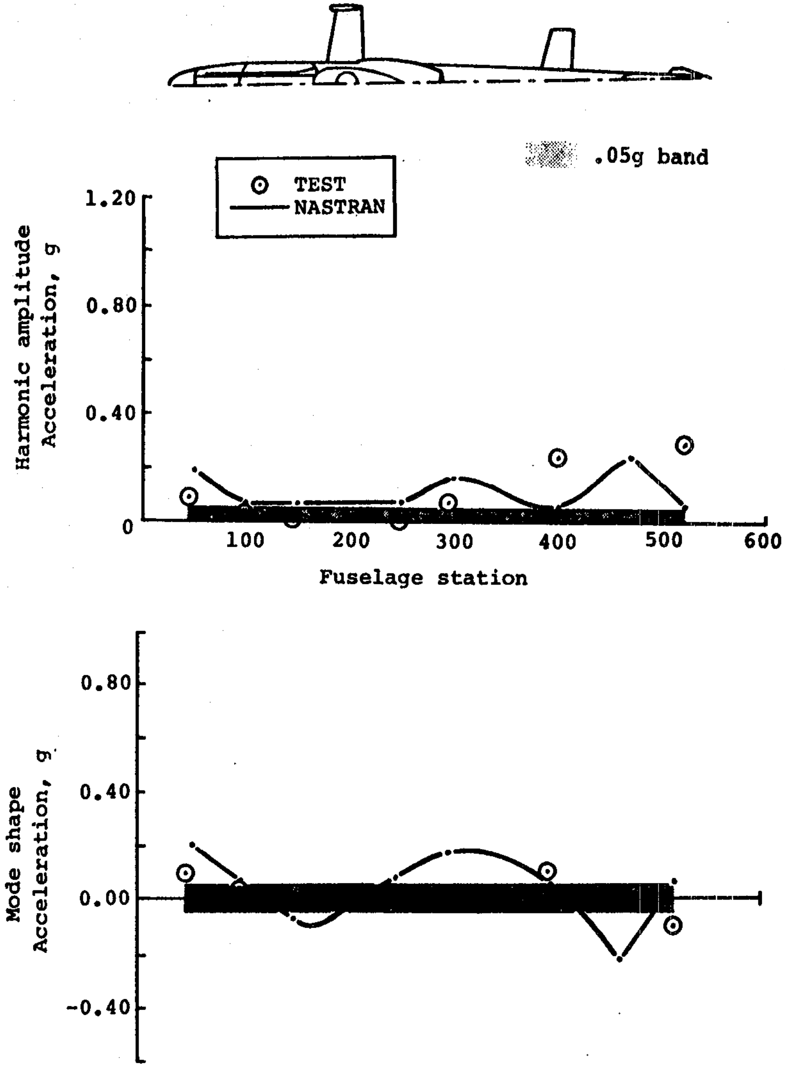

142 KT - CLEAN WING

FLIGHT VIBRATION CORRELATION

The table presents an overall qualitative assessment of the aforementioned flight vibration correlation results. The impact of this study on design is emphasized. The results are considered adequate if response magnitude and trends appear reasonable. The results are considered inadequate if the response magnitude and trends cannot be assessed because of insufficient data.

FLIGHT VIBRATION CORRELATION

CONDITION	DIRECTION	HARMONIC	CORRELATION			PROBLEM AREA	EXPLANATION
			LOW	MID	HIGH		
CLEAN WING	VERTICAL	2/REV	GOOD	GOOD	GOOD	NOSE AT 142 KT, LOW	PITCH ISOLATION, NOSEBOOM
CLEAN WING	LATERAL	2/REV	POOR	POOR	POOR	RESPONSE LOW ESPECIALLY AT TAIL	ROLL ISOLATION, MAIN ROTOR DOWNWASH ON VERTICAL FIN
CLEAN WING	VERTICAL	4/REV	FAIR	FAIR	GOOD	RESPONSE WAS REDUCED BY A FACTOR OF TEN BASED ON LOADS	ARTIFICIAL RESONANCE DUE TO BIG MASS USED FOR HUB ACCELERATIONS
CLEAN WING	LATERAL	4/REV	POOR	POOR	POOR	RESPONSE VERY HIGH ESPECIALLY AT TAIL	LATERAL COUPLING WITH ARTIFICIAL VERTICAL MODE IN RESONANCE
CLEAN WING	VERTICAL	6/REV	FAIR	FAIR	FAIR	MAST HIGHER, ELEVATOR AND TAIL LOWER	SUSPECT ELEVATOR MODE NEAR 6/REV IN TEST
CLEAN WING	VERTICAL	6/REV	FAIR	FAIR	FAIR	MAST HIGHER, ELEVATOR AND TAIL LOWER	SUSPECT ELEVATOR MODE NEAR 6/REV IN TEST

AIRSPEED

CONCLUSIONS - FLIGHT VIBRATION

Test data from an AH-1G operational loads survey (Eustis Contract DAAJ02-73-C-0105) were compared to a NASTRAN analysis. Measured vibration responses of the airframe for level flight conditions were compared to a NASTRAN vibration model. Measured hub accelerations and control loads were used to excite the analytical model. The correlation was based on comparing vibration amplitude and mode shape curves at three main rotor harmonics: two-, four-, and six-per-rev. Guidelines used for evaluating the correlation were discussed and used in judging the correlation.

Conclusions from the flight vibration correlation study are as follows:

1. There was good agreement between calculated and measured vertical two-per-rev vibration. This predominant excitation frequency of the BHT two-bladed rotor produces vibration levels that are normally higher than those at the higher harmonics.

2. Lateral two-per-rev vibration levels were calculated to be much lower than those measured in test, primarily at the tail. Poor prediction of roll isolation from the main rotor pylon or main rotor downwash excitation on the fin are suspect.

3. Vertical stiffness of the main rotor pylon was extremely important in the vibration analysis. This problem was caused by using hub accelerations without control of the applied load. Since the applied vertical hub acceleration was very small, vertical deflections on the order of a few thousandths of an inch had a significant effect on the applied load. Pylon designs with vertical isolation, such as the nodal beam, should not be as sensitive to vertical deflections of the mast and transmission.

4. Pendulum stiffening due to rotor thrust, elastomeric mount rotational stiffness, and increased pylon modal damping were analyzed to determine the effect on two-per-rev isolation of the main rotor pylon. The results of the analysis showed there was not a significant effect at two-per-rev.

CONCLUSIONS - FLIGHT VIBRATION (concluded)

5. Except for a resonance of an artificial mode at four-per-rev caused by the method of applying hub accelerations, calculated and measured four- and six-per-rev vibration responses agreed fairly well. It is not surmised that the accuracy of the analysis at these frequencies can be judged, however, since the vibration response at these frequencies was not strongly influenced by modes in close proximity to the forcing frequency. From the results of vibration testing, the airframe vibration prediction was quantitatively accurate through four-per-rev, but deviated from measured results significantly at six-per-rev. In addition, when exciting at the main rotor hub through the pylon, the correlation obtained was poorer than that obtained when exicting directly on the airframe. Considering these factors, the agreement of four- and six-per-rev may have been coincidental. More information is needed in order to judge the NASTRAN analysis for prediction of airframe vibration at these frequencies.

Recommendations for further investigations are as follows:

1. Investigate the effect of pylon dynamics on airframe vibration by a combined analytical and test correlation program.

2. Investigate the main rotor two-per-rev downwash environment on the AH-1G fin.

3. Investigate validity of current rotor analyses for prediction of two-, four-, and six-per-rev excitation for pylon/airframe NASTRAN analysis. A valid analytical model of the airframe will not accurately predict the vibration response of the airframe if the excitation is not accurate. In addition, a convenient method for measuring hub shears should be developed.

CONCLUSIONS - FLIGHT VIBRATION

- TWO-, FOUR-, AND SIX-PER-REV CORRELATION
  - TWO-PER-REV VERTICAL GOOD
  - TWO-PER-REV LATERAL POOR
  - FOUR- AND SIX-PER-REV FAIR

- FURTHER WORK NEEDED
  - INVESTIGATE PYLON DYNAMICS
  - CORRELATION OF ROTOR ANALYSES
  - MEASURE MAIN ROTOR DOWNWASH ON FIN
  - DEVELOP HUB SHEAR MEASUREMENT TECHNOLOGY

6. TAILBOOM EFFECTIVE SKIN INVESTIGATION

TAILBOOM AND VERTICAL FIN STATIC TEST

In addition to flight vibration correlation, deflection, and internal load data from static tailboom tests are compared with a NASTRAN analysis. The purpose of the tailboom test correlation study is to better quantify the effects of buckled skin under compression loading on the stiffness and internal loads of the semimonocoque tailboom structure. Rather than use the elastic line model of the tailboom, a built-up NASTRAN tailboom model was developed for the analysis. This was considered necessary so that the many load paths that were instrumented in test were represented in the model for direct comparison.

In the previous tailboom static test comparison, the NASTRAN elastic line model agreed well with measured deflections. The tailboom stiffness properties for the elastic line model were calculated by considering the skins as fully effective. This is not totally accurate since the tailboom is of semimonocoque sheet-stringer design. This type of design compensates for skin buckling and the corresponding reduced element areas at stress levels near the limit design stress. Since this analysis is based on stress levels resulting at 1g level flight conditions rather than 3.5g limit conditions, consideration of the skins as being fully effective is believed accurate. However, better procedures for determining the effective skin should be developed to determine the stiffness of sheet metal panels under various loadings for use in dynamic analysis. This study is a step in that direction since current methods are evaluated by comparison with test.

The tailboom and vertical fin structure are shown. The tailboom is bolted to the fuselage at four attachment fittings located at the four main longerons of the tailboom and the four main beam caps of the fuselage.

The tailboom is of semimonocoque construction having aluminum skins, stringers, and longerons. The longerons and stringers are supported by bulkhead frames spaced down the length of the boom. The hinged tail rotor drive shaft cover on top of the boom is assumed nonstructural.

The vertical fin has a two-cell cambered airfoil section with two spars and a trailing edge strip. The hinged tail rotor drive shaft cover on the front of the fin is assumed nonstructural as well as the top portion of the fin which extends above the 90-degree gearbox.

TAILBOOM AND VERTICAL FIN STATIC TEST

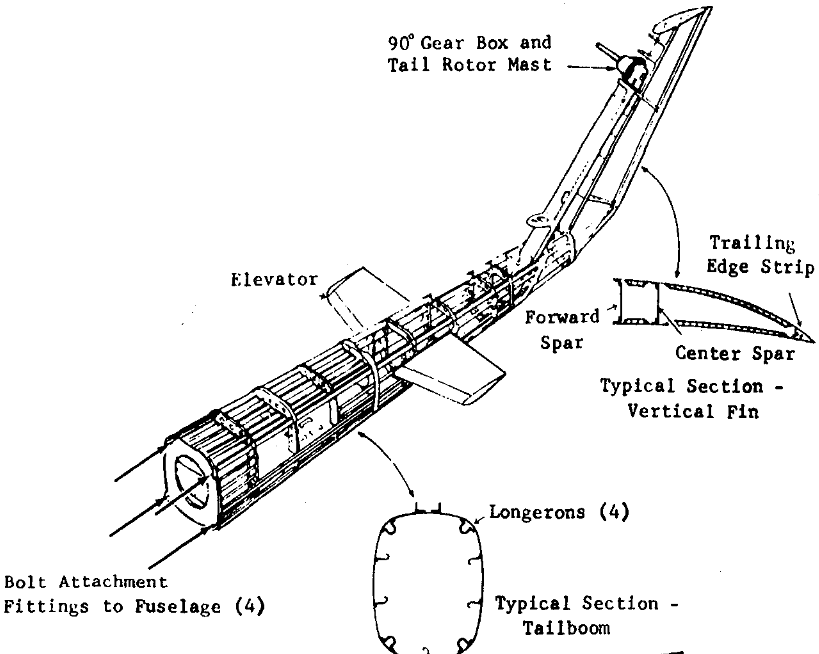
90° Gear Box and
Tail Rotor Mast
Trailing Edge Strip
Elevator
Forward Spar
Center Spar
Typical Section - Vertical Fin
Longerons (4)
Bolt Attachment Fittings to Fuselage (4)
Typical Section - Tailboom

NASTRAN idealized model

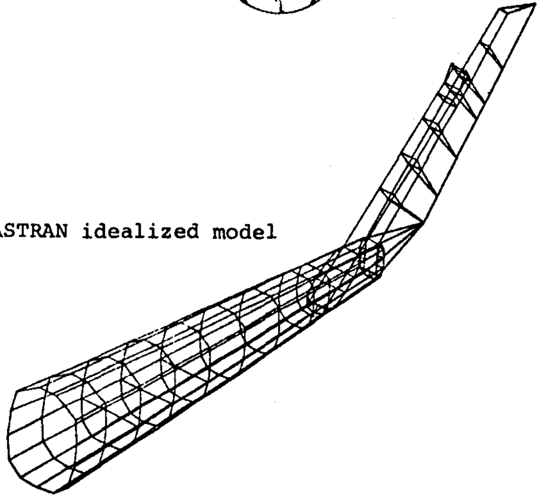

TAILBOOM STATIC TEST SETUP

The tailboom and fin assembly used in this test is from an AH-1G helicopter, ship number 68-15048, obtained from Rock Island Arsenal in Illinois, and is the same specimen used in a previous load-deflection test. The tailboom installation is Part No. 209-030-800-7. The flight history of the tailboom is unknown but no obvious structural defects were present. All cargo and inspection covers were in place and secured for the test. The drive shaft and cover were removed.

The tailboom was cantilevered from a support fixture with the tailboom centerline horizontal as shown. The fixture was bolted to the floor of the BHT Engineering Test Building with the tailboom mounted to the test fixture at the four production fuselage attachment fittings.

Test loads were applied to the tailboom using a hydraulic cylinder and hand pump with a calibrated pressure gage. A contour fitting frame was attached to the tailboom at Boom Station 227 and load was applied through the frame. The applied load was cycled from 0 to maximum at least three times before data were measured. Data were then recorded for three separate test runs for each load condition.

Three separate loads were applied perpendicular to the tailboom centerline at Boom Station 227. Lateral right and lateral left loads of 5604 N maximum were applied at Boom Station 227, W.L. 61.10. A vertical down load of 4448 N maximum was applied at Boom Station 227, B.L. 0.0. The lateral right and left loads were applied in thirteen increasing increments with four decreasing increments. The vertical down load was applied in ten increasing increments with four decreasing increments.

Data were taken during three separate load applications for each load condition. There was no significant difference between results from each load application. The third load application was selected for plotting, since any settling in the joints of the structure would have most likely occurred during the first and second loadings.

TAILBOOM STATIC TEST SETUP

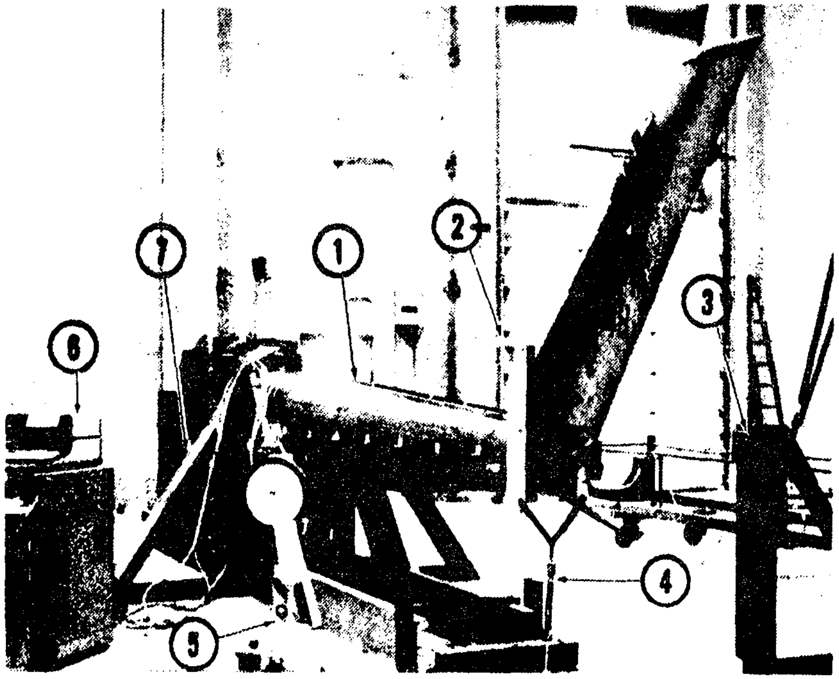

Arrows indicate:

1. AH-1G tailboom test specimen
2. Contour frame for load application
3. Fixture for attaching hydraulic cylinder for lateral right load
4. Hydraulic cylinder for applying vertical down load
5. Hand pump with calibrated pressure gage
6. HP9830A data acquisition system
7. Tailboom mounting fixture

TAILBOOM INSTRUMENTATION

Single active arm strain gages were installed at various locations on the tailboom with the axis of the gage parallel to the tailboom centerline. Other gages were installed inside the tailboom on stringers and longerons.

Data were recorded automatically with a Hewlett Packard 9830A data acquisition system. The strain level for each gage was converted to stress using a conversion factor for aluminum based on a Young's modulus of $E = 7.240 \times 10^{10}$ N/m^2. It should be noted that no correction was made to the indicated stress due to changes in indicated strain caused by Poisson effects. Results were printed out for each increment of load.

TAILBOOM INSTRUMENTATION

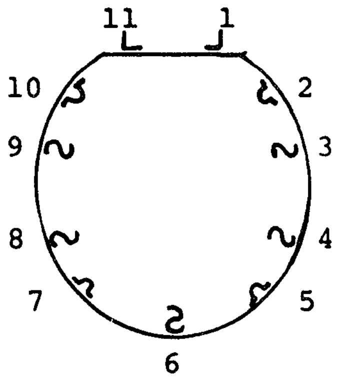
11
1
10
2
9
3
8
4
7
5
6

Section A-A
B.S. 69.97

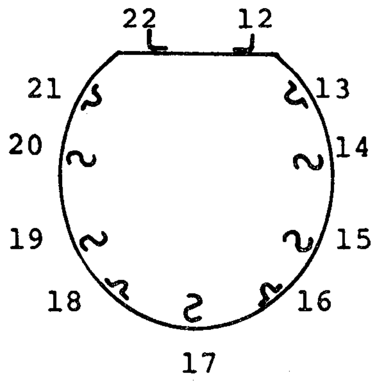
22
12
21
13
20
14
19
15
18
16
17

Section B-B
B.S. 90.91

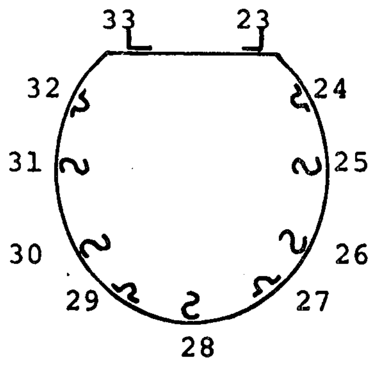
33
23
32
24
31
25
30
26
29
27
28

Section C-C
B.S. 118.85

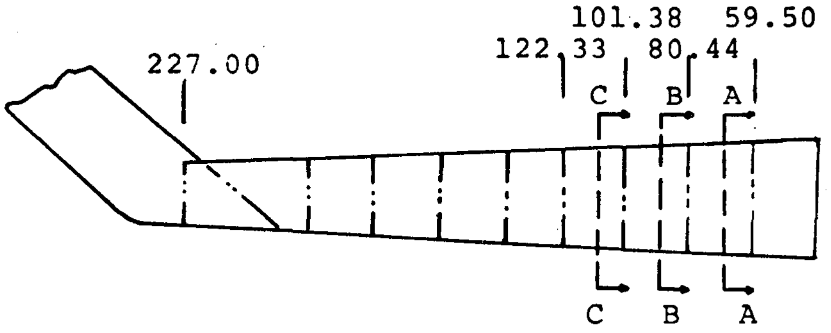
227.00
101.38
59.50
122.33
80.44
C
B
A
C
B
A

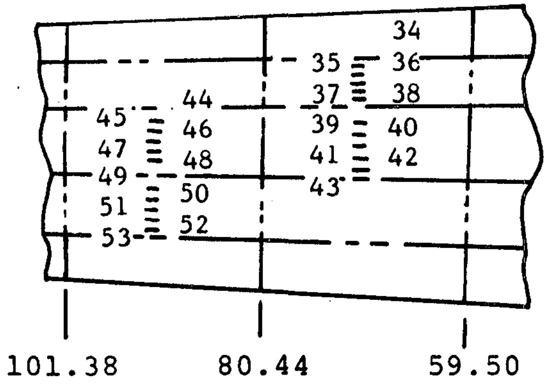
34
35
36
37
38
44
45
46
47
48
39
40
41
42
49
50
43
51
52
53
101.38
80.44
59.50

TAILBOOM MODELING PHILOSOPHY

The objective of the modeling of the tailboom was to provide an analysis for evaluating the test data. To achieve good comparison between the test and analysis, the structural load paths must be correctly represented. These paths are a function of geometry and sectional properties of the structural members. To meet this primary objective it is important that the stiffness of the structure be accurately represented. Some guidelines used in modeling are the following:

1. In the built-up modeling of the tailboom, grid points are located at the intersection of panels. This is done because the axial members (rods) are generally easier to relocate to the grid point than shear panels.
2. Skin panels are modeled with shear panels and are assumed to carry no axial load. If the skin is unbuckled or has some of its material effective, the area of the stringer or longeron is increased to reflect the effective skin.
3. The longerons and stringers are modeled with rod elements that carry only tension or compression axial loads, since their own bending stiffness is assumed negligible compared to the section.
4. The ring bulkheads do not significantly affect the bending stiffness of the overall tailboom. These bulkheads are modeled with bending bars, with stiffness in the plane of the bulkhead to preserve the location of the axial members around the periphery.

TAILBOOM MODELING PHILOSOPHY

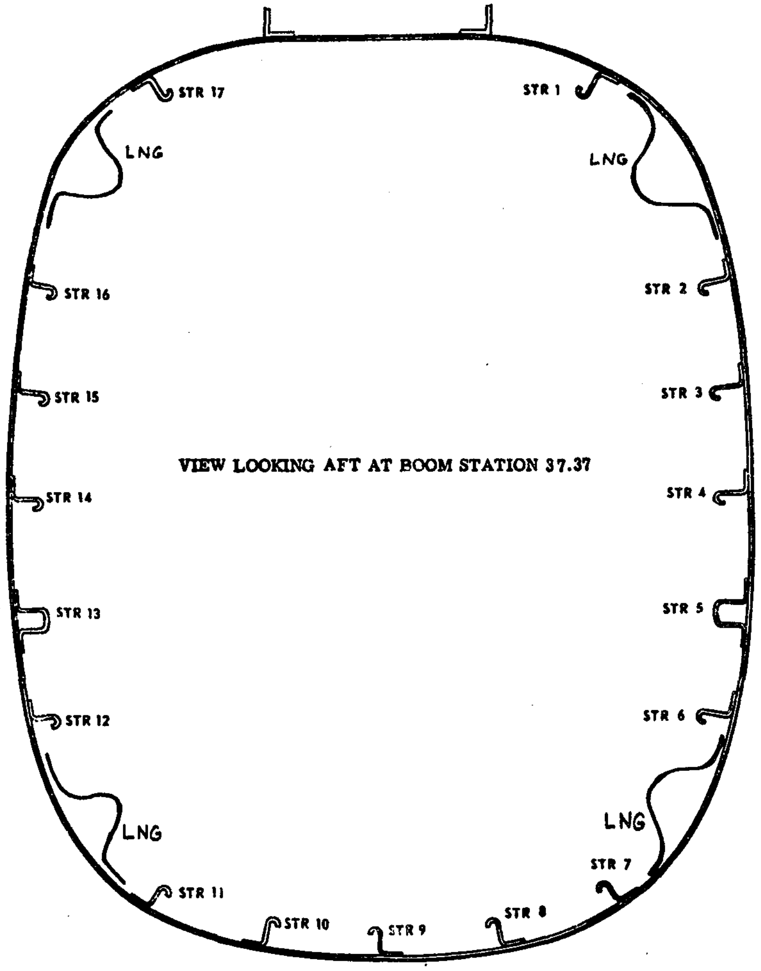
STR 17
STR 1
LNG
LNG
STR 16
STR 2
STR 15
STR 3
VIEW LOOKING AFT AT BOOM STATION 37.37
STR 14
STR 4
STR 13
STR 5
STR 12
STR 6
LNG
LNG
STR 7
STR 11
STR 8
STR 10
STR 9

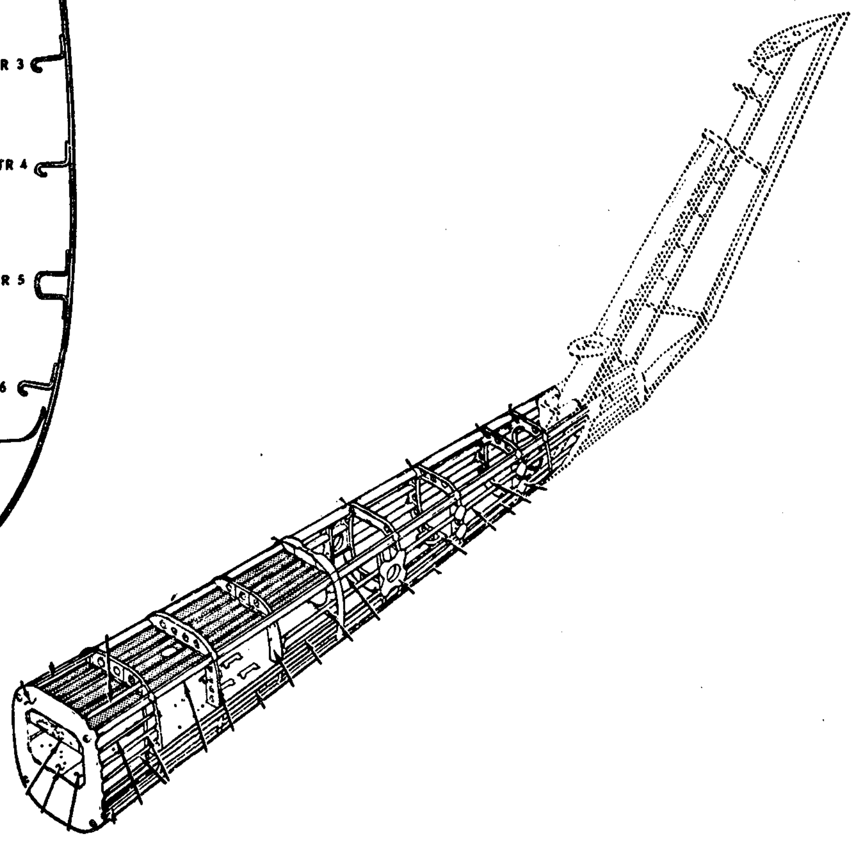

EFFECTIVE SKIN

As discussed in the previous section, the primary objective of the NASTRAN model is to provide an analysis to accurately compare to the test data. To do this, effective axial load carrying skin was accounted for by adding area to the stiffener's cross sectional areas. Each load case was run several times to iterate to the correct amount of effective skin. The method used for determining the portion of the skin panels which are effective in resisting axial loads follows a conventional approach with two exceptions.

These exceptions are:

1. Conventional bending analysis using the classical approach assumes that plane sections remain plane while resisting bending loads. The method contained herein uses a finite element technique for the bending analysis and as such assumes equilibrium and continuity at the model element joints only. Sections which were originally plane in the unloaded state do not necessarily remain plane while resisting bending loads.

2. Conventional bending analysis generally includes some effective skin in the first iteration and adds additional effective skin for each successive iteration. The methods used in this study assumes no effective skin for the initial iteration but progressively adds the skin areas which are calculated to be effective for each succeeding iteration.

To calculate the effective skin for each iteration, the following methods were used:

1. The skin elements on the tension side of the neutral axis are considered 100 percent effective in resisting axial load. The area of these skins is distributed equally to adjacent longerons or stringers. Also, at the longeron locations where skin overlap occurs, the skins between the longeron-to-skin attachments are assumed to be 100 percent effective in both tension and compression.

EFFECTIVE SKIN (continued)

2. An effective width of skin, W, centered on the line of skin-to-stringer attachments can carry the same compression stress as the stringer. Effective skin widths W_1, W_2, W_3, etc., are shown on the typical tailboom cross section in the figure and can be calculated by:

$$W = (2)(.85)\ t\sqrt{\frac{E}{\sigma_{axial}}}$$

where W is the effective skin width on both sides of a stringer, t the skin thickness, σ_{axial} the applied axial stress of the attached longeron or stringer, and E is the modulus of elasticity of the skin material.

3. The remainder of the curved skin between axial members carries a maximum compressive stress of:

$$\sigma_{critical} = \frac{.3Et}{R} \text{ for } v = .3 \text{ and } \frac{R}{t} < 500$$

$$\sigma_{critical} = E\left|9\left(\frac{t}{R}\right)^{1.6} + 0.16\left(\frac{t}{L}\right)^{1.3}\right| \text{ for } 500 < \frac{R}{t} < 3000$$

$$\text{and } 0.1 < \frac{L}{R} < 3000$$

$$\sigma_{critical} = KE\left(\frac{t}{b}\right)^2 \text{ for flat sheet } (R = \infty)$$

where $\sigma_{critical}$ is the buckling stress of the skin element, R the radius of curvature of the skin element, L is the tailboom bay depth, K is a constant and is 3.62 minimum, and b is the distance between axial members.

EFFECTIVE SKIN (concluded)

Thin curved skin between the axial members normally buckles at a compressive load less than that required to buckle the axial members. In this analysis, the curved skin is treated as an element with varying effective area which depends on the ratio of the curved skin's buckling stress, $\sigma_{critical}$, to the axial member's stress, σ_{axial}. Hence, the effective skin area, $A_{eff'}$, for the buckled skin panels can be written,

$$A_{eff} = b't\ (\sigma_{critical}/\sigma_{axial})$$

where b' is the width of the curved skin between the effective skin widths W_1, W_2, W_3, etc.

EFFECTIVE SKIN

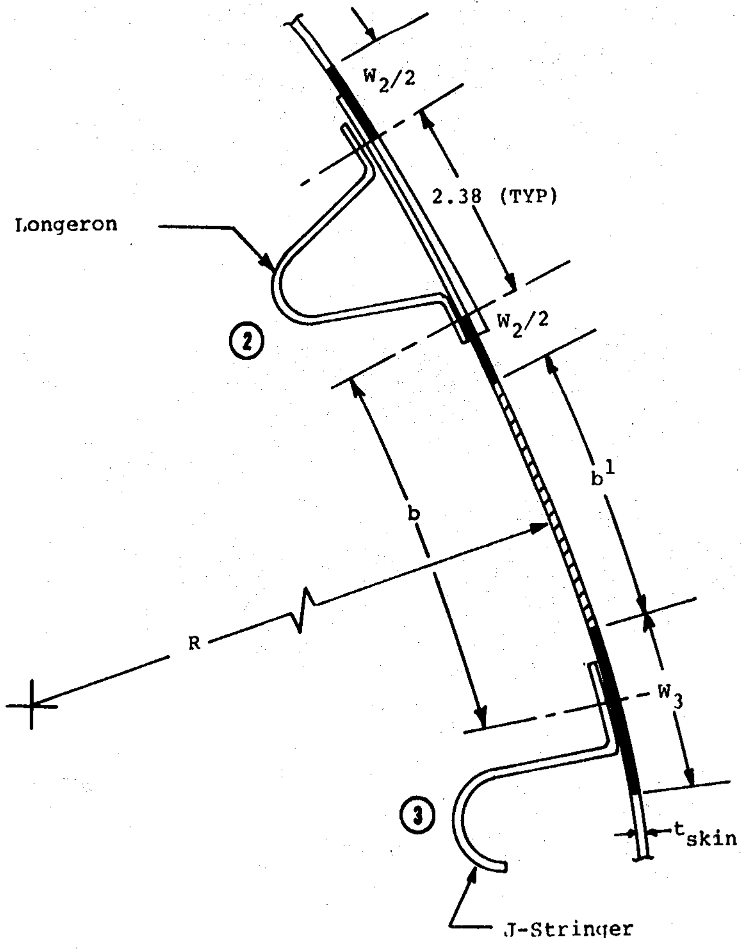
$W_2/2$
2.38 (TYP)
Longeron
$W_2/2$
②
b
b^1
R
W_3
③
t_{skin}
J-Stringer

STRESS COMPARISON

A comparison between the stresses measured in the test and the stresses calculated in the NASTRAN analysis with full effective skin is given in the table. Each test load was applied three times. The average of three readings are given as the test stress.

In reviewing the comparison of the test and analysis stresses, good correlation as well as poor correlation can be seen. For the right load, a difference of 35 percent is shown for element 4, the compression side, of bay 4 while a 37 percent difference is shown for the tension side, element 10 of bay 4. Similar discrepancies are observed for the left loading. The down loading had generally better correlation with the exception of the bottom stringer, element number 6, which shows a difference of 38 percent for bay 2, 0 percent for bay 3, and 26 percent for bay 4.

For this analysis, the skin was assumed to carry a constant load equal to the buckling load after buckling occurs. Upon examining the strain behavior of the buckled panels, an assumption of the buckled panels carrying no load might give better correlation between test and analysis.

STRESS COMPARISON

Tailboom Bay	Ele. No.	5604 N Rt. Load		5604 N Lft Load		4448 N Down Load	
		TEST	NASTRAN	Test	NASTRAN	Test	NASTRAN
2	1	-1936	-1443	1448	1036	3331	3131
	2	-2969	-4276	3424	3702	1949	3002
	3	-5281	-5269	5063	3958	968	1217
	4	-5432	-6590	4280	4953	-1086	-1311
	5	-4984	-4520	3220	3902	-2548	-3045
	6	211	- 96	53	- 236	-5458	-3371
	7	4839	4242	-3792	-5079	-3516	-3391
	8	5682	5099	-5471	-7247	-1541	-1397
	9	3127	4159	-3555	-6220	948	1284
	10	4957	4329	-7038	-6768	4128	3404
	11	599	1383	-2061	-2147	4187	3191
3	1	-1291	-1294	1613	827	3904	3694
	2	-3516	-3713	4734	3310	2759	2747
	3	-3983	-4084	4707	3556	777	1007
	4	-4075	-2856	3661	2786	- 790	- 685
	5	-5511	-3795	3615	3510	-3035	-2872
	6	20	- 228	59	-1895	-3817	-3877
	7	4957	3511	-3753	-4174	-3681	-2917
	8	3838	2780	-3160	-2843	- 704	- 614
	9	2772	3695	-2791	-4267	626	1100
	10	3575	3826	-4312	-4114	2752	3107
	11	1752	1212	-2679	-1780	4029	3750
4	1	-1185	-1158	1237	787	4319	3757
	2	-3760	-3192	3786	3037	2679	2621
	3	-4470	-2962	4372	3418	790	905
	4	-4300	-2783	3937	2852	- 955	- 754
	5	-3872	-3340	3351	3323	-2904	-2798
	6	- 53	- 281	- 13	- 25	-3141	-3916
	7	3917	2589	-3476	-2808	-2963	-2094
	8	2746	2740	-2607	-3148	- 580	- 603
	9	3193	3404	-2949	-3544	770	943
	10	3970	2486	-4378	-2545	3127	2022
	11	2021	1084	-2568	-1415	4168	3700

1 pound = 4.448 newton
1 PSI = 6895 N/m^2

DEFLECTION COMPARISON

A comparison between the calculated and measured deflections is shown in the figure for vertical and lateral load conditions. Deflections with and without effective skin are given. The effective skin analysis for the vertical deflection agrees well with the test results. The lateral load case shows the NASTRAN analysis to be stiffer than test. The figure also illustrates the load-stress behavior for a buckled panel. The solid line shows the load in the panel as it was assumed to behave for this analysis, constant load equal to the buckling load after buckling occurs. The dashed line curve shows the post buckling behavior of the panel more realistically, with the stress falling off with load. Using the method of calculating effective skin presented in this report, a model that is too stiff may result. This is probably why deflections for the lateral loading do not agree with the test results. Little buckling occurred for the vertical loading while there was considerable buckling for lateral. (Note: Another possible reason the NASTRAN model is too stiff laterally is because the longeron areas are lumped at the grid points on the contour and not at the actual longeron centroids. Therefore, the model has too much area moment of inertia in the lateral direction due to the "Ad^2" terms.)

DEFLECTION COMPARISON

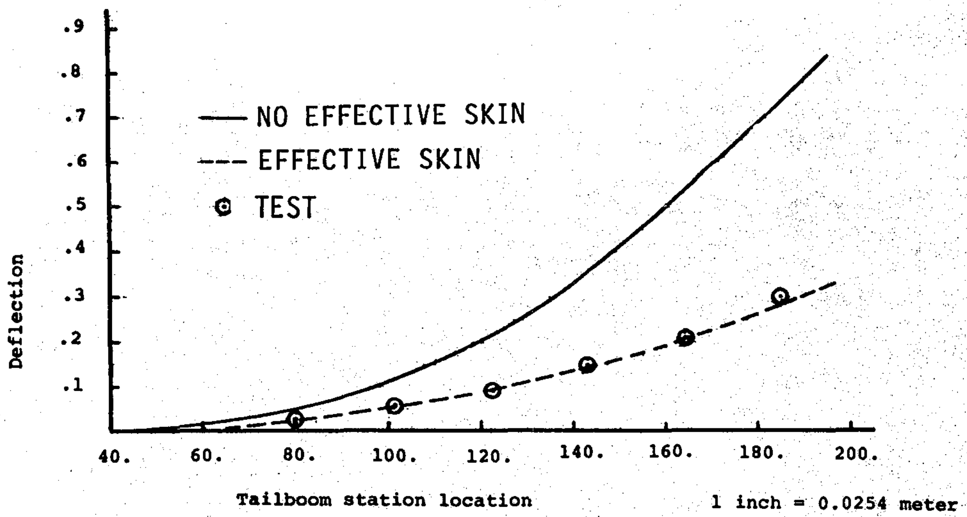

VERTICAL DEFLECTION

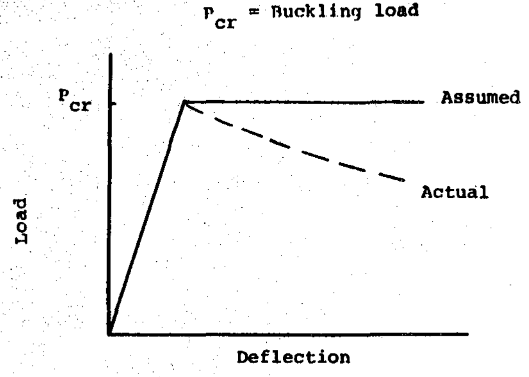

SKIN BUCKLING BEHAVIOR

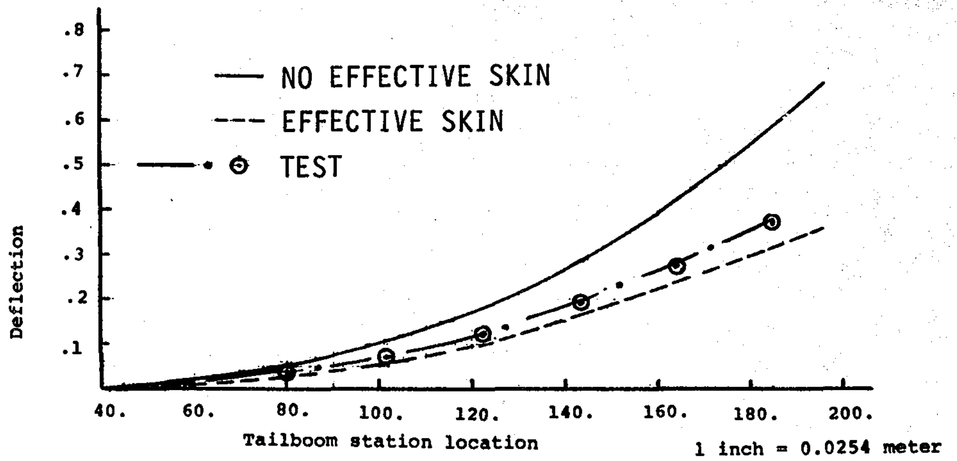

LATERAL DEFLECTION

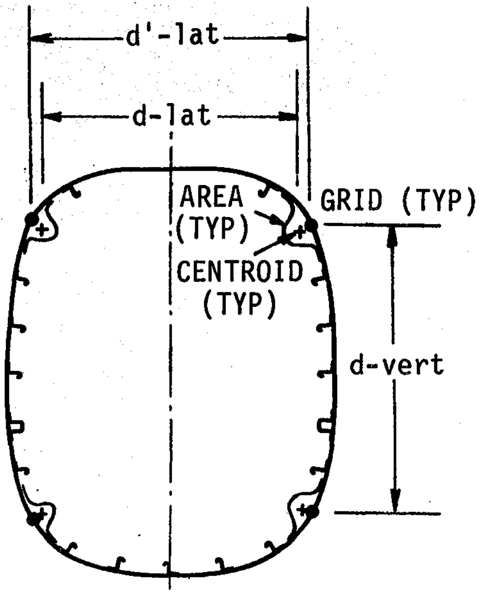

d'-lat
d-lat
AREA (TYP)
GRID (TYP)
CENTROID (TYP)
d-vert

LONGERON OFFSET EFFECT

CORRELATION OF ANALYTICAL RESULTS WITH TEST DATA

As indicated in the static load-deflection data, the AH-1G NASTRAN model with the built-up tailboom has greater lateral bending stiffness than test. Consequently, the first lateral airframe bending mode of the built-up tailboom model (7.39 Hz) is higher than test (7.1 Hz). On the other hand, the stick model load-deflection data agreed well with test and therefore agrees well in frequency placement.

The higher natural frequencies calculated for the AH-1G NASTRAN model with built-up tailboom are lower than test. This may be due to the torsional stiffness of the tailboom. The static tailboom torsion test conducted earlier in the program indicated that the NASTRAN stick model was too soft in the aft end. Further investigation is needed to resolve the difference.

CORRELATION OF ANALYTICAL RESULTS WITH TEST DATA

MODE	NATURAL FREQUENCY - HZ		
	TEST	ELASTIC LINE TAILBOOM	BUILT-UP TAILBOOM
MAIN ROTOR PYLON FORE-AND-AFT ROCKING (PYLON PITCH)	3.9	2.99	2.99
MAIN ROTOR PYLON LATERAL ROCKING (PYLON ROLL)	--	3.86	3.83
FIRST FUSELAGE (TAILBOOM) LATERAL BENDING	7.1	7.12	7.39
FIRST FUSELAGE (TAILBOOM) VERTICAL BENDING	8.0	7.96	7.96
FUSELAGE TORSION	15.5	15.49	15.07
SECOND FUSLAGE VERTICAL BENDING	18.0	17.20	15.78
SECOND FUSELAGE LATERAL BENDING	18.9	16.74	16.64
FUSELAGE ROLL / ENGINE LATERAL	--	18.73	18.70

NOTE: NASTRAN RESULTS ARE FOR FLIGHT 35A GROSS WEIGHT CONFIGURATION.

FREQUENCY RESPONSE COMPARISON - LATERAL

The two lateral frequency response curves shown in the figure represent pilot seat lateral response for excitation at the tail and hub, respectively. The responses shown are comparisons between the responses of the two AH-1G FEM(s), one with a stick tailboom representation and the other with a detailed model of each bay of the tailboom. The comparisons show very good agreement for mode placement and amplitude response throughout the desired range of frequency response (0-30 Hz) between both models and validates the use of the stick tailboom model.

FREQUENCY RESPONSE COMPARISON - LATERAL

PILOT SEAT LATERAL RESPONSE TO LATERAL TAIL SHAKE

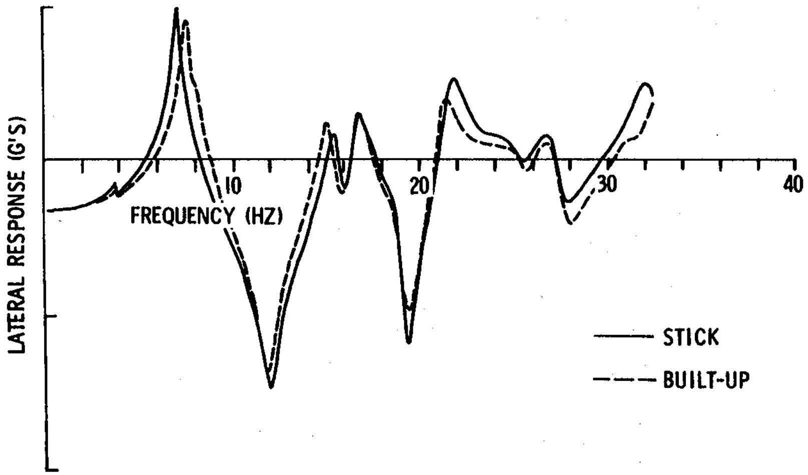

PILOT SEAT LATERAL RESPONSE TO LATERAL HUB SHAKE

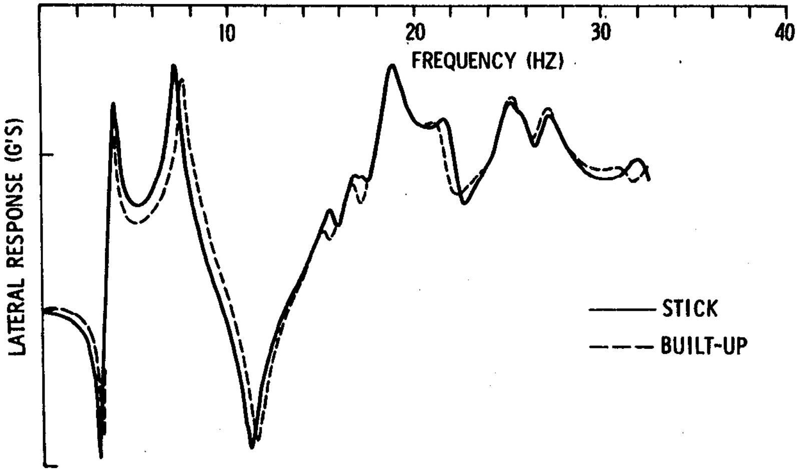

FUTURE WORK NEEDED

The areas having the most potential for improving current FEA vibration modeling techniques are cited. Each of these areas represents an obvious technology that needs further research and/or testing to critically compare common industry experiences needed for improving the state-of-the-art in vibration prediction.

FUTURE WORK NEEDED

- HIGHER FREQUENCY ($\geq$ 4p) VIBRATION PREDICTION
  - NONSTRUCTURAL AIRFRAME PARTS
  - SUBSYSTEM COMPONENTS
  - DAMPING AND NONLINEARITIES
  - LOCAL MODES
- COMPOSITE STRUCTURES
- PYLON ISOLATION SYSTEM MODELING
- ROTOR / AIRFRAME COUPLING
- ROTOR (AERO AND DYNAMIC) EXCITATION AND OTHER SOURCES
- STRUCTURAL OPTIMIZATION
- TESTING METHODS:
  - TEST / FEM COUPLED ANALYSIS
  - MODEL IMPROVEMENT
  - AIRFRAME VIBRATION IMPROVEMENT VIA TEST
  - FORCE DETERMINATION

7. REFERENCES

REFERENCES

1. Shockey, G. A., Williamson, J. W., Cox, C. R., "AH-1G Helicopter Aerodynamics and Structrual Loads Survey," USAAMRDL-TR-76-39, April 1976.

2. Van Gaasbeek, J. R., "Validation of the Rotorcraft Flight Simulation Program (C81) Using Operational Loads Survey Flight Test Data," USAAVRADCOM-TR-80-D-4, November 1979.

3. Cronkhite, J. D., Berry, V. L., Brunken, J. E., "A NASTRAN Vibration Model of the AH-1G Helicopter Airframe," U.S. Army Armament Command Report No. R-TR-74-045, June 1974.

4. Cronkhite, J. D., Berry, V. L., "Correlation of AH-1G Airframe Test Data with a NASTRAN Mathematical Model," NASA CR-145119, February 1976.

5. Cronkhite, J. D., Wilson, H. E., Berry, V. L., "Correlation of AH-1G Helicopter Flight Vibration Data and Tailboom Static Test Data with NASTRAN Results," NASA CR-145120, 1978.

6. Giansante, N., Berman, A., Flannelly, W. G., and Nagy, E. J., "Structural System Identification Technology Verification," USAAVRADCOM-TR-81-D-28, November 1981.

7. Jones, R., Flannelly, W. G., Nagy, E. J., Fabunmi, J. A., "Experimental Verification of Force Determination and Ground Flying of a Full-Scale Helicopter," USAAVRADCOM-TR-81-D-11, May 1981.

APPENDIX A

KAMAN FREQUENCY RESPONSE COMPARISONS
(LOW, MEAN, HIGH GW CONFIGURATIONS)

KAMAN SINUSOIDAL GROUND VIBRATION TEST COMPARISON

A description of ground vibration tests performed by the Kaman Aerospace Corporation (KAC) on a Bell AH-1G and a comparison of the test results with NASTRAN FEM calculations are presented in this section for amplitude and phase frequency response plots. The frequency response plots are presented for a frequency range of 0 - 30 Hz for excitation applied separately at the tail skid location (FS 485) in the vertical direction and at the tail rotor gearbox (FS 521) in the lateral direction. The response accelerometers are identified in the body of the report in the section which introduced this test data.

Three configurations are presented: one clean wing and two wing store configurations. The frequency response comparisons (amplitude and phase) include the following locations:

KAMAN STATION/ACCELEROMETER	NASTRAN GRID	DIRECTION V = VERTICAL L = LATERAL
Nose/Z50	3339	V
C.G/Z195B	19765	V
Left Wing/Z202L	75921	V
Right Wing/Z202R	65921	V
Elevator	40145	V
Aft Tail/Z485	48845	V
Nose/Y46L	4637	L
T/R Gearbox/Y521	520079	L

NATURAL FREQUENCY COMPARISON

VERTICAL TAIL SHAKE - CLEAN WING

MODE	Kaman - Low GW		NASTRAN (Hz)
	Damping	Freq (Hz)	
Fore-aft Pylon	-	-	5.13
First Vertical Bending	0.07	7.19	7.87
Fuselage Torsion	0.10	16.44	15.57
Second Vertical Bending	0.09	17.71	17.34

LATERAL TAIL SHAKE - CLEAN WING

MODE	Kaman - Low GW		NASTRAN (Hz)
	Damping	Freq (Hz)	
Lateral Pylon	-	-	4.95
First Lateral Bending	0.05	7.51	7.11
Fuselage Torsion	0.17	14.66	15.57
Second Lateral Bending	0.10	17.36	17.27
Third Lateral Bending	-	-	-

FREQUENCY RESPONSE COMPARISON - VERTICAL

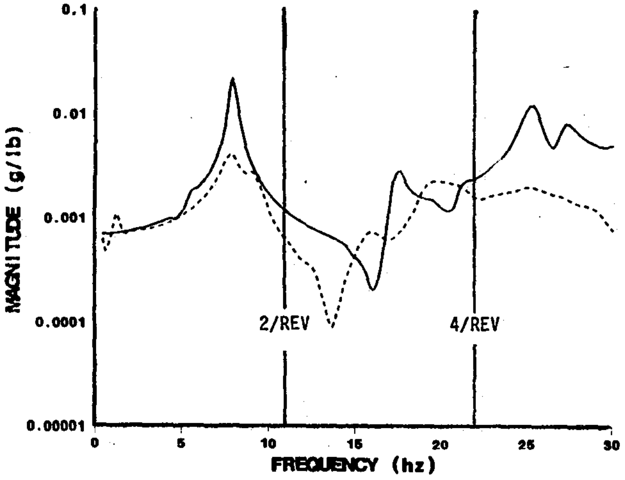

LEGEND

———————— NASTRAN

- - - - - - - - - - Test

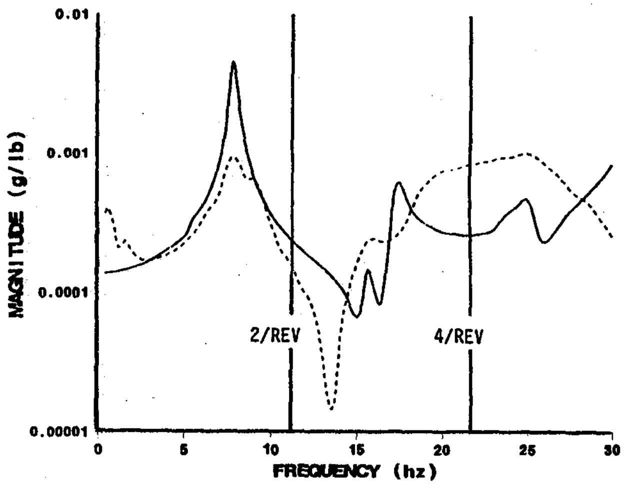

NOSE

CLEAN WING

CG

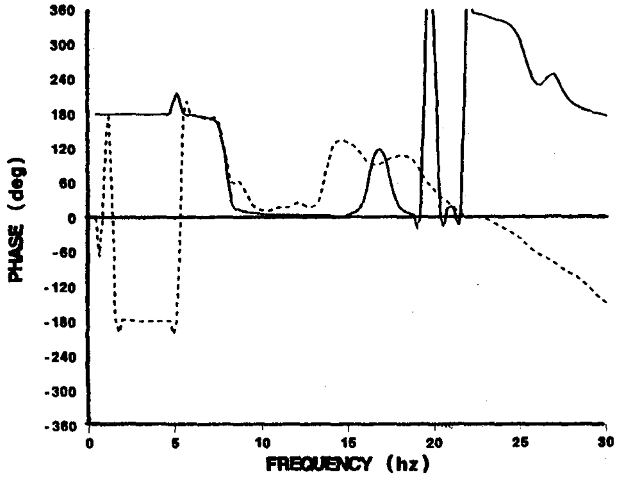

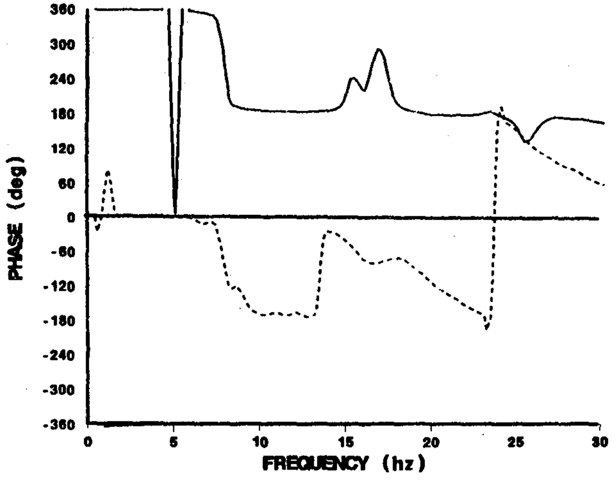

FREQUENCY RESPONSE COMPARISON - VERTICAL

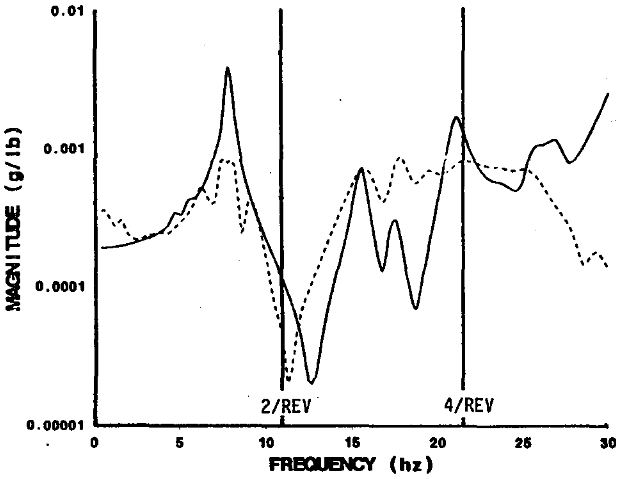

LEGEND

———— NASTRAN

- - - - - - - - - Test

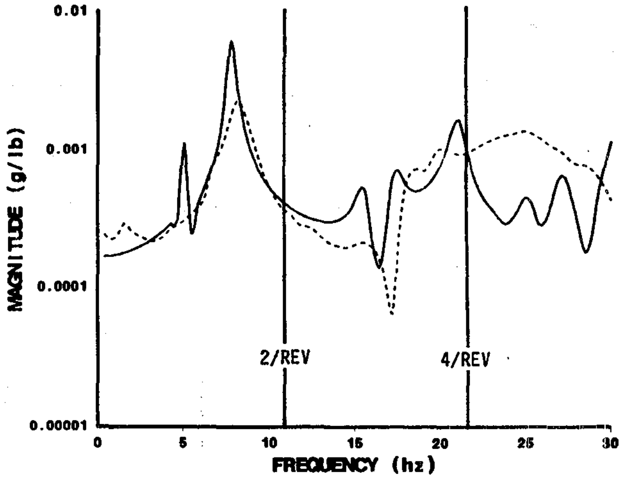

LEFT WING TIP

CLEAN WING

RIGHT WING TIP

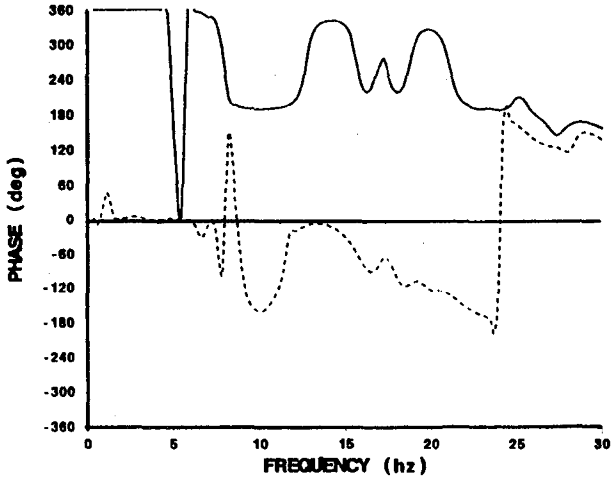

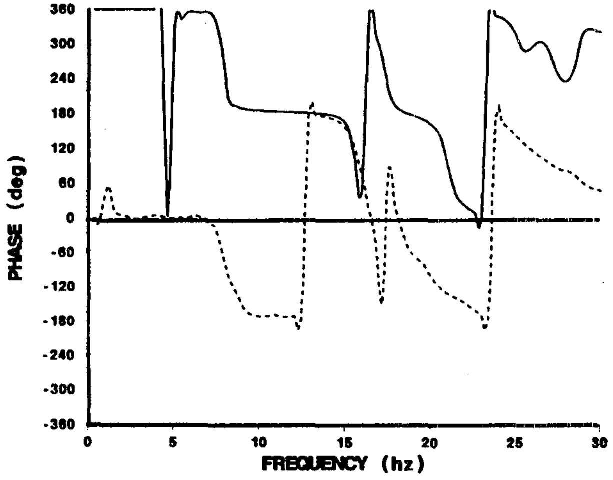

FREQUENCY RESPONSE COMPARISON - VERTICAL

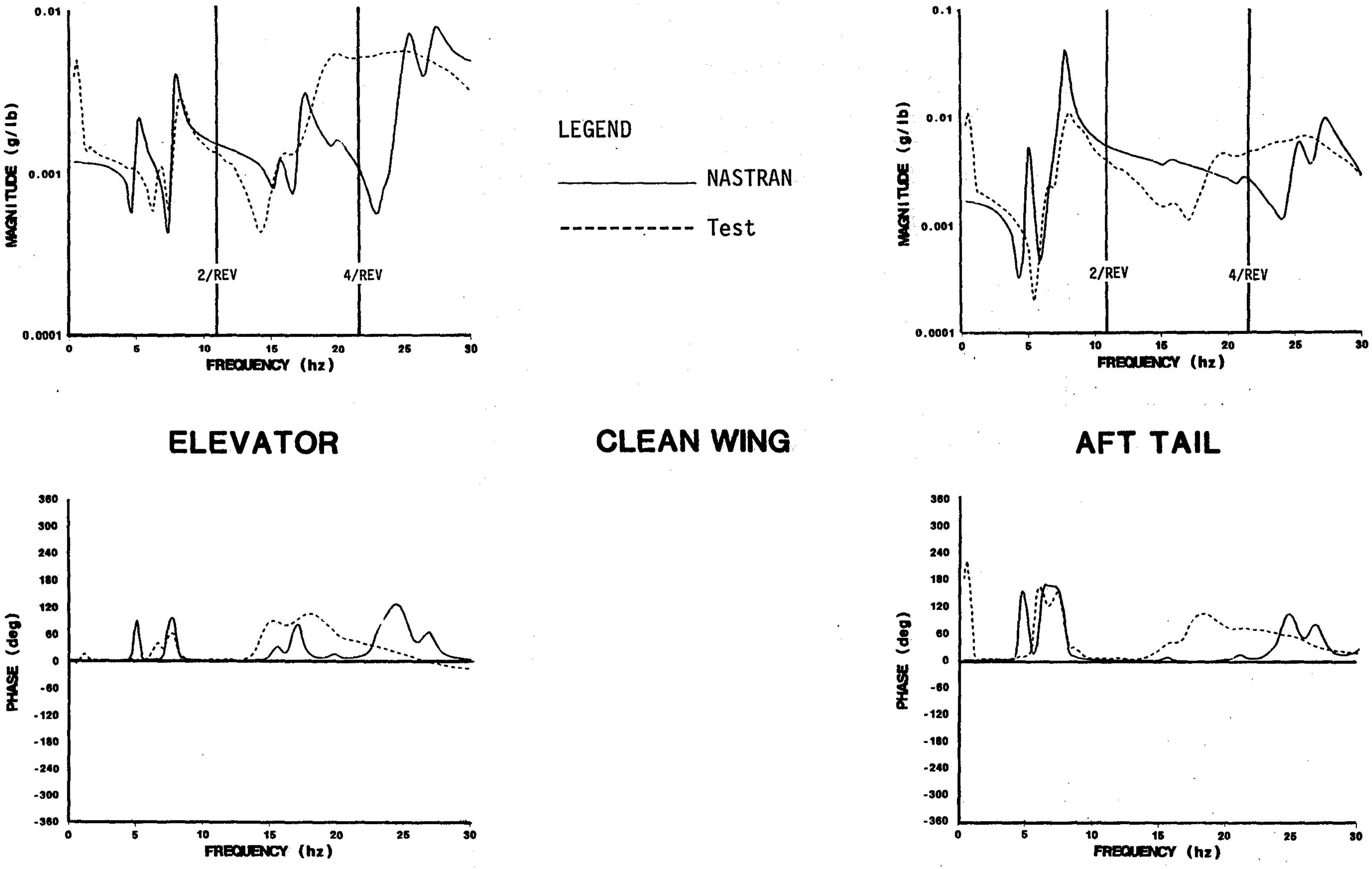

FREQUENCY RESPONSE COMPARISON - LATERAL

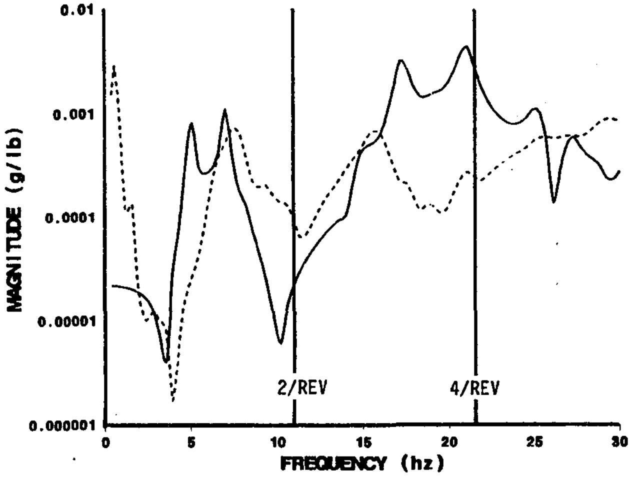

LEGEND

——————NASTRAN

-------- Test

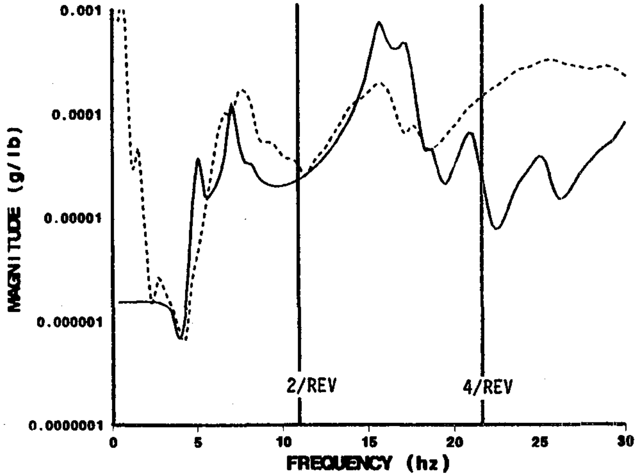

NOSE

CLEAN WING

CG

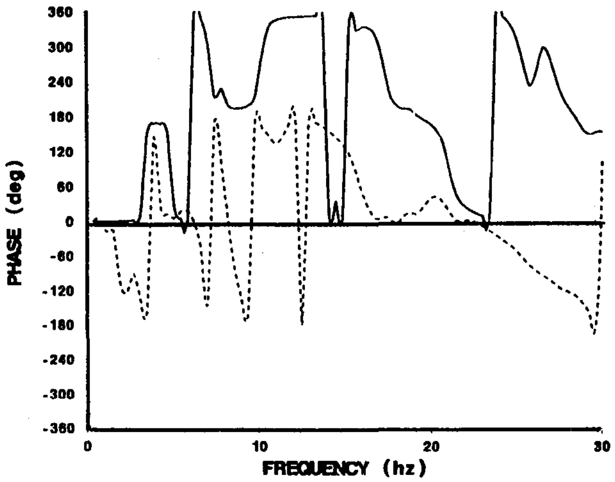

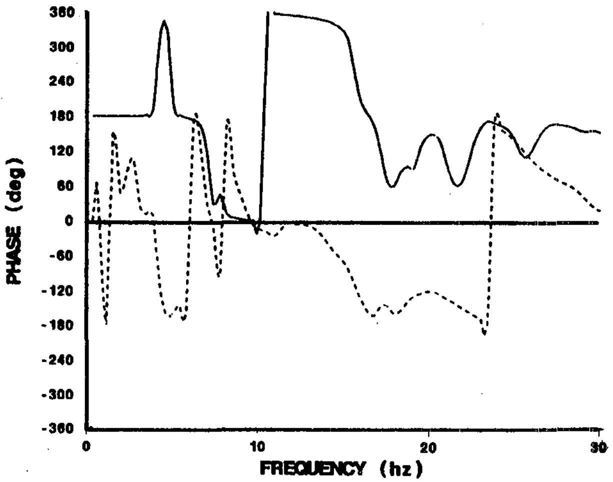

FREQUENCY RESPONSE COMPARISON - LATERAL

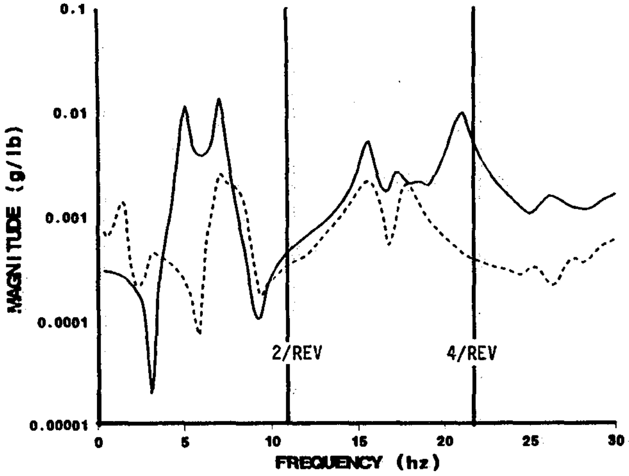

LEGEND

——— NASTRAN

--------- Test

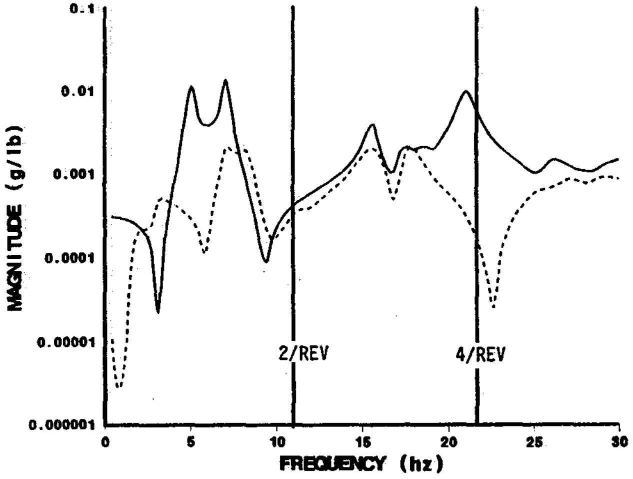

LEFT WING TIP

CLEAN WING

RIGHT WING TIP

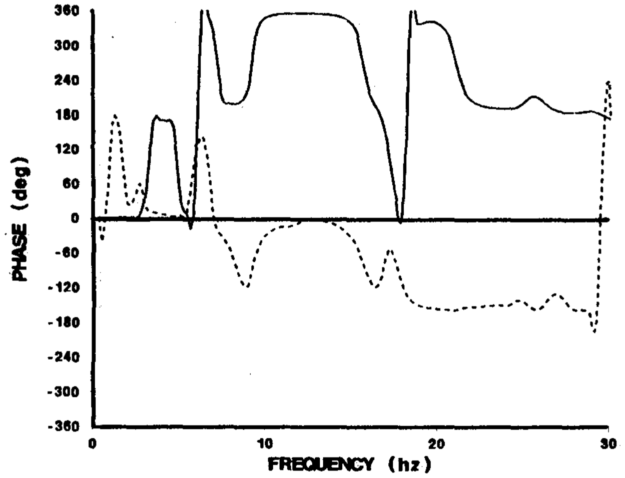

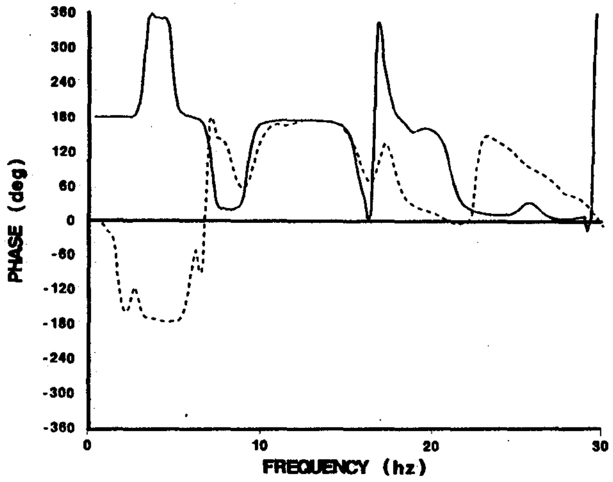

FREQUENCY RESPONSE COMPARISON - LATERAL

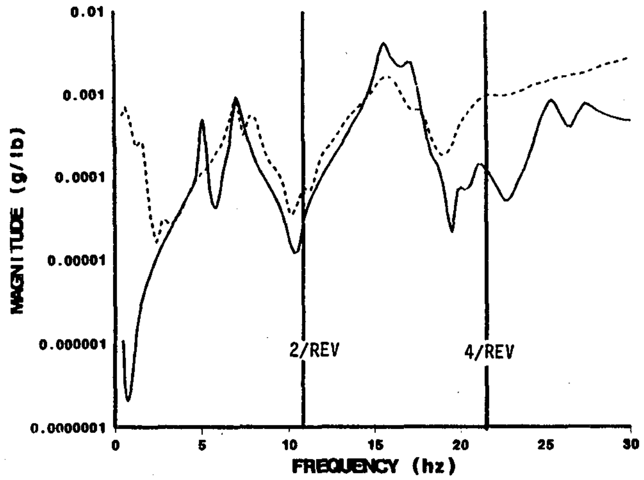

LEGEND

———— NASTRAN

-------- Test

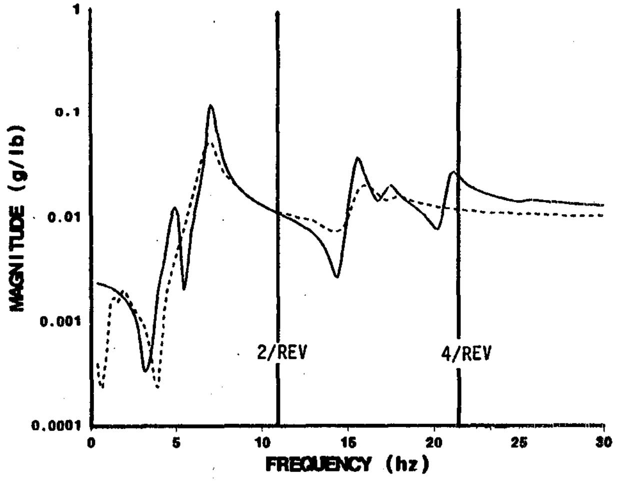

ELEVATOR

CLEAN WING

T/R GEARBOX

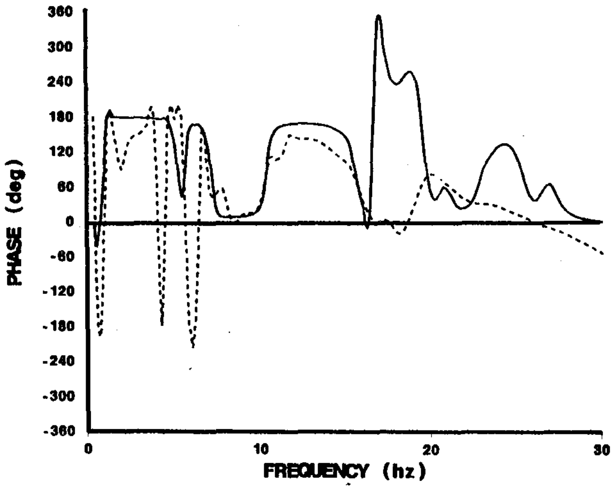

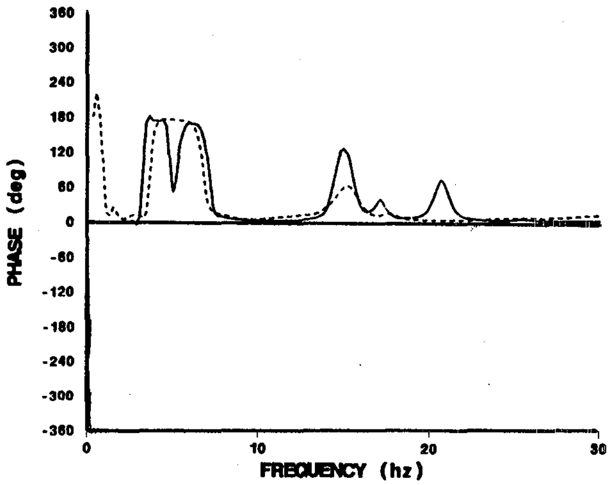

NATURAL FREQUENCY COMPARISON

VERTICAL TAIL SHAKE - OUTBOARD WING STORE

MODE	TEST		NASTRAN (Hz)
	Damping	Freq (Hz)	
Fore-aft Pylon	-	-	5.11
First Vertical Bending	0.08	7.15	7.78
Fuselage Torsion	0.07	15.04	15.36
Second Vertical Bending	0.07	17.88	17.66

LATERAL TAIL SHAKE - OUTBOARD WING STORE

MODE	TEST		NASTRAN (Hz)
	Damping	Freq (Hz)	
Lateral Pylon	-	-	4.34
First Lateral Bending	0.08	7.04	6.84
Fuselage Torsion	0.15	15.08	15.36
Second Lateral Bending	0.09	16.16	16.79

FREQUENCY RESPONSE COMPARISON - VERTICAL

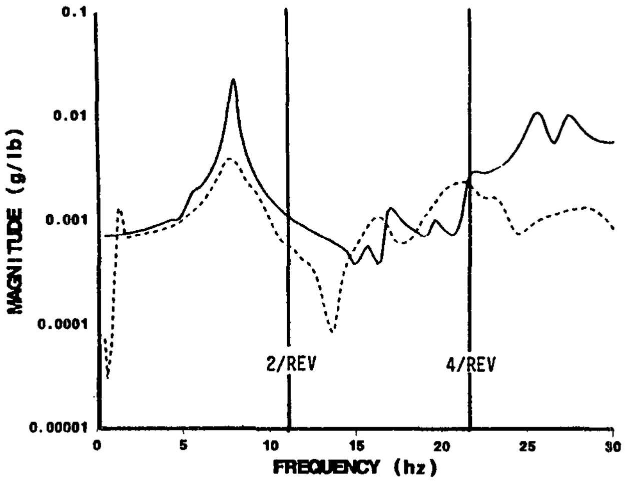

LEGEND

──── NASTRAN

- - - - Test

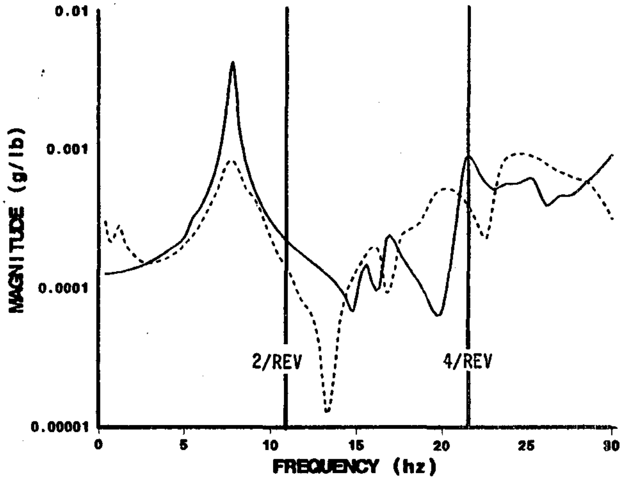

NOSE

OUTBOARD WING STORES

CG

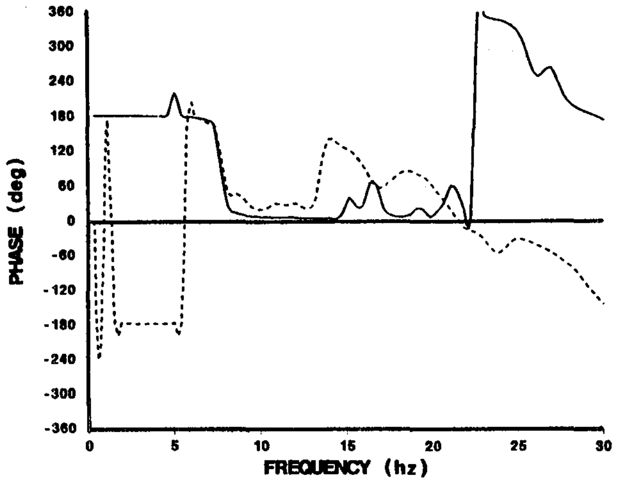

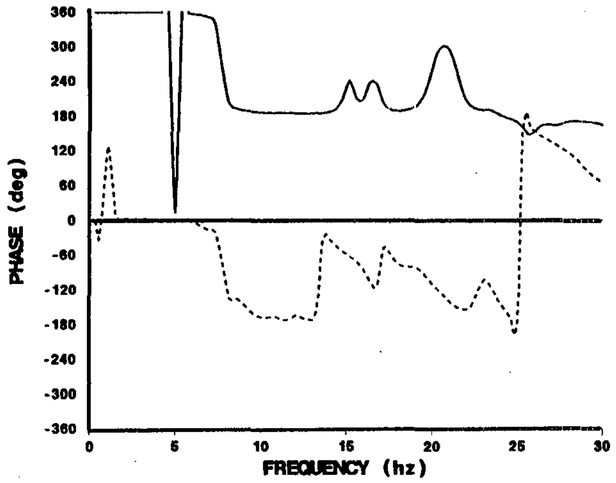

FREQUENCY RESPONSE COMPARISON - VERTICAL

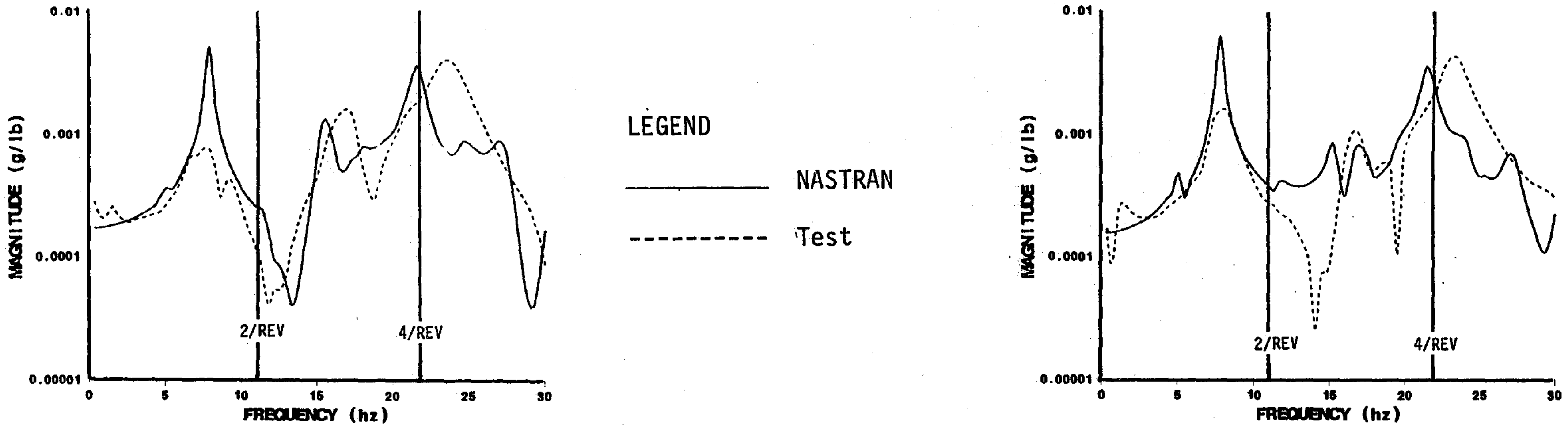

LEFT WING TIP **OUTBOARD WING STORES** **RIGHT WING TIP**

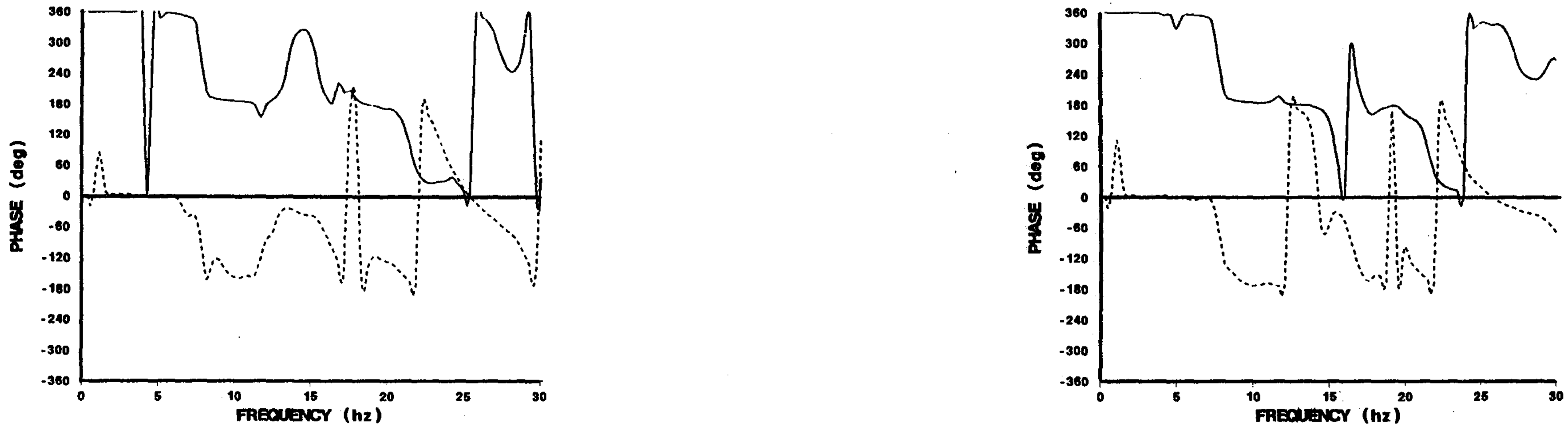

FREQUENCY RESPONSE COMPARISON - VERTICAL

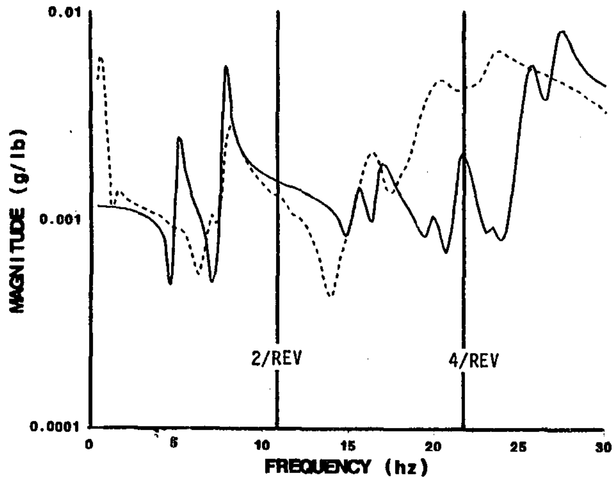

LEGEND

———————— NASTRAN

- - - - - - - - - - Test

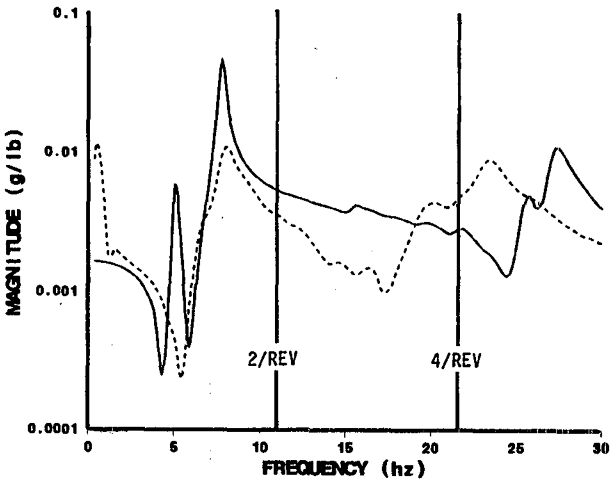

ELEVATOR

OUTBOARD WING STORES

AFT TAIL

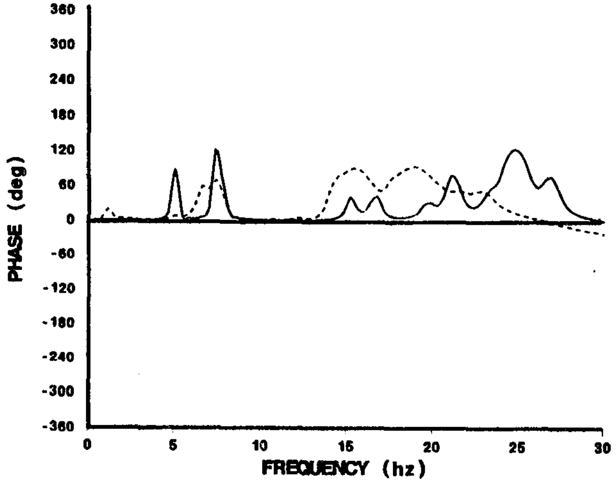

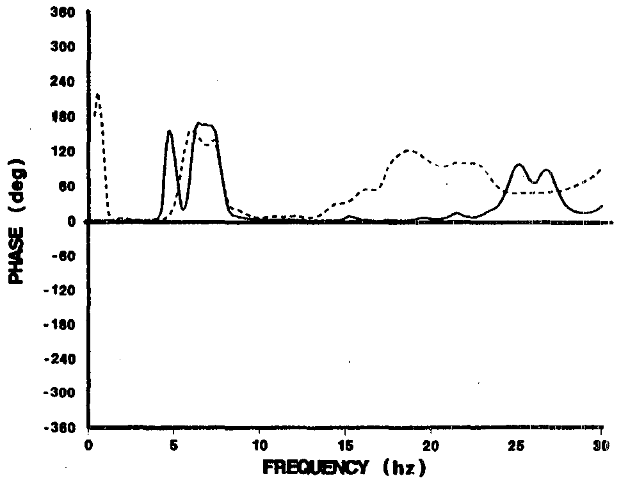

FREQUENCY RESPONSE COMPARISON - LATERAL

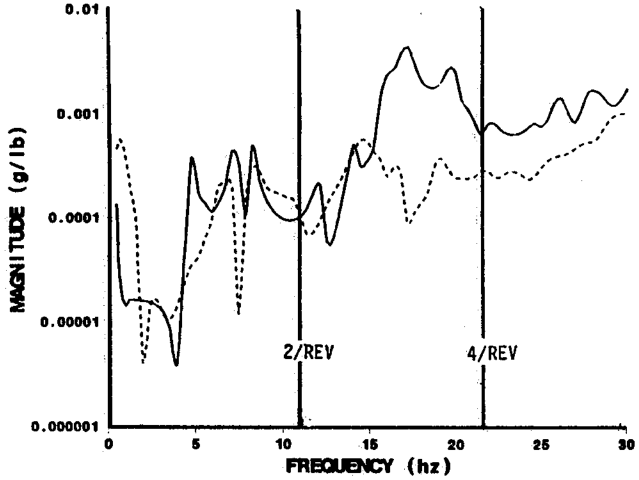

LEGEND

——————— NASTRAN

-------- Test

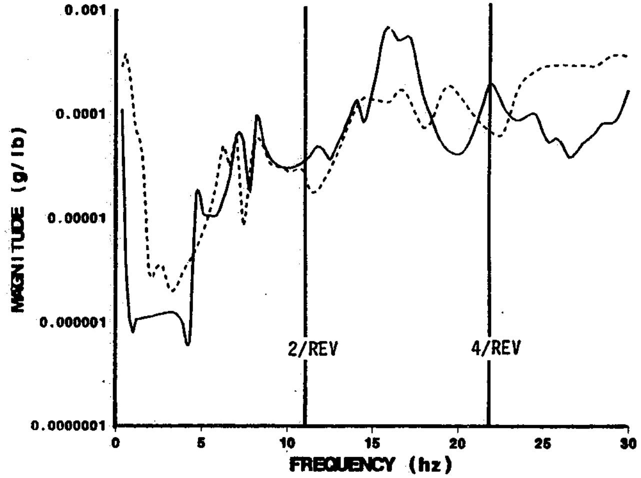

NOSE

OUTBOARD WING STORES

CG

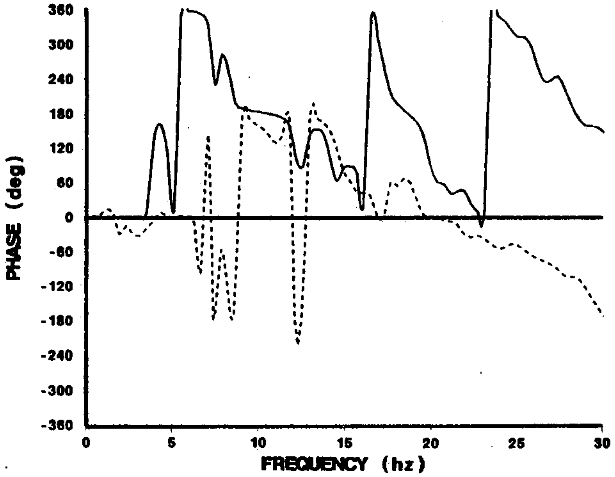

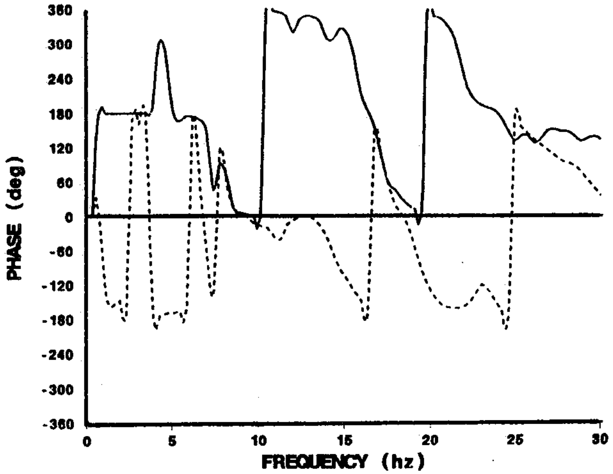

FREQUENCY RESPONSE COMPARISON - LATERAL

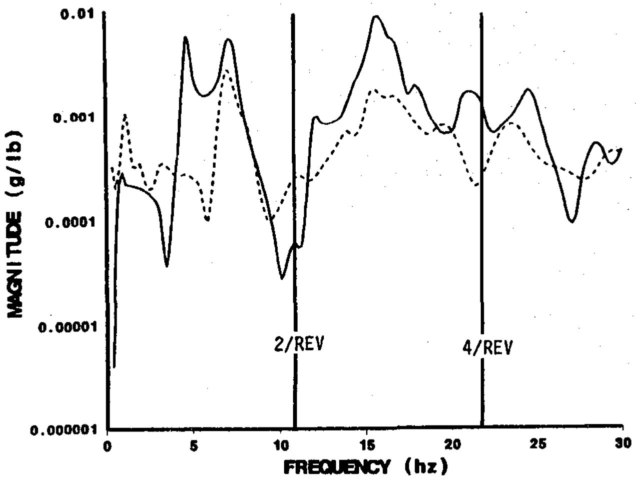

LEGEND

________NASTRAN

-------- Test

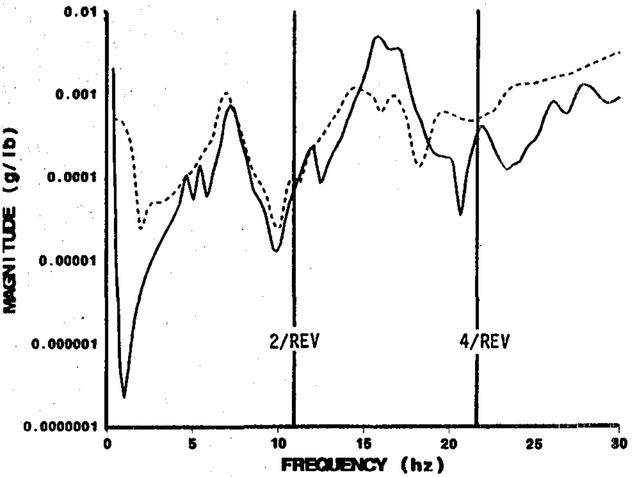

LEFT WING TIP **OUTBOARD WING STORES** **ELEVATOR**

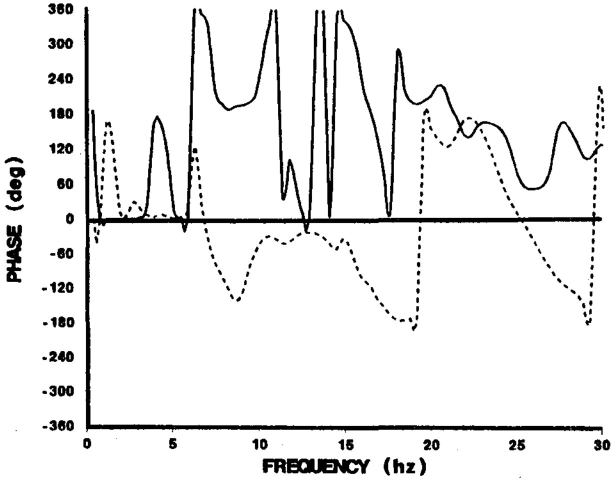

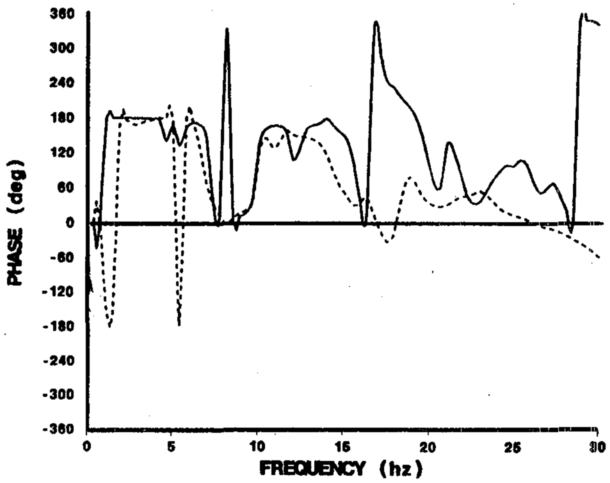

FREQUENCY RESPONSE COMPARISON - LATERAL

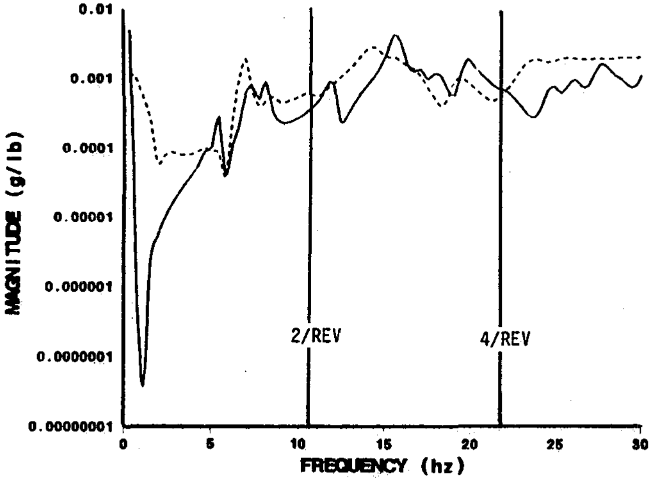

LEGEND

——— NASTRAN

------- Test

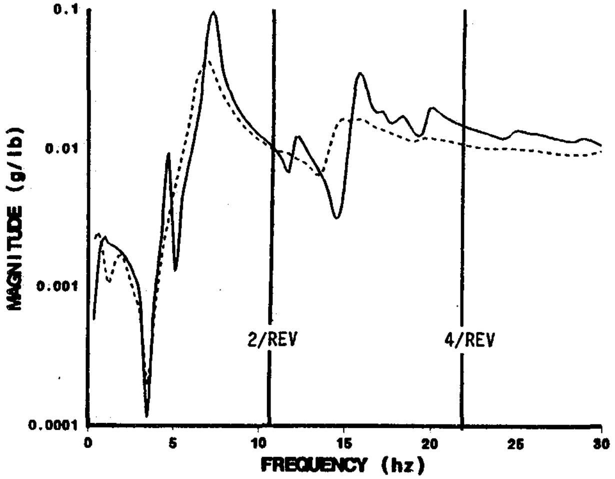

AFT TAIL **OUTBOARD WING STORES** **T/R GEARBOX**

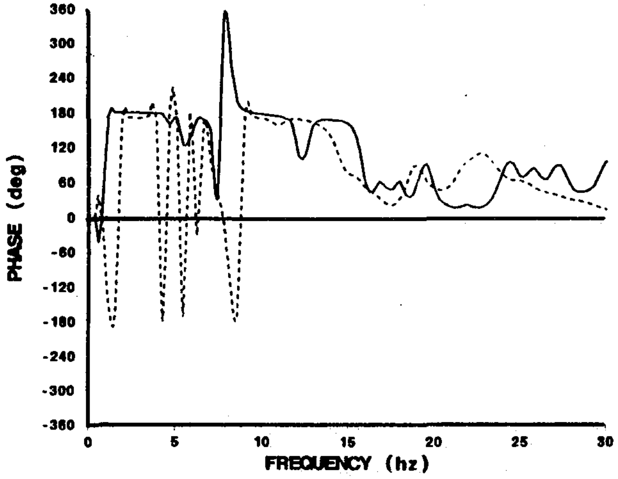

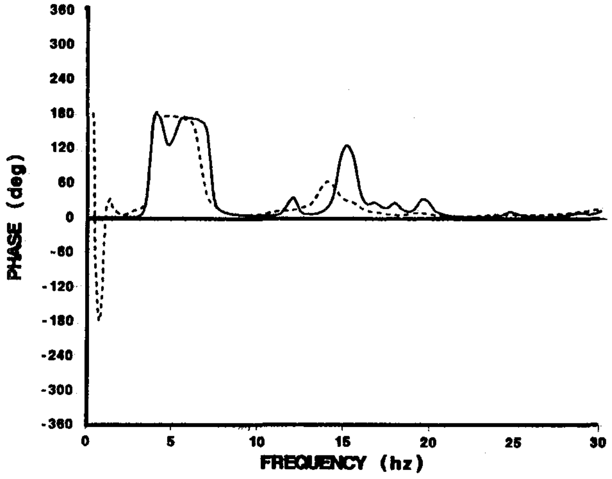

NATURAL FREQUENCY COMPARISON

VERTICAL TAIL SHAKE - OUTBOARD/INBOARD WING STORES

MODE	TEST		NASTRAN (Hz)
	Damping	Freq (Hz)	
Fore-aft Pylon	-	-	5.10
First Vertical Bending	0.07	7.32	7.71
Fuselage Torsion	0.10	15.99	15.54
Second Vertical Bending	0.08	17.60	17.00

LATERAL TAIL SHAKE - OUTBOARD/INBOARD WING STORES

MODE	TEST		NASTRAN (Hz)
	Damping	Freq (Hz)	
Lateral Pylon	-	-	4.15
First Lateral Bending	0.05	7.03	6.65
Fuselage Torsion	0.18	14.35	14.69
Second Lateral Bending	0.07	16.39	15.79

FREQUENCY RESPONSE COMPARISON - VERTICAL

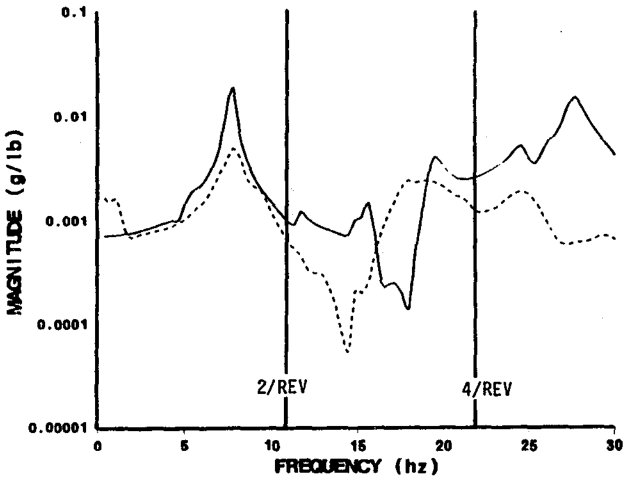

LEGEND

——————— NASTRAN

- - - - - - - - - Test

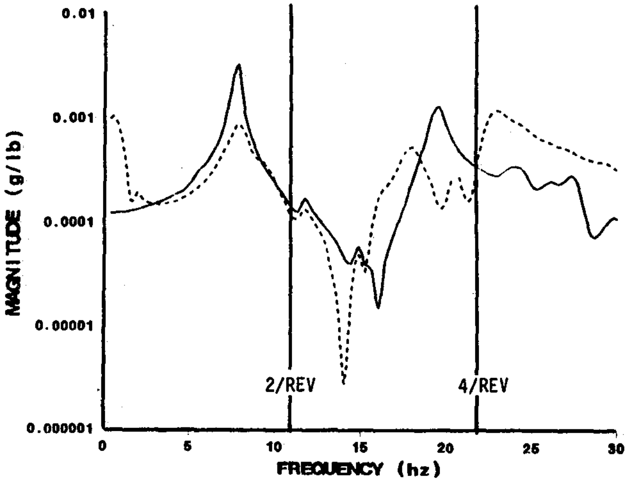

OUTBOARD/INBOARD WING STORES

NOSE

CG

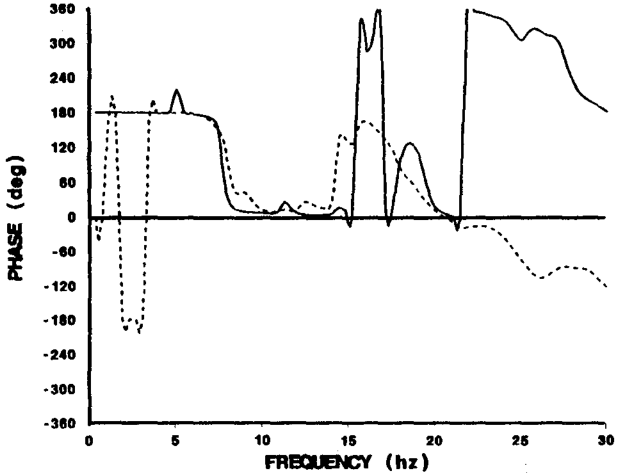

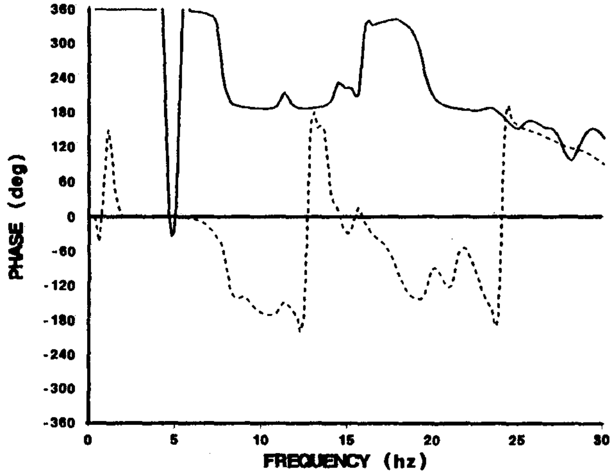

FREQUENCY RESPONSE COMPARISON - VERTICAL

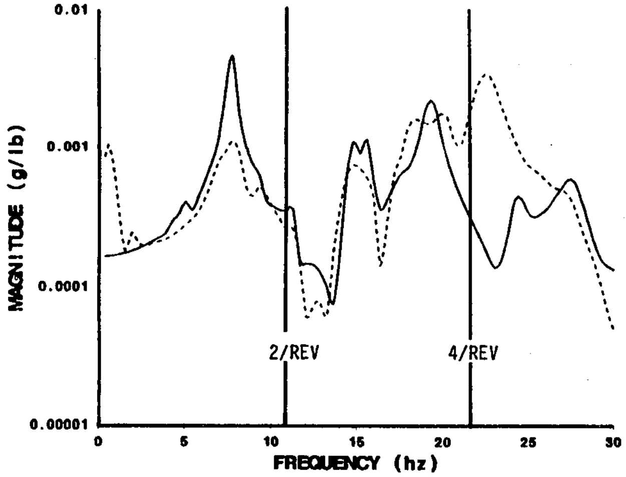

LEFT WING TIP

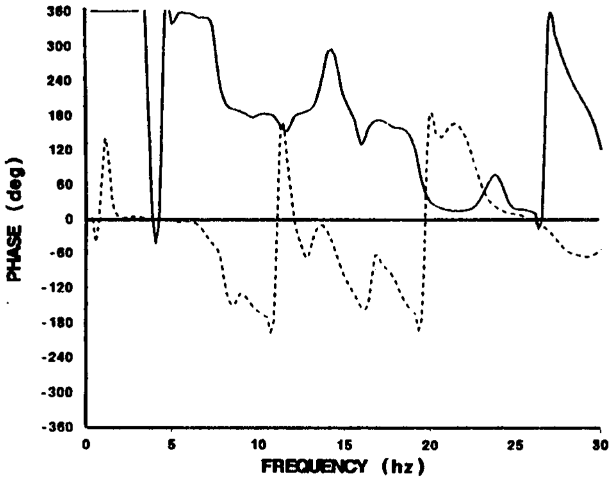

LEGEND

———————— NASTRAN

---------- Test

OUTBOARD/INBOARD WING STORES

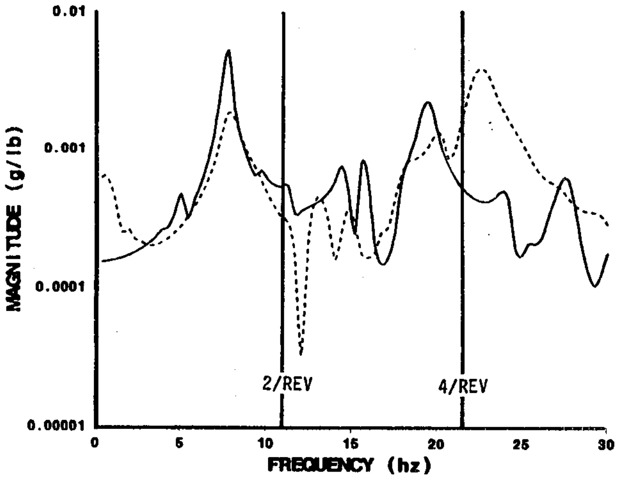

RIGHT WING TIP

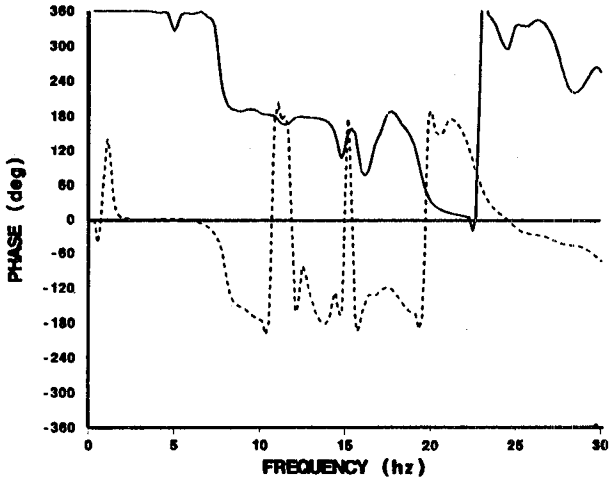

FREQUENCY RESPONSE COMPARISON - VERTICAL

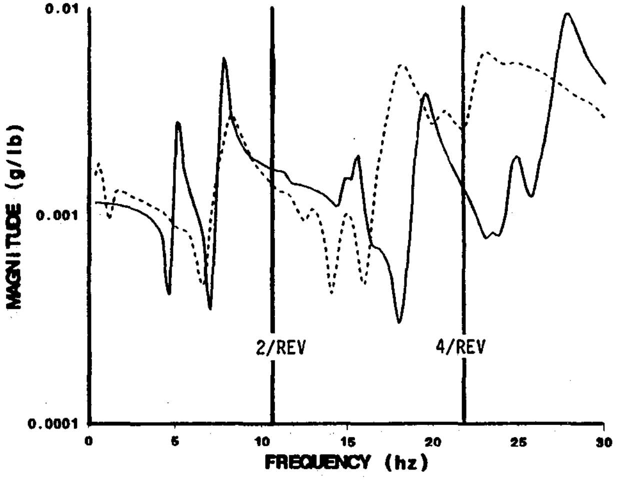

ELEVATOR

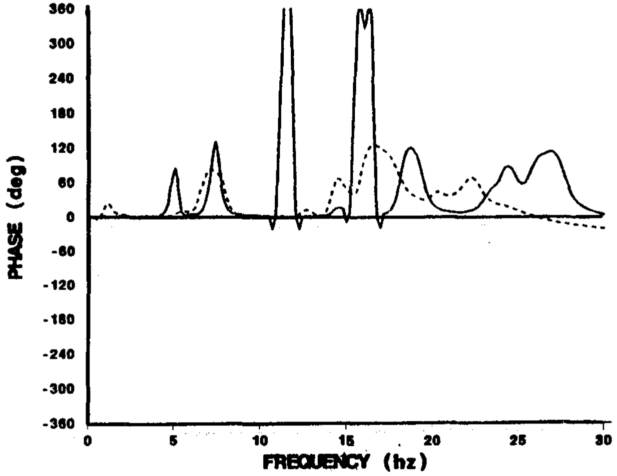

LEGEND

———— NASTRAN

-------- Test

OUTBOARD/INBOARD
WING STORES

FREQUENCY RESPONSE COMPARISON - LATERAL

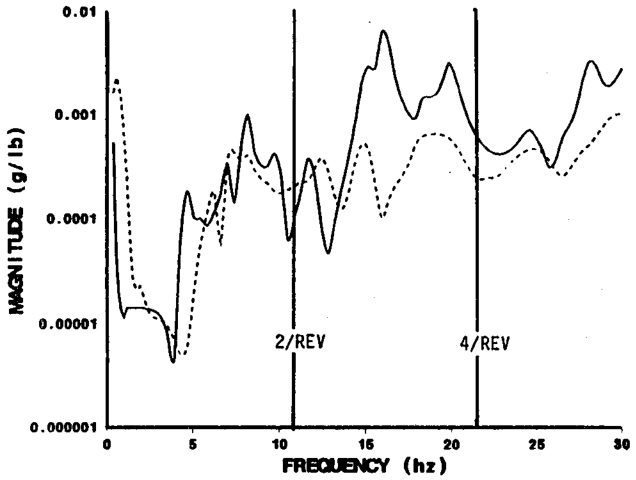

LEGEND

——— NASTRAN

------- Test

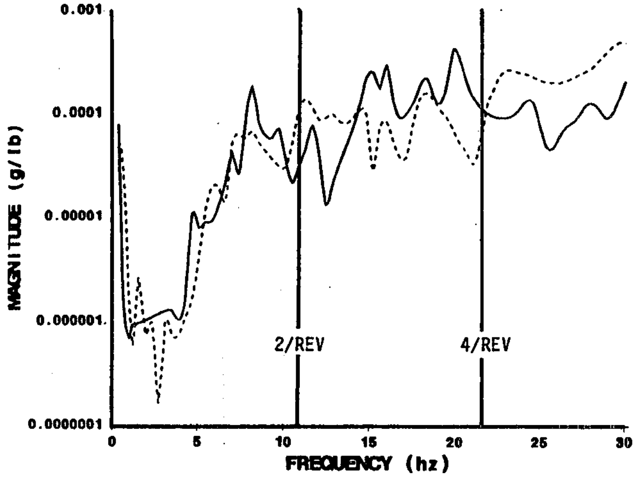

OUTBOARD/INBOARD

NOSE

WING STORES

CG

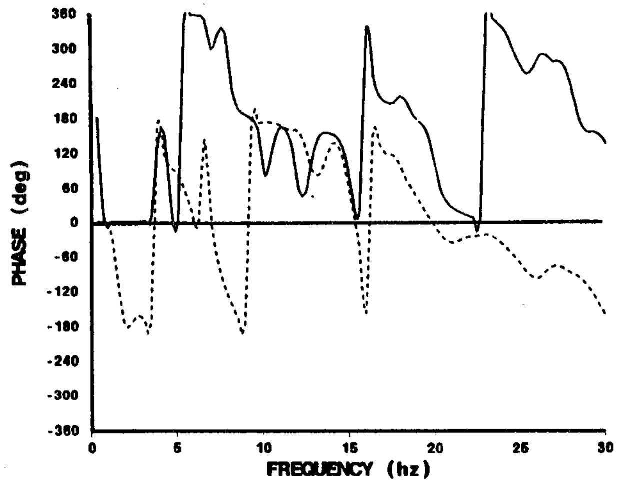

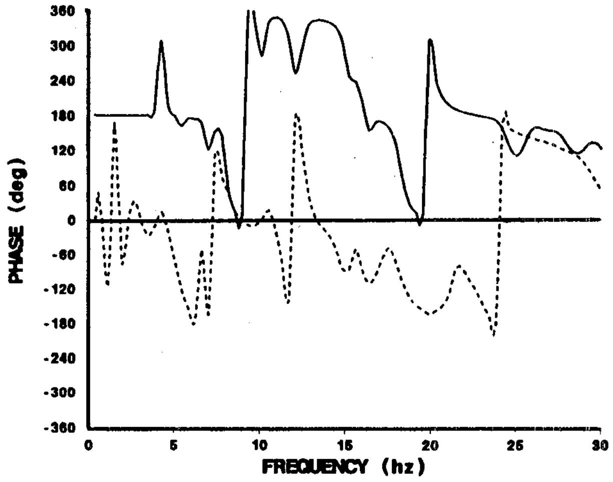

FREQUENCY RESPONSE COMPARISON - LATERAL

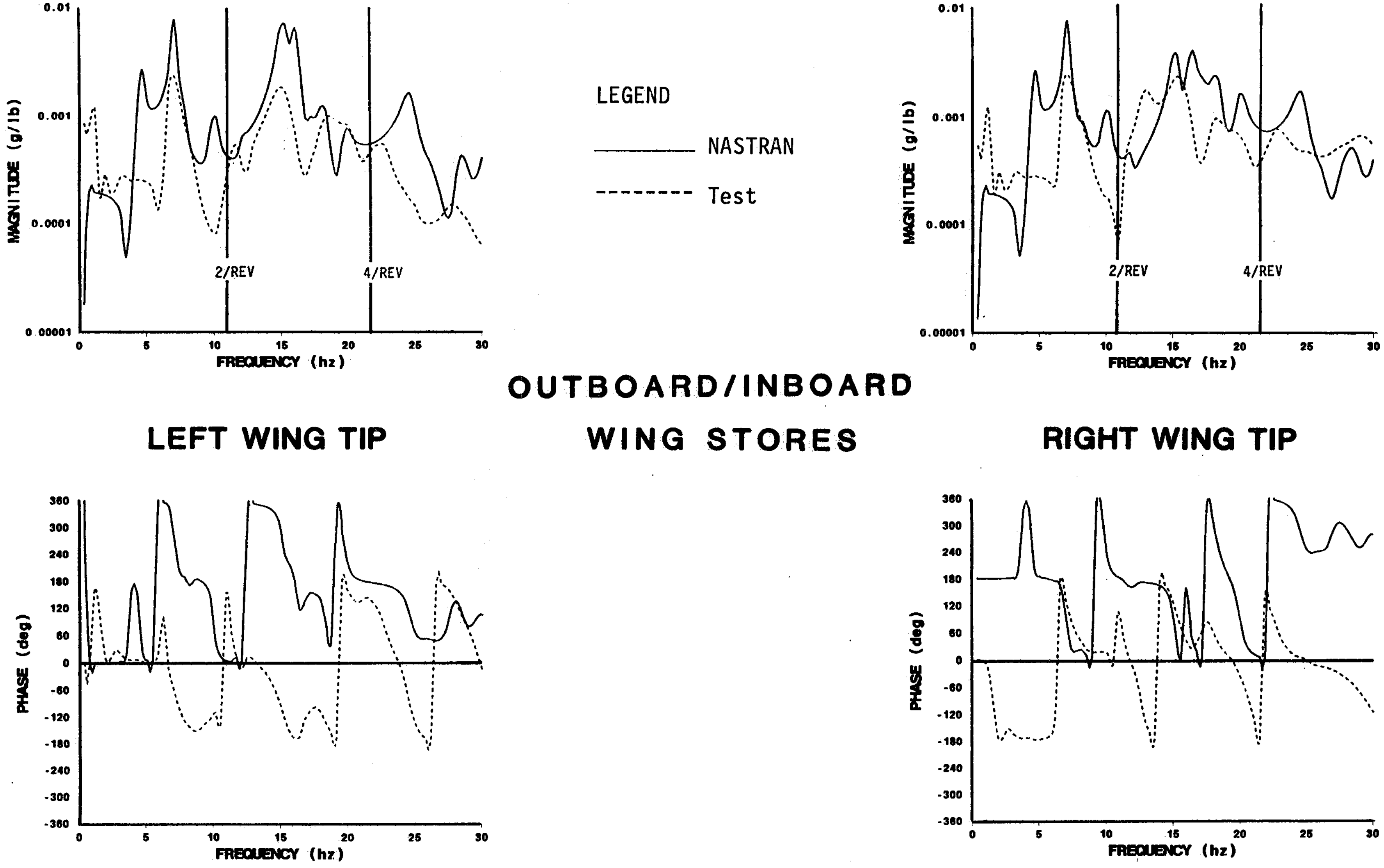

LEGEND

NASTRAN

Test

OUTBOARD/INBOARD

LEFT WING TIP

WING STORES

RIGHT WING TIP

FREQUENCY RESPONSE COMPARISON - LATERAL

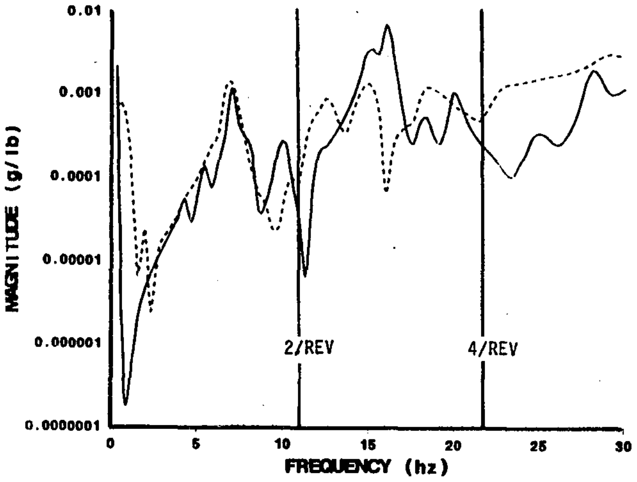

LEGEND

———————— NASTRAN

-------- Test

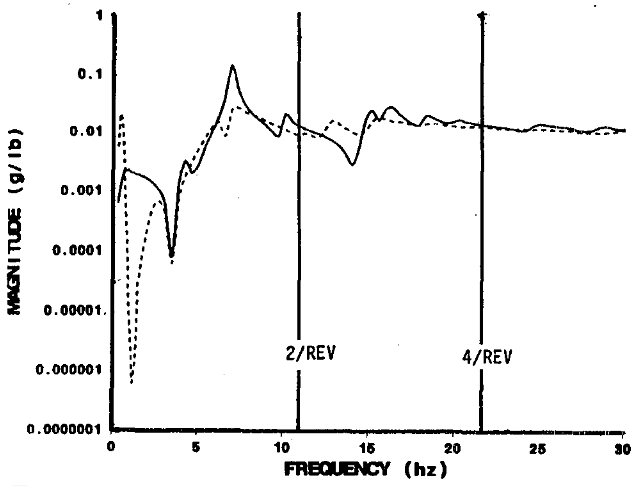

OUTBOARD/INBOARD

ELEVATOR

WING STORES

T/R GEARBOX

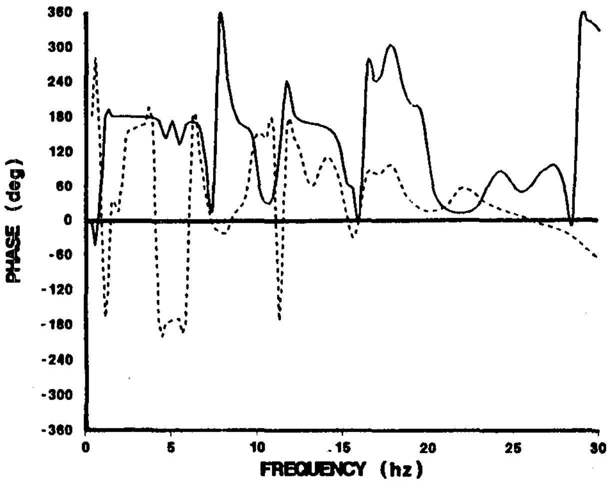

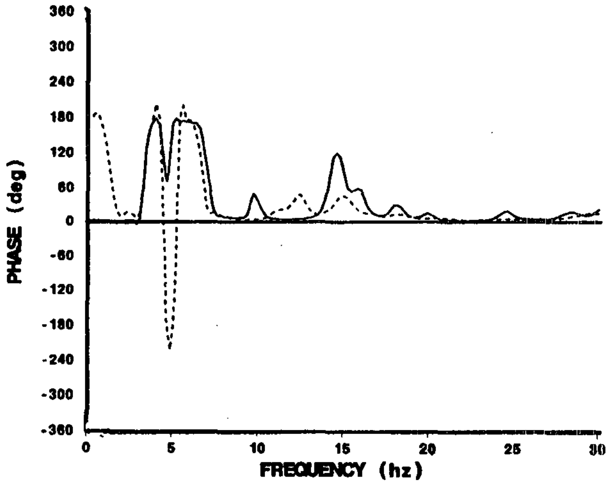

Standard Bibliographic Page

1. Report No.
NASA CR-178201

2. Government Accession No.

3. Recipient's Catalog No.

4. Title and Subtitle
Summary of the Modeling and Test Correlations of a NASTRAN Finite Element Vibrations Model for the AH-1G Helicopter

5. Report Date
January 1987

6. Performing Organization Code

7. Author(s)
J. D. Cronkhite, V. L. Berry, and R. V. Dompka

8. Performing Organization Report No.
699-099-202

9. Performing Organization Name and Address
Bell Helicopter Textron Inc.
P.O. Box 482
Ft. Worth, TX 76101

10. Work Unit No.

11. Contract or Grant No.
NAS1-17496

12. Sponsoring Agency Name and Address
National Aeronautics and Space Administration
Washington, DC 20546

13. Type of Report and Period Covered
Contractor Report

14. Sponsoring Agency Code
505-63-51-01

15. Supplementary Notes
Langley Technical Monitor: Raymond G. Kvaternik
Final Report (1 of 2 final reports for Task #1 of the contract)

16. Abstract

Under a research program designated DAMVIBS (Dynamic Analysis Methods for VIBrationS), four U.S. helicopter industry participants (Bell Helicopter, Boeing Vertol, McDonnell Douglas Helicopter, and Sikorsky Aircraft) are to apply existing analytical methods for calculating coupled rotor-fuselage vibrations of the AH-1G helicopter for correlation with flight test data from an AH-1G Operational Load Survey (OLS) test program. Bell Helicopter, as the manufacturer of the AH-1G, was tasked to provide pertinent rotor data for the two-bladed rotor system and to collect the OLS flight vibration data needed to perform the correlations. The analytical representation of the fuselage structure is based on a NASTRAN finite element model (FEM) developed by Bell which has been extensively documented and correlated with ground vibration test.

This report describes the AH-1G NASTRAN FEM and summarizes the correlations with measured data that have been conducted to verify the model. Comparisons of the AH-1G NASTRAN FEM calculations with measured data include the following: (1) fuselage and tailboom static load-deflection (stiffness) testing, (2) airframe ground vibration testing (0-30 Hz), (3) airframe flight vibration testing (main rotor, 2, 4, and 6/rev), and (4) tailboom effective skin static testing. A description of the modeling rationale and techniques used to develop the NASTRAN FEM is presented in conjunction with all previous correlation work. In general, the correlations show good agreement between analysis and test in stiffness and vibration response through 15 to 20 Hz. For higher frequencies (≥4/rev (21.6 Hz)), the vibration responses generally did not agree well. Also, the lateral (2/rev (10.8 Hz)) flight vibration responses were much lower in the FEM than test indicating that there is a significant excitation source other than at the main rotor hub that is affecting the lateral vibrations, such as downwash impingement on the vertical tail. Recommendations for further work are presented.

17. Key Words (Suggested by Authors(s))
AH-1G helicopter
Dynamic
airframe vibrations
Finite Element structural analysis
helicopter
ground vibration test
rotorcraft
NASTRAN

18. Distribution Statement
Unclassified - Unlimited

Subject Category 39

19. Security Classif.(of this report)
Unclassified

20. Security Classif.(of this page)
Unclassified

21. No. of Pages
300

22. Price
A13

For sale by the National Technical Information Service, Springfield, Virginia 22161

End of Document